

# Sheffield Hallam University

*Pulse time modulation for subcarrier multiplexed systems.*

WICKRAMASINGHE, V. R.

Available from the Sheffield Hallam University Research Archive (SHURA) at:

<http://shura.shu.ac.uk/20532/>

## A Sheffield Hallam University thesis

This thesis is protected by copyright which belongs to the author.

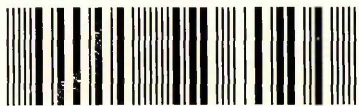
The content must not be changed in any way or sold commercially in any format or medium without the formal permission of the author.

When referring to this work, full bibliographic details including the author, title, awarding institution and date of the thesis must be given.

Please visit <http://shura.shu.ac.uk/20532/> and <http://shura.shu.ac.uk/information.html> for further details about copyright and re-use permissions.

CITY CAMPUS PARK STREET  
SHEFFIELD S1 1WB

101 536 545 0



Bin 12/83

Sheffield Hallam University

**REFERENCE ONLY**

ProQuest Number: 10701179

All rights reserved

INFORMATION TO ALL USERS

The quality of this reproduction is dependent upon the quality of the copy submitted.

In the unlikely event that the author did not send a complete manuscript and there are missing pages, these will be noted. Also, if material had to be removed, a note will indicate the deletion.



ProQuest 10701179

Published by ProQuest LLC (2017). Copyright of the Dissertation is held by the Author.

All rights reserved.

This work is protected against unauthorized copying under Title 17, United States Code  
Microform Edition © ProQuest LLC.

ProQuest LLC.  
789 East Eisenhower Parkway  
P.O. Box 1346  
Ann Arbor, MI 48106 – 1346

# **Pulse Time Modulation for Subcarrier Multiplexed Systems**

**V.R. Wickramasinghe**

A thesis submitted in partial fulfillment of the requirements of  
Sheffield Hallam University for the degree  
of Doctor of Philosophy

*Electronics & Communications Engineering Research Group*  
School of Engineering  
Sheffield Hallam University  
Sheffield, UK

February 1997

To everyone who has helped, loved and held me with  
affection on this treacherous path,

*especially my Mother.*

# *Acknowledgments*

My deepest gratitude is due to the School of Engineering at Sheffield Hallam University for funding the project throughout the three year duration. The project was initiated and carried out under the direct supervision of Dr. Z. Ghassemlooy to whom the author expresses his warmest appreciation for unfailing interest, constructive criticism and helpful suggestions.

Sincere thanks is also due to Dr. Andy Simmonds for his help, advice and proof reading the thesis. The technical help provided by Mr. R.G. Harris to the latter stages of the project is gratefully acknowledged. The advice of Dr. L. Chao and Dr. R. Saatchi has also been valuable.

In addition, the author remembers warmly all the colleagues in the *Electronics & Communications Engineering Research Group* who has helped to create a conducive work environment and for helpful discussions from time to time. The help given by various members of the technical staff is also greatly appreciated.

Without the help and personal support of my dear friends in Sheffield, especially towards the latter stages, the work carried out in this thesis could not have been completed. I would like to express my heartfelt gratitude to those friends and relatives who provided constant encouragement and guidance throughout this project.

## *Declaration*

I hereby declare that this thesis is entirely my own work, and has not been submitted in support of an application of another degree or qualification of this, or any other university, institute of learning, or industrial organisation.

V.R. Wickramasinghe

February 1997.

# *Abstract*

Subcarrier multiplexed (SCM) systems are an attractive alternative to the evolving digital technology for transmitting broadband services, at an affordable price. However, the majority of existing systems are based on analogue signal transmission and therefore, the strict noise and nonlinear requirements undermine the system performance. The work carried out in this thesis presents the feasibility of pulse time modulation (PTM), as a second stage modulator, in SCM systems.

PTM techniques offer simplicity and low cost, and with the additional bandwidth available on optical fibres can trade bandwidth to significantly higher signal-to-noise ratio (SNR) levels, compared to analogue systems. Three different PTM techniques, square wave frequency modulation (SWFM), pulse frequency modulation (PFM) and pulse position modulation (PPM) has been investigated. A prototype system capable of transmitting a video channel, two audio channels and a data channel is implemented for each technique in order to evaluate the performance potential of PTM as a second stage modulator in SCM systems.

The SNR expressions for all three schemes are derived from the first principles and the obtained results were verified experimentally. The optimum SNR performance is delivered by a raised cosine shaped pulse and the PPM technique delivers 5 dB SNR improvement over PFM. For SWFM systems a 3 dB SNR advantage is gained over single-edge detection technique and PFM systems by employing double-edge detection at the receiver.

PPM spectrum contains a clock component which could be employed at the receiver for signal recovery. Demodulation technique, based on clock recovery using a phase locked loop (PLL) is proposed and implemented. This technique is cost effective and less complex compared to the existing demodulation schemes.

The PFM implementation shows a 6 dB improvement in the receiver sensitivity compared to conventional SCM systems, while the PPM system offers an extra 2.5 dB improvement. The improved receiver sensitivity of the SCM-PTM technique, results in an increased optical power budget, where the transmission distance, number of subscribers and the number of channels in a network can be optimized. The nonlinear performance of the overall system is also shown to be within the specified performance levels.

# Contents

<i>Acknowledgements</i>	i
<i>Declaration</i>	ii
<i>Abstract</i>	iii
<i>Glossary of Abbreviations</i>	viii
<i>Glossary of Symbols</i>	xi

## 1 Introduction

1.1	Historical Background	1
1.2	Objective of the Research	4
1.3	Organisation of the thesis	8

## 2 Subcarrier Multiplexed Systems

2.1	Introduction	11
2.2	Motivation to use SCM	13
2.3	Evolution and Applications	15
2.4	Summary	22

## 3 Design Aspects of SCM Systems

3.1	Introduction	23
3.2	Transmitter	24
	3.2.1 Optical modulation index	27
	3.2.2 Laser intensity noise	29
	3.2.3 Intrinsic nonlinear distortion	30
	3.2.4 Clipping distortion	33
3.3	Optical Channel	35
	3.3.1 Attenuation	35
	3.3.2 Dispersion	36
3.4	Receiver	37
	3.4.1 Shot noise	38
	3.4.2 Thermal noise	39

3.5	CNR and System Penalties	40
	3.5.1 CNR expression	40
	3.5.2 System penalties	42
3.6	Summary	47

## **4 Second stage modulators and Pulse Time Modulation**

4.1	Introduction	49
4.2	Second Stage Modulators	50
	4.2.1 Digital modulator for video, voice and data transmission	51
	4.2.2 FM modulator in a micro-cell environment	55
	4.2.3 Pros and cons of implemented techniques	59
4.3	Pulse Time Modulation	61
	4.3.1 Classification of modulation techniques	62
	4.3.2 PTM techniques	63
	4.3.3 PTM spectrum	67
	4.3.4 Comparison of PTM techniques	69
4.4	SCM-PTM concept	73
4.5	Summary	74

## **5 PFM and SWFM systems**

5.1	Introduction	75
5.2	PFM and SWFM Modulation	76
5.3	PFM and SWFM Demodulation	78
5.4	Noise Analysis	85
	5.4.1 Jitter noise	87
	5.4.2 SNR expressions	90
	5.4.2.1 Raised cosine model	91
	5.4.2.2 Guassian / exponential model	92
	5.4.2.3 Trapezoidal model	93
	5.4.3 Performance comparison of the SNR expressions	96
	5.4.4 Threshold analysis	97
5.5	System Optimisation	100
	5.5.1 Nonlinear distortion	100
	5.5.2 Sampling ratio	102
	5.5.3 Transmission bandwidth	106
5.6	Summary	108

## 6 Pulse Position Modulation Systems

6.1	Introduction	109
6.2	PPM Modulation	110
6.3	PPM Demodulation	114
6.3.1	Spectral characteristics	114
6.3.2	The clock component	116
6.3.3	Phase locked loop	119
6.3.4	Alternative demodulation techniques	121
6.4	SNR Analysis	124
6.4.1	Noise analysis	124
6.4.2	SNR expressions	126
6.6	Summary	128

## 7 System Implementation

7.1	Introduction	129
7.2	SCM Signal	131
7.2.1	Video channel	131
7.2.2	Audio channel	134
7.2.3	Data channel	136
7.2.4	Frequency division multiplexer	139
7.3	SWFM and PFM Transmitters	141
7.3.1	The VCO and SWFM generation	143
7.3.2	Pulse generator	145
7.4	PPM Transmitter	147
7.4.1	Ramp generator	147
7.4.2	PPM modulator	149
7.5	Optical Link	152
7.5.1	Optical transmitter	152
7.5.2	Optical receiver	156
7.5.3	Optical power budget and rise time budget	157
7.6	SWFM and PFM Receiver	161
7.7	PPM Receiver	163
7.7.1	Phase locked loop	163
7.7.2	PWM generator	165
7.8	Demultiplexing and Signal Demodulation	168
7.8.1	Video signal recovery	168

	7.8.2	Audio signal recovery	169
	7.8.3	Data signal recovery	172
7.9		Summary	173
<b>8</b>		<b>Results and Analysis</b>	
	8.1	Verification of Spectral Predictions	175
	8.1.1	PFM and SWFM system	176
	8.1.2	PPM system	179
	8.2	SNR and BER Performance	183
	8.2.1	SNR measurement	183
	8.2.2	Performance analysis	189
	8.2.3	BER measurements	192
	8.3	Nonlinear Distortion Performance	195
	8.3.1	PTM sub-system linearity	195
	8.3.2	Overall system linearity	198
<b>9</b>		<b>Conclusions</b>	
	9.1	Conclusions	202
	9.2.	Contributions to Knowledge	206
		<b>References</b>	209
		<b>Appendix A : Analysis of the Laser Bias Circuit</b>	221
		<b>Appendix B : Prototype Schematic</b>	223

# *Glossary of Abbreviations*

<b>Abbreviation</b>	<b>Description</b>
A/D	analogue-to-digital converter
AM	amplitude modulation
AM-VSB	amplitude modulation-vestigial sideband
APD	avalanche photodiode
ATM	asynchronous transfer mode
BD	baseband distortion
B-ISDN	broadband integrated services digital network
BPSK	binary phase shift key
CATV	community antenna television
CDR	carrier-to-distortion ratio
CNR	carrier-to-noise ratio
CSO	composite second order
CTB	composite triple beat
D/A	digital-to-analogue converter
ECL	emitter coupled logic
EDFA	erbium doped fibre amplifier
ELED	edge-light emitting diode
FDM	frequency division multiplexed
FM	frequency modulation
FSK	frequency shift key
FWHM	full width half maximum
HD	harmonic distortion
HDTV	high definition television
IC	integrated circuit
IF	improvement factor
IM/DD	intensity modulation / direct detection
IMD	intermodulation distortion

IMP	intermodulation product
ISDN	integrated services digital network
ISI	inter symbol interference
JPEG	joint photographic experts group
LAN	local area network
LD	laser diode
LED	light emitting diode
MPEG	moving pictures expert group
Nd:YAG	Neodymium Yittrium Aluminium Garnet
NRZ	non return to zero
OMI	optical modulation index
ONU	optical network unit
PCM	pulse code modulation
PECL	pseudo emitter coupled logic
PFM	pulse frequency modulation
PIM	pulse interval modulation
PIWM	pulse interval width modulation
PLL	phase locked loop
POTS	plain old telephone services
PPM	pulse position modulation
PSK	phase shift key
PSM	pulse shape modulation
PSTN	public switched telephone network
PTM	pulse time modulation
PWM	pulse width modulation
RF	radio frequency
RIN	relative intensity noise
rms	root mean square
SCM	subcarrier multiplexed
SDH	synchronous digital hierarchy
SNR	signal-to-noise ratio
SWFM	square wave frequency modulation
TDM	time division multiplexed

TDMA	time division multiple access
TTL	transistor-transistor logic
VCO	voltage controlled oscillator
VPR-BH	vapour phase regrown buried heterostructure
WDM	wavelength division multiplexed

# *Glossary of Symbols*

<b>Symbol</b>	<b>Definition</b>
$A$	pulse amplitude
$A_c$	amplitude of the carrier signal
$B_r$	effective receiver noise bandwidth
$B_t$	transmission bandwidth
$c$	speed of light in vacuum
$CI_3R$	carrier-to-intermodulation ratio
$C_L$	total channel optical power loss
$CNR$	carrier-to-noise ratio
$D$	deviation ratio
$D_f$	fibre dispersion parameter
$d$	duty cycle
$D_3$	third order distortion co-efficient
$F(G)$	excess avalanche noise factor
$f_c$	carrier signal frequency
$f_g$	frequency guardband
$f_m$	modulating signal frequency
$F_n$	noise figure of the optical receiver
$G$	mean avalanche gain
$I_b$	laser bias current
$I_d$	dark current noise
$I_o$	average detected photocurrent
$I_{peak}$	peak signal current
$I_{th}$	laser threshold current
$J_k()$	Bessel function of the first kind, $k^{\text{th}}$ order
$K$	Boltzman constant
$k$	PPM modulation sensitivity

$k_o$	gain factor of the VCO
$k_d$	gain of the phase detector
$M$	PPM modulation index
$m_i$	OMI of the $i^{\text{th}}$ channel
$m_{lin}$	linear OMI
$m_{opt}$	optimum per channel OMI
$m_{rms}$	rms OMI
$M_s$	system margin
$n_1$	refractive index of the fibre core
$n_{i(rms)}$	rms impulse noise power
$n_{j(rms)}$	rms jitter noise power
$\overline{n_{RIN}^2(t)}$	rms intensity noise power
$\overline{n_s^2(t)}$	rms shot noise power
$\overline{n_t^2(t)}$	rms thermal noise power
$P_{av}$	average received optical power
$P_b$	laser bias optical power
$P_p$	peak received optical power
$P_r$	received optical power
$P_t$	transmitted optical power
$\dot{p}(t_s)$	pulse slope at time $t_s$
$q$	electron charge
$r$	transmission bandwidth to carrier frequency ratio
$R$	sampling ratio
$RIN$	relative intensity noise
$R_L$	front-end load resistance
$R_o$	optical receiver responsivity
$T$	pulse period
$T_{ab}$	absolute temperature
$\overline{T_i}$	average time interval of pulses due to impulse noise
$T_f$	optical fibre rise time
$T_r$	receiver rise time
$t_r$	rise time

$T_r$	transmitter rise time
$\overline{w^2}$	average width of pulses due to impulse noise
$x_i(t)$	signal current of the $i^{\text{th}}$ channel
$\alpha_{con}$	optical connector losses
$\alpha_f$	optical fibre attenuation
$\alpha_{splice}$	optical splice losses
$\beta$	PFM/SWFM modulation index
$\beta_{FM}$	FM modulation index
$\Delta f$	peak frequency deviation
$\Delta t$	peak pulse deviation
$\Delta\lambda$	FWHM spectral width of the optical source
$\overline{(\delta P)^2}$	mean square laser intensity fluctuations
$\sigma$	Gaussian FWHM
$\tau$	pulse width
$\omega_c$	angular carrier frequency
$\omega_m$	angular modulating frequency

# Introduction

## 1.1 Historical Background

The invention of the transistor and the integrated circuit (IC)s have revolutionised the electronics industry since the early 1960s. Even today, progress in the micro-electronics industry continues to be the driving force behind the information technology revolution that has emerged within the last decade. Since the early days of ICs, processing capability and the amount of semi-conductor memory on a chip has doubled approximately every 19 months. The increased processing powers and larger memories of computers have been complemented by the continuous ability of the software industry to release more comprehensive and user friendly products to the market [1].

The advances made in computer technology have made it possible to gather mass amounts of data, text, still images, moving images, sound *etc.* and as a result has seen the emergence of multi-media systems [2-3]. With the increased amount of information at

our disposal, the need for sharing this information has greatly increased. Hence, within the last decade the communications industry has experienced a remarkable growth in network traffic.

In the 1980s the capacity of existing transmission channels had reached their limit. A good portion of the radio spectrum had already been allocated to various governmental and commercial organisations and the coaxial cable networks were carrying traffic at a maximum capacity. Therefore, the emergence of optical fibres as a practical transmission medium was critical.

Optical fibres possess two unique characteristics compared to existing transmission channels: one is the enormous transmission channel bandwidth and the other is the extremely low loss of the optical fibres. In communication systems, a rule of thumb is to assume the transmission capacity is approximately 10% of the carrier signal. Since the optical frequencies extend well into the THz region, the transmission capacity of optical fibre communication systems is a few orders of magnitude greater than the existing transmission channels. Therefore, optical fibres provided a means of carrying the ever increasing volume of network traffic and opened up the possibility of providing broadband services.

Today, optical fibre cables with attenuations as low as 0.2 dB/km are available and allow for a greater distance between repeater stations. The emergence of erbium doped fibre amplifier and soliton transmission has helped to increase the transmission distances of optical communication, even further [4]. In addition, optical communication systems are

free from electromagnetic interference and are more secure and reliable compared to conventional transmission mediums [5].

As the demand for broadband services increases, the telecommunication and cable television providers are looking at various options for delivering new services to the home and business environments. The narrowband Integrated Services Digital Network (ISDN) already provides data services in addition to the plain old telephone services (POTS). Although initially restricted to the business environment, home users are increasingly finding ISDN services to be attractive as the prices become affordable [6].

However, the narrowband ISDN network is only capable of providing bandwidth limited applications and in order to deliver high bandwidth services such as real-time video, images, animation, graphics *etc.* a broadband network is required. To upgrade the existing public switched telephone network (PSTN) into a fully integrated broadband network massive infrastructure investments are required. Network operators, service providers and electronic consumer companies are forging new partnerships to stay ahead of competitors in order to grab a slice of the future broadband market.

The ultimate broadband network will be implemented in digital technology incorporating asynchronous transfer mode (ATM) [7] and synchronous digital hierarchy (SDH) [8]. The emerging compression techniques such as moving pictures experts group (MPEG) [9] will also be critical to the delivery of broadband digital information. However, the digital technology is still evolving and the high cost of digital equipment prohibit their wide spread deployment at present.

Meanwhile in the interim, subcarrier multiplexed (SCM) systems offer an attractive alternative for transmitting broadband services at an affordable price. SCM systems offer simplicity and low cost and has the ability to access the high bandwidth available on optical fibres to deliver broadband applications.

The SCM concept was first used in microwave communication systems where a number of subcarriers were used to transmit baseband channels over a wireless or coaxial link. With the advent of optical fibres in the 1980s, SCM concept was implemented in optical communication systems. The mature GHz technology gave access to the high channel bandwidth of optical fibres and also resulted in the cost effectiveness of SCM systems [10].

Initially they replaced the existing coaxial and microwave long-haul links, but later they were extended into point to multi-point applications. Currently SCM is being used in local area network (LAN) applications and in the cable television industry to deliver analogue video channels[11].

## **1.2 Objective of the Research**

The majority of existing SCM systems are based on analogue signal transmission. For all its positive attributes, the low cost of SCM networks is realised by compromising the level of performance. Analogue modulation techniques, such as frequency modulation (FM) and amplitude modulation (AM), employed in SCM are simple and bandwidth efficient and modulate the optical source in a continuous manner. However, due to the analogue nature of the signal, the noise and nonlinearity requirements imposed upon the

system are very stringent. The main noise and nonlinearity contributors in a SCM system are the optical source and the optical receiver. The drawback of stringent noise and nonlinear requirements, from a network design standpoint, is the constraints imposed upon the optical power budget of the system. The limited input dynamic range of the optical source undermine the number of transmission channels, while the restricted power budget results in reduced transmission distance and number of subscribers.

In order to improve the performance of analogue optical link, work has been carried out on linearisation of optical sources, reduction of laser intensity noise, optimisation of optical receivers *etc.* An alternative approach to enhance the performance of a SCM system is to introduce a second stage modulator to improve the input dynamic range and the receiver sensitivity. The second stage modulation systems differ from the conventional SCM systems as the SCM signal is modulated onto a secondary RF/microwave carrier prior to optical modulation. The choice of a second stage modulator is determined by its suitability for optical modulation and transmission, bandwidth efficiency, overall cost and the required level of performance of the signal channels. At the receiver, the optical signal is converted to an electrical signal and fed to the corresponding demodulator in order to recover the original SCM signal. Information is recovered from the SCM signal by employing standard signal recovery techniques used in SCM systems.

Several second stage modulation techniques have been published by leading research centres world-wide, since the early 1990s. **Grace** at *United Telecommunications Inc.*, Kansas, USA [12] has developed a prototype system employing a high speed analogue-to-digital (A/D) converter to digitise the analogue SCM signal for optical transmission.

**Ohmoto** [13] and **Sato** [14] from *Nippon Telegraph & Telecommunication Inc.*, Japan have used FM for transmission of SCM signals to take advantage of wideband FM gain.

Modulation techniques employed in communication systems can be broadly categorised into three groups: analogue, digital and pulse modulation. Analogue modulation is simple and cost effective, but is vulnerable to various noise sources and often fails to deliver the required signal-to-noise ratio (SNR)s over moderate distances in optical fibre communication systems. The nonlinearity of the optical source and optical channel can also severely limit the quality of the received signal through intermodulation.

In contrast, digital modulation has proved to be substantially immune to channel noise and nonlinearities and is capable of producing high SNRs at the receiver. However, digital systems are more complex, largely due to their coding circuitry, and are significantly higher in cost compared to analogue systems. They also carry an intrinsically large bandwidth overhead, restricting the transmission capacity.

Pulse modulation occupies an intermediate position between analogue and digital modulation techniques. In the most widely used pulse modulation scheme, referred to as pulse time modulation (PTM), some time property of a constant amplitude pulse train is modulated in sympathy with the information. The PTM concept was conceived around 50 years ago [15], but applications have been limited until its re-emergence as a preferred modulation format for optical fibre communication systems.

The primary advantage of PTM is its ability to trade cost against system performance. The technique is simple and inexpensive, requiring no complex digital coding and the

pulse format of the carrier improves the noise immunity and nonlinear tolerance. The ability to trade SNR performance against transmission bandwidth is an extremely important property of any modulation technique. With the additional bandwidth available on optical fibres, PTM is an ideal signal carrier which can trade bandwidth to increase the SNR to significantly higher levels compared to analogue systems, and at a relatively low cost compared to digital systems. In addition, PTM traffic can be routed through logic circuits and the majority of PTM schemes do not require complex synchronisation mechanisms at the receiver, reducing cost and complexity. Also narrow pulse PTM formats can operate the optical source at low duty ratios to help maximise the device life time and peak power level [16].

It was mentioned earlier that signal performance, bandwidth efficiency and overall cost are key factors in determining the feasibility of a modulation scheme as a SCM second stage modulator. From the above discussion, PTM proves to be a viable option due to its high performance, low cost, simplicity and suitability for optical transmission.

There are a number of PTM techniques such as pulse position modulation (PPM), pulse frequency modulation (PFM), pulse interval modulation (PIM) *etc.* which have been used in various applications. They range from video distribution, inter-satellite communication to power applications [16].

However, in terms of transmission capacity, applications employing PTM could be restricted due to the limited number of PTM channels that can be multiplexed onto a single transmission channel. Most PTM techniques possess variable time frames, proportional to the information, making multiplexing in the time domain virtually

impossible. Frequency division multiplexing is a possibility, but due to the larger frequency presence of PTM signals (in comparison to analogue modulation schemes), is inefficient.

An alternative multiplexing approach called compound PTM (CPTM), which combines various PTM formats together with a self synchronising mechanism, has also been reported [17]. There are several types of CPTM techniques such as compound pulse frequency and width modulation (CPFWM), compound pulse position and width modulation (CPPWM) and compound pulse interval and width modulation (CPIWM). However, the maximum number of channels that can be accommodated in most compound techniques is two, at a cost of considerable increase in system complexity. Therefore, due to limited multiplexing capability, PTM has been employed mainly in single channel applications.

The objectives of the research can be broadly stated as twofold. Primarily, it is to demonstrate the viability of PTM as a second stage modulator and to evaluate its performance against conventional SCM systems. Secondly, as explained above, PTM systems hitherto has been used mostly in single channel applications. Therefore, the research should investigate the potential of the proposed technique for multi-channel, broadband signal transmission, for PTM formats.

### **1.3 Organisation of the Thesis**

In section 1.1 a brief historical background into SCM systems was presented. Chapter 2 gives a detail account of the concept of SCM, with respect to optical communication

systems, its advantages compared to evolving digital technology, evolution and applications.

The design aspects of SCM systems are considered in Chapter 3. The SCM system is divided into three distinct sections: transmitter, optical channel and receiver. In each section key system parameters, noise and nonlinear sources are presented. For both the transmitter and the receiver, performance critical optical stage is considered in detail. In section 3.5, by combining parameters introduced in the previous sections, an expression for the carrier-to-noise ratio (CNR) of an individual subcarrier channel is derived. The chapter concludes with a discussion on optimisation of system parameters and the penalties of conventional SCM systems.

The concept of second stage modulation is introduced at the beginning of Chapter 4. Several second stage modulation systems and their performance are also considered. A detailed description of PTM techniques is given in section 4.3, including their classification, spectral characteristics and comparison of different PTM schemes in terms of performance, cost and complexity. Section 4.4 introduces the concept of PTM, as a second stage modulator in a SCM system, and the possible techniques which can be incorporated.

Chapter 5 presents two popular PTM techniques: PFM and square wave frequency modulation (SWFM). They are considered in one chapter as their characteristics are closely related. Initial sections are an introduction to modulation and demodulation of each technique. The SNR analysis is carried out in section 5.4, culminating in the

derivation of SNR expressions. Optimisation of PFM and SWFM system parameters are dealt with in section 5.5.

Chapter 6 deals exclusively with PPM systems. Section 6.2 details the characteristics and generation of PPM signals. The PPM demodulation is dealt with in detail in the following section, including a spectral investigation, the behaviour of the PPM clock component and the possibility of employing a phase locked loop (PLL) to recover information. The SNR derivations, using different pulse models, is carried out in section 6.4.

Details of the prototype implementation are listed in Chapter 7. The nature of the subcarrier channels, and their modulation and demodulation formats are presented. Various aspects of system and circuit design for each of the implemented PTM techniques are also presented in detail. The design of the optical link and the associated optical system parameters are presented in section 7.5. The bandpass filtering and the appropriate demodulation techniques employed to recover each signal channel are presented in the final section.

The results and analysis of the PTM signal spectra, SNR and bit error rate (BER) performance and the nonlinear distortion performance are given in Chapter 8.

The concluding remarks and the contributions made to knowledge are presented in Chapter 9.

# Subcarrier Multiplexed Systems

## 2.1 Introduction

Subcarrier multiplexed (SCM) systems were originally used in microwave communication systems, where a number of baseband channels are frequency shifted using subcarriers at different frequencies and the frequency division multiplexed (FDM) signal is transmitted over free space [10]. With the emergence of low loss optical fibres in the 1980s, optical communication began to revolutionise the communication industry and became the preferred medium for high capacity, long distance transmission applications. The SCM concept was incorporated into optical communication systems, because of the ability of the microwave technology to utilise the large channel bandwidth available on optical fibres. In optical SCM systems the FDM signal is modulated on to an optical carrier, which is the primary information carrier. From here on in the text, the SCM systems referred to are optical SCM systems, unless otherwise specified.

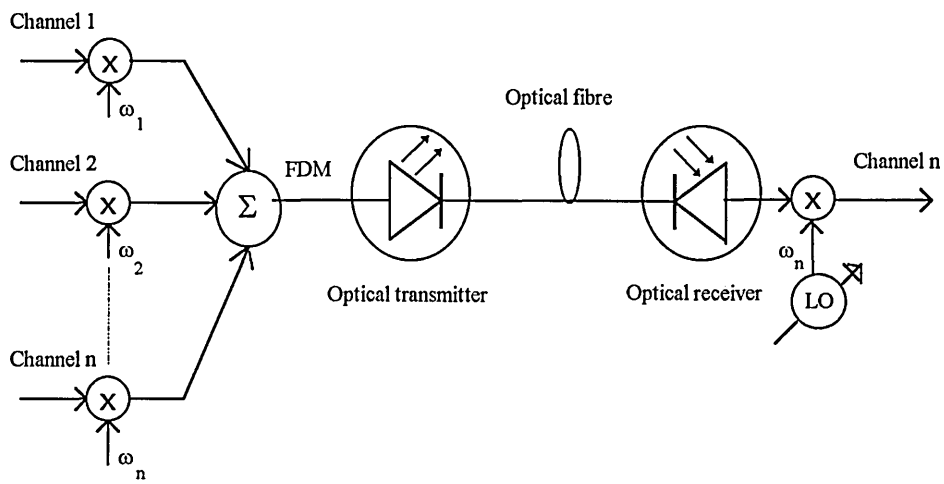


Figure 2.1 A typical SCM system employing a heterodyne receiver.

A typical SCM system employing a heterodyne receiver is shown in Fig. 2.1. Radio frequency (RF) or microwave frequency signals at different frequencies ( $\omega_n$ ) are modulated by analogue or digital baseband signals. The up converted signals are then FDM and the composite signal is used to modulate an optical carrier [18]. The RF or microwave carriers are secondary carriers as opposed to the primary optical carrier and therefore, known as “subcarriers”.

The optical modulation can be either direct or external modulation. In direct modulation, the light source is directly driven by the electrical signal and information is conveyed by the optical intensity (intensity modulation). At the receiver, simple direct detection technique, employing photodiodes is used to recover the electrical signal. This is known as intensity modulation/direct detection (IM/DD) and is widely used because of its simplicity and low cost [5].

External modulation is achieved by applying the optical carrier and the modulating signal to an external modulator and demodulation is carried out by employing coherent optical

detectors at the receiver. External optical modulation belong to the fourth generation optical systems and is still evolving. Although it has advantages over direct modulation, the high cost associated with it prohibit their large scale deployment at present [19-20].

At the receiving end, once the optical signal is converted into the electrical domain the baseband channels can be recovered by employing a heterodyne receiver or bandpass filtering. In heterodyne receivers the local oscillator locks onto the incoming subcarrier of the desired channel and demodulation follows. In bandpass filtering, the desired channel is filtered from the composite signal and appropriate demodulators are used to recover the baseband information.

## **2.2 Motivation to use SCM**

Although SCM is an analogue transmission technique it has a number of advantages over digital multiplexing. Most of these advantages are due to the fact that SCM employs a technology which has matured, compared to the evolving digital technology.

The microwave techniques employed in SCM systems have been around for a number of years. Therefore they have been studied extensively and are optimised for different system applications [21]. Currently available lasers, when operated as intensity modulators can offer modulation bandwidths upto 20 GHz [11]. This far exceeds the speed of modern baseband digital circuitry. Such high bandwidths can only be accessed by employing microwave technology which extend well into the GHz range. Most critically, microwave techniques are cost effective compared to the evolving digital technology and therefore SCM offers system economy [18].

Time division multiplexed (TDM) systems can only transmit digital information. In contrast, SCM systems have the ability to transmit analogue as well as digital channels simultaneously. Baseband digital channels can be frequency shifted using appropriate modulation techniques such as frequency shift keying (FSK), phase shift keying (PSK) etc. and multiplex along with the frequency shifted analogue channels. At the receiver, the information can be recovered by employing a suitable demodulator. This transparency of SCM to digital and analogue traffic has been particularly attractive in the emerging broadband application networks.

In applications where the receiver only needs to access part of the overall bandwidth, SCM employs narrow band receivers with resulting improvements in noise performance. This contrasts with wideband TDM systems where the entire multiplexed bandwidth is usually required at the receiver [22].

In digital networks, sophisticated signalling mechanisms, frame and bit synchronisation, line codes *etc.* increase system complexity and cost. Comparable SCM networks are simpler and offers flexibility and upgradability. Additional service channels can be introduced into the system by simply adding new subcarriers without altering the performance of other channels. Therefore, SCM networks can offer a graceful evolution to future high bandwidth applications such as digital television, high definition television (HDTV), image and graphic applications [18].

The primary disadvantage of SCM systems is that they are less tolerant to noise and non linearities, compared to digital systems, due to the analogue nature of the signal . Also they are required to operate at high frequencies (GHz range) to access the large

bandwidth available on optical fibres, making lower end of the modulation bandwidth redundant. To transmit digital information using the SCM technique, more bandwidth per channel is required compared to TDM systems since baseband digital information has to be modulated on to a carrier [11].

## **2.3 Evolution and Applications**

SCM systems have evolved with optical communication, which was first employed as a commercial transmission medium in early 1980s. In its initial stages they replaced point-to-point transmission links [22], employed in long distance communication. The superior performance of optical links were preferred to the existing coaxial and microwave links, whose transmission capacities were reaching their limits. Pioneering the move towards embracing SCM technology were telephony companies, and SCM was used in the trunk lines of the public telephony network [23].

As the source power and linearity improved the point-to-point systems evolved into point-to-multi-point systems. In multiple access networks employing time division multiple access (TDMA) technology, the bit rate that each user must handle grows linearly as the number of users increase. Hence the cost and complexity of each receiver is a problem in large networks [22]. Since SCM enables the bandwidth per node to remain constant as the number of nodes increase, it has found applications in local area network (LAN)s [24-25], multi-channel video distribution networks and bi-directional broadband networks [26-27].

Two techniques have been widely deployed in LANs using SCM. In the first technique, subcarriers are not part of the access method, but are simply carriers for conventional multiple access procedure. Standard LAN traffic is used as a data source and modulated on to a carrier to be transmitted along other services in a multi service environment [11].

The second technique is to use subcarrier frequencies for addressing in order to implement a multiple access procedure [25]. In these type of networks each node transmits on a given frequency and the receivers wishing to tune in select the appropriate subcarrier frequency. Figure 2.2 illustrates a  $N \times N$  star coupler interconnecting  $N$  users. The user "J" transmits on a given frequency and the receiver can tune into any of the 1- $N$  users. The speed at which the receiver can tune to any given subcarrier is very important, since it directly effect the access delay time of the implemented access procedure.

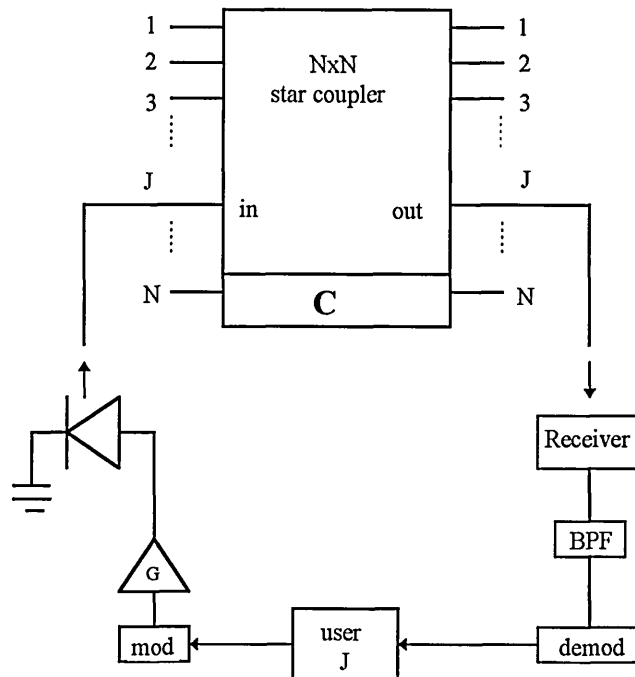


Figure 2.2 Interactive LAN using SCM to interconnect  $N$  users [25].

Alternatively the receivers can be allocated a unique carrier frequency with transmitters capable of transmitting at any of the receiver frequencies. In such a system the access delay depends on the speed of tuning of the subcarriers of the transmitter [11].

One of the most important applications of SCM is the distribution of community antenna television (CATV) channels. In the mid 1980s the feasibility of SCM for multi-channel video distribution was evaluated [28-29] and in early 1990s SCM was adopted as the industry standard to deliver analogue video channels [10, 30, 31]. Amplitude modulation-vestigial sideband (AM-VSB) is used as the modulation format as it is compatible with the current television receivers, but frequency modulation (FM) is also employed, especially in super trunking applications.

SCM-CATV networks offer increased reliability, repeater distance and power budgets, compared to the former coaxial networks. Additionally both CATV and telephone industries seek to extend fibre closer to the home and SCM optical networks are a platform to deliver future broadband services [22].

One of the drawbacks of the present network is the high signal to noise ratio (SNR)s required by AM-VSB channels, which can limit the number of channels and subscribers. *NTT Transmission Systems Laboratories*, Kanagawa, Japan, has developed a fully engineered multi-channel FM-SCM video distribution system (see Fig. 2.3) using FM [31]. The system performance is enhanced, due to FM modulation and upto 50 video channels can be distributed to more than 10,000 customers through three cascaded erbium doped fibre amplifiers. Several tests have also been carried out on the feasibility of SCM to deliver compressed and uncompressed video channels and future networks

may use more complex modulation methods such as multilevel quadrature amplitude modulation [32].

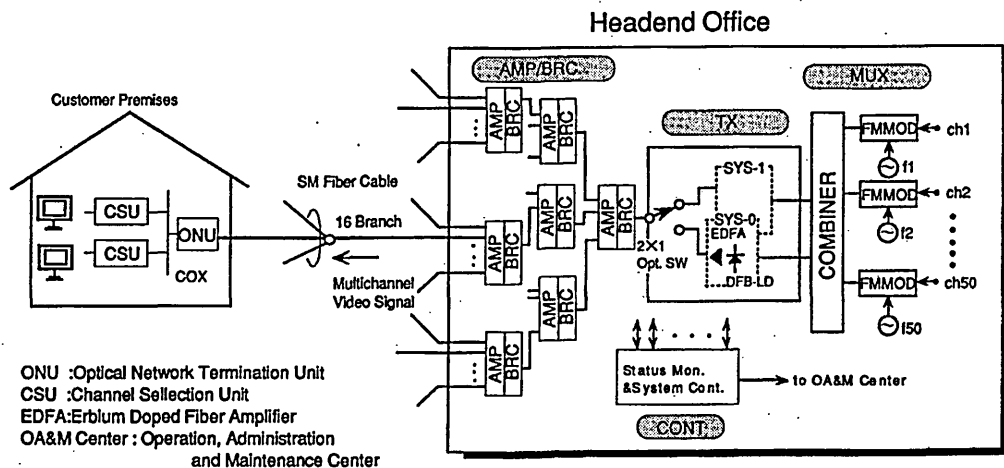


Figure 2.3 System configuration of FM multi-channel video distribution system [31].

As the demand for broadband services grew in the late 1980s, SCM was one of the first techniques to be investigated to evaluate the possibility of broadband services delivery to home and business users. The attraction of SCM in a broadband environment was due to its low cost, high bandwidth, flexibility and upgradability.

The first field test experiment using optical fibres for the distribution of broadband services was implemented by *GTE laboratories* in 1989 [33], employing binary phase shift keying (BPSK) subcarriers. The system consists of 20 digitised video channels (16 broadcast, 4 switched) and one 4 Mbit/s data channel for downstream operation and a video and data channel for upstream operation. Services are distributed to 5 homes and the system is run for a trial period of 5 years to determine the public response to broadband services. A simplified block diagram of the central office downstream transmitter is illustrated in Fig. 2.4.

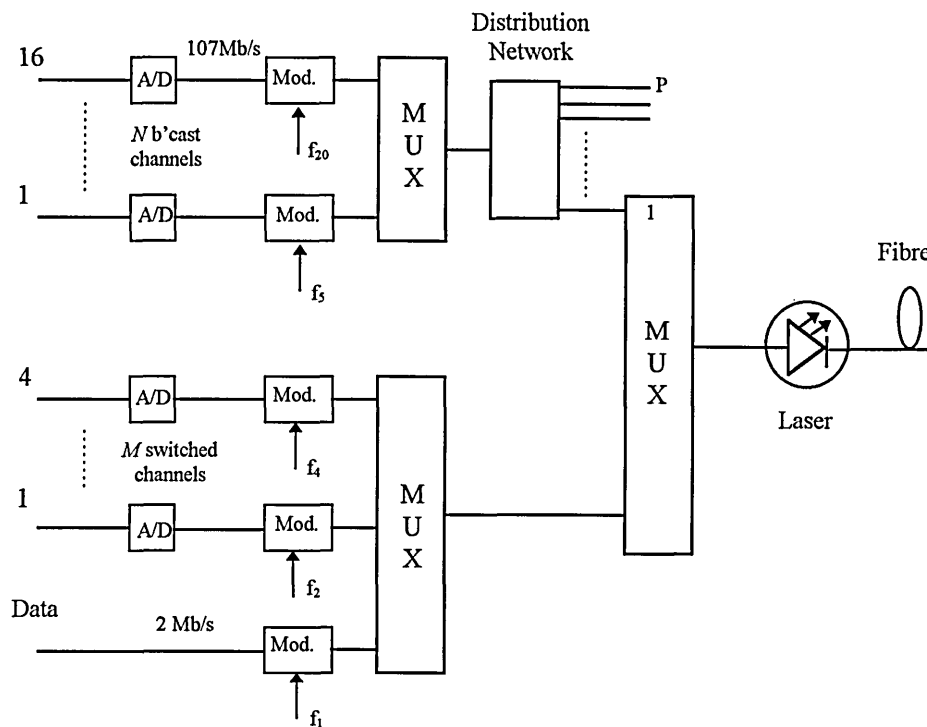


Figure 2.4 Simplified block diagram of the central office transmitter in BPSK subcarrier system [33].

**Olshansky** has also demonstrated a bi-directional hybrid fibre-coax network employing SCM [34]. Downstream traffic consists of 64 FM video channels and 32 data channels, each at a data rate of 1.5 Mbit/s. Thirty two customers are served from four optical network unit (ONU)s, each serving 8 subscribers via coaxial drops. Each subscriber is allocated a 1.5 Mbit/s upstream baseband digital channel which is modulated at the ONU and transmitted upstream to the central office. The topology of the distribution network is shown in Fig. 2.5.

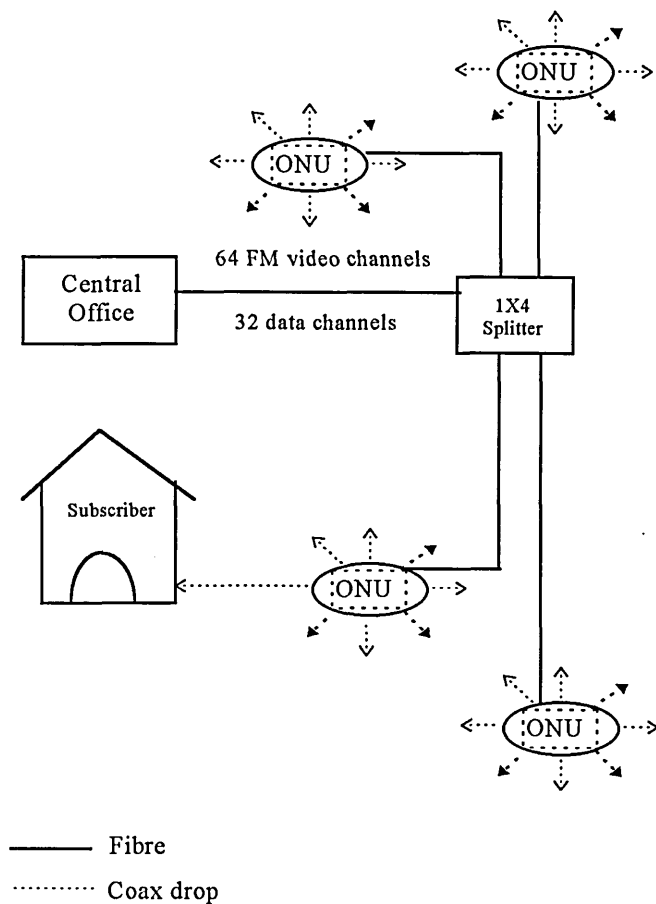
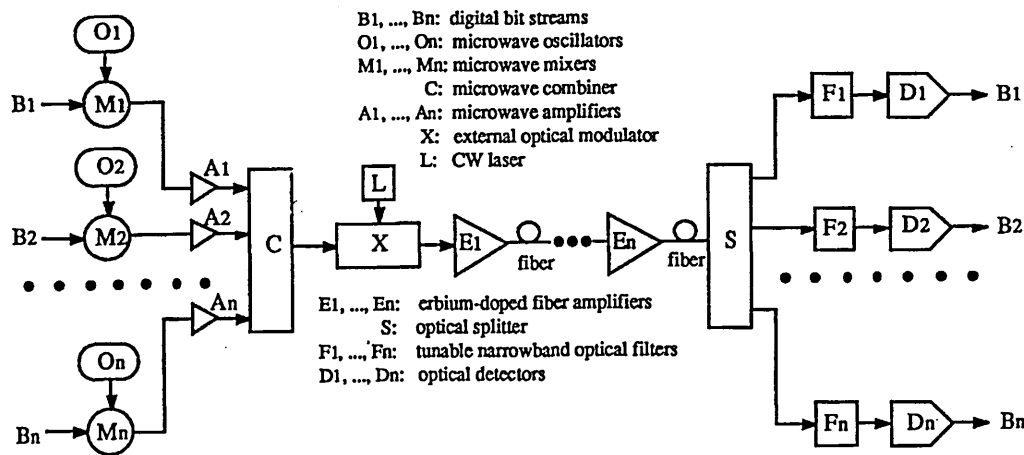


Figure 2.5 Bi-directional hybrid fibre coax network to deliver data and video services to 32 customers employing SCM technology [34].

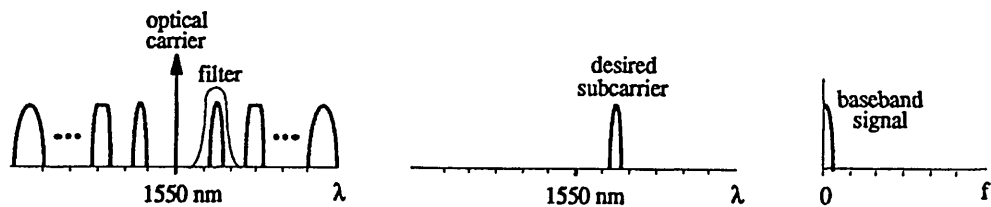
An all fibre multi-service network using TDM and SCM techniques is also being field tested by *British Telecom* in the UK to gain experience with fibre operation in the local network [35]. The network is named broadband integrated distributed star (BIDS) and integrates together the concepts of a switched CATV network and a remote telecom multiplexer to provide telephony, video and digitised radio services.

More recently, the *Lawrence Livermore National Laboratory* in California, USA [36] has demonstrated the potential of SCM to transmit multiple, gigabit data channels over

hundreds of kilometres of conventional optical fibre cables. High bit rate data channels are modulated onto microwave subcarriers and the SCM signal is fed to an external optical modulator. At the receiver end the desired subcarrier channel is optically pre-selected using a narrowband optical filter and an optical detector is employed to recover the electrical data stream. Figure 2.6 shows the conceptual block diagram and the frequency spectrum at different stages of signal demodulation.



(a) conceptual block diagram



(b) frequency spectrums at the receiver

Figure 2.6 A SCM system to transmit multiple, gigabit data channels [36].

The primary limitation in baseband digital transmission of multi-gigabit data is, optical fibre dispersion. In the above technique, the dispersion limitations are overcome by carrying the baseband data on a subcarrier frequency and employing optical pre-filtering

and optical detection at the receiver to recover the original bit stream. A prototype system employing two 2.5 Gbit/s data channels and a transmission distance of 300 km has been demonstrated.

Although the thrust is towards a broadband digital network (B-ISDN), experts predict the initial delivery of multimedia services will employ analogue techniques and SCM is expected to play major role [37].

## **2.4 Summary**

In this chapter the basic concept of SCM with reference to optical fibre communication systems was introduced. The advantages of SCM systems, their evolution and applications were also discussed.

The primary advantage of SCM systems, compared to alternative TDM systems, is its low cost. The microwave technology employed in SCM systems is simple and inexpensive, and can access the large bandwidth available on optical fibres. The compatibility of SCM with the existing RF and microwave systems makes it useful in many applications from CATV to LANs. The flexibility of SCM networks provide a platform to deliver the emerging broadband services, at a lower investment cost compared to the evolving digital technology.

---

# Design Aspects of SCM Systems

## 3.1 Introduction

In order to implement SCM systems, an understanding of the fundamental system parameters is required. In this chapter the parameters which affect the performance of SCM systems and their limitations are presented. Noise and distortion are the major design considerations of analogue systems and therefore, are discussed in detail.

The overall system has been divided into three distinct parts as shown in Fig. 3.1. Section 3.2 presents some key parameters associated with the transmitter, and its noise and distortion contributions. The attenuation and dispersion of the optical channel and the noise introduced by the receiver are discussed in sections 3.3 and 3.4, respectively. The carrier-to-noise ratio and the penalties associated with SCM systems are discussed in section 3.5.

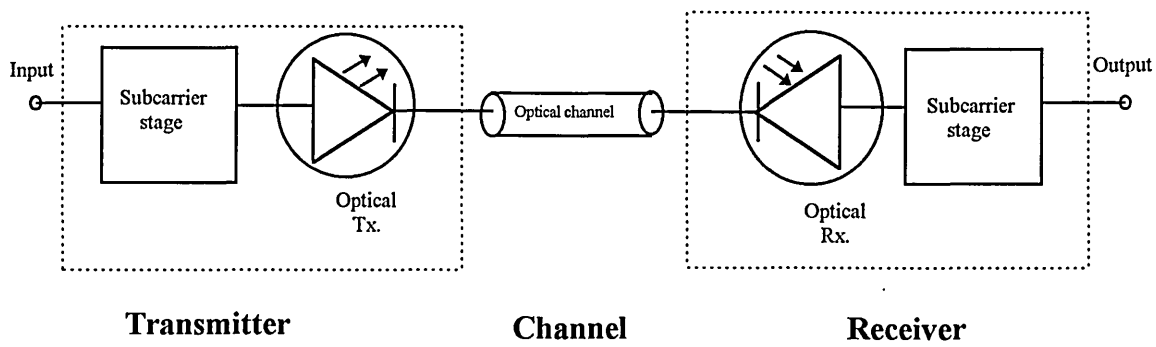


Figure 3.1 SCM system considered in three sections: transmitter, channel and receiver.

### 3.2 Transmitter

The SCM transmitter consists of two stages. The primary stage implements the subcarrier frequency generation, modulation and multiplexing to form the SCM signal from the baseband channels. The secondary stage consists of an optical transmitter, which converts the SCM signal into the optical domain for transmission via the optical channel. The type of optical source can determine the transmission distance, number of channels, noise and nonlinear contributions and therefore, is a major design consideration. Since the primary stage employs standard RF and microwave techniques, it is not discussed here.

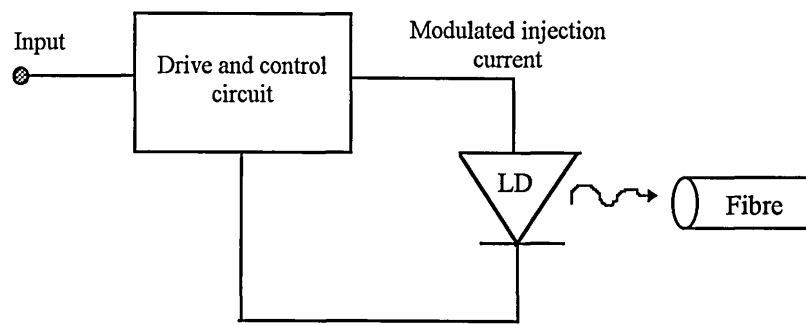
The optical transmitter can either be a direct optical modulator or an external optical modulator (Fig. 3.2). In direct modulation the composite signal is used to modulate the injection current of a laser diode which in turn modulates the intensity and the frequency of the optical carrier [38]. Normally, the receivers respond to the intensity variations of the optical carrier and such systems are known as intensity modulation direct detection

(IM/DD) systems. The receivers which respond to the phase variations of the optical carrier are known as coherent systems.

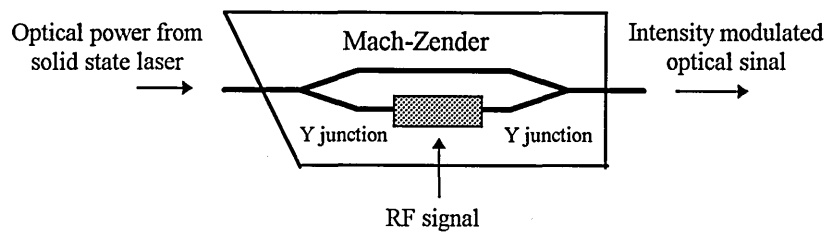
External optical modulators are employed in both intensity modulation (IM) systems as well as coherent systems. In IM systems, a continuous wave laser source and the modulating signal are fed to an external device such as a Mach-Zender or a Y fed directional coupler which acts as the external modulator (see Fig. 3.2(b)) [39]. Solid state laser sources such as Neodymium-Yttrium Aluminium Garnet (Nd:YAG), employed in external modulators, offer extremely high optical power levels. However, the main drawback of external modulators is the nonlinearity of the optical output power and the voltage transfer characteristic of the interferometric device.

In coherent systems, a narrow line-width, continuous wave semiconductor laser and the electrical signal are fed to an external modulator. The external modulator is usually a waveguide device fabricated from a group III-V semiconductor compound, and provide amplitude, frequency or phase modulation of the optical carrier [39].

The majority of SCM systems proposed to date employ IM/DD due to its low cost and simplicity. Coherent optical techniques can be applied in SCM systems [19, 40] providing increased receiver sensitivity, link lengths and a large number of users through dense wavelength division multiplexing (WDM). Against these advantages must be weighed the complexity and cost inherent in coherent systems. It is therefore, only in specific situations where the overall advantages justify the cost, that coherent techniques are employed. Therefore, an IM/DD system has been assumed throughout the analysis.



(a) direct optical modulation



(b) external optical modulation

Figure 3.2 Direct and external optical modulation.

In the following subsections, parameters of the transmitter which influence the system performance are considered. Section 3.2.1 deals with the optical modulation index (OMI), which represent the depth of modulation of the optical source. OMI can determine the transmission capacity and the signal quality of individual channels, and is a key system parameter. The main noise source at the transmitter is laser intensity noise and is considered in section 3.2.2. Nonlinear distortion can be introduced during electro-optic conversion if the laser is driven beyond its linear region. Intrinsic and clipping distortion of the laser are considered in sections 3.2.3 and 3.2.4 respectively.

### 3.2.1 Optical modulation index

The input current  $i(t)$ , for a  $N$  channel SCM signal can be represented as:

$$i(t) = \sum_{i=1}^N x_i(t) \quad (3.1)$$

where  $x_i(t)$  is the signal current of the  $i^{\text{th}}$  channel. The transmitted optical power output  $P(t)$  is given by [41, 42] :

$$P(t) = P_b \left[ 1 + \sum_{i=1}^N m_i x_i(t) \right] \quad (3.2)$$

where  $P_b$  is the biased optical power and  $m_i$  is the optical modulation index (OMI) of the  $i^{\text{th}}$  channel. OMI is an important system parameter, which represents the depth of modulation of the optical source, and for a single subcarrier channel, the OMI is expressed as [42] :

$$m_i = \frac{I_{peak}}{I_b - I_{th}} \quad (3.3a)$$

where  $I_{peak}$  is the peak current of the  $i^{\text{th}}$  signal channel,  $I_b$  is the laser bias current and  $I_{th}$  is the laser threshold current. Alternatively, the OMI can be expressed in terms of optical power as shown in Eqn. (3.3b) [42]

$$m_i = \frac{P_{peak} - P_b}{P_b} \quad (3.3b)$$

where  $P_{peak}$  is the peak optical power of the  $i^{\text{th}}$  channel (see Fig. 3.3)

Equations (3.3a) and (3.3b) are still valid for the overall OMI of the system provided that  $I_{peak}$  and  $P_{peak}$  are values of the composite signal. But in general the overall OMI is defined as either a linear or a rms quantity, depending on the number of channels. When the number of channels are less than 10, signals add coherently and a linear OMI is applicable [42].

$$m_{lin} = \sum_{i=1}^N m_i \quad (3.4a)$$

As the number of channels increase, the probability of all channels attaining a peak value simultaneously, decreases. Since signals add incoherently it is more appropriate to define a rms OMI [43]

$$m_{rms} = \left[ \sum_{i=1}^N m_i^2 \right]^{1/2} \quad (3.4b)$$

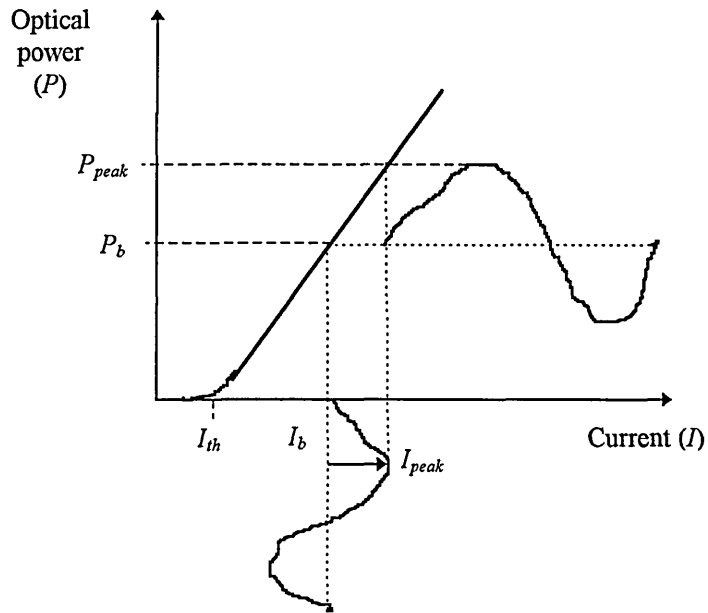


Figure 3.3 The laser  $P$ - $I$  characteristic for a modulating current of peak value,  $I_{peak}$ .

### 3.2.2 Laser intensity noise

The intensity of a semi-conductor laser fluctuates even when the bias current of the laser is constant with negligible fluctuations. These power fluctuations results in intensity noise, which is converted into current fluctuations at the optical receiver resulting in signal-to-noise ratio (SNR) degradation [18]. Since analogue systems operate at high optical power levels, the optical receiver is particularly sensitive to intensity variations of the transmitter and intensity noise is a critical parameter in SCM systems [38].

Intensity noise is expressed as a normalised quantity: relative intensity noise (RIN) [21]

$$RIN = \frac{\overline{(\delta P)^2}}{P^2} \quad (3.5)$$

where  $\overline{(\delta P)^2}$  is the mean square intensity fluctuations and  $P$  is the average intensity of laser light. The RIN value is sensitive to the laser bias level and is inversely proportional, according to Sato [44]. Figure 3.4 shows the variation of RIN for a vapour phase regrown buried heterostructure (VPR-BH) laser, at different bias levels, confirming the inverse relationship. The peaks in the graph correspond to the laser relaxation oscillation frequency.

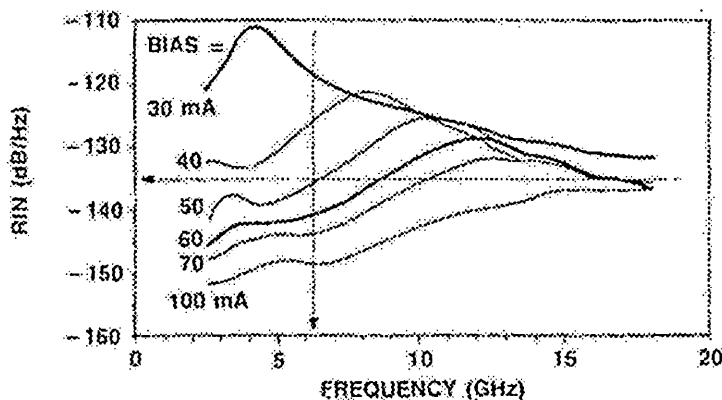


Figure 3.4 Laser RIN variation against modulating frequency [21].

Modern lasers exhibit low intrinsic RIN values, typically in the region -130 to -160 dB/Hz. However, optical reflections due to fibre discontinuities increase the overall intensity noise figure by around 10-20 dB. Optical isolators or low feedback connectors should be employed in single mode laser operation to reduce the effect of external reflections on intensity variations.

The rms noise power due to intensity noise is given by [21]:

$$\overline{n^2_{RIN}(t)} = RIN I_o^2 B_r \quad (3.6)$$

where  $I_o$  is the average detected photocurrent and  $B_r$  is the effective receiver noise bandwidth.

### 3.2.3 Intrinsic nonlinear distortion

Since SCM systems impose strict linearity requirements, nonlinearity is a critical design parameter. Nonlinear distortion can either be harmonic distortion (HD), distortion due to single tones, or inter modulation distortion (IMD), distortion in the presence of multiple tones. In SCM systems signal channels are summed in the frequency domain and the dominant form of non-linear distortion is IMD. The frequencies arising due to IMD are called intermodulation product (IMP)s and they originate from two distinct nonlinear effects: intrinsic nonlinearity and clipping. Intrinsic nonlinearity is considered in this section while clipping distortion is considered in the following. Since IMD is dominant in the presence of HD, only the former is considered further.

Figure 3.5 shows the laser clipping resulting in zero optical power when the drive current falls below the threshold, and the saturation due to operation beyond the linear region.

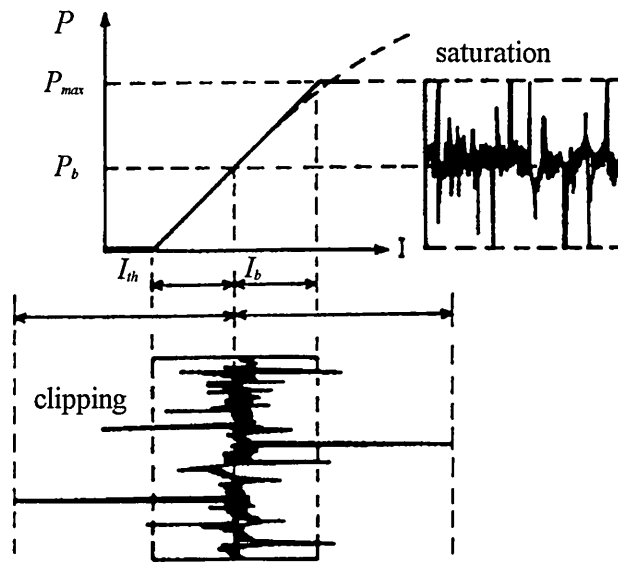


Figure 3.5 Intrinsic and clipping distortion of lasers.

The  $P$ - $I$  characteristic of a laser operating above the threshold can be represented by a polynomial of the following form [45]:

$$P = a_0 + a_1 I + a_2 I^2 + a_3 I^3 + \dots \quad (3.7)$$

The second and third order terms of the polynomial are significant and give rise to second and third order nonlinear distortion. This is called intrinsic nonlinearity and originates from the nonlinear rate equations [41] and leakage current [21] of the laser.

When IMPs fall inside a channel bandwidth, distortion results, and the carrier-to-distortion ratio (CDR) of an individual channel depends on the number of IMPs that reside within the channel. The precise number of nonlinear terms for a given transmission bandwidth is best assessed by computer combinatorial analysis based on the initial frequency plan. Therefore, by evaluating the number of IMPs the scale of distortion can be determined at a design stage. In the following sections the IMPs resulting from

second and third order nonlinear distortion and their dependence on the subcarrier frequencies are considered.

Second order IMPs are of the form  $f_i \pm f_j$ , where  $f_i$  and  $f_j$  are the subcarrier frequencies [46]. If the subcarrier frequencies are limited to a single frequency octave, second order distortion falls outside the pass band and therefore has no bearing on the system. But for systems whose frequency band exceeds a single octave, second order terms are the dominant form of distortion. The number of second order IMPs are dependent on the frequency plan and can be determined using the tables given in [47] and [48].

The distribution of second order IMPs for 35 equally spaced CATV subcarrier channels, passed through a nonlinear model, defined by Eqn. (3.7), is shown in Fig. 3.6 [18]. This indicates that for a system operating beyond a frequency octave the number of inband IMPs are greatest for signal channels at the end of SCM transmission band. The number at the lower frequency end is twice the number at the higher frequency edge.

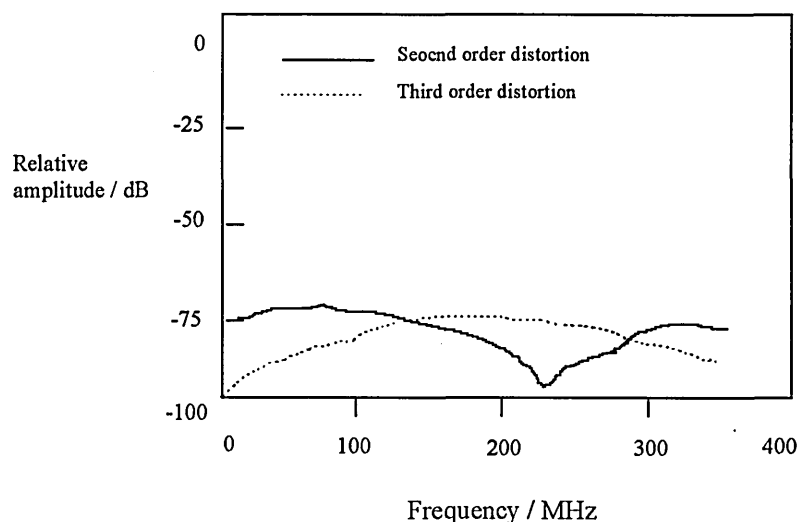


Figure 3.6 Distribution of second and third order IMPs for a 35 channel CATV signal passed through a nonlinear model [18].

For systems operating below a frequency octave, third order IMPs are the dominant form of nonlinear distortion. They can be subdivided into triple beat IMPs and two tone IMPs, according to the number of frequencies making up a product [46]. Triple beat IMPs are a combination of three subcarrier frequencies and are of the form:

$$f_i \pm f_j \pm f_k$$

The number of triple beat IMPs are given by  $N(N-1)(N-2)/2$ , and the highest number falls on the mid-band channel (Fig. 3.6). Two tone IMPs are of the form  $2f_i + f_j$ , and their number is given by  $N(N-1)$  [18]. Generally, triple beat IMPs are greater in number and therefore, tend to dominate third order distortion contributions. Figure 3.6 also indicates the distribution of third order IMPs for the 35 channel CATV system. The mid-band channels contain the most number of third order IMPs, falling to low levels at either side of the transmission band.

### 3.2.4 Clipping distortion

Intrinsic nonlinear analysis is only valid for a limited operating range and for systems with a large number of channels the dominant form of distortion is clipping. Clipping occurs when the modulating current falls below the threshold value  $I_{th}$ , and the LD is switched off resulting in zero optical power (see Fig. 3.5).

A number of models have been developed to calculate distortion power due to clipping. The earlier models have calculated clipping distortion by evaluating the total mean square power of the clipped portion, and distributing it uniformly among the signal channels [49, 50]. But the later models [51, 52] have shown that not all the clipped power fall within the transmission band (Fig. 3.7) and therefore, earlier calculations are overvalued. A review of clipping distortion models can be found in [53].

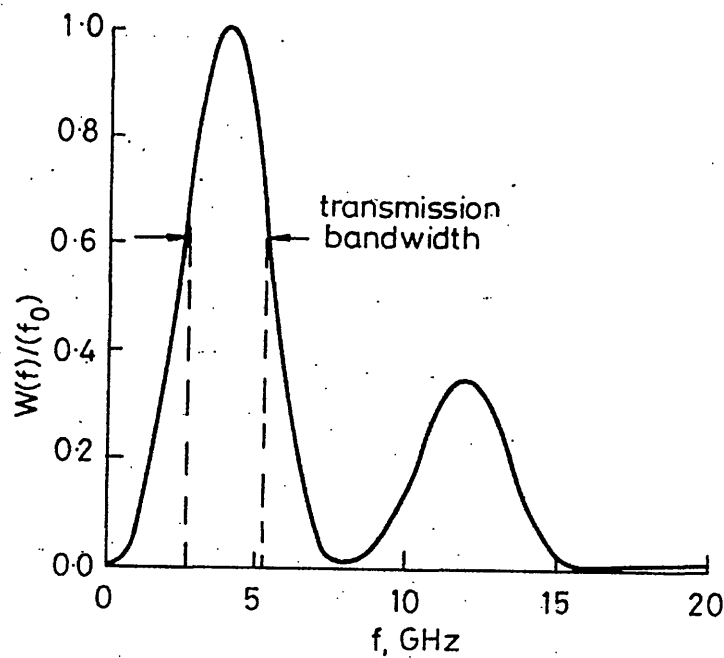


Figure 3.7 Clipping distortion power distribution, indicating that a substantial part of distortion noise spectrum falls outside the transmission bandwidth [51].

It is common to express the distortion for a specific channel by adding the power of IMPs, that fall within the channel, and express it with respect to the carrier. Composite second order (CSO) distortion defines the total power of second order IMPs that fall within a channel, normalised to the carrier power of that channel. CSO is expressed in dBc units where 'c' represents normalisation with respect to the carrier power. Third order IMPs are also expressed in a composite form known as composite triple beat (CTB) distortion, and as in the second order case is given in dBc units. Typically both CSO and CTB distortion values should be below -60 dBc for adequate system performance [9]. It should be pointed out that clipping distortion analysis is very involved and is not generally carried out at a design stage. However, the determination of IMPs, resulting from intrinsic nonlinearity, helps to allocate the subcarrier frequencies

so that the distortion within individual channels could be minimised. Clipping distortion can be kept to acceptable levels by restricting the rms OMI below unity.

### **3.3 Optical Channel**

Optical fibres are the most widely used transmission medium for optical communication systems. Although optical fibres are superior in performance compared to other transmission mediums, signal impairments occur during transmission. Attenuation and dispersion are the major degradations and are discussed below.

#### **3.3.1 Attenuation**

During optical transmission signal power attenuates, limiting the transmission distance. Although modern optical technology offers attenuations less than 0.5 dB/km (in the 1300 nm and 1500 nm optical windows), repeaters or optical amplifiers are required for long haul links. Repeaters convert the signal into the electrical domain for amplification and therefore introduces noise and distortion in the process. The emergence of erbium doped fibre amplifiers [54, 55] has made it possible to amplify optical signals without conversion, thus offering low noise figure amplifiers.

In erbium doped fibre amplifier (EDFA)s, a section of the fibre is doped with erbium atoms and an external laser source excites the electrons into a high energy state (see Fig. 3.8). At the incidence of the optical signal, the excited electrons emit photon energy by stimulated emission, boosting the optical power level. Current amplifiers can offer gains upto 20 dB at a theoretical minimum noise figure of 3 dB [38]. Although these amplifiers

offer advantages compared to conventional repeaters, current technology allows their operation only at 1550 nm wavelength.

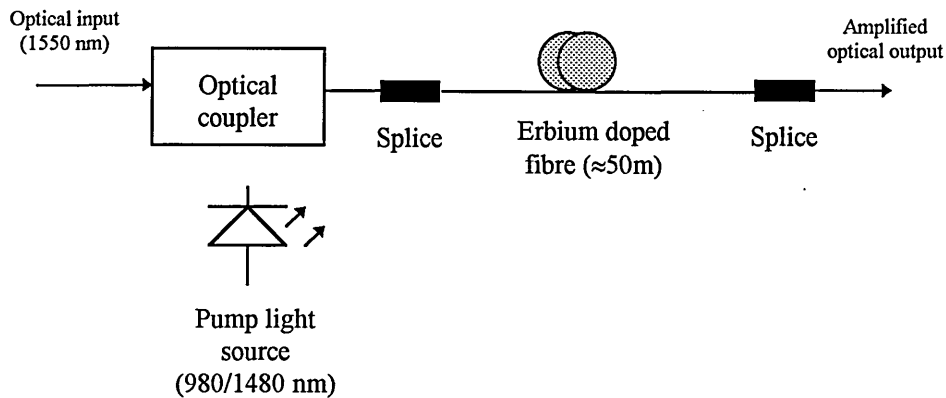


Figure 3.8 Erbium doped fibre amplifier.

### 3.3.2 Dispersion

Dispersion results due to different optical modes arriving at the receiver at different times. In digital systems the effect of dispersion is to introduce pulse spreading resulting in inter symbol interference (ISI). In intensity modulated subcarrier systems, dispersion induces harmonic and intermodulation distortion and can set an upper transmission limit [56].

The scale of dispersion induced distortion depends on the subcarrier frequencies, the dispersion constant, length of the fibre and modulation indices. Therefore, the assignment of channels and communication bands (i.e. a group of channels) is influenced. **Ih** and **Gu** [57] have shown that the magnitude of dispersion induced IMD sum terms are comparable to those of HD of the same order, provided the frequencies considered are

not far apart. The IMD difference terms are though, much smaller compared to HD of the same order.

Multi-mode fibres suffer from intermodal dispersion (dispersion due to several optical modes travelling within the fibre) and can severely limit the transmission bandwidth-distance product. However, single mode fibres only suffer chromatic dispersion (dispersion due to different materials within the fibre) and the effects are not as limiting as intermodal dispersion. Today single mode fibres operating at 1300 nm and dispersion shifted fibres at 1500 nm optical windows can offer extremely low dispersion values. Therefore, the dispersion induced distortion can be comparably much smaller to laser induced distortion, discussed previously.

### **3.4 Receiver**

The SCM receiver consists of an optical stage, where the optical signal is converted back into an electrical signal, followed by further processing in order to recover the baseband channels from the composite signal. The main requirements of the optical receiver are that it should convert the optical signal into an electrical signal efficiently, be able to operate with an appropriate bandwidth and add as little noise as possible [38]. As stated in section 3.2, coherent optical techniques are not considered and the optical receiver is assumed to employ direct detection. The baseband recovery from the composite signal employs either heterodyning or bandpass filtering and will not be discussed due to their common usage in communication systems [58].

Direct detection optical receivers convert the optical intensity variations into an electric current. These receivers exhibit good linearity and the distortion contribution is insignificant. However, the noise performance is critical since the optical receivers must be able to operate at low optical power levels. The main noise sources are shot noise generated by the photodiode and thermal noise of the post amplifier.

In optical communication systems two types of receivers are employed: PIN-FETs and avalanche photodiode (APD)s [39]. PIN-FET receivers show good noise performance at low frequencies and therefore are used in narrowband applications. On the other hand, APDs can offer additional signal gains at the expense of cost, complexity and higher power consumption. However, APDs have superior sensitivities and better SNRs at higher frequencies and therefore, are preferred to PIN-FETs for broadband applications.

The bandwidth of the receiver is also critical in SNR performance. In order to process the entire signal, the receiver bandwidth must be at least as large as that of the information. However, if the receiver bandwidth is too high additional noise is introduced, resulting in poor SNRs. Low noise receivers have bandwidths that range from little more than, to twice, the signal bandwidth [5].

Shot noise and thermal noise contributions of the receiver are discussed in the following sub-sections.

### 3.4.1 Shot noise

The optical power incident on photodetectors arrives in the form of energy packets, known as photons. Each photon produces a discrete electric charge carrier called an electron. The arrival of photons over a time period is not consistent and due to its random nature, the produced current deviates from a mean value. These fluctuations of the photocurrent constitute quantum or shot noise and set a lower limit on the minimum noise level in optical communication systems.

In addition, even when no optical power is incident, the detector produces discrete charge carriers due to spontaneous generation of electron-hole pairs. This electrical current is known as dark current. Combining the noise currents due to the charge quantum and the dark current, the mean square noise current induced is: [39]

$$\overline{n^2_s(t)} = 2q(I_d + I_o)B_r G^2 F(G) \quad (3.8)$$

where  $q$  is the electron charge,  $I_d$  is the dark current,  $I_o$  is the average detected photocurrent,  $B_r$  is the effective receiver noise bandwidth,  $G$  is the mean avalanche gain of the APD and  $F(G)$  is the excess avalanche noise factor. For a  $p-i-n$  receiver  $G$  and  $F(G)$  are unity.

The above equation shows that shot noise is proportional to the received optical power. In fact, when the optical receiver operates at high power levels, shot noise is the dominant noise source and can set an upper limit on receiver sensitivity. Operation of SCM systems in the shot noise dominant region is known as quantum limited operation.

### 3.4.2 Thermal noise

Electric current is carried by discrete electric charges. The random fluctuations of the charge carriers due to thermal energy produce a random noise current, known as thermal noise. In optical receivers, thermal noise is generated in the front end load resistor. In addition, thermal noise is also introduced by other electronic components in the receiver (e.g. amplifiers), and can be accounted for by specifying a noise figure,  $F_n$ .

The thermal noise current contribution is given by the following equation [39]:

$$\overline{n^2_i(t)} = \left( \frac{4KT_{ab}}{R_L} \right) F_n B_r \quad (3.9)$$

where  $K$  represents the Boltzman constant,  $T_{ab}$  is the absolute temperature,  $R_L$  is the front end load resistance and  $B_r$  is as defined before. At low optical power levels thermal noise dominates system performance; this is known as thermal noise limited operation.

## 3.5 CNR and System Penalties

In analogue transmission systems the signal performance is measured by the ratio of signal power to noise power at the receiver end. So far in this chapter, SCM system parameters and noise and nonlinear sources have been identified. By combining these it is possible to derive an expression for the signal-to-noise ratio (SNR) at the output of the SCM receiver. As the noise and distortion due to electronic processing i.e. the subcarrier stage, is assumed negligible, the SNR can be derived at the output of the optical receiver. Since individual signal channels at the output of the optical receiver are present as modulated subcarrier channels, the SNR is referred to as a carrier-to-noise ratio (CNR). In section 3.5.1 the CNR expression for a subcarrier channel is derived followed by a discussion on the performance limiting factors of SCM systems in section 3.5.2.

### 3.5.1 CNR expression

Ignoring the nonlinear distortion due to optical conversion and transmission, the received optical power  $P_r(t)$  is:

$$P_r(t) = P_{av} \left[ 1 + \sum_{i=1}^N m_i x_i(t) \right] \quad (3.10)$$

where  $P_{av}$  is the average detected optical power and other symbols are as defined in section 3.2.1. The resulting photocurrent  $i_p(t)$ , for an optical detector of responsivity  $R_o$  and avalanche gain  $G$  is:

$$i_p(t) = R_o G P_r(t) \quad (3.11)$$

Therefore the recovered signal current of the  $i^{\text{th}}$  channel can be written as:

$$i_r(t) = R_o G P_{av} m_i x_i(t) \quad (3.12)$$

Hence the mean square signal current or the rms signal power into a  $1 \Omega$  resistor is:

$$\overline{i_r^2(t)} = (R_o G P_{av} m_i)^2 \overline{x_i^2(t)} \quad (3.13)$$

As we have shown earlier, SCM systems are affected by three main noise sources: laser intensity noise of the transmitter, shot noise and thermal noise of the receiver. The rms noise power  $n_{rms}$ , can be expressed by combining Eqns. (3.6), (3.8) and (3.9), as shown below.

$$n_{rms} = \left[ RIN(R_o G P_{av})^2 + 2q(I_d + R_o G P_{av})G^2 F(G) + \left( \frac{4KT_{ab}}{R_L} \right) F_n \right] B_r \quad (3.14)$$

Therefore, the rms carrier-to-rms noise power ratio  $CNR$ , for the  $i^{\text{th}}$  signal channel can be expressed as:

$$CNR = \frac{(R_o G P_{av} m_i)^2 \overline{x_i^2(t)}}{\left[ RIN(R_o G P_{av})^2 + 2q(I_d + R_o G P_{av})G^2 F(G) + \left( \frac{4KT_{ab}}{R_L} \right) F_n \right] B_r} \quad (3.15)$$

Also, system nonlinearities introduce distortion in the recovered signal. As was shown in sections 3.2.3 and 3.2.4, laser nonlinearity is the most significant nonlinear contributor in SCM systems. As most systems operate below a frequency octave, the primary concern is with third order products and, by defining a third order distortion co-efficient  $D_3$ , the carrier-to-intermodulation ratio  $CI_3R$ , can be expressed as [25]:

$$CI_3R = \frac{1}{D_3 N^2 m_i^4} \quad (3.16)$$

The carrier-to-noise ratio for the overall system  $CNR_{sys}$ , which takes into account intermodulation distortion as well as rms noise, can be expressed by combining Eqns. (3.15) and (3.16):

$$\frac{1}{CNR_{sys}} = \frac{1}{CNR} + \frac{1}{CI_3R}$$

$$CNR_{sys} = \frac{(R_o GP_{av} m_i)^2 \overline{x_i^2(t)}}{\left[ RN(R_o GP_{av})^2 + 2q(I_d + R_o GP_{av})G^2 F(G) + \left( \frac{4KT_{db}}{R_L} \right) F_n \right] B_r + (R_o GP_{av})^2 \overline{x_i^2(t)} m_i^6 D_3 N^2} \quad (3.17)$$

### 3.5.2 System penalties

To get information from one place to another various communication techniques are employed. In all these techniques the prime requirement is that noise and distortion are limited to such levels, that the recovered information is of a pre-determined quality. The SNR required to deliver the quality of service defined by some standard, is known as system fidelity [59]. For example, in video transmission the recovered weighted SNR must be 56 dB to deliver studio quality video signals [60]. In the case of telephony channels this figure is around 30 dB [58].

So far SCM system parameters and its noise and nonlinear contributors have been presented, with the derivation of CNR for an analogue SCM channel in section 3.5.1. As can be seen from Eqn. (3.17) the signal power strongly depends on the OMI and the fundamental noise level is set by the shot and thermal noise of the receiver. At higher optical power levels nonlinear distortion and RIN can increase the noise contribution. From a system point of view the optimisation of an optical network can be achieved in two ways. The CNR can be maximised for a specified power level or alternatively, the optical power level can be minimised to deliver a specified CNR. Once the system fidelity is defined the latter approach helps to optimise the optical power budget, i.e. the optical power available for transmission and distribution (see Eqn. (3.21)).

The improvement factor of a modulation technique defines the SNR improvements that can be delivered as a result of modulation. Hence, it is defined as the ratio of the recovered SNR to the CNR of the modulated signal. In SCM systems signals are modulated at the subcarrier stage and the SNR improvements are delivered by the modulation techniques employed. For AM subcarrier systems the improvement factor is unity and therefore the SNR is equivalent to the CNR. FM systems can deliver a higher SNR for the same CNR, due to the FM improvement factor. This implies that SCM receivers require high CNRs to deliver adequate signal performance.

As stated earlier, the receiver thermal and shot noise can set a fundamental limit to the achievable CNR. The signal power is strongly influenced by the OMI allocated for each channel and increases as  $m_i^2$ , as indicated by Eqn. (3.13). However, this increase is not without penalties as the intermodulation distortion will also increase at higher values of

$m_i$ . In fact, from Eqn. (3.17), the intermodulation distortion can be represented as a noise current  $\overline{i_m^2}$  [61]:

$$\overline{i_m^2} = (R_o G P_{av})^2 \overline{x_i^2(t)} N^2 D_3 m_i^6 \quad (3.18)$$

Therefore, the signal power gains due to larger  $m$  values can be offset by increased nonlinear distortion. This implies an optimum modulation index for which CNR can be maximised. The optimum per-channel modulation index,  $m_{opt}$ , can be represented by the simple relationship shown below [61]:

$$m_{opt} = \frac{1}{(3D_3 N^2 CNR)^4} \quad (3.19)$$

The above equation indicates that the optimum modulation index can be determined independent of thermal, shot and intensity noise. **Walker *et al.*** [23] has shown an experimental verification of the existence of an optimum modulation index: the two tone third order IMP of a 1300 nm Fabry-Perot laser, modulated by 2.0 and 2.1 GHz frequencies has been measured. Figure 3.9 shows the relationship between CNR (measured in a 1 MHz bandwidth) and the total modulation index for two different bias levels.

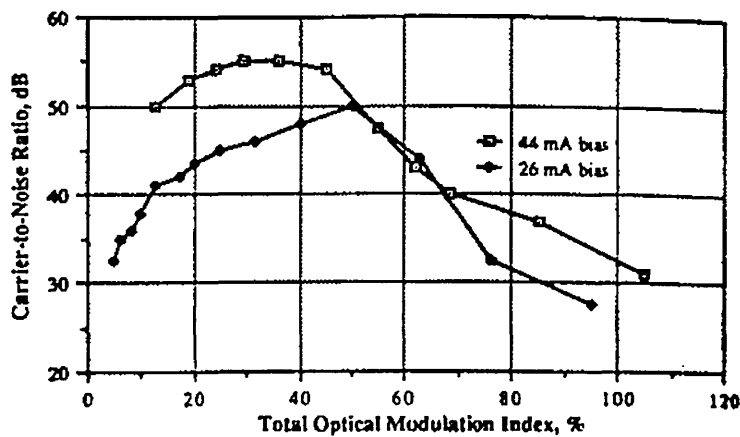


Figure 3.9 Carrier-to-noise ratio vs. total OMI [23].

In standard optical fibre communication systems employing LED transmitters, intensity noise is not accounted for, owing to the high optical power levels required for it to become significant [62]. However, in the case of laser diodes RIN can be a limiting factor, especially for high frequency and high optical power operation. The RIN limited CNR can be expressed as:

$$CNR = \frac{m_i^2}{2 RIN B_r} \quad (3.20)$$

where the symbols are as defined in section 3.2

The RIN limited operation for a broadcast AM and FM system is calculated in Fig. 3.10. As the OMI value allocated for each channel increases so does the RIN value hence, no change in SNR. To achieve the same SNR values, RIN has to be limited to lower levels for AM, compared to FM systems.

Another limitation of increased OMI, not taken into account in Eqn. (3.19), is laser clipping. Statistical analyses have shown that limiting the optical source strictly to the linear region is too conservative, and a degree of over modulation can be beneficial without causing significant increase in distortion [50]. However, clipping effects determine a fundamental limit to total laser modulation index and the limited input dynamic range of the laser sources has been one of the major limitations of SCM systems todate. In particular, if the system requirements dictate that high CNRs are required, signal channels must be operated at high OMIs and therefore, the system capacity is undermined.

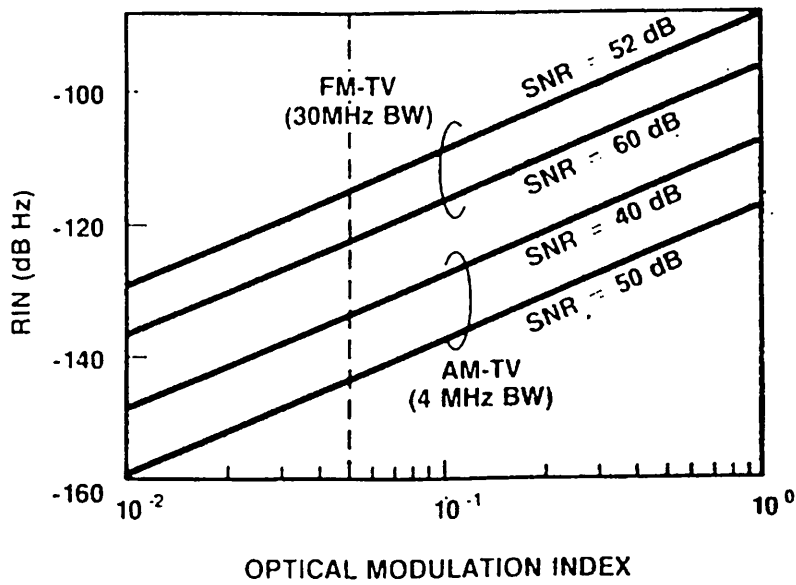


Figure 3. 10 RIN vs. OMI/channel for broadcast AM and FM systems [16].

In summary the above discussion has shown that SCM systems require high CNRs at the receiver, and the strict noise and linearity requirements can further undermine the achievable CNRs. As a consequence SCM systems have poor receiver sensitivities, requiring high optical power levels at the receiver.

In optical communication systems an optical power budget is defined to ensure that enough optical power reaches the receiver for reliable operation during system lifetime, and is expressed as [59]:

$$P_t = P_r + C_L + M_s \quad (3.21)$$

where  $P_t$  is the transmitted optical power,  $P_r$  is the received optical power,  $C_L$  is the total channel losses due to fibre, connectors, splices *etc.* and  $M_s$  is the system margin, allowed for unforeseen losses. As  $P_r$  needs to be high, SCM systems have to be operated with

restricted power budgets. A restricted power budget limits the transmission distance and also the number of subscribers in a network.

A comparison between optical power budgets for AM and FM systems has been made in [18] and is shown in Fig. 3.11. This shows the increase in power budget with OMI for AM and FM systems. Due to the improved receiver sensitivity, to deliver similar SNR levels, FM systems have a much larger optical power budget available compared to AM systems.

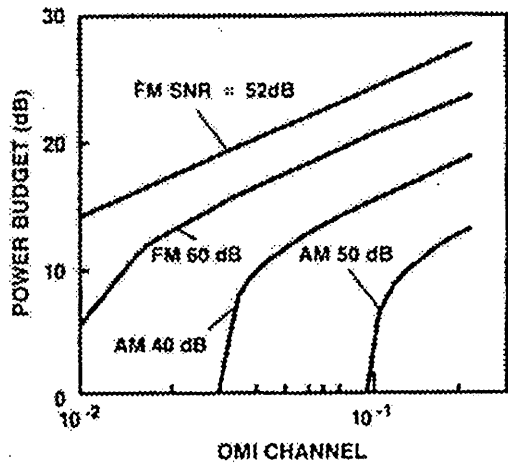


Figure 3.11 OMI/channel vs. power budget for AM and FM [18].

### 3.5 Summary

In this chapter the design parameters of SCM systems were considered in detail. The key parameters of the transmitter were identified as the optical modulation index, and intensity noise and nonlinear distortion of the laser diode. In order to limit intensity noise a laser diode which has a low intrinsic RIN value and techniques to limit back reflection must be employed. Clipping distortion was identified as the dominant form of nonlinear distortion for systems operating a large number of channels. Techniques to evaluate the amount of nonlinear distortion at a preliminary design stage were also introduced.

The attenuation and dispersion of the optical channel and its impact on the SCM signal was presented in section 3.3. Shot noise and thermal noise were identified as the dominant noise sources of a SCM receiver and can set a fundamental limit to the achievable CNR. The stringent requirements imposed on laser RIN and nonlinear distortion, to achieve the high levels of CNR levels required in SCM systems, restrict the optical power budget limiting the transmission distance, number of channels and the subscribers in a network.

---

# Second Stage Modulators and Pulse time Modulation

## 4.1 Introduction

Around 1870, John Tyndall, a British physicist, demonstrated to the Royal Society that light can be guided along a curved stream of water. Some 100 years later the same phenomenon was used to guide light over the first truly low loss glass fibre, making optical fibre communication a practical proposition [5]. Since then optical fibre technology has developed very rapidly and operational fibre systems are now common place. The potentially infinite information capacity of optical fibre channels promises to take global communications to new heights.

With the emergence of broadband communications, optical fibre networks are being used to distribute video, data and voice services. The choice of modulation format on the optical carrier is a principal factor in realising a high performance, bandwidth efficient

system at an acceptable cost. Analogue modulation schemes such as FM and AM are simple and bandwidth efficient and modulate the optical source in a continuous manner. A number of such analogue channels can be combined as in SCM systems, described in chapters 2 and 3, to distribute various services to subscribers at a low cost.

However, the low cost of SCM systems is realised by compromising the level of performance. As outlined in section 3.5.2, the poor receiver sensitivity of SCM receivers and the strict noise and nonlinearity requirements imposed upon the optical source undermine the network capacity, transmission distance and the number of subscribers.

## **4.2 Second Stage Modulators**

In order to improve the performance of analogue optical links, work has been carried out on linearisation of optical sources, reduction of laser intensity noise, optimum optical receivers *etc.* [63-65]. An alternative technique employed to enhance system performance of a SCM optical link is to introduce a second stage modulator to improve the input dynamic range and the receiver sensitivity. In such systems, the frequency division multiplexed signal channels, i.e. the SCM signal, is modulated onto a secondary carrier prior to optical transmission. Therefore the SCM signal acts as the baseband signal of the second stage modulator. The modulation format of the second stage modulator is determined by its suitability for optical transmission, the required level of performance, bandwidth efficiency and overall cost. At the receiver, the optical signal is converted into an electrical signal and fed to the corresponding demodulator, in order to recover the SCM signal. Information can be recovered from the SCM signal by

employing standard signal recovery techniques used in SCM systems. Figure 4.1 shows the concept of second stage modulation in SCM systems.

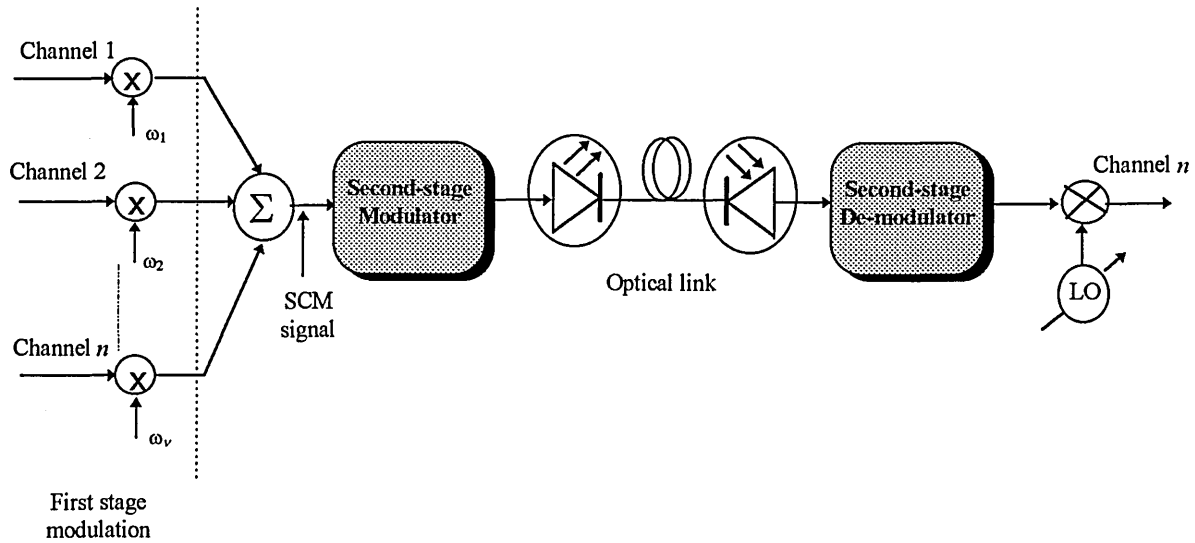
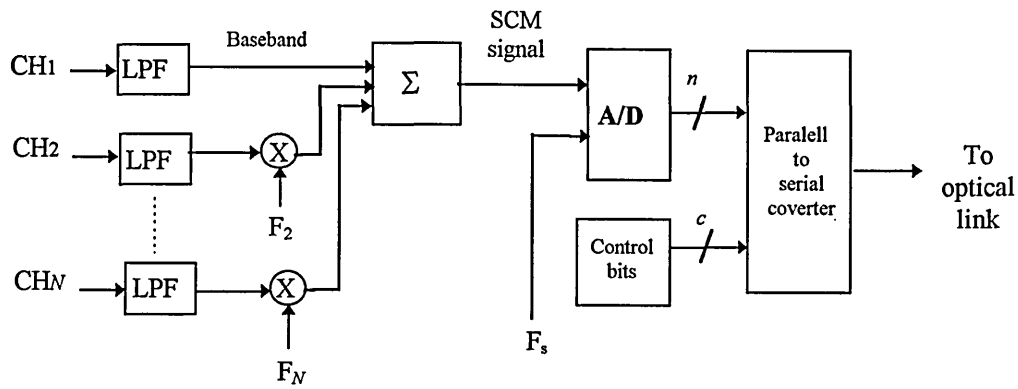


Figure 4.1 A SCM system employing a second stage modulator.

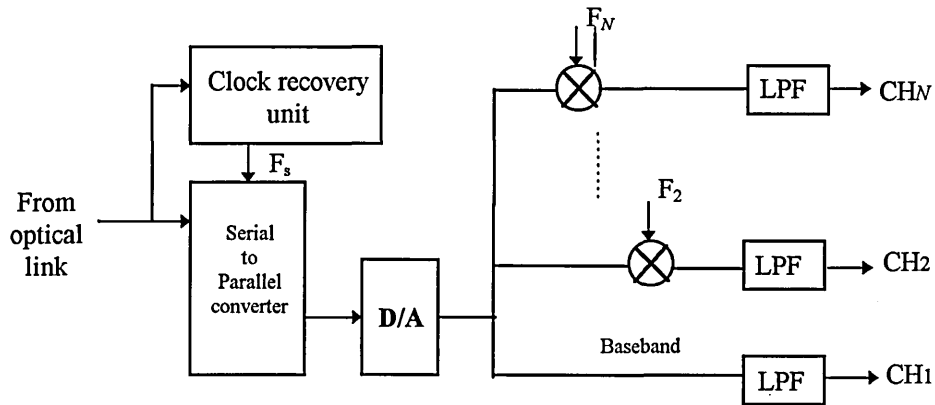
Work on second stage modulators in SCM systems has been reported by several leading research centres across the world and in the ensuing subsections two different system implementations are presented. Pros-and-cons of each technique are weighed in section 4.2.3.

#### 4.2.1 Digital modulator for video, voice and data transmission

Grace at *United Telecommunications Inc.*, Kansas, USA [12] has developed a prototype system employing a high speed analogue-to-digital (A/D) converter to digitise an analogue SCM signal for optical transmission. Figure 4.2 illustrates the concept of a SCM quantiser/transmitter subsystem and the receiver/demultiplexer subsystem.



(a) SCM multiplexer -transmitter



(b) receiver-demultiplexer

Figure 4.2 Block diagram of a quantising SCM transmitter-receiver subsystem [12].

In the transmitter, the  $N$  channel SCM signal is fed to a  $n$  bit A/D converter. The parallel data stream of the A/D converter is serialised and transmitted via an optical fibre link. The composite signal resulting from the application of conventional SCM techniques, is acceptable for digitisation, provided the following conditions are satisfied.

- (a) the composite signal never exceeds the dynamic range of the A/D converter.
- (b) bandwidth information of the composite signal does not violate the Nyquist criteria.
- (c) bit resolution of the A/D is adequate to limit the quantisation noise.

Additional control bits are inserted into the data stream, prior to optical transmission, to convey frame and clock information to the receiver.

The process of information recovery is a simple reversal of the multiplexing process. The bit stream is digital-to-analogue (D/A) converted, yielding the composite signal from which each channel is then recovered.

The prototype system was configured to multiplex two NTSC video signals and a single 192 kbit/s bipolar bit stream to represent voice and data information. An 8 bit A/D converter, operating at a sampling rate of 28 MHz, was employed to digitise the SCM signal. A laser diode operating at 1300 nm, 12 km of single mode fibre and a *p-i-n* photodetector was employed in the optical link.

Figure 4.3 shows the spectrum of the recovered composite signal at the output of the D/A converter. The information from dc to 5 MHz represent the baseband video channel, the data channel is centred at 7 MHz and the second video channel is modulated to a subcarrier at 14 MHz. The weighted SNR of the baseband video channel exceeded 52 dB, while for the highband video channel the SNR exceeded 50 dB. Performance of the data channel is indicated by the eye pattern shown in Fig. 4.4, and the measured BERs ranged from  $10^{-7}$  to  $10^{-11}$ . The response of the prototype system to a 310 kHz test tone is compared with a directly modulated laser, as shown in Fig. 4.5. It can be seen that the quantiser produces low level, higher order spectra, compared to pre-dominantly second and third order harmonics of the directly modulated laser.

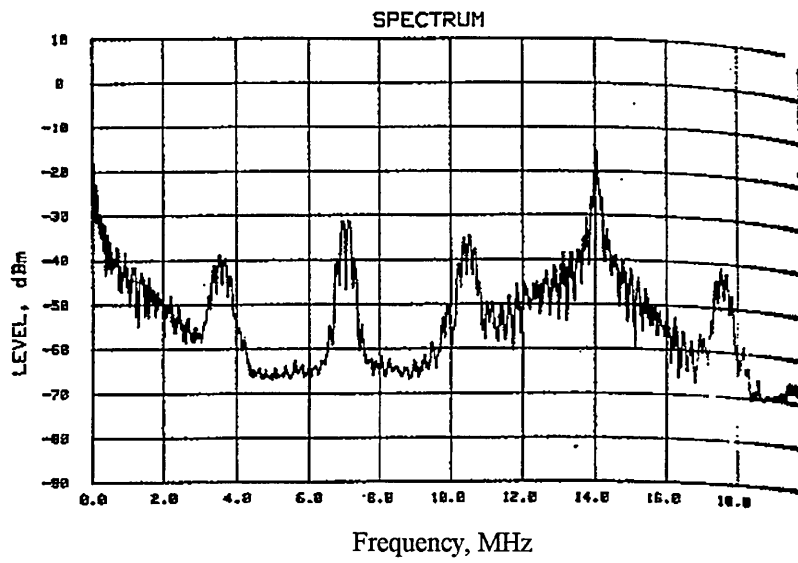


Figure 4.3 Spectrum of the reconstructed composite signal at the receiver [12].

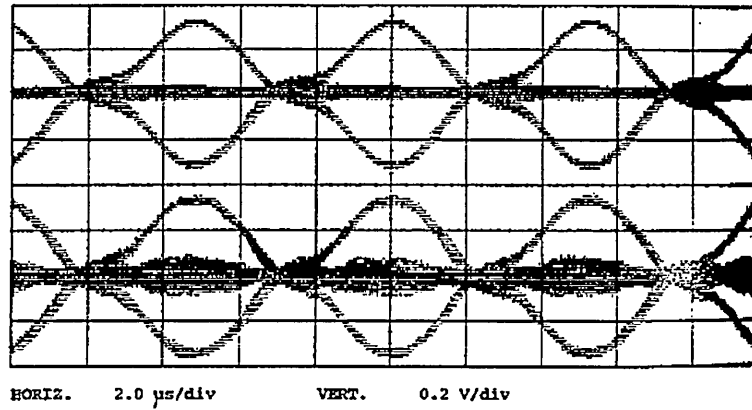
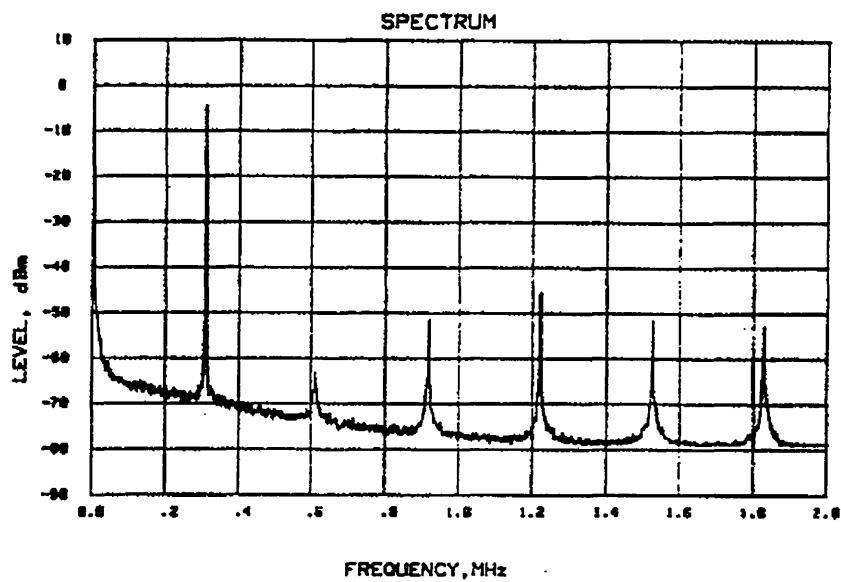


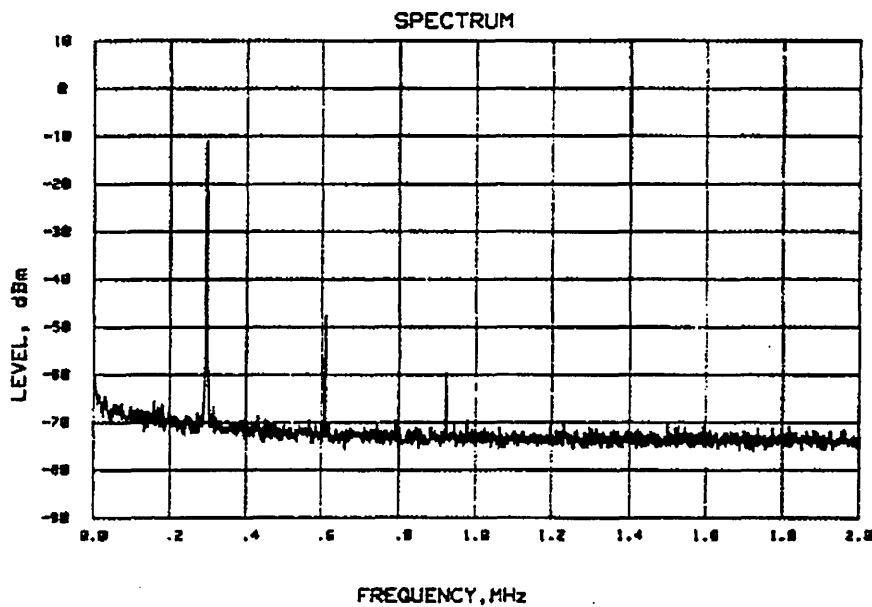
Figure 4.4 Eye pattern of the data channel [12].

top trace : transmitted data

bottom trace : received data



(a) the prototype system response



(b) 1300 nm laser operated at a modulation index of 0.5

Figure 4.5 Response to a 310 kHz test tone [12].

#### 4.2.2 FM modulator in a micro-cell environment

In a micro-cell radio environment, the number of base station (BS)s required are greater than in conventional cellular systems. Therefore, due to its low cost and simplicity, SCM

is a feasible method of connecting each BS to the central station (CS). However, the input dynamic range of the link is limited due to laser RIN and nonlinearity constraints. *NTT Radio Communication Systems Laboratories*, Yokosuka-shi, Japan, [13] have reported a FM second stage modulator to improve the dynamic range of the SCM optical link. The SCM signal is fed to a FM modulator, prior to optical transmission, and at the receiver, the optically converted signal is fed to the FM demodulator in order to recover the original SCM signal. The required input dynamic range of the optical source is fixed because the FM signal is a constant amplitude signal and the CNR performance is improved due to wideband FM gain.

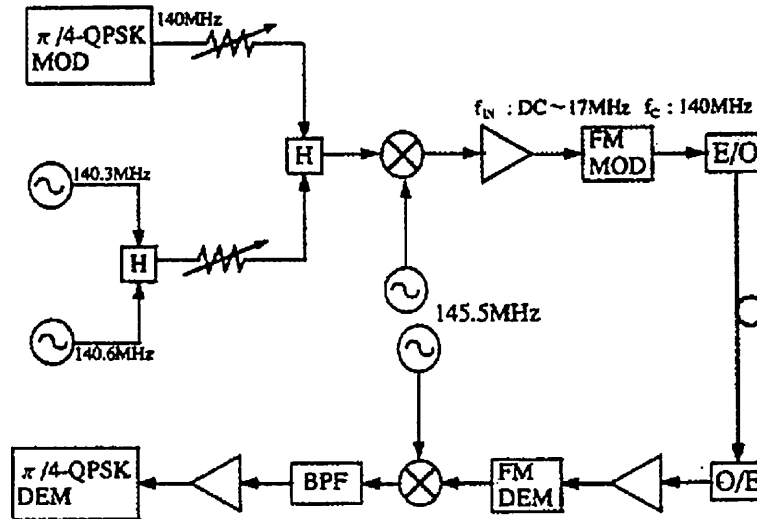


Figure 4.6 Block diagram of the FM second stage prototype system [13].

The concept of FM second stage modulation was tested for a QPSK modulated subcarrier system. The employed FM modulator has a centre frequency of 140 MHz and a baseband frequency response of upto 17 MHz. A single QPSK subcarrier, modulated by a data rate of 300 kbit/s, was used to test the BER performance of the system. The block diagram of the system setup is illustrated in Fig. 4.6 and system parameters are

summarised in table 1. System configuration shows that the QPSK signal is down converted prior to FM modulation and at the receiver upconverted following the FM demodulator, prior to QPSK demodulation.

<b>QPSK modulator</b>	Modulation format	$\pi/4$ QPSK
	Demodulation	differential detection
	Roll-off-factor	0.5
	Signal bandwidth	300 kHz
	Baseband frequency	DC to 17 MHz
<b>FM modulator</b>	Centre frequency	140 MHz
	Modulation index	0.15
<b>Optical link</b>	Optical output power	3.6 mW
	Photodiode responsivity	0.6 A/W
	Fibre	1.3 $\mu\text{m}$ , single mode

Table 1 Experimental specification of the prototype system.

The measured and calculated BER performance as a function of the input power, defined at the optical source for the conventional method and at the FM modulator for the proposed method, is shown in Fig. 4.7. The second stage FM modulator technique improved the input power sensitivity by 23 dB compared to the conventional system, when the delivered bit error rate (BER) was  $10^{-3}$ .

The technical feasibility of FM second stage modulation technique was first demonstrated by *Sato et al* at *NTT Electrical Communications Laboratory*, Yokusaka,

Japan [14] in 1985. They have implemented a prototype system to distribute audio, video and data services, operating at an optical wavelength of 1300 nm, using 9 km of multi-mode fibre.

A novel analogue-digital hybrid technique has been adopted by **Andrawis** and **Jacobs** at *South Dakota State University*, Brookings, USA [66] to overcome noise and nonlinear limitations in analogue multi-channel video transmission systems. Each baseband video channel is modulated onto a FM carrier and the modulated channels are sampled at the Nyquist rate in order to be multiplexed in the time domain. The technique is illustrated by the block diagram of Fig. 4.8. By means of simulation and system analysis, performance of the proposed technique has been compared with existing modulation schemes.

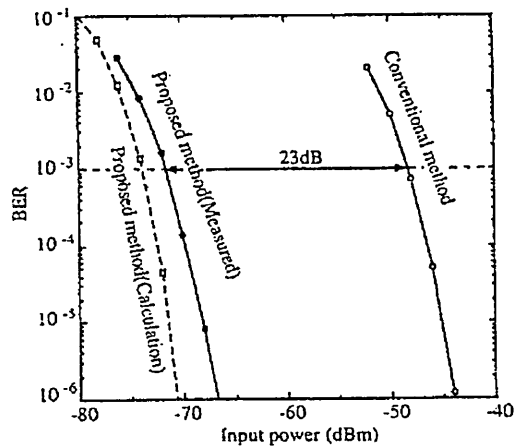
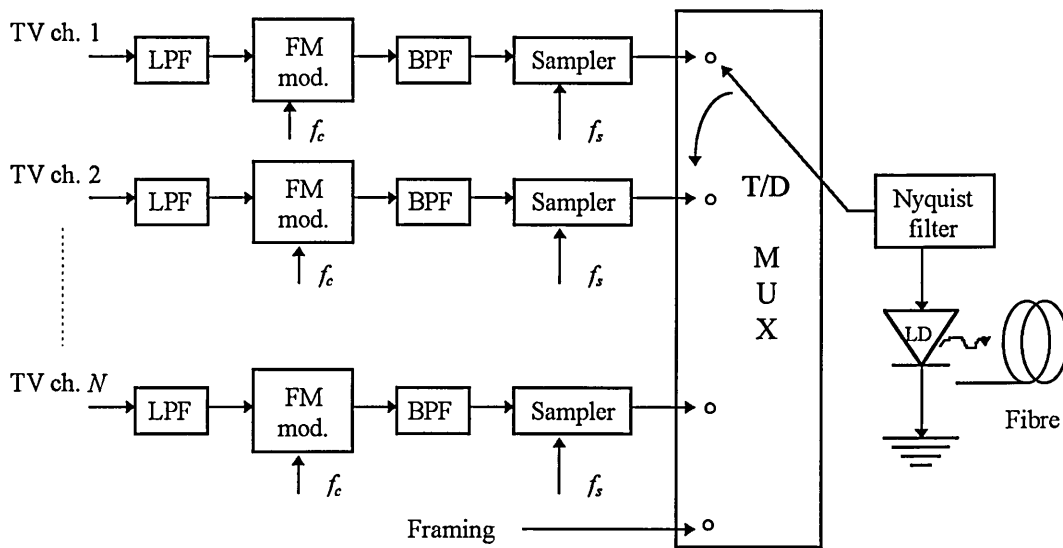
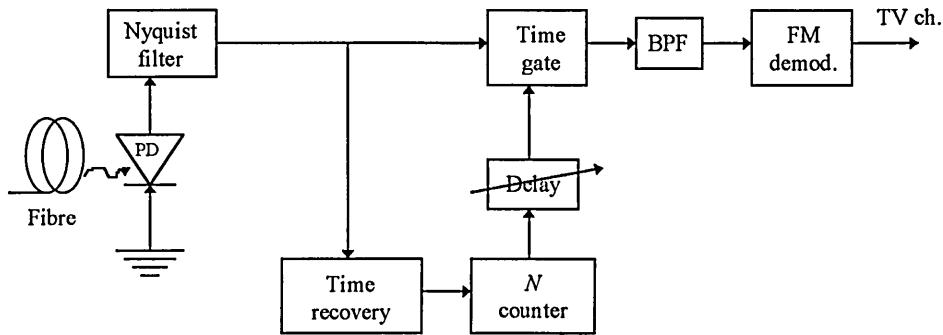


Figure 4.7 Measured and calculated BER performance as a function of the input power

[13]



(a) transmitter



(b) receiver

Figure 4.8 Transmitter and receiver block diagram of FM-TDM technique [66].

### 4.2.3 Pros-and cons of implemented techniques

In sections 4.2.1 and 4.2.2, two second stage modulation techniques, incorporating digital modulation and analogue FM modulation respectively, have been described. The quantised SCM approach can deliver SNRs comparable to pulse code modulation

(PCM), since a digitised signal is employed for optical transmission. However, applications of this technique can be limited due to the following:

(a) speed of the A/D converter:

currently available digital encoders, at most, can sample upto frequencies of 100 MHz. Therefore, the modulation bandwidth of the digital modulator is severely restricted, limiting the number of subcarrier channels.

(b) digital encoding is a complex and expensive process.

(c) digital signals carry an intrinsically large bandwidth overhead and therefore, require extremely high channel bandwidths.

On the other hand FM modulation is simple and cost-effective. FM modulator can have a significantly higher input dynamic range compared to digital modulators, allowing for greater number of subcarrier channels to be transmitted. The constant amplitude of the FM signal allow for the optical source to be operated without stringent nonlinear restrictions. The SNR performance is improved considerably compared to AM systems, due to wideband FM gain, but is lower compared to PCM systems.

The analogue-digital hybrid technique introduced in [66] can also offer sensitivity to nonlinearities comparable to digital systems. As this method employs time multiplexing, intermodulation and cross modulation associated with FDM systems is eliminated. The reported results indicate an optical power budget improvement of approximately 8.5 dB compared to conventional FDM systems. However, bandwidth requirements are higher compared to FDM systems and timing recovery at the receiver increases the cost and complexity of the system.

### 4.3 Pulse Time Modulation

As we have already discussed in this chapter analogue modulation schemes are vulnerable to various noise sources and often fail to deliver the required SNRs over moderate distances in optical fibre communication systems. The nonlinearity of the optical source, optical channel and associated circuitry can also severely limit the quality of the received signal through intermodulation and crosstalk.

In contrast, digital schemes such as PCM have been demonstrated to be substantially immune to channel noise and nonlinearities, and are capable of producing high SNRs at the receiver. However, digital systems are significantly more complex, largely due to their coding circuitry, and therefore, costly compared to simple analogue systems. Digital systems also carry an intrinsically large bandwidth overhead, restricting the transmission capacity. The emerging compression techniques such as moving pictures experts group (MPEG) [9] and joint photographic experts group (JPEG) [67] address the bandwidth overhead of digital systems and will play a crucial role in future broadband digital services distribution.

For example, current compression technology is capable of transmitting upto 10 compressed digital video channels within a single analogue video channel [68]. However, the complexity of compression techniques and the need to have a decompression unit in each receiver significantly increases the cost, and therefore is not financially viable at present.

### 4.3.1 Classification of modulation techniques

The classification of modulation techniques employed in communication systems is shown in Fig. 4.9. The modulation occupying an intermediary position to analogue (AM, FM etc.) and digital (PCM) techniques is known as pulse modulation. Although at present there is no general method of classifying pulse modulation techniques, two broad categories, according to the nature of the modulating signal, can be identified [69].

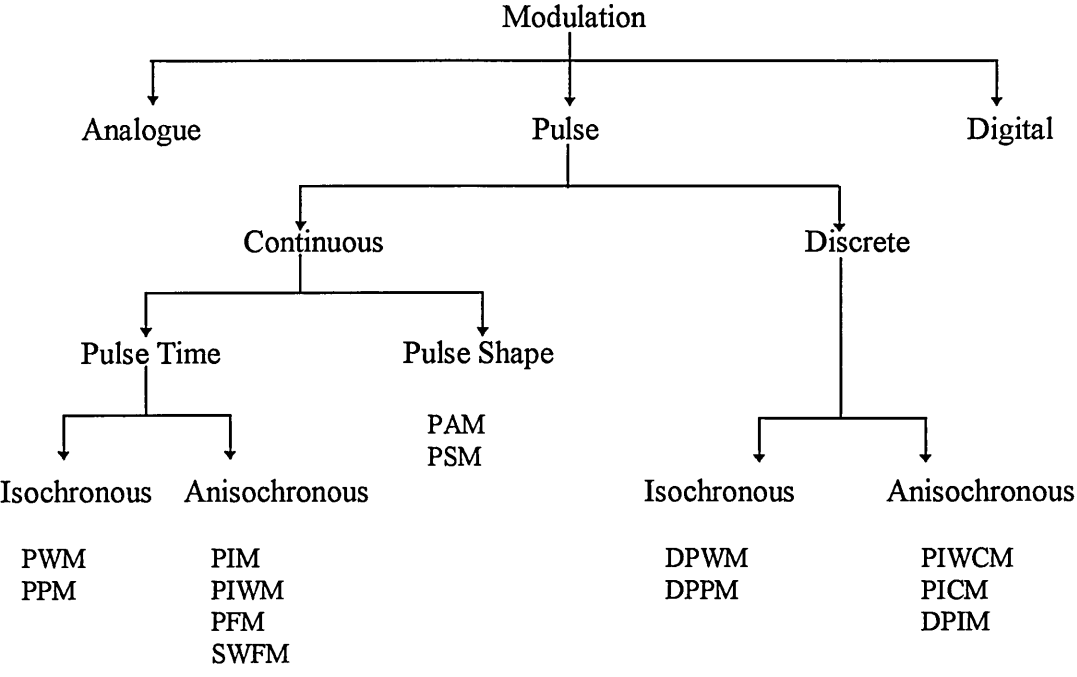


Figure 4.9 Classification of modulation techniques

One category is continuous pulse modulation, where a continuous signal vary a time property or alternatively, the physical appearance, of the pulse train. According to the form of modulation it can be subdivided into two categories: pulse time modulation (PTM) and pulse shape modulation (PSM). PTM is the variation of some time property, such as pulse width, frequency, position *etc.* of a constant amplitude pulse train.

The PTM concept was conceived around 50 years ago and was first reported in the 1940s [15, 70], but its applications were limited in the early years. However, with the advent of optical fibre communication, PTM has re-emerged as a preferred modulation format for the optical carrier and is the most widely used pulse modulation technique.

In contrast, PSM is the modulation of the physical appearance of a pulse, such as pulse slope or pulse amplitude [71], and is limited in its applications. Different PTM techniques will be considered in the following sub-sections, but PSM systems will not be considered as they are not employed in this work.

The second category is discrete pulse modulation [72], where the modulating signal is discrete, such as binary PCM. The primary discrete pulse modulation technique is digital pulse position modulation (DPPM) [73], where the position of a pulse within a time frame is determined by the value of the corresponding PCM word. This technique has shown substantial improvements in receiver sensitivity over equivalent binary PCM, when the fibre bandwidth is several times that required by PCM. Discrete pulse modulation has found applications in deep space communication but, is not considered here as it is as complex and costly as PCM systems.

### **4.3.2 PTM techniques**

The primary advantage of PTM is its ability to trade cost against system performance. Modulation is simple and inexpensive, requiring no complex digital coding, and the pulse format of the modulated carrier improves the noise immunity and tolerance to nonlinearities. Moreover, PTM is unique in its ability to trade performance with

bandwidth overhead, which is a particularly exploitable feature in optical fibre systems. For example, certain short distance applications such as local area networks (LANs), may use multi-mode or singlemode fibre with a dispersive optical carrier, which imposes a significant bandwidth limitation in the optical channel. In these applications low speed optical sources such as light emitting diodes (LEDs) can be used, while still achieving the required SNR. In contrast, the available bandwidth on long distance terrestrial and undersea routes may be many orders of magnitude broader where optical amplification and soliton techniques are employed. This additional bandwidth can be readily exploited, at a low cost, by PTM to improve SNR performance. Therefore, PTM has the ability to trade bandwidth against SNR, to significantly high levels compared to analogue systems, and at a relatively low cost compared to digital systems [16].

Additional advantages of PTM include its ability to be routed through logic circuits and switching nodes in networks, and the lack of synchronisation requirements at the receiver, offering circuit simplicity and low cost.

The adoption of PTM techniques has certain beneficial consequences from the standpoint of opto-electronic subsystem specifications as well. Since PTM deals exclusively with a pulse format, there are no concerns over LED or laser diode linearity, as would be the case with direct intensity modulation or subcarrier multiplexing techniques (sections 3.2.3 and 3.2.4). In addition, for narrow pulse PTM formats the peak optical output may be maintained at a high level to ensure good noise performance at the receiver without compromising device lifetime through elevated mean power levels at the transmitter. An optical transmitter for a PTM system may therefore be chosen primarily for its maximum

peak power level, with little regard to device linearity, in order to maximise transmission distance [74].

In all PTM methods, one of a range of time dependent features of a pulse carrier is varied to convey information. Table 4.2 lists the different PTM techniques and the pulse variables associated with each technique.

<b>PTM technique</b>	<b>Variable</b>
PPM	position
PWM	width (duration)
PIM	interval (space)
PIWM	interval and width
PFM	frequency
SWFM	frequency

Table 4.2 Different PTM techniques and associated pulse variables

According to the structure of the time frame, PTM can be sub-divided into isochronous and anisochronous techniques [75]. In isochronous systems, there exists a fixed time frame equivalent to the pulse period of the carrier at all times, and information is conveyed by modulating some pulse property within that fixed time frame. Pulse position modulation (PPM) and pulse width modulation (PWM) belongs to the isochronous PTM category. In PPM information is carried by virtue of a continuously variable position of a narrow pulse within the fixed time frame. In PWM, the width of the pulse within a pre-determined time frame is modulated to carry the signal. Time domain representation of isochronous PTM techniques are illustrated in Fig. 4.10.

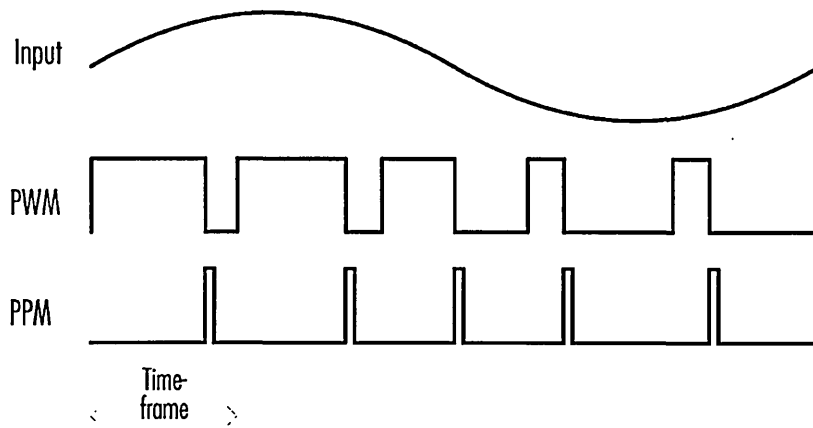


Figure 4.10 Isochronous PTM techniques in the time domain.

Anisochronous systems do not have a fixed time frame and the period between consecutive pulses is determined by the modulating signal amplitude. Pulse frequency modulation (PFM), square wave frequency modulation (SWFM), pulse interval modulation (PIM) and pulse interval width modulation (PIWM) are classified as anisochronous PTM techniques and are illustrated in Fig. 4.11.

In PFM, the instantaneous frequency of a train of narrow pulses is determined by the modulating signal amplitude. SWFM is closely related to both PFM and analogue FM, consisting essentially of a series of square wave edge transitions occurring at the zero crossing points of FM.

As its name suggests, in PIM the variable intervals between adjacent narrow pulses are determined by the modulating signal. PIWM is derived directly from PIM to produce a waveform in which both mark and space convey information in alternating sequence.

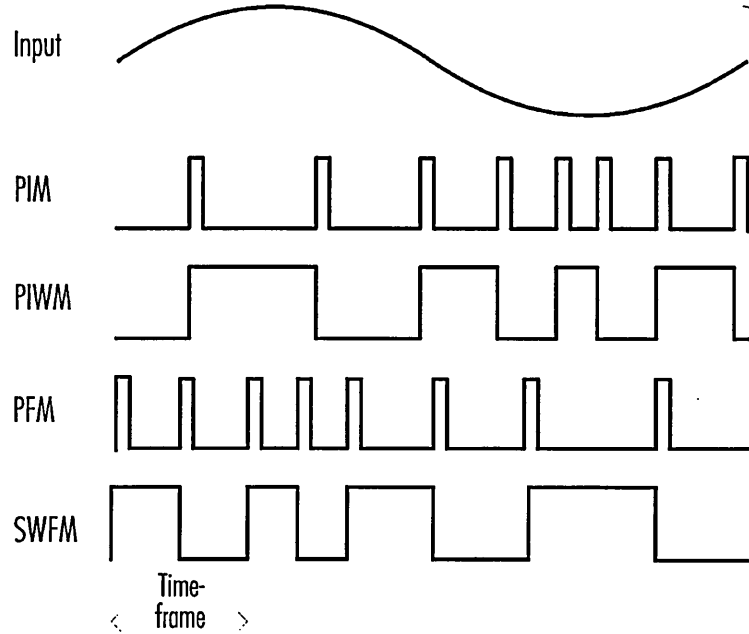


Figure 4.11 Anisochronous PTM techniques

### 4.3.3 PTM spectrum

All PTM techniques produce a modulation spectra which shares a common set of features and therefore the general profile of PTM spectrum is considered in this section. In each PTM technique, modulation gives rise to a diminishing set of sidetones centred around the carrier frequency and its harmonics, separated in frequency by an integer multiple of the signal frequency, as shown in Fig. 4.12. The number and strength of the sidetones is a function of the modulation index and in most cases can be predicted by Bessel functions of the first kind. Generally the number of sidetones around the  $n^{\text{th}}$  harmonic is  $n$  times the number around the fundamental. Thus the frequency deviation around the  $n^{\text{th}}$  harmonic is  $n$  times greater compared to the deviation about the fundamental. A baseband component is also present for some PTM methods, along with harmonics, depending on the form of sampling employed in the modulator.

Either natural or uniform sampling of the input signal may be adopted for PTM. Naturally sampled modulators operate directly on the input signal, and the precise sampling instants are variable, determined by the location of the modulated pulse edges. For uniform sampling, the input signal is routed via a sample-and-hold circuit which produces flat topped amplitude modulated pulses, so that the PTM modulator operates on uniformly spaced and stored input samples.

Demodulation in naturally sampled systems is carried out by converting the PTM signal into a form with a baseband component and recovering it with a lowpass filter. When uniform sampling is employed, a sample-and-hold circuit is included to recreate an amplitude modulated pulse form, followed by a lowpass filter. Uniform sampling is capable of complete signal recovery without distortion, at the expense of system cost and complexity [74].

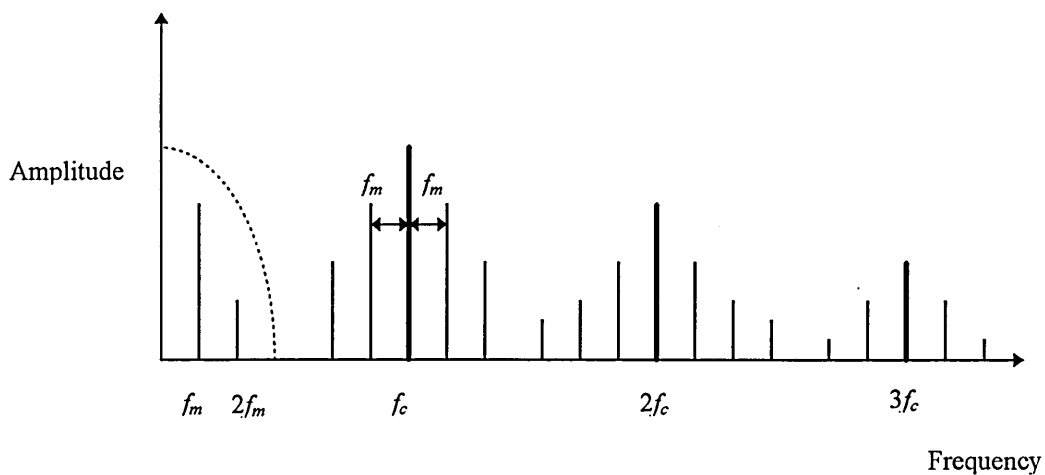


Figure 4.12 A typical PTM spectrum.

#### 4.3.4 Comparison of PTM techniques

The performance of a modulation technique is measured by its ability to deliver high SNRs and low distortion values. Bandwidth efficiency, complexity and cost are also important system parameters in selecting a modulation format and a trade-off has to be made for conflicting requirements in order to achieve an optimised system [59].

As has already been shown, the spectrum of different PTM techniques share commonalties, resulting in similar bandwidth requirements. The cost of PTM is also low compared to digital systems requiring elaborate coding techniques. PFM and SWFM are relatively less complex to other PTM techniques, as they can be operated with commercially available VCOs. All the other PTM schemes require a high speed linear ramp generator at the transmitter and sometimes at the receiver too, depending on the demodulation technique adopted. A common approach is used for signal demodulation in all PTM systems: regenerating a PTM signal with a baseband component at the receiver and employing a lowpass filter.

However, the distortion and SNR performance of different PTM techniques are variable and are considered here. Hitherto, relatively little work has been published on PIM [76-77] and PIWM [78] systems, for two reasons. Primarily, they have shown no performance advantage over PPM systems, but are more complex in their circuit implementation. Secondly, the input dynamic range of PIM and PIWM modulators are limited since the most negative transitions of the modulating signal could produce pulses at very short intervals, increasing the instantaneous frequency of the signal [79]. Therefore, only PFM, SWFM, PPM and PWM are considered further.

PTM techniques rely on a baseband component, regenerated at the receiver to recover information. Depending upon the sampling ratio, side tones around the carrier fundamental can enter the baseband region, introducing baseband distortion (BD). The distortion levels in the recovered signal can be determined by the spectral profile of the PTM signal employed in signal demodulation. For PFM the BD level, defined as the ratio between the peak sidetone in the baseband region and the recovered baseband signal amplitude, when modulated by a single tone of frequency  $f_m$ , can be given as [75]:

$$BD_{PFM} = \frac{2J_k(M) \sin[\pi(f_c + f_m)\tau]}{\pi f_m M \tau} \quad (4.1)$$

where  $M$  is the modulation index,  $f_c$  is the carrier frequency and  $\tau$  is the pulse width and  $J_k(\cdot)$  is the Bessel function of the first kind, order  $k$ .

Similarly, for a double edge regenerated SWFM signal the BD is given as [75]:

$$BD_{SWFM} = \frac{J_k(2M) \sin[\pi(2f_c + f_m)\tau]}{\pi f_m M \tau} \quad (4.2)$$

Repeating the analysis for PWM and narrow pulse PPM, the BD can be expressed as [16]:

$$BD_{PWM/PPM} = \frac{2J_k(\pi M)}{\pi M} \quad (4.3)$$

Figure 4.13 shows the sampling ratio requirements for different PTM techniques, calculated using Eqns. (4.1) to (4.3). Each curve is defined for a BD level of -40 dB, and can be used to allocate the modulation index and sampling ratio for the various modulation techniques. It can be seen that the lowest sampling ratio requirements are for SWFM, followed by PFM. Both PWM and PPM require comparably higher sampling ratios to achieve the same level of distortion.

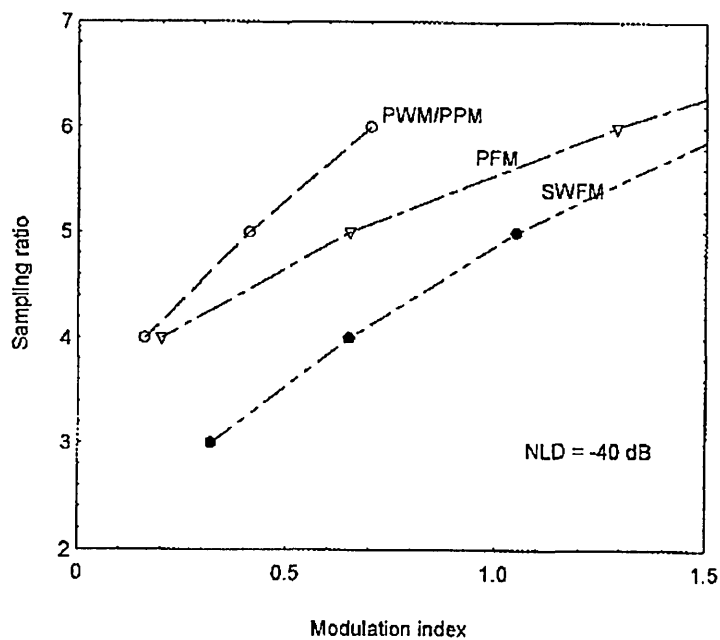


Figure 4.13 Sampling ratio vs. modulation index for a BD level of -40 dB.

The improvement factor (IF) of a modulation technique is the difference between the recovered SNR and the carrier-to-noise ratio (CNR) at the input of the demodulator, expressed in dB units. In communication systems, an optimum modulation technique is one which delivers a high SNR for a low CNR, without compromising other system parameters. As all PTM techniques rely on a time-amplitude conversion to recover information, jitter noise determines system performance. However, if the CNR at the demodulator is lowered too much, impulse noise begins to dominate system performance. The CNR, below which impulse noise begins to dominate, represents a threshold value in PTM SNR performance and is around 20 dB for most PTM systems [80].

For PTM systems operating above the noise threshold value, the IF factor is proportional to the square of the ratio of channel bandwidth to carrier frequency, when peak signal

power is considered in the SNR expressions. The constant of proportionality is slightly different for each of the PTM techniques and is listed below for pulses of raised cosine shape [16]:

$$\text{PWM} \quad IF = \frac{\pi^2}{8} \left( \frac{MB_t}{f_c} \right)^2 \quad (4.4)$$

$$\text{PPM} \quad IF = \frac{\pi^2}{4} \left( \frac{MB_t}{f_c} \right)^2 \quad (4.5)$$

$$\text{PFM} \quad IF = \frac{3}{4} \left( \frac{MB_t}{f_c} \right)^2 \quad (4.6)$$

$$\text{SWFM} \quad IF = \frac{3}{2} \left( \frac{MB_t}{f_c} \right)^2 \quad (4.7)$$

#### 4.4 SCM-PTM Concept

In section 4.2 some of the characteristics desired of a second stage modulator were outlined. The ability to deliver high SNRs, bandwidth efficiency, low overall cost and immunity to laser nonlinearities were identified as some of these characteristics. Second stage modulators employing digital PCM and analogue FM modulation, and their performance potential were investigated in sections 4.2.1 and 4.2.2, respectively. The PCM system can deliver high SNRs, but is limited in applications due to complexity and cost. On the other hand FM technique is simple and low cost but, its noise and nonlinear performance is limited.

In section 4.3.1 the concept of PTM was introduced and its advantages over other modulation techniques were listed. The simplicity, low cost and its ability to trade-off system performance against transmission bandwidth makes PTM an ideal candidate for a

second stage modulator in SCM systems. The pulse format of the PTM signals also has a number of beneficial consequences from the stand-point of opto-electronic subsystem specification.

A PTM modulator incorporated as a second stage modulator in a SCM system is illustrated in Fig. 4.14. The performance potential of different PTM techniques were considered in section 4.3.4. It was shown that PIM and PIWM techniques are considerably more complex compared to other PTM techniques, without any added performance gain. It will also be shown in Chapter 6 that PWM is an inefficient technique as it carries a considerable amount of power which conveys no information. Therefore, the above techniques are not considered further in this work. The following two chapters deal with PFM, SWFM and PPM techniques, in the context of a second stage SCM system.

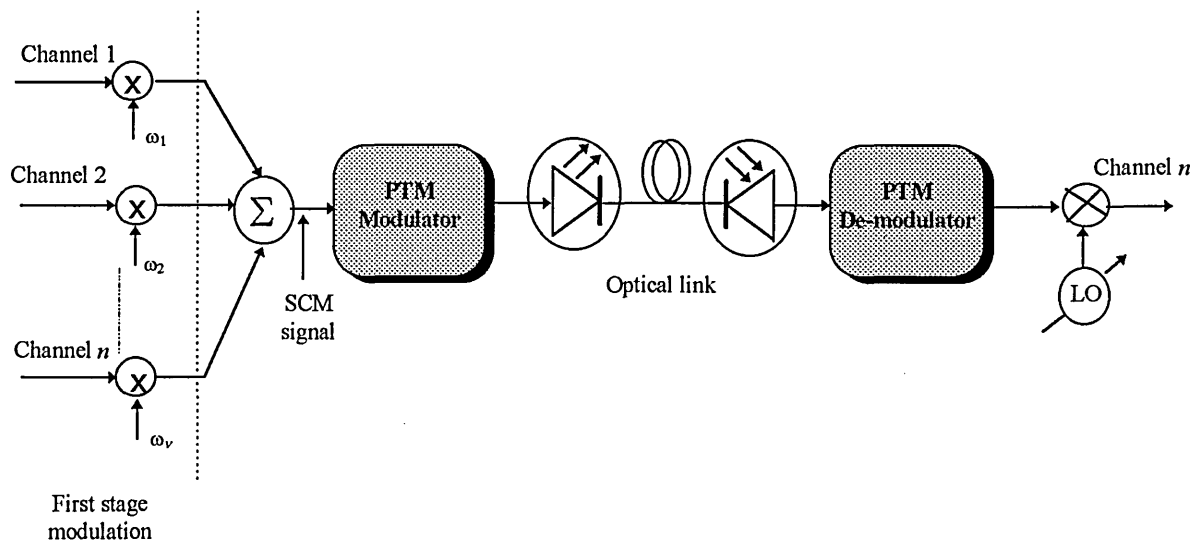


Figure 4.14 PTM as a second stage modulator in a SCM system.

## 4.5 Summary

In this chapter the concept of a second stage modulator, to improve the performance of a SCM system, was introduced. Implementation and performance of several second stage modulator systems, incorporating digital PCM and analogue FM modulation, were presented. The concept of PTM, an intermediary modulation technique, was introduced. Different PTM techniques, their spectral characteristics and performance were also presented. The low cost, simplicity, bandwidth to signal performance trade-off and its ability to exploit the high bandwidth available on optical fibres makes PTM an ideal candidate for a second stage modulator in SCM systems.

---

# Pulse Frequency Modulation and Square Wave Frequency Modulation Systems

## 5.1 Introduction

Pulse frequency modulation (PFM) and square wave frequency modulation (SWFM) are anisochronous PTM techniques which can deliver adequate signal performance for transmission over small and moderate distances [80]. Both modulation schemes are closely related to each other as well as to conventional FM systems. PFM and SWFM can be implemented using simple digital circuitry offering low cost and simplicity. The signal to noise ratio (SNR) performance can be traded-off for transmission bandwidth and therefore are particularly suited for wideband channels such as optical fibres.

Since PFM and SWFM have similar characteristics they are considered together in this chapter. Modulation and demodulation techniques and the characteristic of the frequency spectra are considered in sections 5.2 and 5.3 respectively.

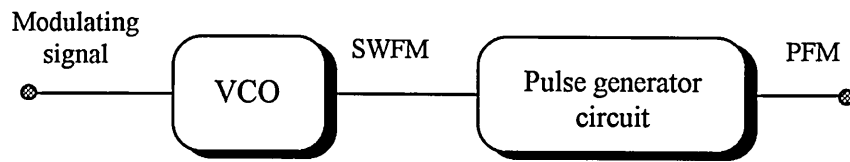
SNR is a primary performance indicator of any communication system. Therefore, in section 5.4, the SNR of PFM and SWFM are derived from the first principles and expressed for different pulse models. The threshold effect of frequency modulated systems is also discussed.

In order to optimise system performance the parameters upon which the SNR is dependent must be optimised. In the final section of this chapter the parameters and their optimisation, in the context of a SCM system, is presented.

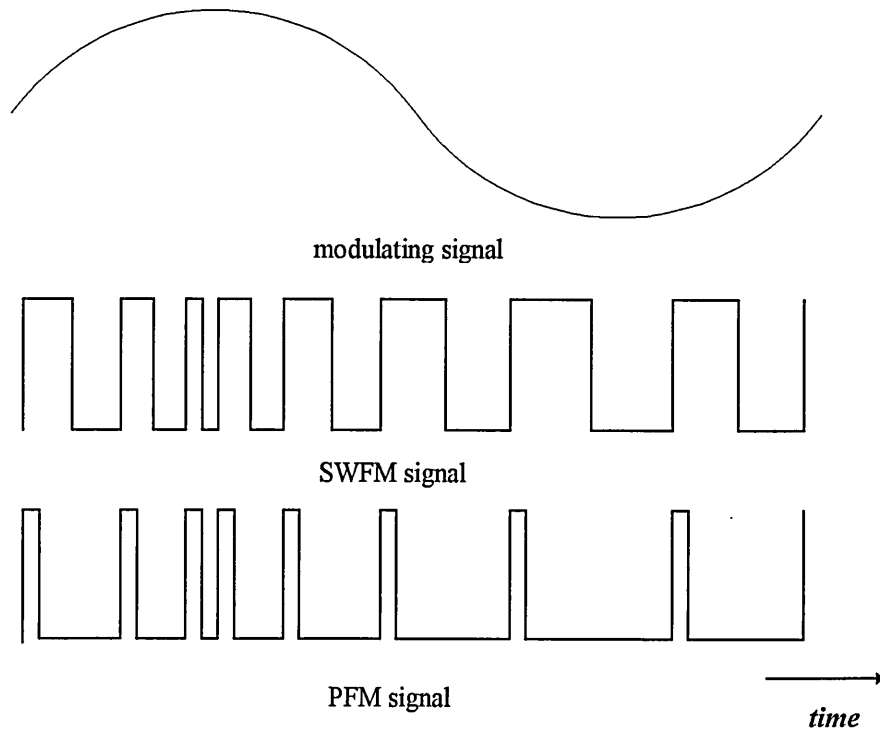
## **5.2 PFM and SWFM Modulation**

In PFM, the instantaneous frequency of a constant amplitude pulse train, having a fixed pulse width, is varied according to the modulating signal. In SWFM the carrier signal is a square wave of fixed duty cycle (approximately 50%) and the modulated signal is essentially a series of square wave edge transitions occurring at the zero crossing points of a sine wave FM signal [81].

SWFM can be conveniently and simply generated by driving the input of a square wave output VCO with the modulating signal. Alternatively a sine wave FM signal can be generated first and then passed through a voltage comparator to convert it into a SWFM signal. A PFM signal can be generated by feeding the SWFM signal into a pulse generating circuit such as a monostable. Below carrier frequencies of 30 MHz, standard VCOs from the TTL logic family are suitable for signal generation, but above this frequency emitter coupled logic (ECL) devices become increasingly necessary [16]. PFM and SWFM signal generation and the time domain waveforms are illustrated in Fig. 5.1.



(a) block diagram



(b) signals in the time domain

Figure 5.1 PFM and SWFM modulation.

By representing the change in repetition of the pulses through the phase change at pulse edges, PFM and SWFM signals can be represented in the time domain by Eqns. (5.1) and (5.2), respectively [82].

$$f(t) = A \sum_{n=-\infty}^{\infty} \frac{1}{2\pi j n} \left\{ \begin{array}{l} \exp \left[ jn \left( \frac{\omega_c \tau}{2} + 2\pi \Delta f \int x(y) dy \right) \right] \\ - \exp \left[ -jn \left( \frac{\omega_c \tau}{2} - 2\pi \Delta f \int x(y) dy \right) \right] \end{array} \right\} \exp(jn \omega_c t) \quad (5.1)$$

$$f(t) = AD \sum_{n=-\infty}^{\infty} \text{Sinc}(n\pi D) \exp \left[ jn \left( \omega_c t + 2\pi \Delta f \int x(y) dy \right) \right] \quad (5.2)$$

Here  $x(y)$  is the normalised modulating signal,  $A$  is the carrier amplitude,  $\omega_c$  is the carrier frequency,  $\Delta f$  represent the maximum frequency deviation,  $\tau$  is the pulse width and  $D$  is the square wave duty cycle.

The depth of modulation is indicated by the parameter, modulation index. Assuming the modulating signal is band limited to  $f_m$  the modulation index for both PFM and SWFM is expressed as [82]:

$$\beta = \frac{\Delta f}{f_m} \quad (5.3)$$

### 5.3 PFM and SWFM Demodulation

In order to gain a better understanding of PFM and SWFM, their spectral characteristics must be studied. Since the derivation for a generalised modulating signal would be extremely difficult, it is prudent to derive the spectral characteristics for a single tone modulating signal and generalise the results.

The PFM spectrum for a series of pulses of width  $\tau$  and carrier frequency  $\omega_c$ , when modulated by a sine wave of frequency  $\omega_m$ , may be represented by [83]:

$$f(t) = \frac{A\omega_c\tau}{2\pi} \left\{ \begin{aligned} &1 + \frac{2\beta}{\omega_c\tau} \sin\left(\frac{\omega_m\tau}{2}\right) \cos\left(\omega_m t - \frac{\omega_m\tau}{2}\right) \\ &+ 2 \sum_{n=1}^{\infty} \sum_{k=-\infty}^{\infty} J_k(n\beta) \frac{\sin(n\omega_c + k\omega_m)\tau/2}{n\omega_c\tau/2} \cos\left[(n\omega_c + k\omega_m)t - k\omega_m\tau/2\right] \end{aligned} \right\} \quad (5.4)$$

Similarly, the expression for SWFM is [84]

$$f(t) = AD \sum_{n=1}^{\infty} \text{Sinc}(n\pi D) \sum_{k=-\infty}^{\infty} J_{|k|}(n\beta) \exp[j(n\omega_c + k\omega_m)t] \quad (5.5)$$

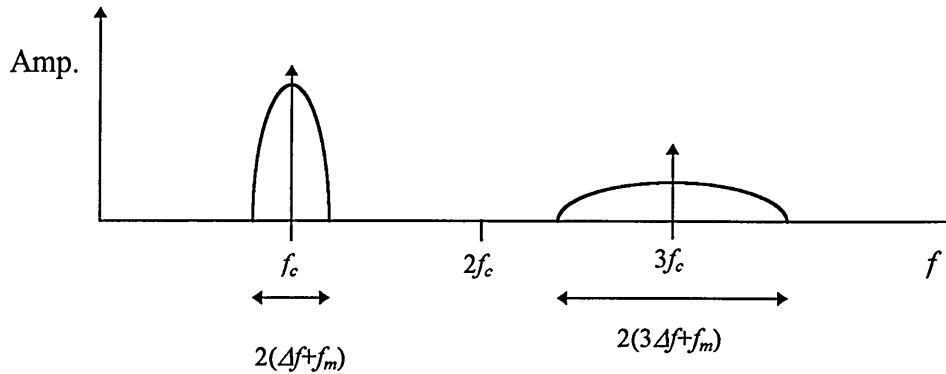
The spectra are plotted in Fig. 5.2 and the general characteristics attributed to PTM spectrums (section 4.3.3) can be identified. The presence of the baseband component in PFM signal indicate that information can be recovered directly from the PFM signal. The strength of the baseband presence is determined by the modulation index, carrier frequency, pulse width and the modulating frequency.

For a multi-tone modulating signal, the baseband frequency response depends on the relationship between the pulse width and the modulating signal. Provided that

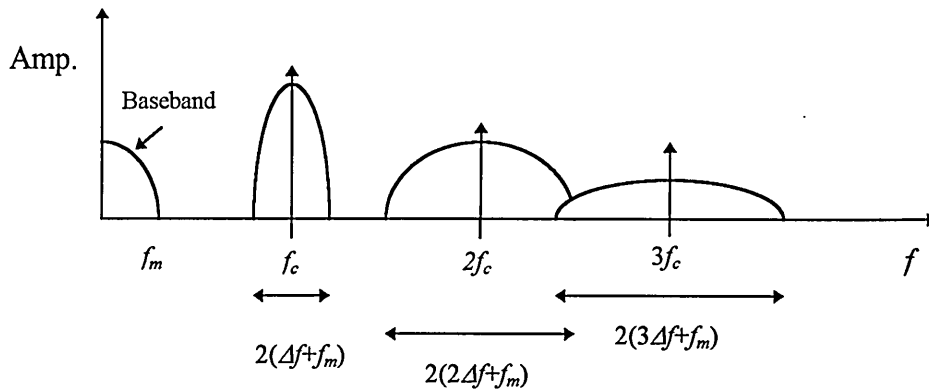
$$f_m \ll \frac{1}{\tau}$$

the original baseband signal will be present in the PFM signal without any amplitude distortion [82]. The sideband structure of the PFM signal is slightly asymmetric compared to conventional FM spectrum. However, Carson's rule [85] can still be used to give an upper limit of spectrum spreading.

The baseband component and the even carrier harmonics are not present in a SWFM signal, provided the square wave duty cycle is 50%. However, in practice the duty cycle tends to deviate slightly from the 50% value resulting in a small baseband and even harmonic presence [82].



(a) SWFM



(b) PFM

Figure 5.2 SWFM and PFM spectrum distribution.

The demodulation techniques of PFM and SWFM can be deduced from their spectral characteristics. Ordinary FM demodulation techniques may be adopted, locked on to the carrier or its harmonics using a phase locked loop (PLL). However, this approach usually

results in limited linearity and noise performance as a consequence of selecting only a restricted spectral slice. The presence of a distortionless baseband component indicate that information can be recovered directly from the PFM signal and baseband recovery is indeed the technique widely employed in PFM and SWFM demodulation [70].

The simplest form of demodulation would be to recover the baseband component directly from the incoming PFM signal. However, this technique generates poor SNR performance as both leading and trailing edges of the PFM signal are affected by noise. Therefore, in PTM systems, the incoming signal is regenerated at the receiver before employing baseband recovery [81].

The PFM regenerator consists of a threshold detector and a constant width pulse generator. The incoming PFM or SWFM signal is passed through a threshold detector with a threshold crossing set at half the pulse amplitude for optimum pulse detection, as will be explained in section 5.4.2. The output of the threshold detector is fed to a monostable in order to trigger constant width pulses at the leading or lagging edge. The baseband component of the regenerated PFM signal can be recovered by employing a low pass filter (see Fig. 5.3).

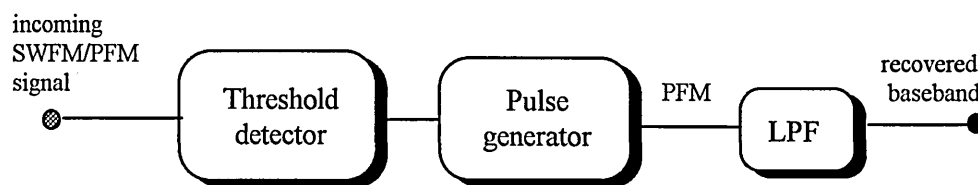


Figure 5.3 PFM and SWFM demodulation by baseband recovery.

The transmitted PFM pulse width is determined by the required level of signal performance and the available channel resources, as will be shown later in the chapter. It was stated earlier that one of the parameters which influence the strength of the baseband component present in a PFM signal, is the pulse width. Therefore, when employing baseband recovery technique, the width of the regenerated PFM pulse influences the recovered signal power level.

The baseband signal power at the output of the PFM regenerator can be optimised by choosing an optimum width for the regenerated pulse train. The relationship between baseband signal power and the regenerated pulse width can be determined by further examining the PFM spectral expression (Eqn. 5.4). Hence, the baseband signal power  $S_b$ , can be expressed as:

$$S_b = \left(\frac{A\beta}{\pi}\right)^2 \sin^2\left(\frac{\pi d}{R}\right) \quad (5.6)$$

where  $d$  is the duty cycle of the regenerated signal,  $R$  is the sampling ratio and other symbols are as defined before.

The above equation is plotted against  $d$ , for a range of  $R$  values, in Fig. 5.4. Here the baseband signal power is normalised to the amplitude of the carrier frequency and a  $\beta$  value of 1 is assumed. A parabolic increase can be identified for the baseband signal power as  $d$  increases. The baseband distortion level dictates the  $R$  value in PTM systems (see section 5.5) and therefore, for a chosen  $R$ , the baseband signal power is maximised by optimising the duty cycle of the regenerated PFM pulses.

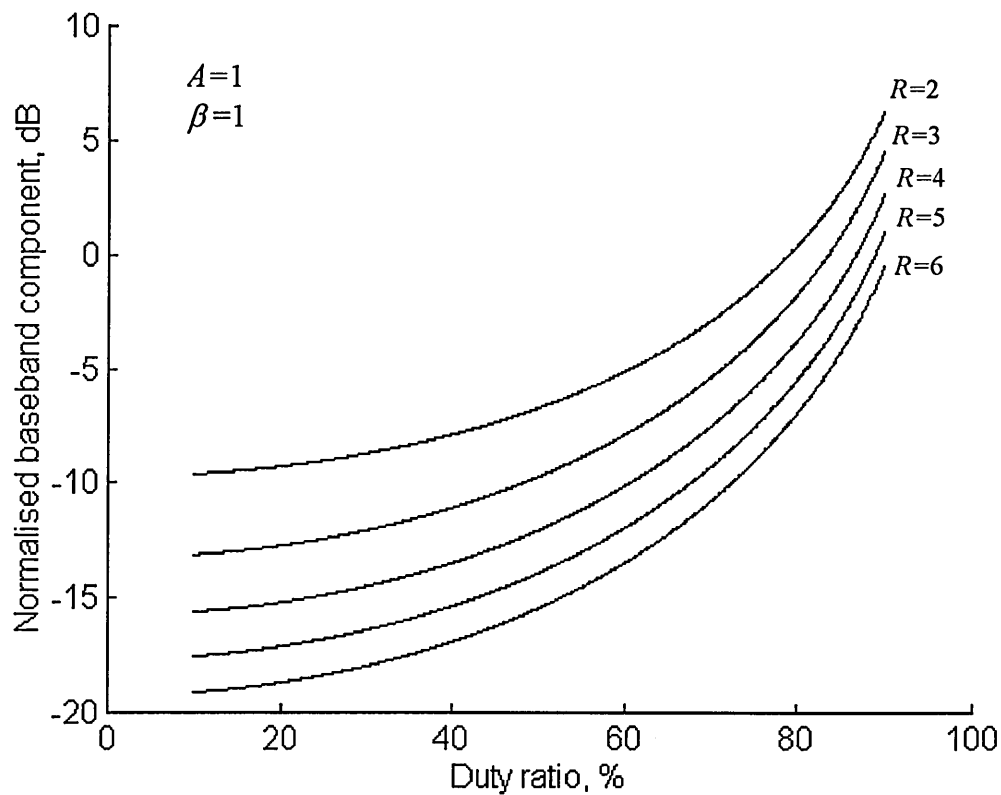
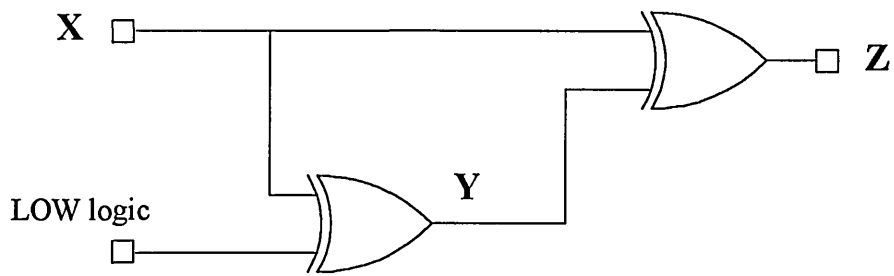
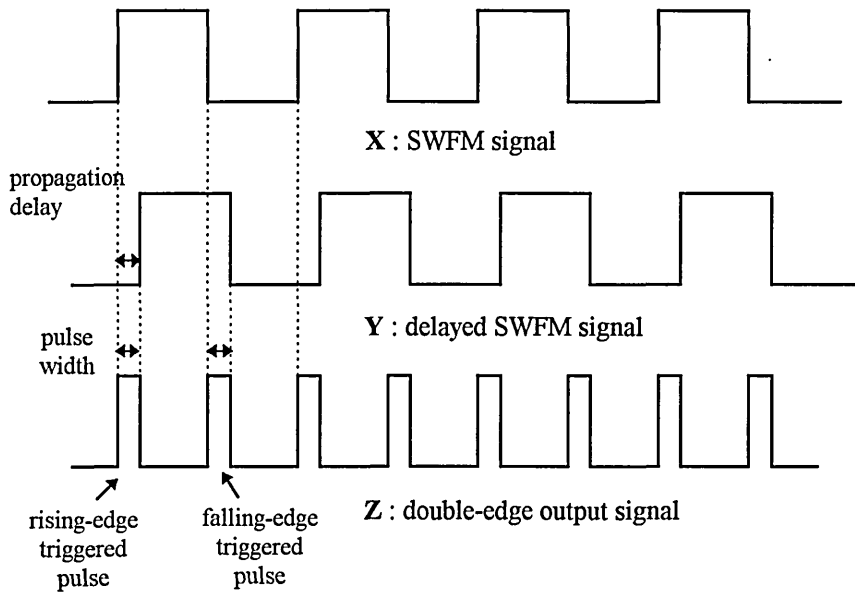


Figure 5.4 Baseband signal power variation in regenerated PFM signals.

In SWFM systems, it is also possible to generate pulses at both the leading and lagging edges of the SWFM signal, resulting in a 3 dB SNR improvement compared to single-edge detection technique [81]. The sampling ratio requirements are also lowered by nearly half, as will be explained in section 5.5.2. Practical circuit implementation of the double-edge demodulation is particularly simple using a number of EX-OR gates in a logic rectification and delay circuit. The logic circuit diagram and the associated signal waveforms are illustrated in Fig. 5.5, where pulses are generated at both the rising and falling edges of the SWFM signal. The pulse width is determined by the number of gates, and the propagation delay of each gate, included in the delay path [82].



(a) logic circuit diagram



(b) illustrated waveforms

Figure 5.5 SWFM double-edge demodulation.

## 5.4 Noise Analysis

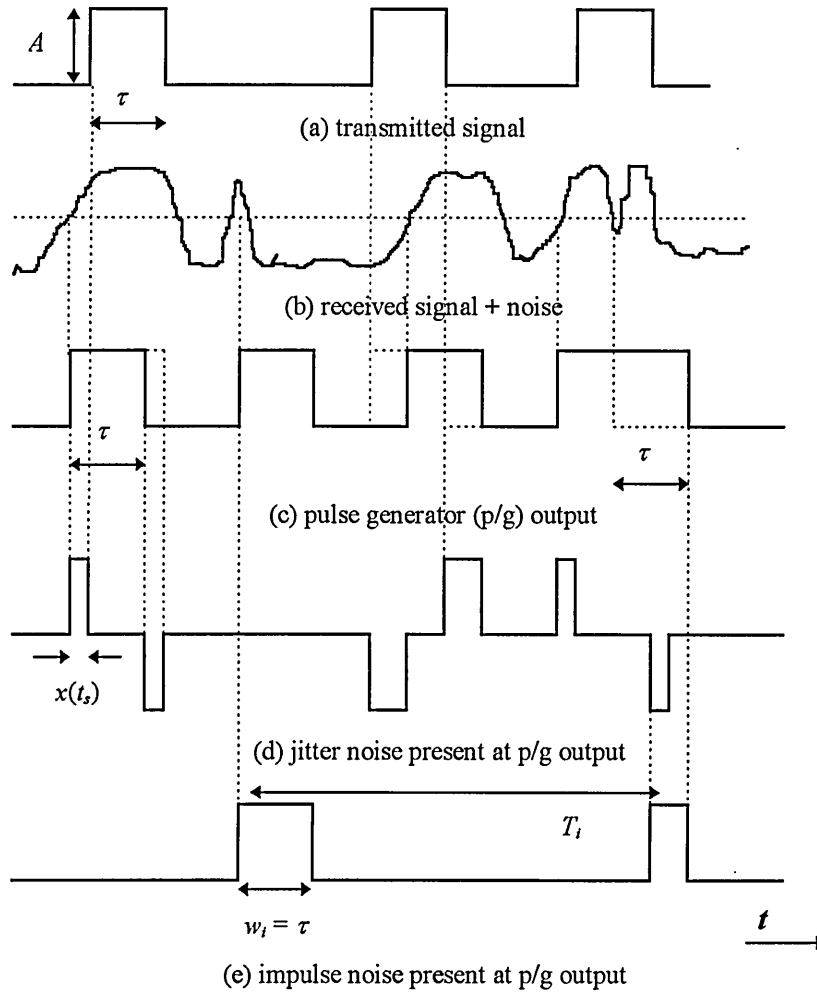
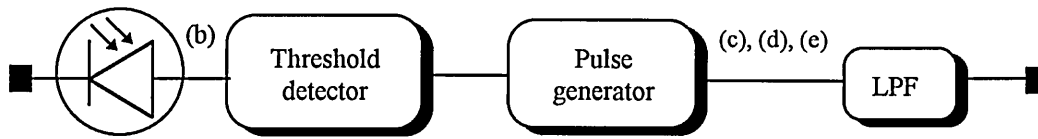
The performance of analogue communication systems are determined in terms of their ability to deliver adequate SNRs. In this section the SNR for PFM and SWFM are derived from the first principles. A number of pulse models, applicable to communication channels are employed in the derivation.

Figure 5.6 shows the effect of noise on the received PFM pulse train (the PFM receiver is repeated here, for clarity). As can be seen from this figure, there are two forms of noise which effect the performance of PFM systems. One is the noise imposed on the pulse edges which causes the signal to cross the threshold at the wrong time instant, causing time displacements in the recovered pulse signal. This is known as jitter noise or edge noise. The other noise source is the occasional noise impulses which cause the signal to cross the threshold erroneously, introducing pulse errors [80].

Hence, the SNR of a PTM system can be expressed as follows,

$$SNR = \frac{S}{n_{j(rms)} + n_{i(rms)}} \quad (5.7)$$

where  $S$  is signal power and  $n_{j(rms)}$  and  $n_{i(rms)}$  represent the rms noise power due to jitter noise and impulse noise, respectively. Typically the input SNR and the detection threshold of a PFM system are such that jitter noise determines the overall noise performance of the system. The situation when impulse noise power become close to jitter noise represents the SNR threshold and is discussed in section 5.4.4. The SNR expressions of section 5.4.2 are derived by assuming the signal operation is above the threshold level and therefore the noise performance is determined by jitter noise alone.



- $\tau$  = pulse width
- $A$  = pulse height
- $x(t_s)$  = pulse displacement
- $w_i$  = width of impulse noise pulses
- $T_i$  = interval between impulse noise pulses

Figure 5.6 Noise effect on PFM signal [80].

### 5.4.1 Jitter noise

When the SNR at the input of the PFM/SWFM demodulator is above a threshold value the output SNR performance is determined by the random jitter present in the PFM and SWFM pulses. The sources of random jitter can be identified as follows [82]:

- (a) jitter produced at the modulator, owing mainly to VCO frequency noise.
- (b) optical pulse jitter due to optical source response time variation.
- (c) jitter produced at the receiver during amplitude phase conversion.

In most systems, the jitter produced by (a) and (b) is insignificant, thus only source (c) is taken into account in the analysis. The random noise referred to throughout the analysis is assumed to be white Gaussian in nature.

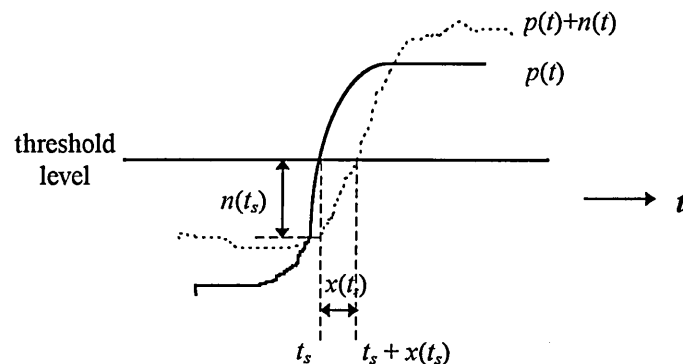


Figure 5.7 Time displacement due to jitter noise.

Figure 5.7 shows the effect of jitter noise on threshold crossings. The time displacement  $x(t_s)$  due to the noise  $n(t)$  can be expressed as

$$x(t_s) = - \frac{n(t)}{\dot{p}(t_s)} \quad (5.8)$$

where  $\dot{p}(t_s)$  represents the pulse slope at time  $t_s$ . For an unmodulated pulse train, the leading edge crosses the threshold periodically at

$$t = t_s + mT$$

where  $m$  is an integer and  $T$  is the pulse period. The pulse displacement at the leading edges can be represented by a train of impulses  $x_n(t)$ , where each impulse is co-incident with a threshold crossing and weighted by its displacement (see Fig. 5.8).

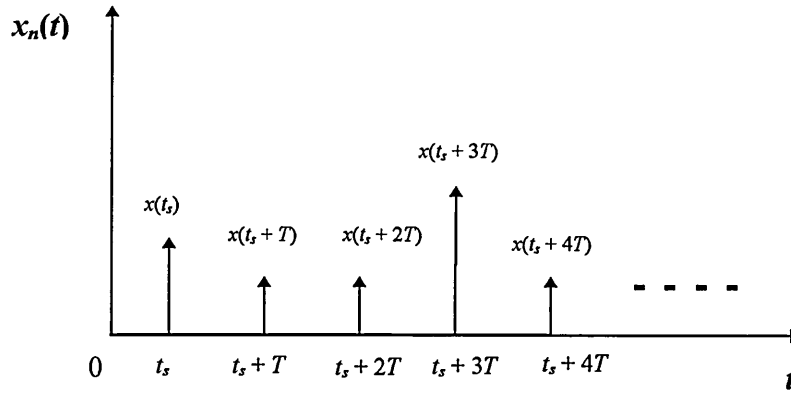


Figure 5.8 The error pulse train  $x_n(t)$ .

$$x_n(t) = \sum_{m=-\infty}^{\infty} x(t_s + mT) \delta(t - t_s - mT) \quad (5.9)$$

Combining Eqns. (5.8) and (5.9)

$$x_n(t) = -\frac{1}{\dot{p}(t_s)} \sum_{m=-\infty}^{\infty} n(t) \delta(t - t_s - mT) \quad (5.10)$$

Equation (5.10) shows that  $x_n(t)$  is a sampled version of the input noise, weighted by the inverse of the pulse slope  $\dot{p}(t_s)$ , and its double sided noise power spectral density is given as [86]:

$$X(f) = \left[ \frac{f_c}{\dot{p}(t_s)} \right]^2 \sum_{k=-\infty}^{\infty} N_i(f - kf_c) \quad (5.11)$$

where  $f_c$  is the carrier frequency and  $N_i(f)$  is the double sided input noise power spectral density.

The displacement of the PFM pulses due to jitter noise can be represented as a noise pulse  $y(t)$ , being added to the uncorrupted PFM pulse, to produce the displaced pulse as shown in Fig. 5.9. For PFM systems  $y(t)$  is defined as:

$$y(t) = \begin{cases} -A & 0 \leq t \leq x(t_s) \\ A & \tau \leq t \leq \tau + x(t_s) \end{cases} \quad (5.12)$$

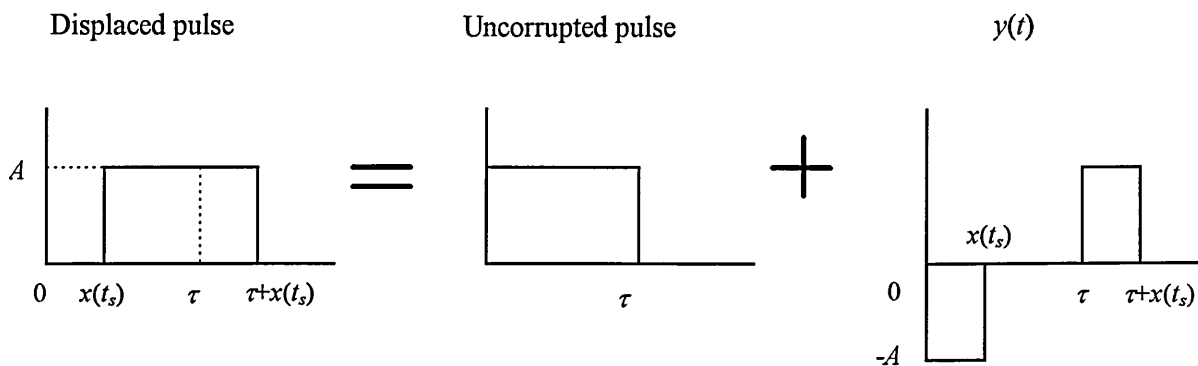


Figure 5.9 Pulse displacement due to noise pulse,  $y(t)$

Assuming  $x(t_s)$  is small for practical systems, the Fourier transform of  $y(t)$  is

$$Y(f) = Ax(t_s)[e^{-j2\pi f\tau} - 1] \quad (5.13)$$

$y(t)$  represents the noise added to the monostable output for a single pulse. Since the noise output is approximately independent of the modulating signal  $x(t)$  [87], and only frequencies passed by the lowpass filter are of interest, assuming

$$x(t) = 0$$

$$f \ll \frac{1}{\tau}$$

the power spectral density of the noise added to the monostable output due to the impulse train  $x_n(t)$ , can be expressed as :

$$N_o(f) = A^2(2\pi f\tau)^2 X(f) \quad (5.14)$$

Substituting for  $X(f)$ , the single sided noise power spectral density at the demodulator output can be expressed as [86]

$$N_{i'o}(f) = \left[ \frac{2\pi f_c \tau A}{\dot{p}(t_s)} f \right]^2 \left[ N_i'(f) + \sum_{k=1}^{\infty} \{N_i'(kf_c - f) + N_i'(kf_c + f)\} \right] \quad (5.15)$$

where  $N_i'(f)$  is the single sided noise power spectral density at the input of the threshold detector, and for a uniform response optical channel can be expressed as below [10]:

$$N_i'(f) = RIN(R_oGP_p)^2 + 2q(R_oP_p + I_d)G^2F(G) + \frac{4kT_{ab}}{R_L} \quad (5.16)$$

where the symbols are as defined in Eqn. (3.14).

#### 5.4.2 SNR expressions

The peak signal level  $v_p$  is produced by the maximum deviation  $\Delta f$  and the rms signal power  $S_{rms}$ , at the output of the PFM demodulator is equivalent to:

$$S_{rms} = \frac{v_p^2}{2} = \frac{(A\Delta f\tau)^2}{2} \quad (5.17)$$

As the PFM noise power is dependent on pulse slope, the shape of incoming pulses influence the SNR. The PFM pulses can be approximated by different pulse models, according to the applications. Three pulse models, which are good approximations to real world situations, have been employed in the derivation. The derived expressions are used to evaluate the optimum pulse model which can deliver a maximum SNR.

In digital systems, the bit errors due to false alarm and erasure errors are minimised by a threshold set at half the bit amplitude. Similarly in PTM systems, pulse errors due to the signal crossing the threshold erroneously, can be minimised by a threshold level set at

half the pulse amplitude. Therefore an optimum threshold level of  $A/2$  is assumed throughout the analysis.

#### 5.4.2.1 Raised cosine model

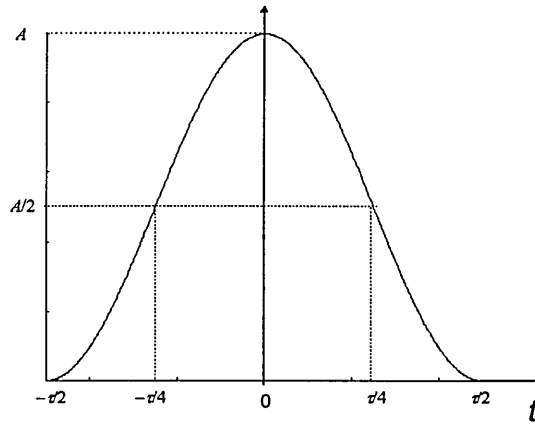


Figure 5.10 Time domain representation of a raised cosine pulse.

Raised cosine pulses, illustrated in Fig. 5.10, are widely deployed in communication systems and therefore, is appropriate to represent the PFM pulses. A raised cosine pulse in the time domain can be expressed as:

$$p(t) = A \cos^2\left(\frac{\pi t}{\tau}\right) \quad (5.18)$$

where  $A$  is the pulse height and  $\tau$  is the end-end pulse width. The pulse slope  $\dot{p}(t_s)$  at the threshold crossing is:

$$\dot{p}(t_s) = \frac{A\pi}{\tau} \quad (5.19)$$

By substituting for  $\dot{p}(t_s)$  in Eqn. (5.15), the rms noise power at the demodulator output  $N_{o(rms)}$ , can be expressed as

$$N_{o(rms)} = \frac{1}{3} \left( \frac{2\pi f_c \tau^2}{\pi} \right)^2 f_m^2 N_{i(rms)} \quad (5.20)$$

Using Eqns. (5.17) and (5.20) the rms signal to rms noise power ratio can be expressed in terms of the peak received optical power  $P_p$ , as:

$$SNR_{rms} = \frac{3}{8} \left( \frac{\beta}{f_c \tau} \right)^2 \frac{(R_o GP_p)^2}{N_{i(rms)}} \quad (5.21)$$

where the product  $R_o GP_p$  represent the pulse height,  $A$ .

An expression in terms of the average received optical power  $P_{av}$ , can prove useful as sometimes the optical power measurements are given as an average quantity. For a pulse train of width  $\tau$  and period  $T$ , the pulse height can be expressed as [88]:

$$A = \frac{R_o GP_{av} 2T}{\tau} \quad (5.22)$$

where rest of the symbols are as defined previously. Combining the above equation and Eqns. (5.17) and (5.20), the PFM SNR expression can be re-written in terms of average received optical power as:

$$SNR_{rms} = \frac{3}{2} \beta^2 \left( \frac{1}{f_c \tau} \right)^4 \frac{(R_o GP_{av})^2}{N_{i(rms)}} \quad (5.23)$$

#### 5.4.2.2 *Gaussian / exponential model*

The pulse nature of PFM makes it particularly attractive for optical communication. During optical transmission pulses are dispersed, and for most practical systems can be approximated by either a Gaussian or an exponential pulse model.

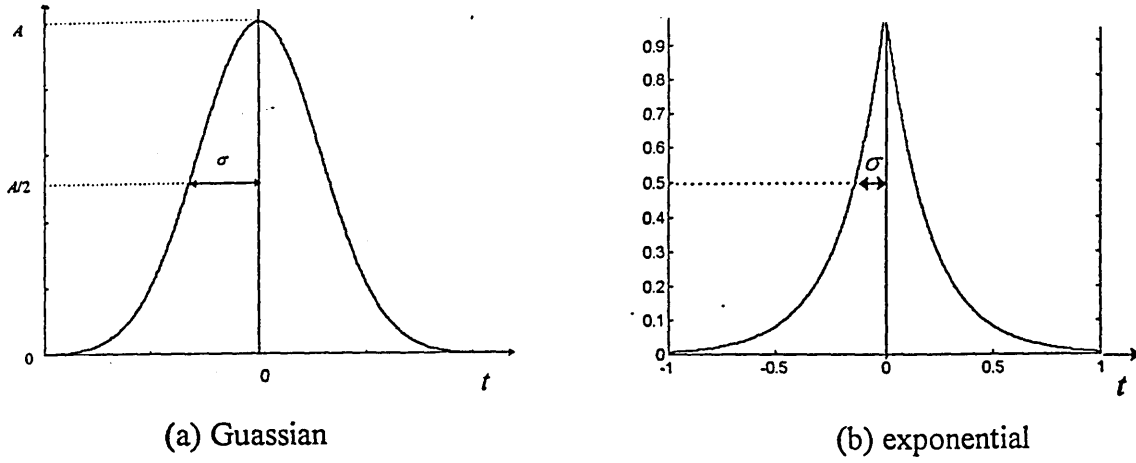


Figure 5.11 Pulse models in optical fibre transmission.

A Gaussian and an exponential pulse are shown in Fig. 5.11(a) and 5.11(b), respectively.

A Gaussian pulse of pulse width  $\sigma$ , defined to the half amplitude point, can be expressed in the time domain as:

$$p(t) = A \exp\left(\frac{-t^2}{2\sigma^2}\right) \quad (5.24)$$

Similarly, for an exponential pulse:

$$p(t) = \exp\left(\frac{-t}{\sigma}\right) \quad (5.25)$$

For both models  $\dot{p}(t_s)$  at the half amplitude point can be represented as:

$$\dot{p}(t_s) = \frac{6A}{5\sigma} \quad (5.26)$$

As before, substituting for  $\dot{p}(t_s)$  in Eqn. (5.15), the expression for  $N_{o(rms)}$  is:

$$N_{o(rms)} = \frac{1}{3} \left( \frac{5\pi f_c \sigma^2}{3} \right)^2 f_m^2 N_{i(rms)} \quad (5.27)$$

Combining Eqns. (5.17) and (5.27), the rms signal to rms noise power ratio when the PFM pulses are assumed to be Gaussian or exponential shaped, is derived to be:

$$SNR_{rms} = \frac{3}{2} \left( \frac{3\beta}{5\pi f_c \sigma} \right)^2 \frac{(R_o G P_p)^2}{N_{i(rms)}} \quad (5.28)$$

where the symbols are as defined previously. Following the procedure in the previous section, the SNR in terms of average received optical power  $P_{av}$ , is:

$$SNR_{rms} = \frac{54}{25} \beta^2 \left( \frac{1}{f_c \tau} \right)^4 \frac{(R_o G P_{av})^2}{N_{i(rms)}} \quad (5.29)$$

#### 5.4.2.3 Trapezoidal model

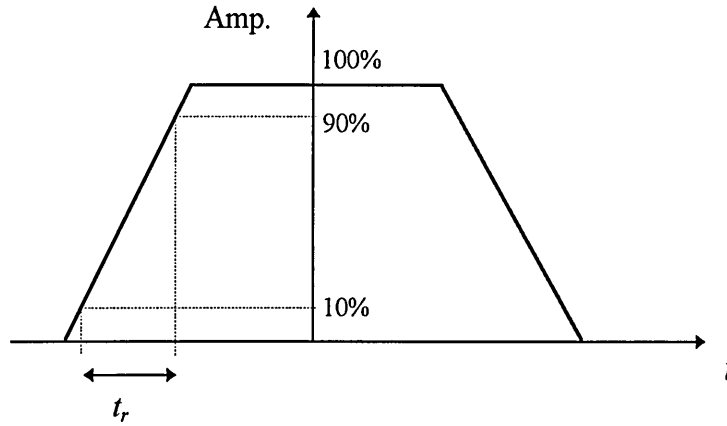


Figure 5.12 A trapezoidal pulse representation in the time domain.

A trapezoidal pulse model is shown in Fig. 5.12. It is a piece-wise linear approximation to PFM pulses and represents a simple mathematical model for the derivation of SNR. Defining the rise time,  $t_r$ , of the pulse as the time taken for the signal to rise from 10-90% of the peak amplitude, the pulse slope  $\dot{p}(t_s)$  is

$$\dot{p}(t_s) = \frac{4A}{5t_r} \quad (5.30)$$

Substituting for the pulse slope in Eqn. (5.15), the rms noise power at the output of the demodulator is

$$N_{o(rms)} = \frac{1}{3} \left( \frac{5\pi f_c \tau t_r}{2} \right)^2 f_m^2 N_{i(rms)} \quad (5.31)$$

The rms signal to rms noise power ratio for a trapezoidal model, where peak optical power is considered, can be derived by combining Eqns. (5.17) and (5.31), yielding,

$$SNR_{rms} = 6 \left( \frac{\beta}{5\pi f_c t_r} \right)^2 \frac{(RP_p)^2}{N_{i(rms)}} \quad (5.32)$$

The electrical 3 dB bandwidth and system rise time are inversely related. For linear systems, the relationship can be approximated by Eqn. (5.33) and can be used as a conservative guideline in optical systems [10].

$$B_t = \frac{0.35}{t_r} \quad (5.33)$$

Therefore, rms SNR can be re-written in terms of transmission bandwidth as:

$$SNR_{rms} = \frac{192}{49\pi^2} \left( \frac{\beta B_t}{f_c} \right) \frac{(RP_p)^2}{N_{i(rms)}} \quad (5.34)$$

As in PFM systems, the amplitude noise of SWFM pulses at the threshold crossing is converted into time jitter of the constant width pulses produced at the demodulator. When amplitude noise added to the SWFM signal is white Gaussian, and the rate of change of the signal at threshold crossing can be represented by the derivatives of the pulse models employed above, the output noise power spectral density is equivalent to PFM systems. Since SWFM demodulation is achieved by generating a PFM signal and recovering the baseband, the rms signal power at the output of the SWFM demodulator is also equivalent to Eqn. (5.17). Hence the SNR expressions derived for PFM is also valid for SWFM systems, provided the above conditions are satisfied.

The SNR of SWFM systems employing double-edge detection, differs from PFM and single-edge SWFM systems due to increased signal power. Assuming the slope of the

SWFM signal for both rising and falling edges is the same, the rms noise power increases by twofold, compared to PFM and single-edge systems. However, this is offset by a fourfold increase in signal power, resulting in an overall 3 dB improvement in SNR, compared to PFM and single-edge detection systems.

### 5.4.3 Performance comparison of the SNR expressions

The energy distribution of PFM signals indicate that approximately 98% of the signal energy is contained within a bandwidth corresponding to the inverse of the PFM pulse width  $\tau$ , see section 5.5.3. Therefore, assuming the transmission bandwidth  $B_t$ , is limited to  $1/\tau$  in the raised cosine and Gaussian models, and representing the carrier-to-noise ratio term in each equation by the symbol  $CNR$ , the SNR expressions derived in terms of peak optical power  $P_p$ , are summarised below.

$$\text{Raised cosine} \quad SNR_{rms} = \frac{3}{8} \left( \frac{\beta B_t}{f_c} \right)^2 CNR \quad (5.35)$$

$$\text{Gaussian/Exponential} \quad SNR_{rms} = \frac{108}{25\pi^2} \left( \frac{\beta B_t}{f_c} \right)^2 CNR \quad (5.36)$$

$$\text{Trapezoidal} \quad SNR_{rms} = \frac{192}{49\pi^2} \left( \frac{\beta B_t}{f_c} \right) CNR \quad (5.37)$$

As described before, the performance potential of a modulation technique is evaluated in terms of the SNR that can be delivered for a given CNR. To provide an illustrative comparison, the SNR versus CNR relationship for the three pulse models are shown in Fig. 5.13. A  $\beta$  value of 1 and a  $B_t/f_c$  ratio of 10, which provides a baseband distortion level of better than -45 dB, are assumed in the calculations [89]. The performance of ordinary FM is also shown for reference.

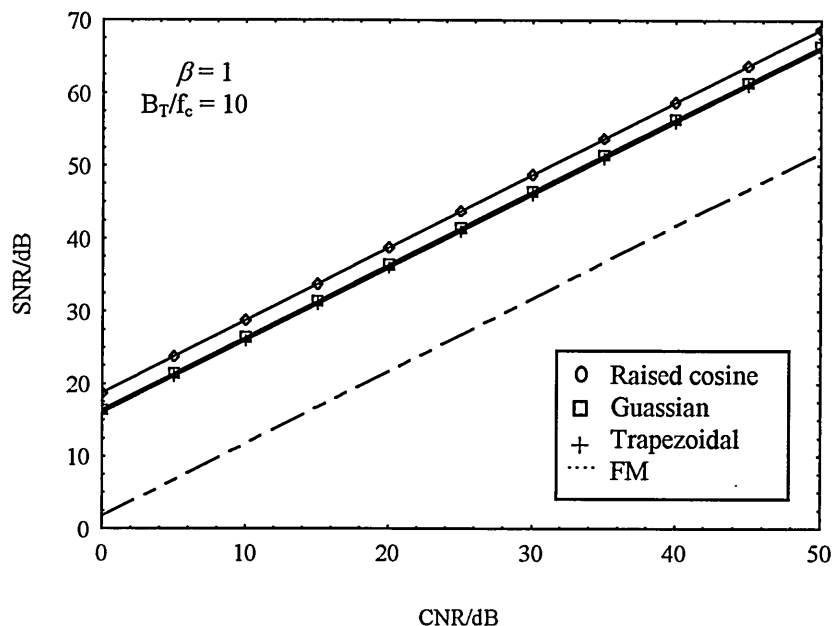


Figure 5.13 SNR vs. CNR for different pulse shapes in PFM systems [89].

The above figure illustrates that for Gaussian, exponential and trapezoidal pulses the SNR is almost equal for a given CNR, while raised cosine pulses offer approximately 3 dB improvement. The pulses in optical transmission systems are best approximated by a Gaussian or an exponential model. Therefore, a raised cosine filter must be employed after the optical receiver in order to achieve an optimum SNR level.

It can be recalled that the above noise analysis was carried out for additive white Gaussian noise, and signal dependent noise in fibre optic systems is not Gaussian. However, it has been demonstrated that Gaussian approximation gives a reasonably good estimate of a receiver performance. The optimum detection point for signal dependent noise systems could also differ from the  $A/2$  position [80].

#### 5.4.4 Threshold analysis

As described at the beginning of section 5.4, the occasional noise impulses can cause the PFM signal to cross the threshold erroneously, introducing pulse errors in the regenerated signal. Impulse noise becomes significant when the SNR at the input of the PFM demodulator falls below a threshold value, resulting in a rapid deterioration of the SNR at the system output. The analysis in section 5.4.1 was carried out assuming the input SNR is above the threshold value, so that the noise performance is determined by jitter noise alone. Although this corresponds to typical operating conditions found in PFM systems, knowledge of the threshold is important for evaluation of the operating range of a system. In this section the behaviour of the SNR threshold is investigated.

According to **Durakev** [80], the power spectral density of an impulse noise waveform, represented by a train of pulses of amplitude  $A$ , average pulse width  $\overline{w^2}$  and an average time interval  $\overline{T_i}$ , can be written as follows.

$$N_{im}(f) = \frac{A^2 \overline{w^2}}{\overline{T_i}} \quad (5.38)$$

Assuming signal independent white Gaussian noise and a trapezoidal pulse model, the SNR performance due to the presence of impulse noise alone, can be characterised by the following equation,

$$SNR_{im} = \frac{1}{1 + \frac{\sqrt{3}}{4\pi^2} \left( \frac{\overline{w^2}}{\tau^2} \right) \left( \frac{B_t}{f_c f_m^2 t_r^2} \right) CNR \exp(-CNR/8)} \quad (5.39)$$

where the detection threshold is assumed to be at  $A/2$ ,  $CNR$  is the carrier signal to rms noise power ratio at the input of the demodulator, and the other symbols are as defined before.

Assuming a worst case impulse noise of  $\overline{w^2} = \tau^2$  and a rise time to bandwidth relationship of  $B_t = 0.35/t_r$ , Eqn. (5.39) can be re-written in the following form.

$$SNR_{im} = \frac{1}{1 + \frac{\sqrt{3}}{4\pi^2} \frac{B_t^3}{(0.35)^2 f_c f_m^2} CNR \exp(-CNR/8)} \quad (5.40)$$

The above equation can be combined with Eqn. (5.37) in order to determine the behaviour of the SNR threshold of PFM. The combined equation is shown below, where  $r$  is the ratio of  $B_t/f_c$  and  $R$  is the sampling ratio.

$$SNR_{rms/im} = \frac{192/49\pi^2 (\beta r)^2 CNR}{1 + \frac{\sqrt{3}}{4\pi^2} \frac{r^3}{(0.35)^2} R^2 CNR \exp(-CNR/8)} \quad (5.41)$$

The SNR at the demodulator output and the input CNR is plotted, using Eqn. (5.41), in Figure 5.14. A threshold value can be identified for the input CNR, below which the signal output starts to deteriorate very rapidly. The threshold value is close to 20 dB and is almost independent of different PFM system parameters, as shown for a range of  $r$  values.

## 5.5 System Optimisation

The system design is based upon the trade-offs between the performance and cost, where performance is measured in terms of noise, distortion and available bandwidth. The SNR expressions derived in section 5.4 show that the SNR is primarily determined by modulation index, transmission bandwidth and sampling ratio. Therefore, in order to maximise SNR, the above parameters must be optimised. Sections 5.5.1 to 5.5.3 deal with optimisation of these parameters.

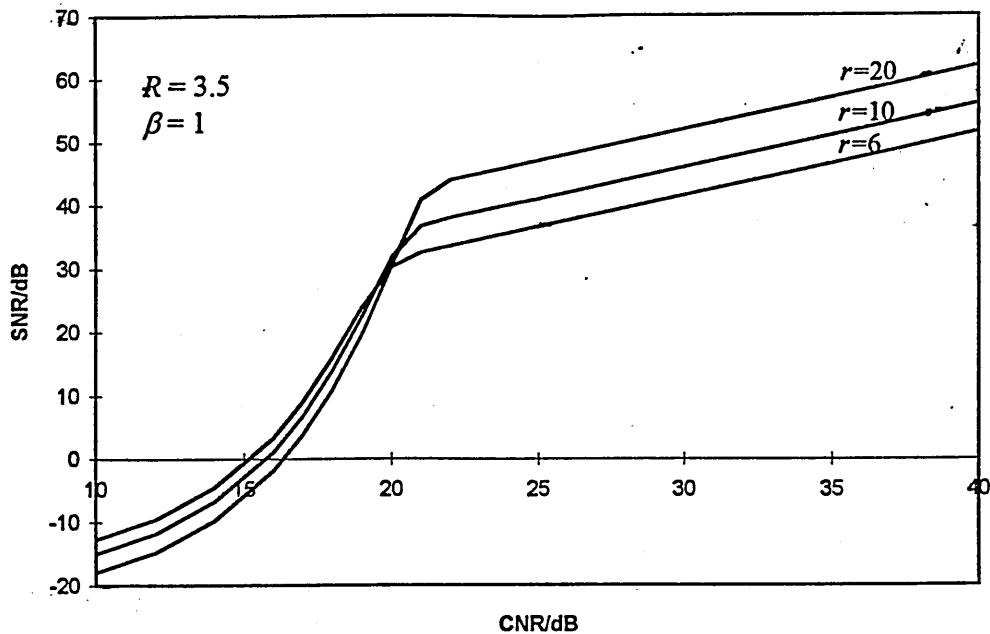


Figure 5.14 Input SNR threshold for PFM systems.

### 5.5.1 Non-linear distortion

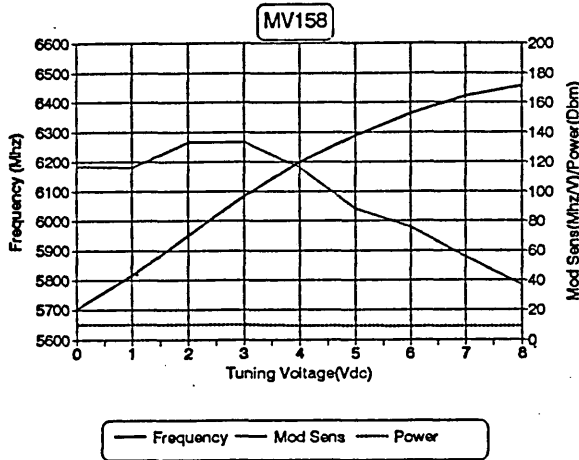
The pulse format of PTM signals render them immune to optical source and channel nonlinearities. Thus, system linearity in PTM schemes is determined by the electronic circuitry associated with signal modulation and demodulation. In PFM and SWFM systems, two factors contribute towards nonlinear distortion. One is the nonlinear voltage-to-frequency conversion characteristic of the VCO and the second is the duty cycle variation of the carrier waveform at different frequencies, resulting in a degree of phase modulation [82].

Typically the nonlinear characteristic of the VCO dominates distortion performance. A typical voltage-to-frequency conversion characteristic for a commercially available VCO is shown in Fig. 5.15.

**GUARANTEED MINIMUM PERFORMANCE DATA**

Linear tuning range:	5900 - 6400 MHz	Frequency Pulling (20 dB rtn):	35 MHz
Control Voltage (max):	1 to 10 Vdc	Frequency Drift (Typ):	400 KHz / C
Power Output (min):	+ 7 dBm	Temperature Range:	-20 to +70 C
Input Power (Vdc):	11 @ 22 mA	Power vs. Temperature (Typ):	0.015 dB / C
Harmonics (worst case):	-20 dBc	FM Noise, 100 KHz - dBc/Hz:	-100
Frequency Pushing:	8 MHz / V	FM Noise, 10 KHz - dBc/Hz:	-75

**Typical Frequency / Mod Sens / Power VS Tuning Voltage**



**Typical Phase Noise**

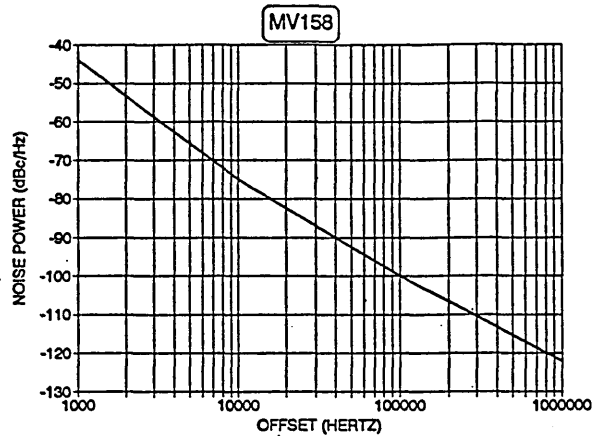


Figure 5.15 Typical voltage-to-frequency conversion characteristic of a commercially available VCO [90].

The transfer characteristic of the VCO can be modelled by a polynomial similar to the one used to model the intrinsic nonlinearity of a laser diode, Eqn. (3.7). When operated beyond the linear region, harmonic distortion (HD) and intermodulation distortion (IMD) results, but the latter is dominant since the input parameter is a frequency combined signal. The spectrum allocation, IMD categories and intermodulation product (IMP) estimations presented in section 3.2.3 are also equally applicable here.

When the number of subcarrier channels are small, the overall modulation index can be expressed as a linear quantity, as explained in section 3.2.1. In conventional SCM

systems operating with a large number of channels, laser clipping can severely limit the input dynamic range, restricting the transmission capacity (see section 3.2.4). A major advantage of the VCO, compared to the laser diode, is the absence of clipping. The overall modulation index for a SCM-PTM system operating more than 10 subcarrier channels, can be defined as a rms quantity,  $\beta_{rms}$ :

$$\beta_{rms} = \sqrt{\sum_{i=1}^N \beta_i^2} \quad (5.42)$$

where  $\beta_i$  is the modulation index per channel and  $N$  is the number of channels.

The transmission capacity of the system is determined by the input dynamic range of the modulator, in this case the VCO, and the  $\beta$  value allocated to each channel. Obviously, the highest SNRs for each channel are obtained by allocating a high  $\beta_i$  value. However, the signal power gains due to larger  $\beta_i$  values can be offset by increased nonlinear distortion, as explained in section 3.5.2. An optimum  $\beta_i$  value can be allocated for each channel according to the input dynamic range of the VCO and the required system capacity. Assuming a  $\beta$  value of unity for each channel and an incoherent signal addition, the VCO in Fig. 5.15 has the capacity to transmit 6944 AM-VSB television channels.

### 5.5.2 Sampling ratio

Minimisation of the carrier frequency leads to an optimum SNR value as indicated by the SNR expressions for PFM and SWFM. However, as indicated in Chapter 4, for a given value of  $\beta$  there is a lower limit for the sampling ratio (defined as the carrier frequency to modulating signal bandwidth ratio) below which, distortion due to the incursion of the lower sidetone components around the carrier fundamental into the baseband region,

becomes significant. Therefore, there exists a trade-off between the minimum sampling ratio and distortion within the baseband.

For PFM, the ratio of recovered signal component amplitude  $A_m$ , to the amplitude of the carrier sidetone  $A_k$ , for single tone modulation may be expressed as [74]:

$$A_m/A_k = \pi\Delta f\tau / \sin[\pi(f_c + kf_m)\tau] J_k(\beta) \quad (5.43)$$

where  $k = R-1$ ,  $R$  being the sampling ratio, and the rest of the symbols are as defined before.

In double-edge regeneration of SWFM, the sidetones are generated around the carrier second harmonic  $2f_c$ , with complete suppression of the spectral structure around the carrier fundamental, for a unity mark-to-space ratio carrier wave. All the odd harmonics are also suppressed due to the doubling of frequency, as shown in Fig. 5.16. Hence, the ratio of the recovered signal-to-sidetone level for SWFM, with double-edge pulse generation, may be written as [74]:

$$A_m/A_k = 2\pi\Delta f\tau / \sin[\pi(2f_c + kf_m)\tau] J_k(2\beta) \quad (5.44)$$

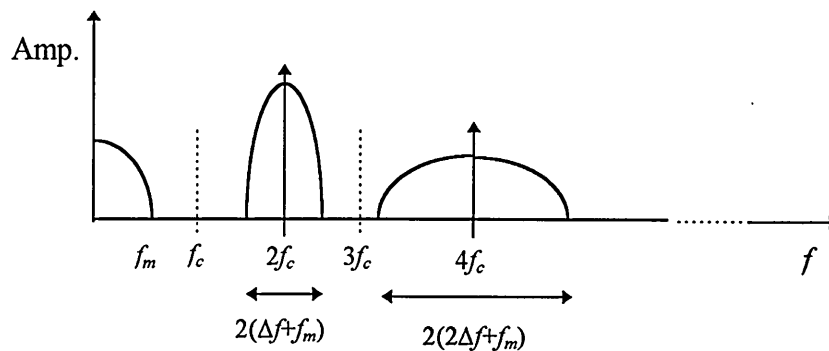


Figure 5.16 Spectrum produced by double-edge SWFM demodulator.

Wilson and Ghassemlooy [16] have evaluated the baseband distortion as a ratio of the peak recovered signal level to the peak sidetone level, inside the baseband, for different modulation indices and sampling ratios. The minimum required sampling for both PFM and SWFM is plotted for a range of distortion levels as function of modulation index in Fig. 5.17. It can be seen that for a modulation index of 1, PFM requires a sampling ratio in excess of 5 to achieve a baseband distortion level of -40 dB, while under the same conditions the sampling ratio requirement of SWFM is below 4. The superior performance of SWFM is due to the suppression of sidetones around the carrier fundamental and increase in the baseband signal level, due to double edge regeneration at the receiver.

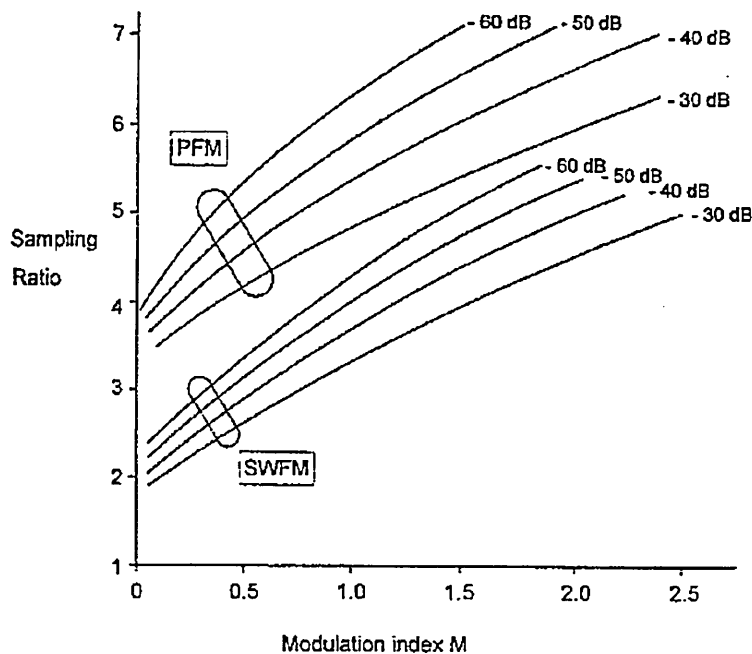


Figure 5.17 Sampling ratios for single tone modulated PFM and SWFM systems [84].

Since single-tone modulation is assumed in these calculations, if they are to be used in a SCM-PTM system, the following factors must be taken into account.

- a) the highest frequency component of the SCM signal, and the modulation index induced by that frequency component can be used to allocate the sampling ratio.
- b) identify any significant frequency components within the SCM signal and modulation index produced by such components. If the sampling ratio predicted for such frequencies is greater than the value predicted by (a), the former should be allocated as the sampling ratio.

It has also been shown that a minimum carrier frequency  $f_{cmin}$ , can be predicted by allowing for a guard band  $f_g$ , between the baseband component and the sidetones around the carrier fundamental [91]. As the sidebands around the carrier frequency is equivalent to a FM sideband structure, defining a deviation ratio  $D$ , as the ratio of overall frequency deviation to signal bandwidth  $f_m$ ,  $f_{cmin}$  can be deduced to be (see Fig. 5.18):

$$f_{cmin} = f_m + f_g + (D + 1)f_m \quad (5.45)$$

Hence, the minimum sampling ratio  $R_{min}$  is:

$$R_{min} = (2 + f_g/f_m) + D \quad (5.46)$$

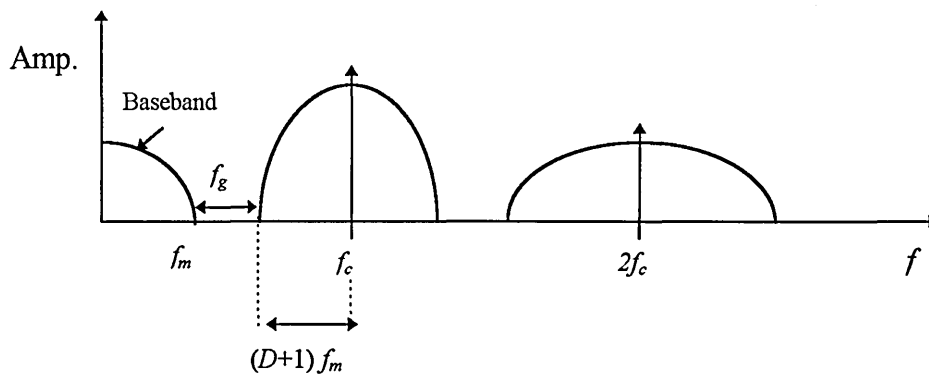


Figure 5.18 Minimum carrier frequency for PFM/SWFM systems.

For a given value of  $D$ , the baseband distortion increases, as the modulation bandwidth becomes greater and the guard band remains constant. Therefore, as indicated by Eqn. (5.46) the guard band should be allocated according to the  $f_m$  value. System measurements on  $R_{min}$  have shown that adequate system margin can be allowed for by choosing the guard band to be 50% of the modulating signal bandwidth.

### 5.5.3 Transmission bandwidth

PFM and SWFM have the ability to trade-off SNR performance against transmission bandwidth, provided the system is operated above the CNR threshold level (section 5.4.4). In deriving the SNR expressions in section 5.4.2, one of the assumptions made was that the transmission bandwidth  $B_b$ , was limited to  $1/\tau$ ,  $\tau$  being the PFM pulse width. In this section that assumption is justified by considering the energy distribution of PFM signal.

Figure 5.19 shows the distribution of the PFM signal energy against the transmission bandwidth to carrier frequency ratio  $r$ , at different duty cycles. When the transmission bandwidth is limited to  $1/\tau$ , the duty cycle  $d$ , defined as the ratio of  $\tau$  over  $f_c$ , is inversely related to  $r$ . The corresponding values of  $r$ , for different values of  $d$  used in the graph, are also indicated.

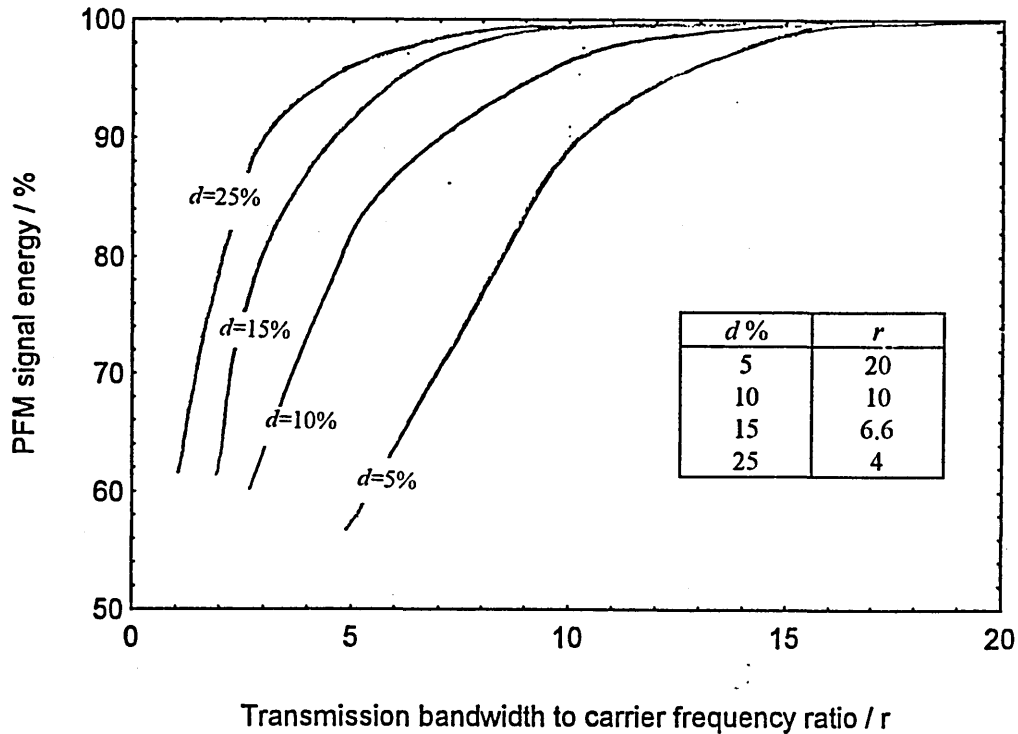


Figure 5.19 Energy distribution of PFM signals.

In sine wave FM, according to Carson's rule [58] the minimum transmission bandwidth is defined as the bandwidth which contains 98% of the signal energy. Choosing a similar criterion for PFM, Fig. 5.19 shows that when the duty cycle is below 10%, 98% of the signal energy is confined within the  $r$  value, corresponding to a transmission bandwidth of  $1/\tau$ . For duty ratios beyond 10%, band limiting the signal to  $1/\tau$  violates the Carson's rule as less than 98% of signal energy is confined within the defined bandwidth. However, the increase in signal energy beyond  $1/\tau$  is only minimal provided the duty cycle is kept below 25%. Therefore, in conclusion it can be stated that adequate signal performance can be delivered by limiting the transmission bandwidth to  $1/\tau$ , when the duty cycle of the PFM signal is kept below 25%.

## 5.6 Summary

In this chapter modulation and demodulation techniques, SNR performance and optimisation of PFM and SWFM systems were presented. The simplicity, spectral characteristics and the similarities of the two modulation techniques were illustrated. It was also shown, the double-edge detection SWFM technique has lower sampling ratio requirements and a 3 dB SNR advantage over single-edge SWFM and PFM systems.

Jitter noise is the primary noise source in PTM systems operating above the CNR threshold. Performance comparison of the derived PFM SNR expressions has shown that the raised cosine pulses deliver the optimum SNR level. The CNR, below which the SNR starts to deteriorate significantly, was shown to be close to 20 dB. In section 5.5, optimisation of PFM and SWFM systems in the context of a SCM-PTM sub-system, was presented. The VCO voltage-to-frequency transfer characteristic is critical to nonlinear distortion performance and commercially available devices are capable of transmitting a large number of subcarrier channels. A transmission bandwidth, which corresponds to the inverse of the pulse width, was shown to be adequate for PFM signal transmission.

# Pulse Position Modulation Systems

## 6.1 Introduction

Pulse position modulation (PPM) is an isochronous PTM technique, which carries information by virtue of a continuously variable position of a narrow pulse within a fixed time frame. This modulation scheme is closely related to pulse width modulation (PWM), where information is conveyed by the variable width of a pulse within a pre-determined time frame. However, a fundamental advantage of PPM over PWM is that a significant portion of the transmitted power which conveys no information in PWM is eliminated, resulting in a more efficient modulation technique [74]. PPM also has better SNR performance compared to other PTM techniques. The complexity of PPM is marginally higher than PFM and SWFM systems dealt with in the last chapter, but considerably lower compared to PCM systems.

This chapter exclusively deals with PPM systems. Section 6.2 introduces PPM modulation and is followed by a spectral characterisation and various options available for signal demodulation, in section 6.3. The SNR expression for a PPM system is derived in section 6.4.

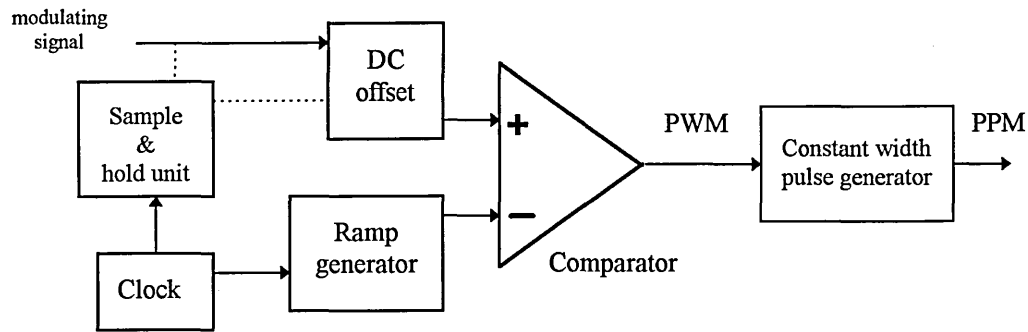
## 6.2 PPM Modulation

In PPM, the position of a narrow pulse within a fixed time frame is varied in proportion to the amplitude of the modulating signal. It is known as an isochronous PTM technique, as there exists a fixed time frame at all times. Typically, PPM pulses are generated by differentiating the trailing edge of a PWM signal [92], and various aspects of PPM generation are discussed in this section.

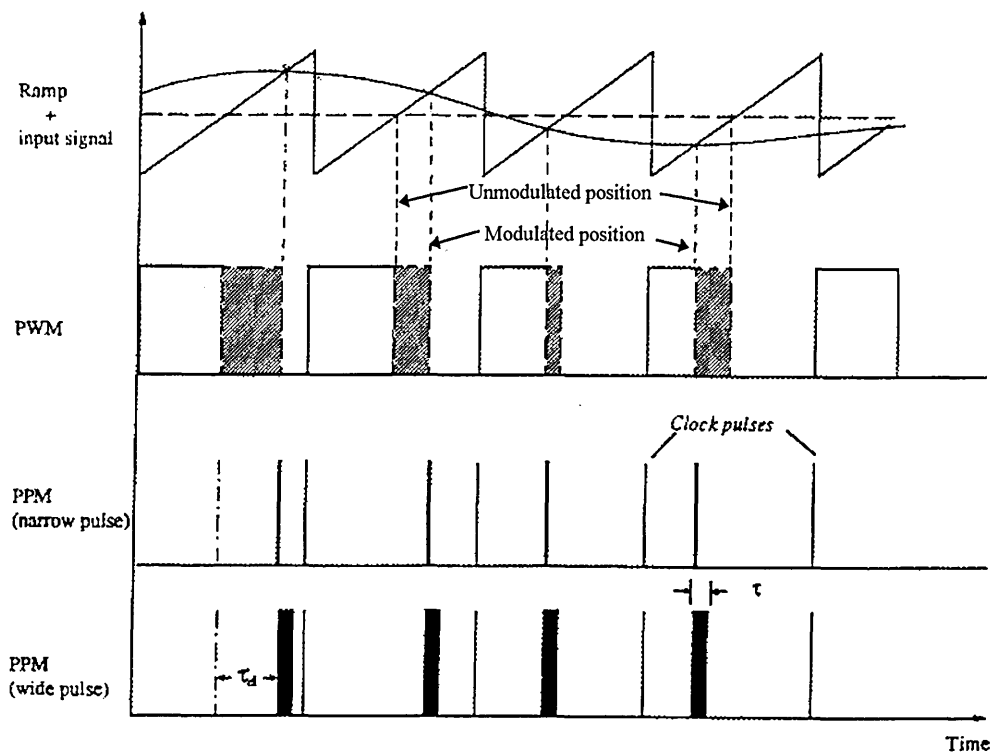
Figure 6.1 shows the block diagram of a PPM modulator and the associated waveforms. Fundamental to the PPM generation is a high speed, linear ramp generator, which determines key parameters such as the modulation sensitivity, input dynamic range and the amount of nonlinear distortion. The PWM signal is generated by comparing the ramp signal with the modulating signal and driving the comparator to a low state at the detection of equivalence. The PPM signal may be derived by differentiating the trailing edge of the PWM signal and a constant width pulse generator is generally used for this purpose [16].

PPM may be divided into two categories, according on how the incoming information is processed. When the modulating signal is directly compared with the linear ramp,

naturally sampled PPM signals are generated. Consequently, the sampling instants are not equally spaced but depend upon the amplitude of the input signal. The other technique, known as uniformly sampled PPM, a sample-and-hold circuit is included in the signal path and therefore, the PPM modulator operates on uniformly spaced, stored input samples.



(a) circuit block diagram



(b) signal waveforms

Figure 6.1 PPM modulation.

When natural sampling is employed, information can be recovered directly from the recreated PTM format containing the baseband component. However, in a system employing uniform sampling, a sample-and-hold unit needs to be included to recreate an amplitude modulated pulse form, prior to lowpass filtering. The choice between natural sampling and uniform sampling is essentially one of performance-cost trade-off. Uniform sampling, in principle, is capable of complete signal recovery without distortion, but at the additional expense of a premium specification of a sample-and-hold unit [75].

It was stated in the last chapter that raised cosine pulses are used commonly in communication system applications. Therefore, in order to mathematically model the PPM signal, a raised cosine pulse train of amplitude  $A$ , pulse period  $T$  and pulse width  $\tau$ , defined to the full width half maximum (FWHM) point, can be written as [93]:

$$P(t) = \sum_{n=-\infty}^{\infty} \frac{A}{2} \left\{ 1 + \cos \left[ \frac{\pi(t - nT)}{\tau} \right] \right\} \quad (6.1)$$

where at all times,  $\tau < |t - nT|$ .

The modulated PPM signal  $f(t)$ , where the time deviation of the  $n^{\text{th}}$  pulse is  $\Delta t_n$  can be represented by:

$$f(t) = \sum_{n=-\infty}^{\infty} \frac{A}{2} \left\{ 1 + \cos \left[ \frac{\pi(t - nT - \Delta t_n)}{\tau} \right] \right\}, \quad |\tau| < |t - nT - \Delta t_n| \quad (6.2)$$

Figure 6.2 illustrate the deviation of a PPM pulse within the time frame  $T$ . For a modulation sensitivity of  $k$  (expressed in units sec/V), the peak pulse deviation  $\Delta t$ , is:

$$\Delta t = kA_m \quad (6.3)$$

where  $A_m$  is the peak amplitude of the modulating signal. The equality defining the peak deviation can be expressed as:

$$\Delta t \leq \frac{T}{2} - \frac{\tau}{2} \tag{6.4}$$

In practical systems this could be a too conservative estimate for the modulation range, as two PPM pulses could only overlap if the modulating signal makes an instantaneous transition from the most positive excursion to the most negative.

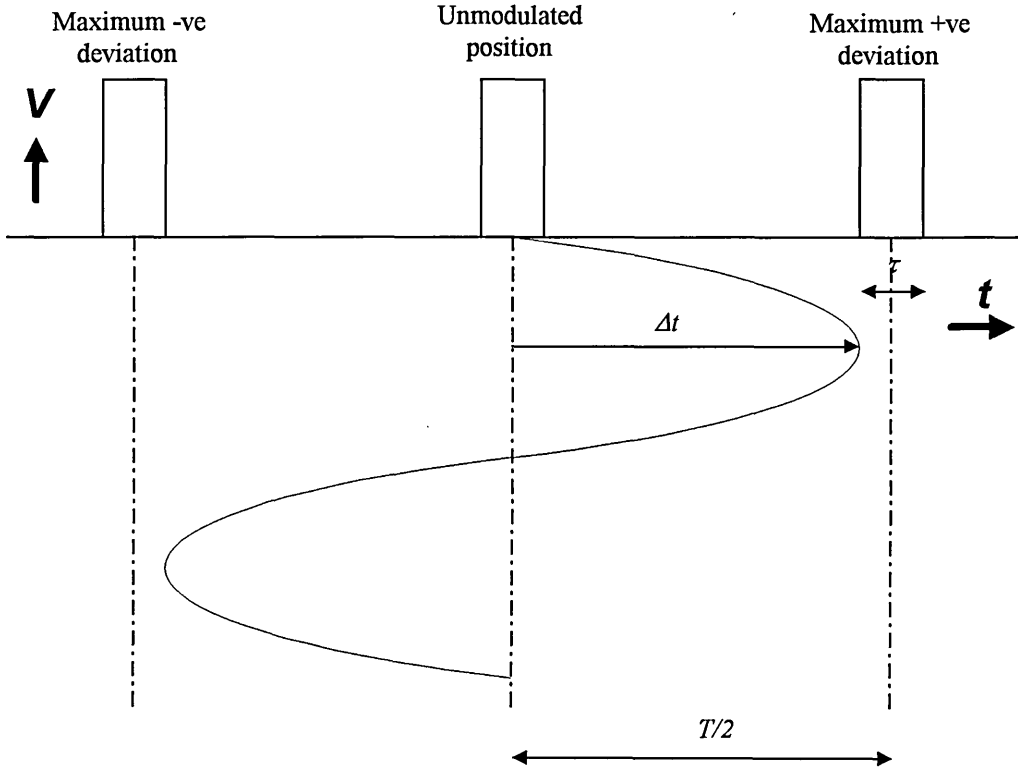


Figure 6.2 Pulse deviation within a PPM time frame.

Using the time relationship for the PPM frame, the modulation index  $M$ , can be defined as:

$$M = \frac{2\Delta t}{T} \tag{6.5}$$

As stated earlier the main feature of PPM is its power efficiency. Therefore, no additional pulses are transmitted for frame alignment, these being reconstructed within the demodulator, as will be shown in section 6.3. Provided that channel bandwidth is large enough, PPM pulses can be made very narrow and therefore, is well suited for optical communication employing injection laser diodes.

## 6.3 PPM Demodulation

In Chapter 4 the general characteristics of the PTM spectrum were presented. It was also stated that all PTM techniques rely on a baseband signal component to recover information and therefore in order to determine the demodulation technique, an investigation of the PPM and PWM spectrums is called for.

### 6.3.1 Spectral characteristics

There are two approaches to developing a mathematical expression for naturally sampled PPM systems. The first approach is based on the assumption that the PPM waveform is a series of impulses modulated in phase. Under this assumption **Stuart** [94] has summarised the Fourier series for PPM as:

$$f(t) = \frac{A\omega_c}{2\pi} \left[ 1 + 2 \sum_{n=-\infty}^{\infty} \sum_{k=1}^{\infty} J_n(k\phi) \cos(k\omega_c + n\omega_m)t \right] \quad (6.6)$$

where  $\omega_c$  is the carrier frequency,  $\omega_m$  is the modulating frequency,  $A$  is the pulse height and  $J_n()$  is the Bessel function of the first kind. The expression indicates that there is no baseband spectral term, hence the PPM signal cannot be directly employed to recover information.

The other approach is to assume that PPM pulses are of finite width, as is the case in practical systems, and to compose the pulses from negative and positive step functions. Employing this approach, the expression for constant width PPM is derived to be [94]:

$$f(t) = \frac{A\omega_c\tau}{2\pi} + AM \sin(\omega_m\tau/2) \cos\omega_m t + \frac{2A}{\pi} \sum_{n=1}^{\infty} \sum_{k=-\infty}^{\infty} J_k(n\pi M) \frac{\sin[(n\omega_c + k\omega_m)\tau/2]}{n} \cos[(n\omega_c + k\omega_m)t] \quad (6.7)$$

where  $\tau$  is the PPM pulse width and rest of the notation is as defined before. The third term of the equation represents the carrier fundamental and the harmonics, and the sidetones generated around them. The second term indicates the presence of a baseband component, which is a differentiated version of the modulating signal. Therefore, an option for signal demodulation in PPM systems, is to extract the baseband component from the regenerated PPM signal and to pass it through an integrator to recover the information. A typical PPM spectrum is plotted in Fig. 6.3, using Eqn. (6.7).

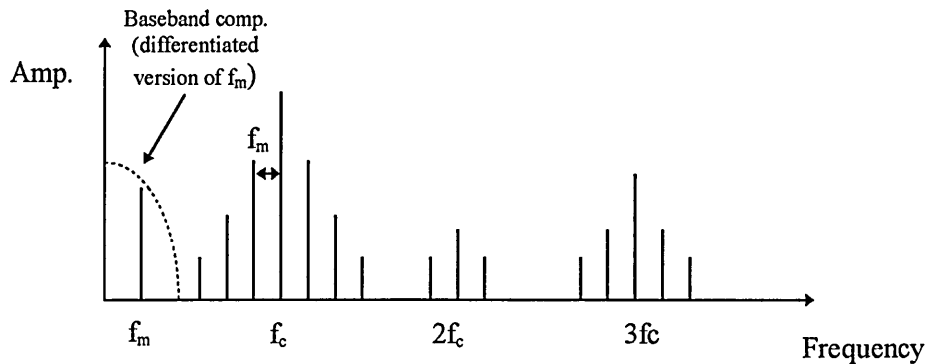


Figure 6.3 A typical PPM spectrum.

At this stage it is appropriate to investigate the spectral characteristics of the PWM signal. A comprehensive Fourier analysis on single tone modulated PWM has been

carried out by several authors [94, 95-96-97]. A naturally sampled, trailing-edge modulated PWM waveform, with a unity unmodulated mark-to-space ratio can be expressed as [16]:

$$w(t) = \frac{1}{2} - \frac{M}{2} \sin \omega_m t + \sum_{n=1}^{\infty} \frac{\sin(n\omega_c t)}{n\pi} - \sum_{n=1}^{\infty} \frac{J_0(n\pi M)}{n\pi} \sin(n\omega_c t - n\pi) - \sum_{n=1}^{\infty} \sum_{k=\pm 1}^{\pm \infty} \frac{J_k(n\pi M)}{n\pi} \sin[(n\omega_c + k\omega_m)t - n\pi] \quad (6.8)$$

and all the symbols are as defined before. Equation (6.8) shows the presence of a baseband component, which is an inverted version of the modulating signal. This suggests that PPM demodulation can be carried out by reconstructing the PWM signal from the incoming PPM signal, and employing a lowpass filter to recover the baseband component.

### 6.3.2 The clock component

The timing diagram in Fig. 6.4 illustrates how a PWM signal can be generated by combining the PPM pulses and a clock signal derived from the incoming signal. Here, it is assumed, that the transmitted PPM signal is generated by differentiating the trailing edge of a PWM signal. Therefore, the reference pulses are generated at the rising edges of the recovered clock signal (also refer to Fig. 6.1).

Since PPM is categorised as an isochronous technique, a distinct clock frequency component should be present under all modulation conditions. In order to verify this, Eqn. (6.7) should be investigated further.

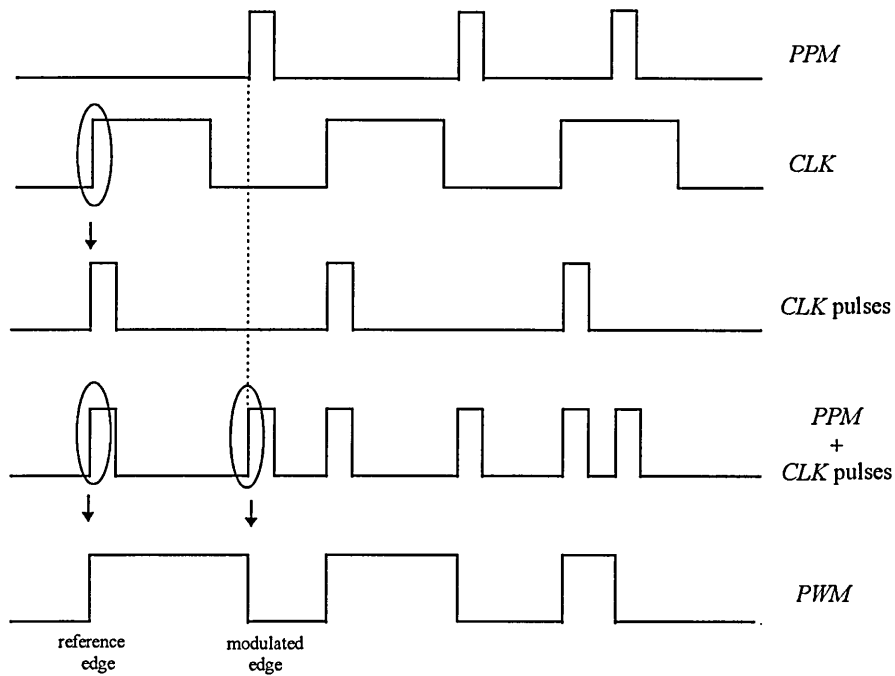


Figure 6.4 Generation of PWM using PPM pulses and a clock reference signal.

The amplitude  $A_c$ , of the carrier frequency in PPM is: [98]

$$A_c = \frac{2A}{\pi} J_0(\pi M) \sin(\pi f_c \tau) \quad (6.9)$$

Equation (6.9) indicates that the value of  $A_c$  is strongly dependent on the modulation index,  $M$ . The normalised value of  $A_c$  with respect to the unmodulated carrier is plotted against  $M$  in Fig. 6.5. This shows a strong presence of the carrier frequency at low modulation indices, rapidly decreasing to lower levels under higher modulation, sinking to its lowest value at approximately 80% modulation.

A device known as a phase locked loop (PLL) can be employed in communication systems to extract distinct frequency components from an incoming signal. The above behaviour of the PPM clock component suggests the possibility of employing a PLL to extract the clock signal from the incoming PPM signal.

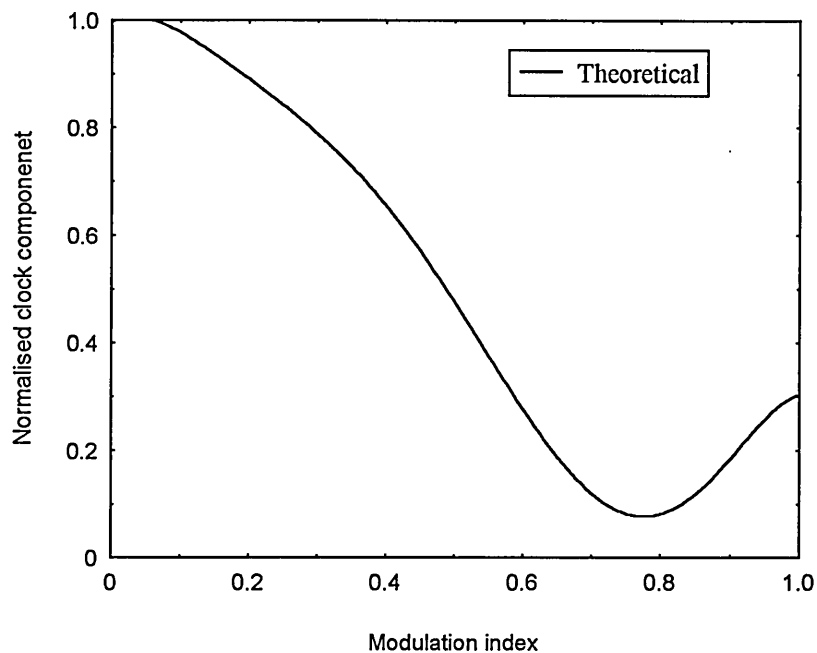


Figure 6.5 Normalised clock component vs. modulation index.

The access to a clock signal at the receiver imply that the technique illustrated by signal waveforms in Fig. 6.4 can be used for PPM demodulation. A block diagram of the demodulator, employing this technique, is shown in Fig. 6.6. Here, the PLL recovered clock component is multiplexed with incoming PPM signal and is used to trigger a bi-stable in order to generate the PWM signal, containing the baseband component.

The critical part of the PPM demodulator is the PLL and therefore, its operation and design parameters are discussed in the following section.

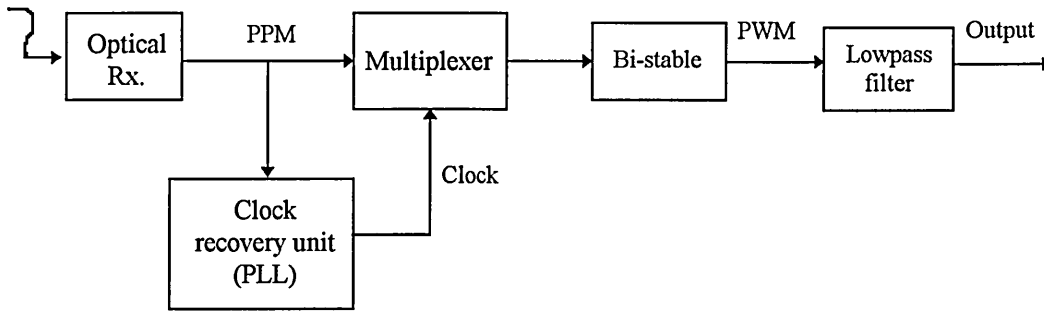


Figure 6. 6 PPM demodulator employing a clock signal recovery.

### 6.3.3 Phase locked loop (PLL)

A phase locked loop (PLL) is a device which enables the phase of a feedback control VCO to follow that of the input signal. It consists of three components, as shown in Fig. 6.7 : phase detector, VCO and lowpass filter. The error voltage produced by the phase detector is proportional to the phase difference between the input signal and the output of the VCO, and is given as:

$$v_e = k_d \sin(\theta_i - \theta_o) \quad (6.10)$$

where  $k_d$  is the gain of the phase detector,  $\theta_i$  is the phase of the input signal and  $\theta_o$  is the phase of the VCO output signal. The error voltage, which is lowpass filtered to eliminate higher order harmonics and to provide a stable loop with a controlled response, is fed to the VCO in order to align its output phase with the incoming signal.

The VCO is initially set to a free running frequency, a frequency close to the incoming signal. When the VCO phase is in a fixed phase relationship to the incoming signal, the PLL is said to have acquired lock. The closed loop phase transfer function of the PLL can be written as [99]:

$$H(s) = \frac{\psi\theta_o(s)}{\theta_i(s)} = \frac{k_o k_d F(s)}{s + k_o k_d F(s)} \quad (6.11)$$

where  $k_o$  is the gain factor of the VCO,  $F(s)$  is the transfer function of the loop filter and the product  $k_o k_d F(s)$  is the forward loop gain.

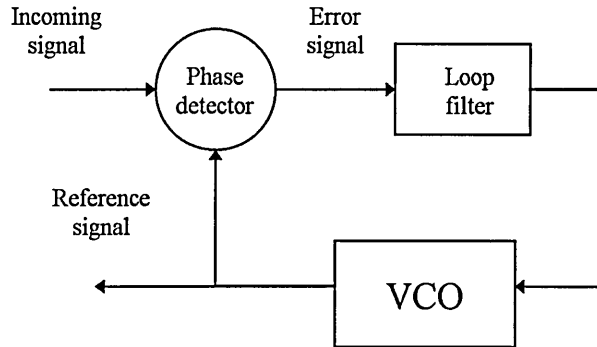


Figure 6.7 PLL block diagram.

Some important system parameters of a PLL are defined below [58].

**Lock acquisition time** : the time required by the PLL to acquire lock.

**Capture range** : the frequency range centred about the free running frequency of the VCO over which the loop can acquire lock with the input signal. Also known as lock-in-range.

**Hold-in-range** : the frequency range over which the loop maintains lock once initial lock is acquired.

**Loop bandwidth** : set by the bandwidth of the lowpass filter.

The transfer function of the loop filter has considerable influence on the PLL parameters listed above. The desired level of PLL performance can be achieved by a judicious choice of the loop bandwidth. For instance, when the difference between the free running frequency and the average incoming signal frequency is less than the loop bandwidth, the

PLL will acquire lock almost immediately. This is achieved with a wide loop bandwidth, which also allows for an extended lock-in-range as its value is equivalent to the loop bandwidth. The drawback of a wide loop bandwidth is that it admits more noise making the hold-in-range smaller [99].

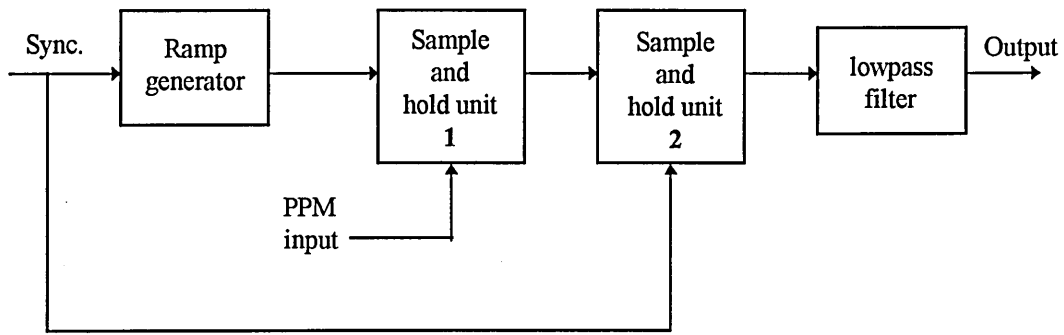
On the other hand a narrow loop bandwidth ensures good noise performance and will tolerate a larger amount of frequency change without losing lock i.e. an extended hold-in-range. However, acquiring lock is difficult, making the lock acquisition time longer and resulting in a narrower lock-in-range.

#### **6.3.4 Alternative demodulation techniques**

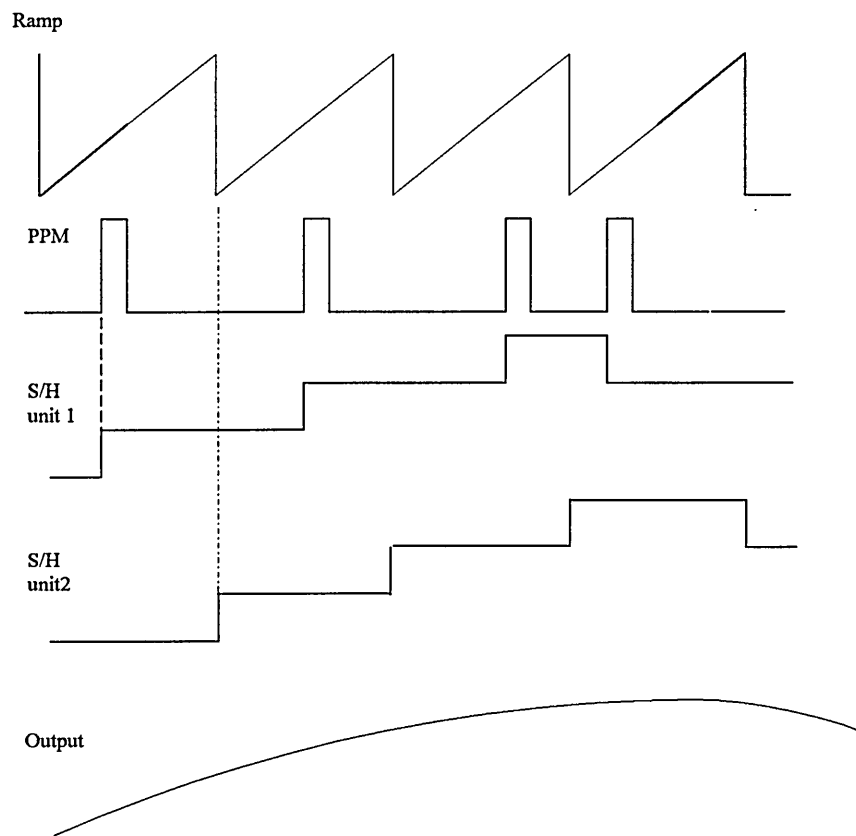
An alternative PPM demodulation technique has been demonstrated by **Holden** [100], where a ramp generator and sample-and-hold circuits are employed in conjunction with a lowpass filter at the receiver. The block diagram of the demodulator circuit and the associated signal waveforms are illustrated in Fig 6.8.

As shown in Fig. 6.8(a), the demodulator consists of two sample-and-hold circuits, the first of which is triggered by the PPM pulses and samples the ramp signal. The output signal is a staircase waveform, where the amplitude and width of each step varies as a function of the position of received pulse in the time slot. In order to generate a constant width step, the signal is fed to a second sample-and-hold unit, which is triggered by a sync pulse. Filtering this constant width step waveform removes the high frequency components introduced by sampling circuits and yields the original information.

The cost and complexity of this technique is higher due to two reasons. One is the additional circuitry required at the receiver due to the inclusion of a ramp generator and two sample-and-hold circuits. The other is the lack of synchronisation between the transmitter and the receiver. The ramp generator at the receiver is allowed to free run at approximately the same frequency as the transmitter, but in order to align the two signals in phase a reference signal is transmitted via separate link.



(a) block diagram



(b) signal waveforms

Figure 6.8 PPM demodulator nominated by **Holden** [100]

## 6.4 SNR Analysis

A comprehensive noise analysis on PFM and SWFM systems was carried out in section 5.4. The concept of jitter noise, its sources and its effect on the recovered pulses were presented. All PTM techniques rely on a phase-to-amplitude conversion to recover information and therefore, a substantial part of the jitter noise analysis in section 5.4.1 is also applicable for PPM systems. As previously, throughout the following analysis a half amplitude threshold detection level, white Gaussian noise and signal operation above the CNR threshold level is assumed.

### 6.4.1 Noise analysis

As explained in section 5.4.1, the jitter noise in PTM systems can be expressed as a pulse train, weighted by the displacement at each threshold crossing. The double sided noise power spectral density at the output of the threshold detector was given by Eqn. (5.11) and is repeated here:

$$X(f) = \left[ \frac{f_c}{\dot{p}(t_s)} \right]^2 \sum_{k=-\infty}^{\infty} N_i(f - kf_c)$$

where  $f_c$  is the carrier frequency,  $\dot{p}(t_s)$  is the pulse slope at threshold detection and  $N_i(f)$  is the double sided input noise power spectral density.

It was shown in the previous section that the desired technique for PPM demodulation is to generate a PWM signal which contains the baseband information. The impact of jitter noise on the regenerated PWM signal is shown in Fig. 6.9. Due to the noise, represented

as an error pulse  $y(t)$  of width  $x(t_s)$ , added to the signal, the modulated edge of the PWM signal is displaced from its original position.

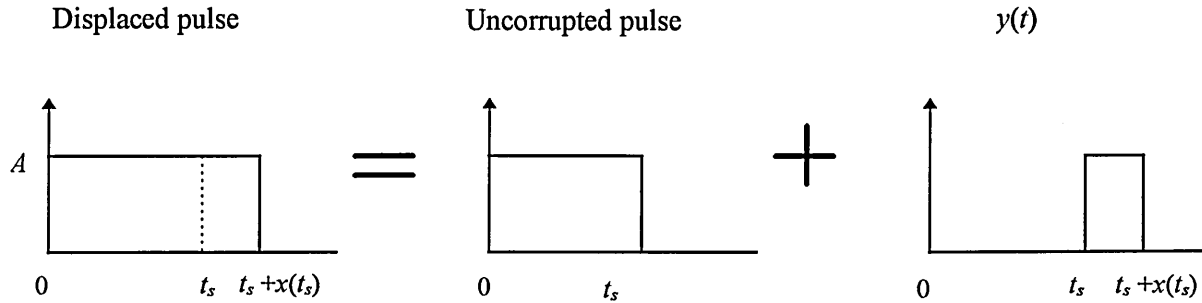


Figure 6.9 Pulse displacement due to noise pulse,  $y(t)$

For small values of  $x(t_s)$ , as the case for practical systems, the Fourier transform of  $y(t)$  is:

$$Y(f) = Ax(t_s)e^{-j2\pi ft_s} \quad (6.12)$$

$y(t)$  represents the noise added to the bi-stable output for a single pulse. Since the noise output is approximately independent of the modulating signal  $x(t)$  [87], and only frequencies passed by the lowpass filter are of interest, assuming

$$x(t) = 0$$

$$f \ll \frac{1}{\tau}$$

the power spectral density of the noise added to the monostable output due to the impulse train  $x_n(t)$ , can be expressed as [88]:

$$N_o(f) = A^2 X(f) \quad (6.13)$$

Using Eqn. (5.11) to substitute for  $X(f)$ , the single sided noise power spectral density at the demodulator output can be expressed as:

$$N'_o(f) = \left[ \frac{Af_c}{\dot{p}(t_s)} \right]^2 \left[ N'_i(f) + \sum_{k=1}^{\infty} \{N'_i(kf_c - f) + N'_i(kf_c + f)\} \right] \quad (6.14)$$

where  $N'_i(f)$  is the single sided noise power spectral density at the input of the threshold detector and for a uniform response optical channel is expressed by Eqn. (5.16).

#### 6.4.2 SNR expressions

The peak signal level  $v_p$  is produced by the maximum pulse deviation  $\Delta t$ , and the rms signal power  $S_{rms}$ , at the output of the PPM demodulator is equivalent to

$$S_{rms} = \frac{v_p^2}{2} = \frac{(k\Delta t)^2}{2} \quad (6.15)$$

where  $k$  is the modulation sensitivity. Using the modulation index  $M$ , and assuming the ramp height is equivalent to the pulse height  $A$ , the rms signal power can be expressed as:

$$S_{rms} = \frac{(AM)^2}{8} \quad (6.16)$$

Assuming an optimum threshold level set at half the pulse amplitude and a PPM pulse modelled by a raised cosine, the rms signal-to-noise power ratio can be expressed as:

$$SNR_{rms} = \frac{1}{8} \left( \frac{M\pi B_t}{f_c} \right)^2 \frac{(R_o G P_p)^2}{N_{i(rms)}} \quad (6.17)$$

where  $B_t$  is the transmission bandwidth assumed to be  $1/\tau$  as in the case of PFM and  $P_p$  is the peak received optical power. As previously, an expression in terms of average received optical power  $P_{av}$ , is useful and is shown below.

$$SNR_{rms} = \frac{(M\pi)^2}{2} \left( \frac{B_t}{f_c} \right)^4 \frac{(R_o G P_{av})^2}{N_{i(rms)}} \quad (6.18)$$

It was stated in Chapter 5 that pulses in optical communication systems are best approximated by Gaussian or exponential pulses. Using the equations in section 5.4.2.2, the rms SNR for a PPM system, modelled by a Gaussian or an exponential pulse, and expressed in terms of peak received optical power is:

$$SNR_{rms} = \frac{18}{25} \left( \frac{MB_t}{f_c} \right)^2 \frac{(R_o GP_p)^2}{N_{i(rms)}} \quad (6.19)$$

Similarly, the  $SNR_{rms}$  in terms of average received optical power is:

$$SNR_{rms} = \frac{72}{25} M^2 \left( \frac{B_t}{f_c} \right)^4 \frac{(R_o GP_{av})^2}{N_{i(rms)}} \quad (6.20)$$

As in the case of PFM, it is useful to examine the relationship between the output SNR and input CNR. Using Eqns. (6.17) and (6.19), and the system parameters in section 5.4.3, the relationship between SNR and CNR for PPM systems is shown in Fig. 6.10. Once again the raised cosine pulse model delivers an optimum level of performance, exceeding the SNR of the Gaussian model by approximately 3 dB. The performance of PFM is also shown for comparison, and falls behind PPM performance by around 5 dB.

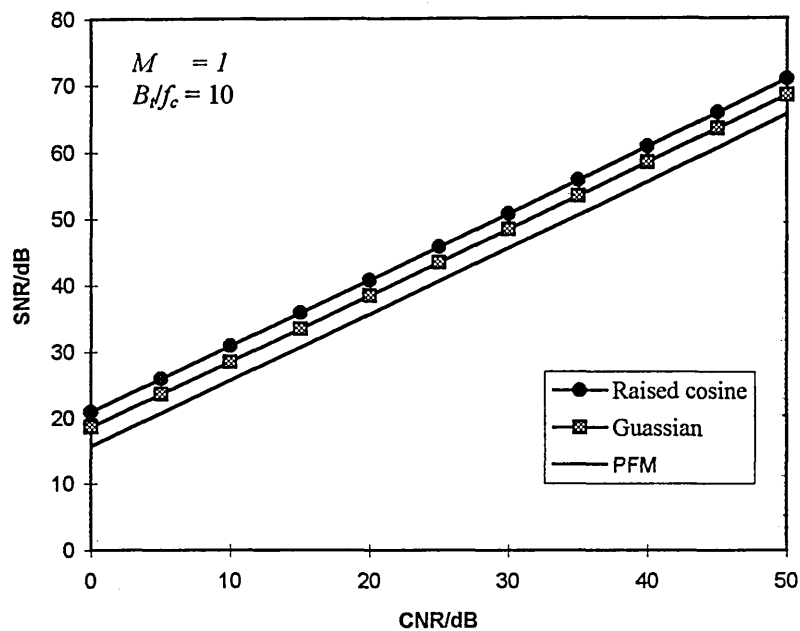


Figure 8.10 SNR vs. CNR for PPM systems.

## 6.5. Summary

In this chapter the modulation and demodulation techniques and SNR performance of PPM systems were considered. PPM was shown to be an efficient derivative of PWM, well suited for optical channel applications. A study of the PPM spectrum has shown that under moderate modulation conditions a clock signal can be extracted from incoming PPM signal. Hence, a novel detection technique, where a PWM signal containing the baseband information is reconstructed at the receiver by virtue of the recovered clock signal, was demonstrated. Alternative demodulation techniques and their disadvantages were also considered. Using the jitter noise analysis of Chapter 5, the SNR expression for a PPM system was derived. Optimum performance is delivered by raised cosine pulses, and PPM has an approximately 5 dB SNR advantage over PFM systems.

---

# System Implementation

## 7.1 Introduction

In order to evaluate the performance of SCM-PTM technique a prototype system to transmit a broadband SCM signal was designed and built. The PTM schemes incorporated into the system are PFM, SWFM and PPM. Video, audio and data signal channels were employed in the subcarrier stage to demonstrate the broadband transmission capability of the SCM-PTM technique. The overall system block diagram is shown in Fig. 7.1.

The prototype system was built on colander ground plane vero boards, using high frequency circuit techniques, and the emphasis was to use commercially available custom and semi-custom built IC devices. Each PTM technique was implemented using emitter coupled logic (ECL), due to its superior performance at high speeds over other logic

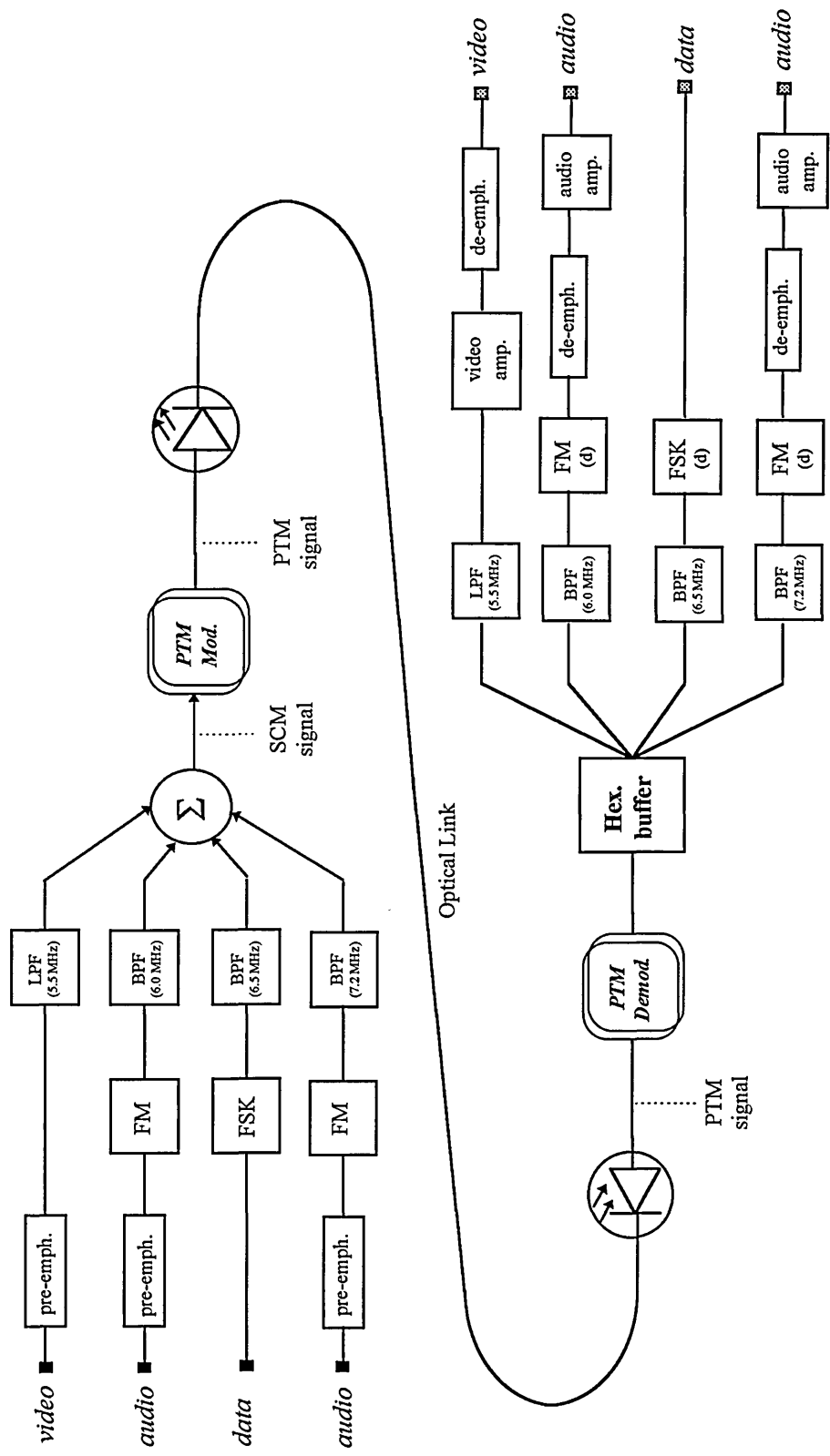


Figure 7.1 System block diagram

families. A semi-conductor laser diode and a *p-i-n* photodiode-transimpedance optical receiver, operating at 1300 nm were employed for the optical link. After PTM demodulation bandpass filtering technique was favoured to recover each subcarrier channel, mainly due to the fact that the required filters were readily available in the market.

In the following sections each stage of hardware implementation of the prototype system is presented. Section 7.2 presents the implementation of the subcarrier stage while sections 7.3 and 7.4 deals with the PFM/SWFM transmitter and PPM transmitter, respectively. In section 7.5 details the optical link and its power budget and rise time budget calculations are given. Sections 7.6 and 7.7 presents the implementation of each PTM receiver, and the baseband signal recovery is dealt with in section 7.8.

## **7.2 SCM Signal**

The SCM signal consists of a baseband video channel, two audio channels and a data channel. In the following sub-sections the implementation of each signal channel is presented.

### **7.2.1 Video channel**

A PAL 625-line colour signal, employed within the UK for television transmission, was used for the video channel. The signal employs 625 lines of interlaced scanning per frame at a rate of 25 frames/second. The total video bandwidth extends to 5.5 MHz and the colour subcarrier is placed at a frequency of 4.43 MHz. The frequency distribution of the signal is shown in Fig. 7.2 [60].

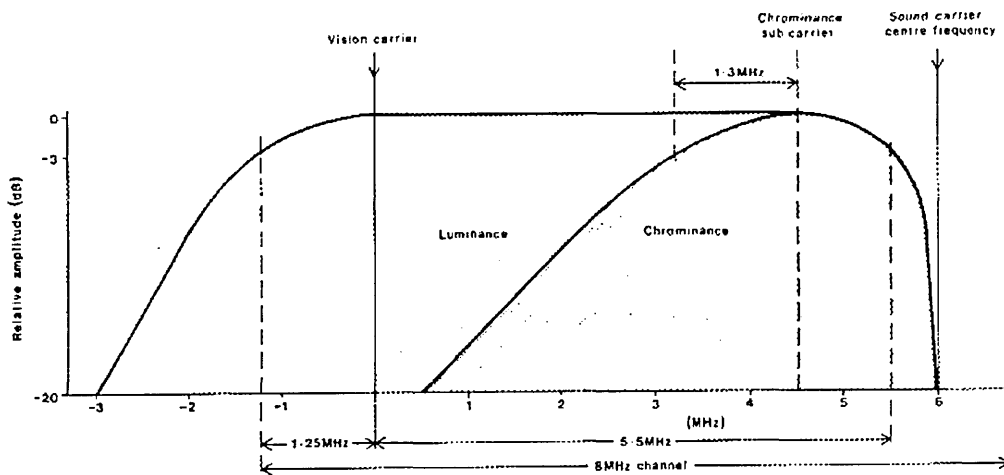
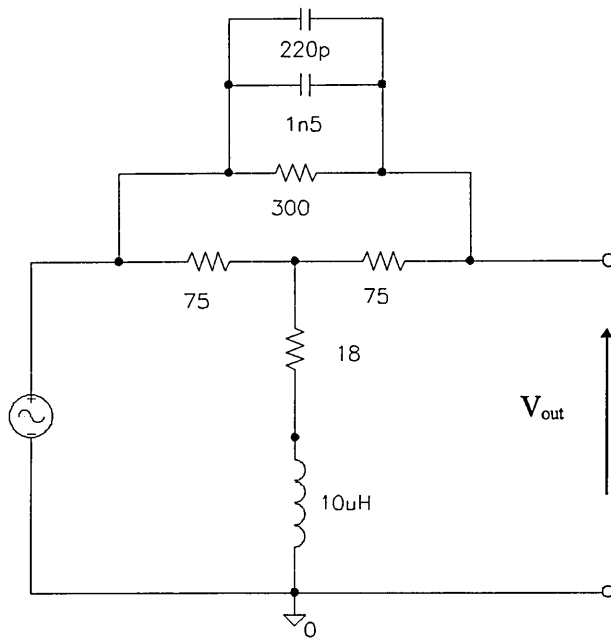


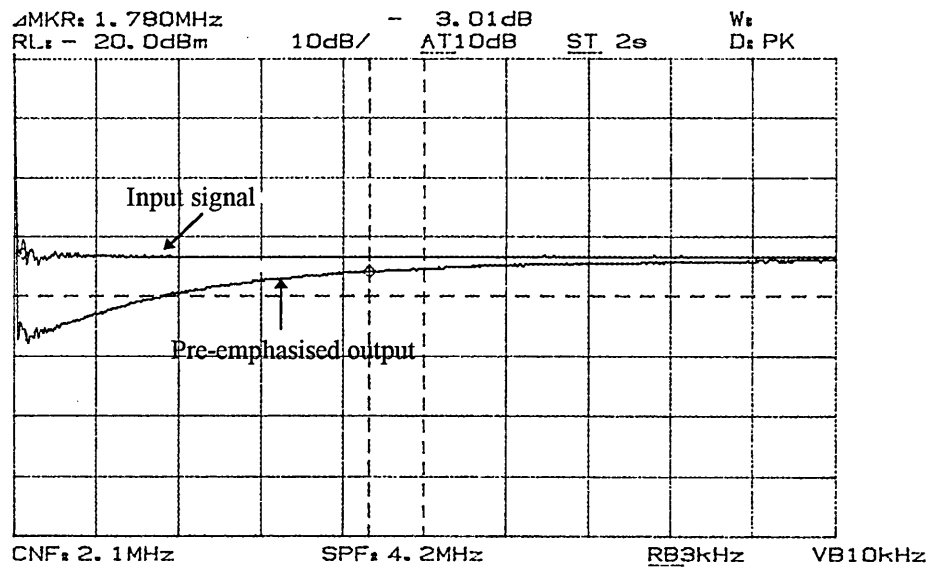
Figure 7.2 The frequency distribution of a PAL 625-line colour video signal [60].

The noise power spectral density of PFM and SWFM has a parabolic relationship against the modulating frequency. Therefore, the noise power at higher frequency components of the modulating signal is greater than the noise level at lower frequencies, degrading the SNR at higher frequencies. To improve the SNR in FM systems, signal level at the top end of the spectrum is boosted to a higher level, prior to modulation. This is known as pre-emphasis and is employed in audio broadcasting and FM transmission of satellite video channels [85].

The video pre-emphasis characteristic, which conforms to CCIR-405 standard, was adopted for PFM and SWFM transmission of the video signal. The pre-emphasis network and its frequency response are shown in Fig. 7.3(a) and 7.3(b), respectively.



(a) circuit diagram



(b) frequency response

Figure 7.3 PAL-625 video pre-emphasis conforming to CCIR-405 standard.

## 7.2.2 Audio channel

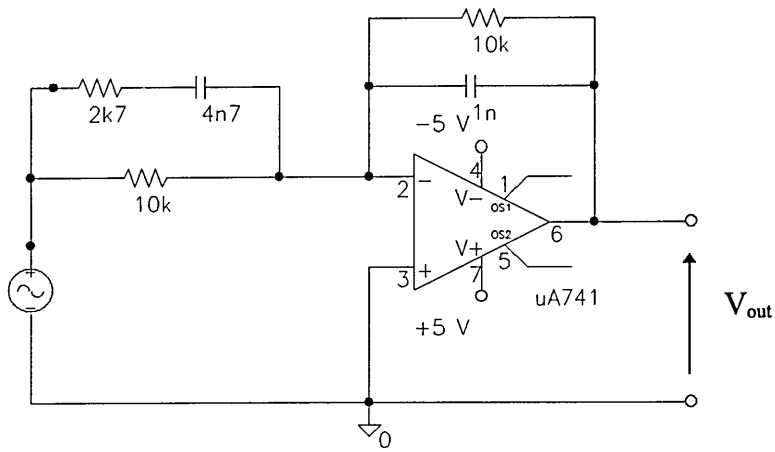
Two audio channels, conforming to the TV sound broadcasting standards, are implemented. The first audio channel is modulated onto the TV audio subcarrier at 6.0 MHz and the second channel is allocated a subcarrier frequency of 7.2 MHz. The characteristics common to the audio channels are tabulated below.

Audio bandwidth / kHz	15
Modulation	FM
Max. deviation / kHz	50
Pre-emphasis / $\mu$ s	50

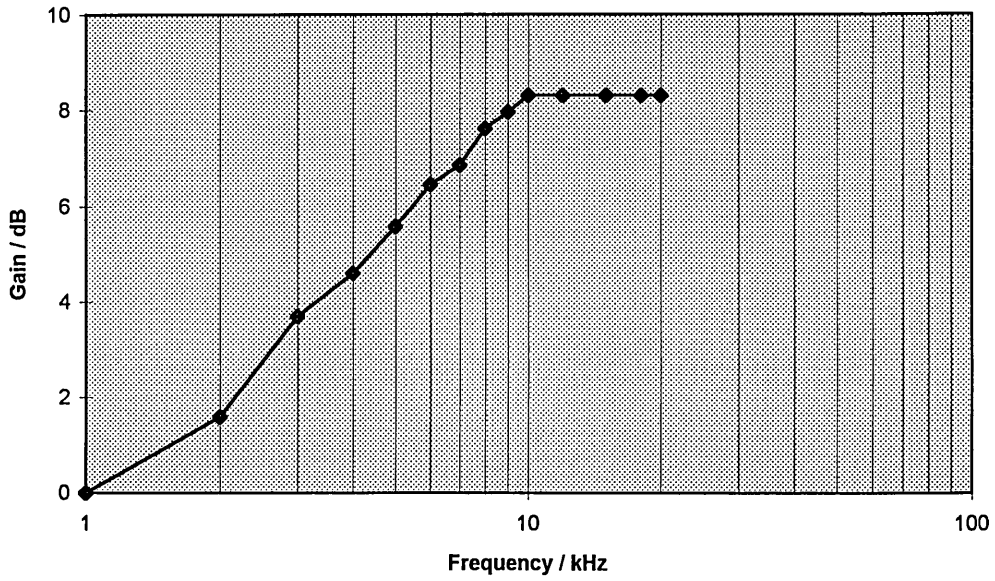
Table 7.1 Characteristics of the audio channels

Since FM is used to frequency shift the baseband audio channels, pre-emphasis can be employed to improve the SNR performance. Both channels were pre-emphasised using the 50  $\mu$ s TV sound broadcasting pre-emphasis standard, which defines a first corner frequency of 3.18 kHz. The pre-emphasised FM signal is actually a combination of FM and phase modulation (PM) and combines the advantages of both modulation techniques with respect to noise performance. The audio pre-emphasis network and its frequency characteristic is shown in Fig. 7.4(a) and 7.4(b), respectively.

**MC 1376** [101] is a monolithic IC, custom built for television sound broadcasting, and was used to implement the two audio channels. The device can be used as a FM modulator in the frequency range 1.4-14 MHz, with the centre frequency set by the resonance of the



(a) circuit diagram



(b) frequency response

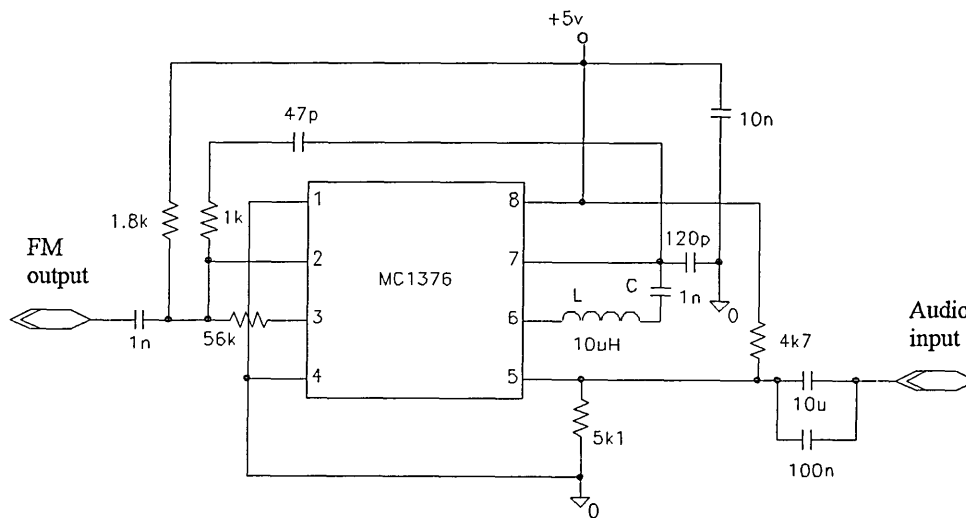
Figure 7.4 Audio pre-emphasis.

inductor (L) between pin 6 and 7, and the capacitance (C) from pin 7 to ground. The modulation sensitivity of the device varies with the centre frequency and is equivalent to approximately 0.3 MHz/V at a carrier frequency of 6 MHz. The best linear characteristics of the device can be realised by biasing the input signal between 2.6-2.7 V. The circuit diagram of the FM modulator for the 6.0 MHz audio channel is shown in Fig. 7.5. Also shown in the figure is the spectrum of the FM audio channel, modulated by a 10 kHz sine wave, at a maximum deviation of 50 kHz.

### **7.2.3 Data channel**

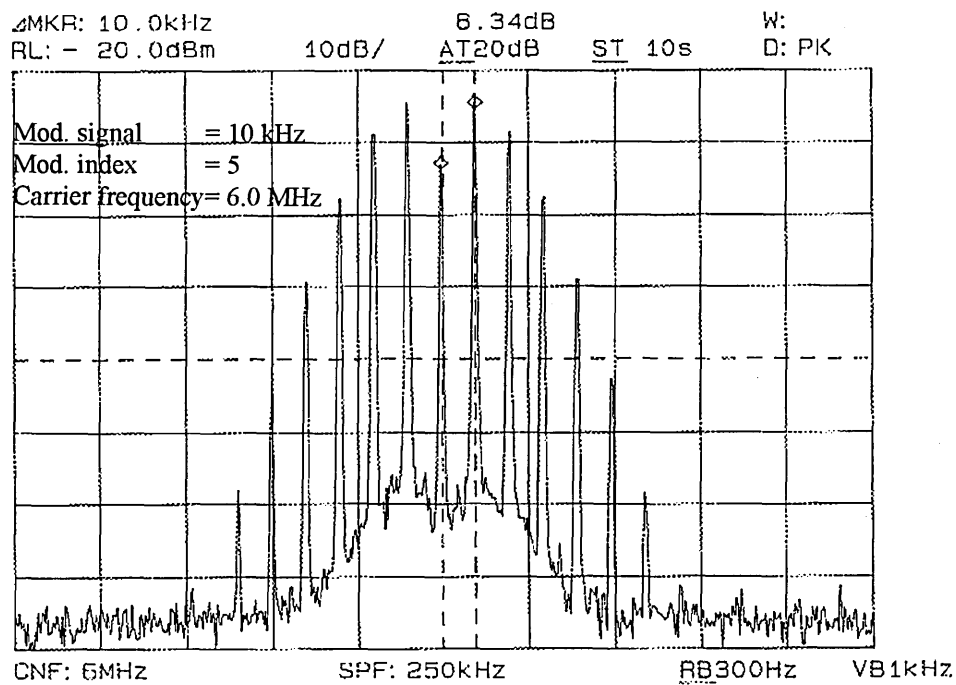
A data channel capable of carrying a maximum non-return to zero (NRZ) data rate of 500 kbit/s was implemented using frequency shift keying (FSK). A channel bandwidth of 780 kHz was allocated at a carrier frequency of 6.552 MHz. The pseudo random bit stream used to simulate the data, is shown in Fig. 7.6.

FSK modulation was implemented using a dual voltage control oscillator [102]. The two VCOs can be operated independently upto a frequency of 85 MHz. The centre frequency is set by a combination of external capacitance (between pin 4 and 5) and the dc voltage on pin 2 (Frequency Control). The deviation range is set by the dc bias on pin 3 (Range input). The circuit diagram of the FSK modulator is shown in Fig. 7.7. Since the output of the VCO is a square wave a bandpass filter is used to reduce the harmonics.



The value of C for the 7.2 MHz channel was 55 pF.

(a) circuit diagram



(b) frequency spectrum

Figure 7.5 FM modulator for the 6.0 MHz audio channel.

hp stopped

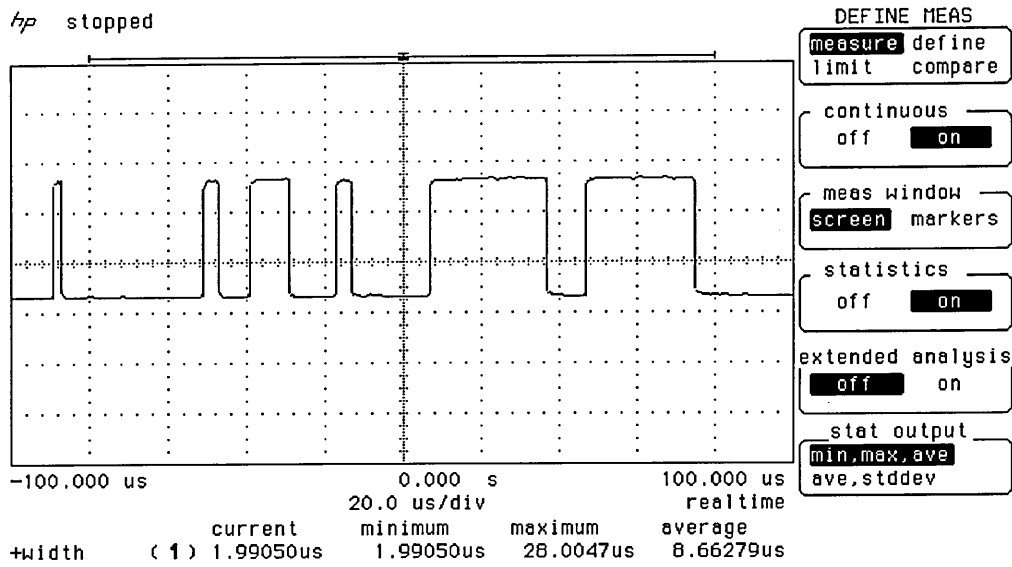


Figure 7.6 A 500 kbit/s PRBS data stream.

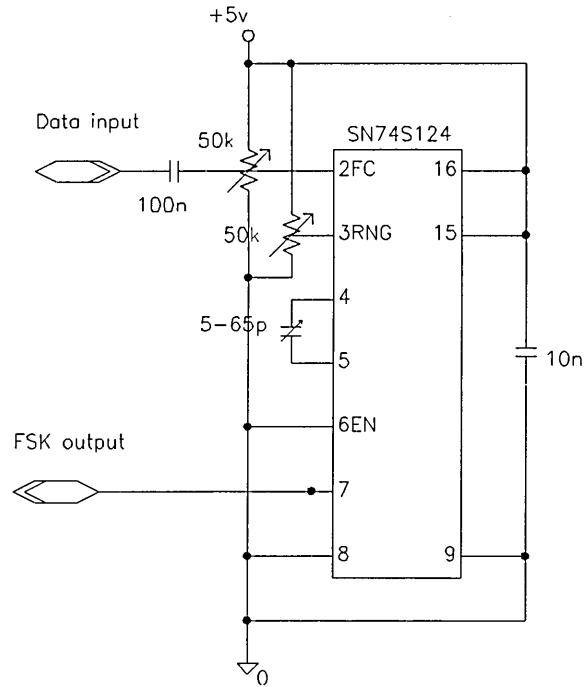


Figure 7.7 FSK modulator circuit diagram.

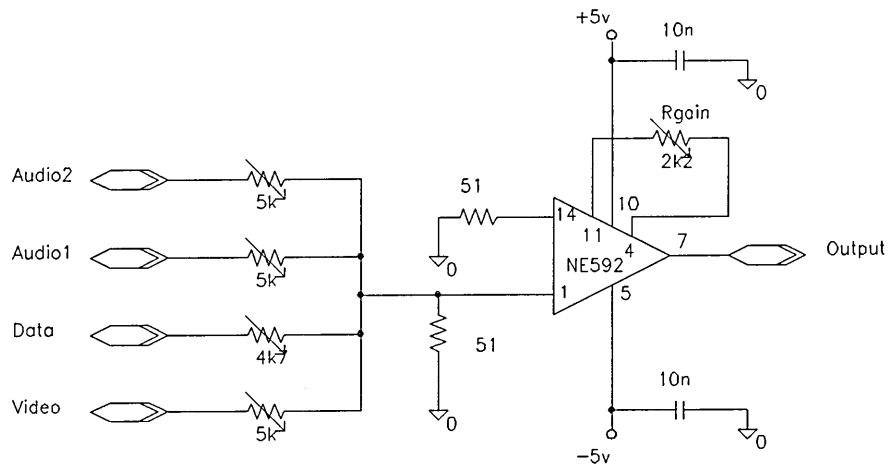
## 7.2.4 Frequency division multiplexer

The signal channels presented so far, are summarised in Table 7.2. Also shown in the table is the output SNR values required to deliver the expected level of performance for signal each channel.

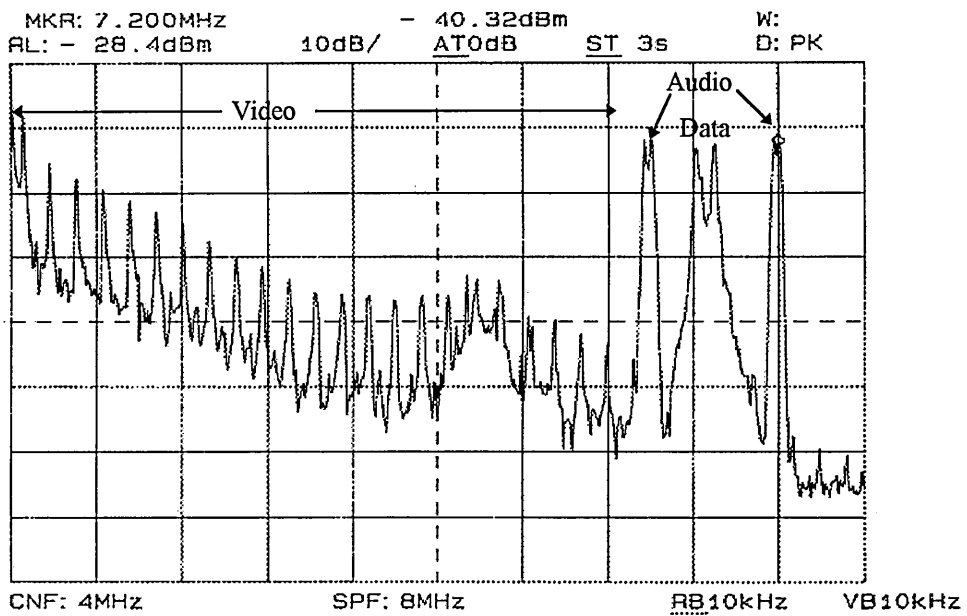
<i>Channel</i>	<b>Signal type</b>	<b>Subcarrier and modulation format</b>	<b>Channel fidelity</b>
<i>Video</i>	PAL 625-line colour bandwidth 5.5 MHz pre-emphasis CCIR-405	Baseband	40 dB
<i>Audio</i>	bandwidth 15 kHz peak dev. 50 kHz pre-emphasis 50 $\mu$ s	6.0 and 7.20 MHz FM	49 dB
<i>Data</i>	bit rate 500 kbit/s code NRZ	6.552 MHz FSK	$10^{-9}$ (BER)

Table 7.2 Subcarrier channel specification.

The SCM signal is formed by adding each signal channel in the frequency domain. A differential video amplifier [103], operating in a summing amplifier configuration, was used to add the subcarrier channels. The frequency spectrum of the SCM signal, consisting of a baseband video channel, two FM audio channels and a data channel is shown in Fig. 7.8, as is the circuit diagram.



(a) circuit diagram



(b) SCM signal spectrum, consisting of video, audio and data channels

Figure 7.8 The frequency division multiplexer.

### 7.3 SWFM and PFM Transmitters

The PTM modules of the prototype system operate at high frequencies and therefore, a high speed logic is required to deliver adequate system performance. Emitter coupled logic (ECL) is one of the fastest forms of digital logic available today and is used to implement each PTM technique employed in the SCM-PTM system.

The monolithic emitter coupled logic (MECL) family was first introduced by Motorola in 1962. Presently there are three MECL families which are commonly used in commercial applications: MECL III, MECL 10K and MECL 10H. Table 7.3 shows some general characteristics of the MECL logic families [104].

		MECL 10 K			
Feature		MECL 10H	10,100 series	10,200 series	MECL III
Gate propagation delay	ns	1.0	2.0	1.5	1.0
Rise/fall time	ns	1.0	3.5	2.5	1.0
Gate power	mW	25	25		60
DC noise margin	V	0.27	0.21		0.20
Power supply	V	V <sub>cc</sub> at ground potential and V <sub>EE</sub> at -5.2 results in maximum noise immunity. 10 nF low inductance, decoupling capacitors should be present every 4 to 6 packages.			
Output termination	Ω	50-150 resistors to -2.0 V dc. 270-2k resistors to V <sub>EE</sub>			
Output impedance	Ω	approximately 7			

Table 7.3 General characteristics of the MECL family.

ECL devices are operated from a single voltage power supply of -5.2 V and have propagation delays in the order of 1 ns. The fast rise and fall times of ECL technology is illustrated in Fig. 7.9, by a narrow pulse generated using ECL devices.

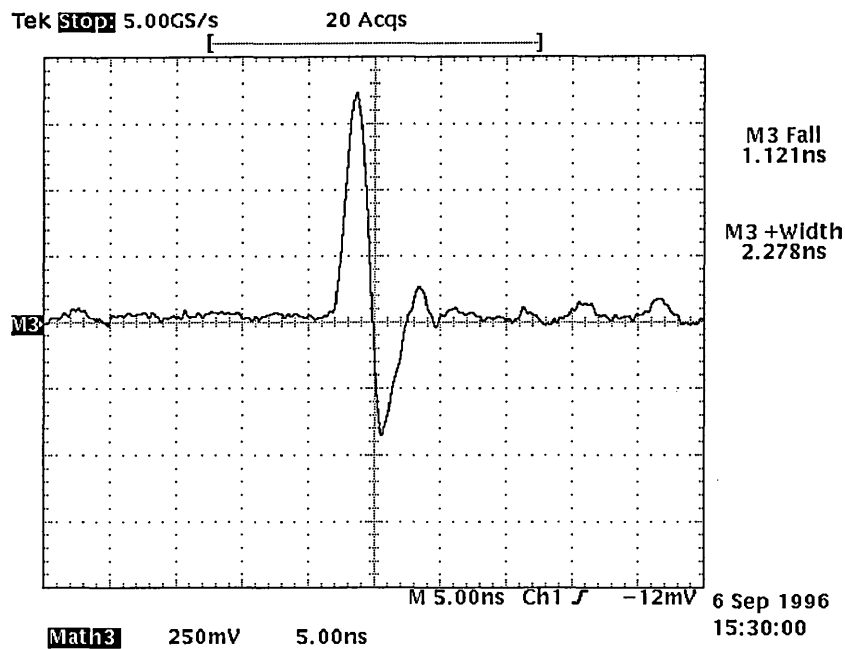


Figure 7.9 A pulse generated using MECL 10H devices, with rise and fall times in the order of 1 ns.

A block diagram of the SWFM and PFM transmitters was given in Fig. 5.1. Fundamental to the PFM and SWFM generation is the VCO, and its implementation is presented in the following section. Additional circuitry of the PFM technique is considered in section 7.3.2.

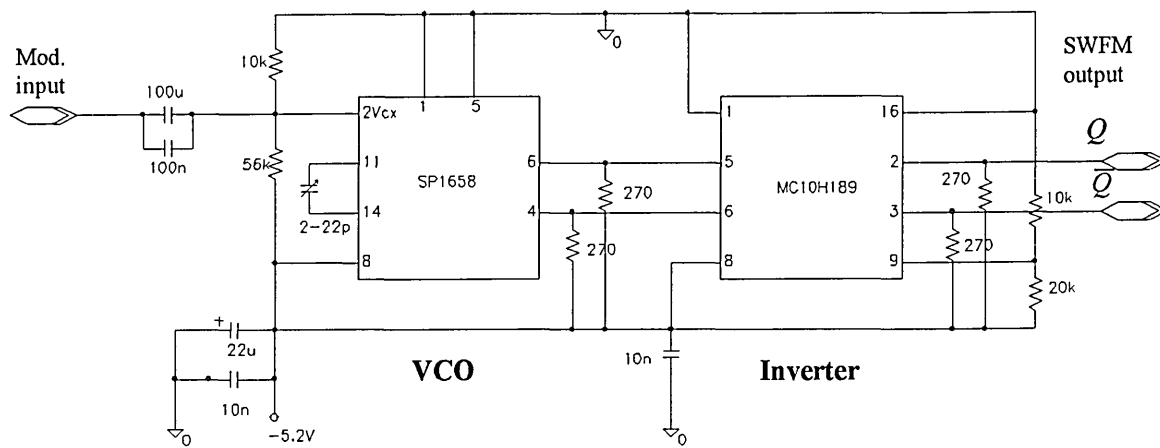
### 7.3.1 VCO and SWFM generation

SP 1658 [105] is a VCO, with a maximum output frequency of 190 MHz, which generates complementary ECL outputs. Frequency control of the square wave VCO output is accomplished through using a voltage controlled current source, which controls the slew rate of a single external capacitor. An input filter is available to decouple noise from the modulating signal and a bias filter eliminates ripple from the output signal at high frequencies.

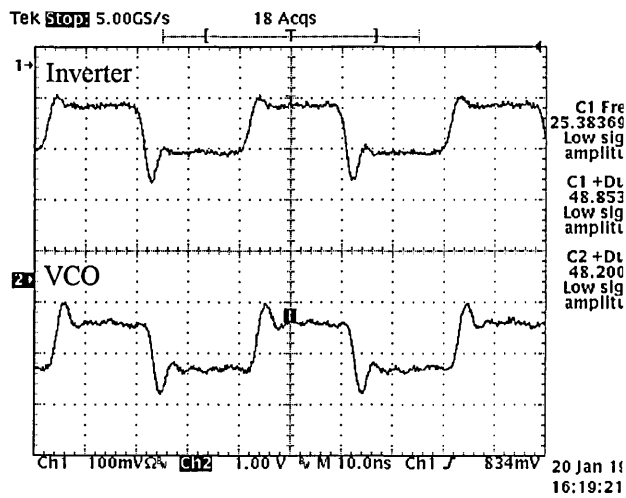
The voltage-to-frequency conversion characteristic of the VCO determine the amount of non-linear distortion generated at the SWFM/PFM transmitter (refer to section 5.5.1). The linearity test of the SP 1658 device, carried out for the intended frequency range of operation for this application, is given in Chapter 8.

It was shown in section 5.5.2 that in double-edge regeneration of SWFM, the spectral profile of PFM is translated on to the even harmonics, with the complete suppression of the sidetone structures around the carrier fundamental and odd harmonics, provided the duty cycle is 50%. Any deviations of the duty cycle would result in partial generation of the fundamental and odd harmonics, increasing the baseband distortion.

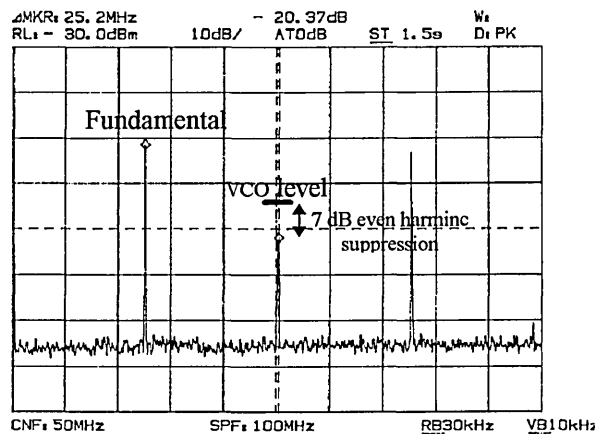
The time domain and frequency domain signals of the VCO output are shown in Fig. 7.10, indicating a strong presence of a second harmonic. In order to achieve a duty cycle closer to 50% and improve the even harmonic suppression, the VCO outputs were fed through an inverter.



(a) circuit diagram



(b) time domain signals



(c) signal spectrum (at inverter output)

Figure 7.10 SWFM modulation

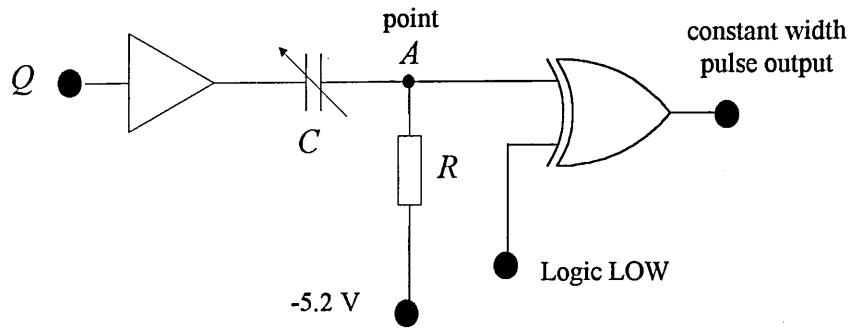
### 7.3.2 Pulse generator

The PFM signal is generated by triggering pulses on the leading edge of a SWFM signal (refer to section 5.2). The lack of commercially available monostables at high frequencies prompted the design of a pulse generator circuit. The gate delay technique, described in section 5.4, has been employed in several PFM implementations to generate constant width pulses from a SWFM signal [82]. Both PFM and SWFM demodulation rely on the regeneration of a PFM signal at the receiver. The circuit technique implemented at the transmitter would therefore, be also used at the receiver in order to regenerate the PFM signal.

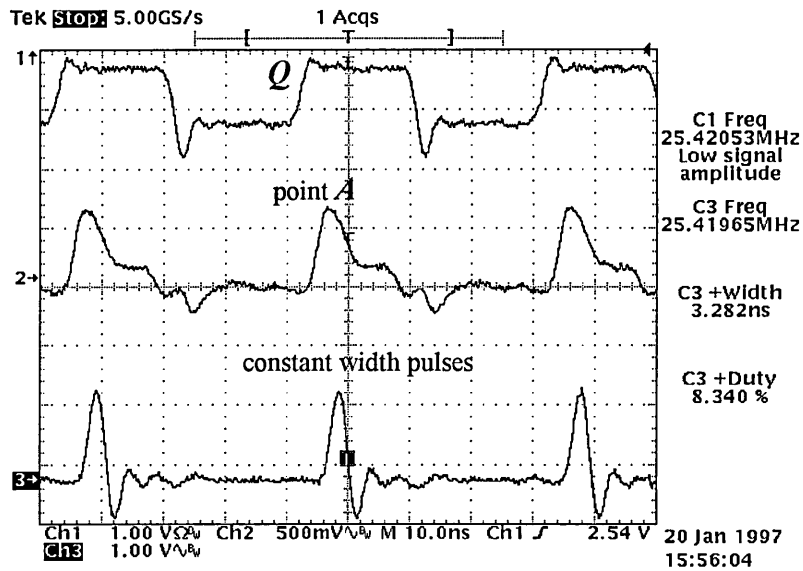
The signal waveforms associated with a pulse generator employing a gate delay technique was shown in Fig. 5.4(b). In this technique, the width of the generated pulses is determined by a combination of the propagation delay of the logic elements and the threshold crossing of the incoming signal. The effect of jitter noise on threshold crossing of PTM signals was graphically illustrated in Fig. 5.7. Due to the random nature of jitter noise, the threshold crossing of consecutive edges of the delayed signal, with respect to the undelayed signal, is variable. This introduces a degree of width modulation to the generated PFM signal, resulting in spectral distortion.

As a result, an alternative approach for pulse generation was called for. Figure 7.11 illustrates a pulse generation technique, employing a differentiator circuit. The width of the generated pulses is determined by the time constant  $RC$ , of the variable capacitor and the resistor. As the pulse generating edge transitions are determined by the external circuit components, rather than the threshold crossings of the incoming signal, this

technique has the ability to generate constant width pulses. The pulses generated by the technique are also shown.



(a) circuit block diagram



(b) signal waveforms

Figure 7.11 Constant width pulse generator.

## 7.4 PPM Transmitter

PPM modulation was dealt with in section 6.2. The process of PPM signal generation, by triggering pulses on the modulated edge of a PWM signal, was illustrated in Fig. 6.1. A critical part of the PPM modulator is the high frequency ramp generator used to generate the PWM signal, and is discussed in the following section. The PPM signal generation using the ramp signal is presented in section 7.4.2.

### 7.4.1 Ramp generator

PPM modulation requires a linear, high frequency ramp signal in order to implement voltage-to-pulse position conversion. There are various techniques of generating a ramp signal, but some of these are only suitable for low frequency applications.

An appropriate high frequency ramp generation technique is to charge a capacitor with a constant current source and to discharge through a high frequency switch. During the charging of the capacitor the ramp voltage rises to its maximum value, and discharging of the capacitor resets the ramp to its initial value. The linear characteristic of the ramp is governed by the following equation,

$$\frac{dV}{dt} = \frac{I}{C} \quad (7.1)$$

where  $I$  is the value of the constant current source and  $C$  is the capacitance. For example to generate a ramp of height 2 V in a duration of 25 ns, using a constant current source of 5 mA, the required value of capacitance is 62.5 pF.

Figure 7.12 shows the circuit diagram for a highly stable constant current source using general purpose pnp transistors. The voltage between  $T_2$  base and the positive supply line is held constant by the voltage reference source, usually a temperature compensated zener diode, forcing  $T_2$  to act as a constant current source. Thermal variations in  $V_{be2}$  are compensated by the use of an identical transistor  $T_1$ , connected in a base-collector diode arrangement. Assuming that  $T_2$  has a sensibly high current gain, the output current  $I_{e2}$  will be given simply by  $V_r/R_1$ . A very low overall temperature co-efficient of less than 50 ppm can be achieved by using a glazed ceramic resistor formulation for  $R_1$ .

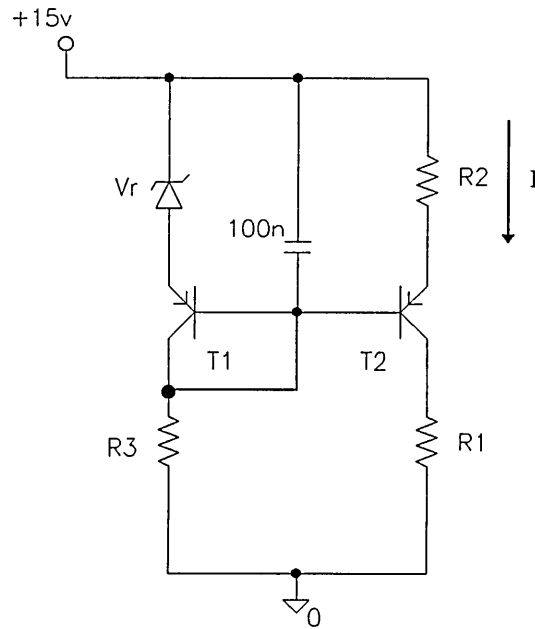


Figure 7.12 The constant current source.

Very short reset times are desired for the ramp signal, in order to improve the input dynamic range of the PPM modulator. **BFR 183** [106] is a npn, RF transistor with a gain bandwidth upto 8 GHz, which can be switched at extremely high frequencies. This device was used as a switch to discharge the capacitor, resulting in reset times in the order of 2 ns.

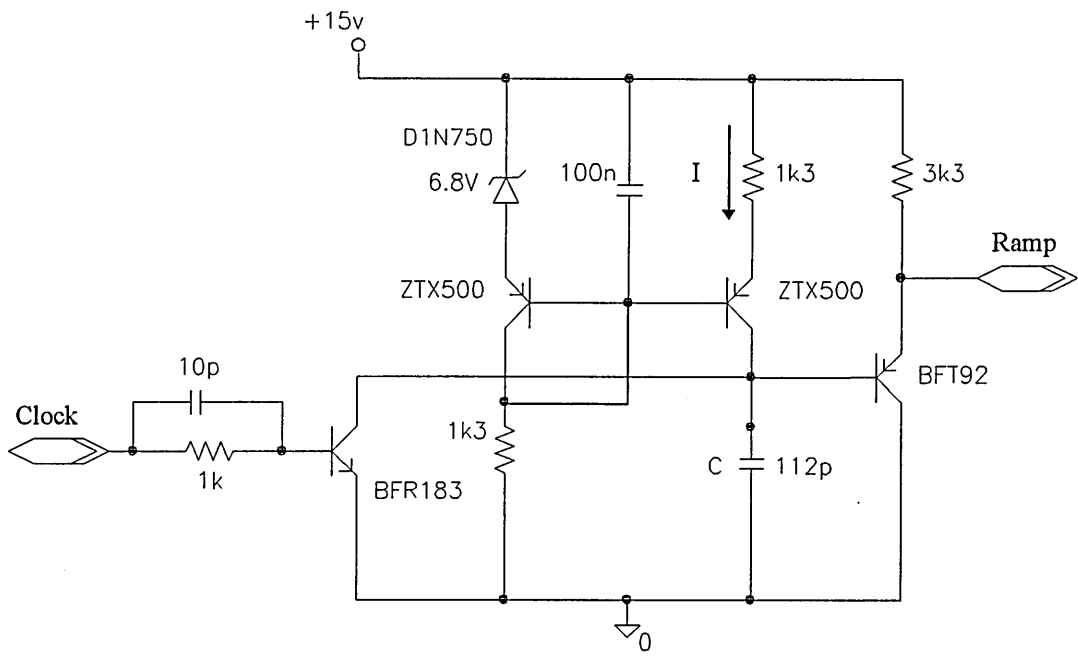
At high frequencies the charge storage in the base-emitter capacitance can be significant under saturated switching conditions, allowing the current flow to continue briefly, even after the switching pulses have been removed. A speed up capacitor is required in the base drive circuit for rapid removal of this excess base charge. The length of the lead from the capacitor to the collector of the switching transistor must also be kept to a minimum in order to limit unwanted inductances. **HP 8081A** rate generator from *Hewlett Packard* was used to generate the narrow width pulses required to reset the ramp.

Figure 7.13(a) shows the complete circuit diagram for the ramp generator, with an additional output transistor used as an output buffer. The oscilloscope traces of the clock pulses and the generated ramp output are also shown.

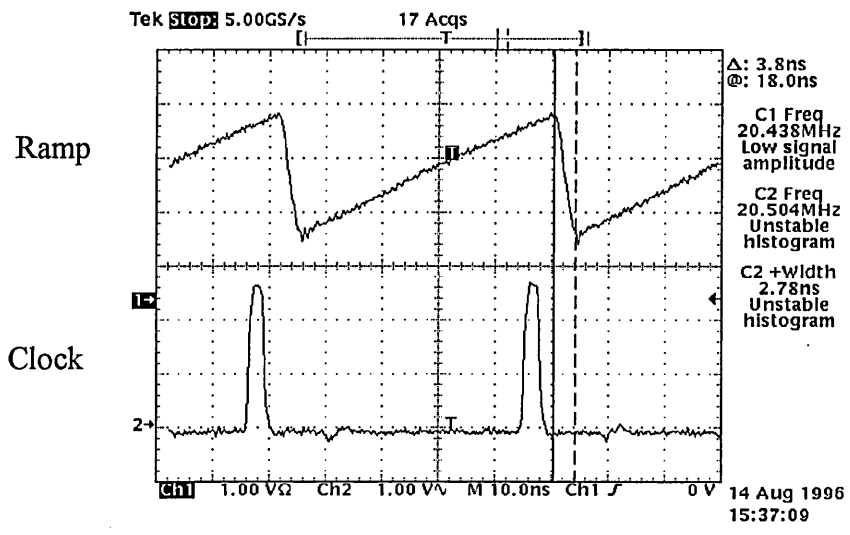
#### **7.4.2 PPM modulator**

The timing and circuit block diagram for PPM generation, employing a ramp signal, was illustrated in Fig. 6.1. A PWM signal is first generated by comparing the ramp signal with the modulating signal, using an ultra fast ECL comparator [107]. The PPM signal is generated by triggering pulses on the modulated edge of the PWM signal. The circuit diagram of the PPM modulator and the associated signal waveforms are shown in Fig. 7.14.

In section 6.3.2 it was shown that a clock component can be extracted at the receiver, from the incoming PPM signal. The extracted clock signal and the PPM pulse stream is used in signal demodulation. Therefore, no reference signal is required to be transmitted with the PPM signal.

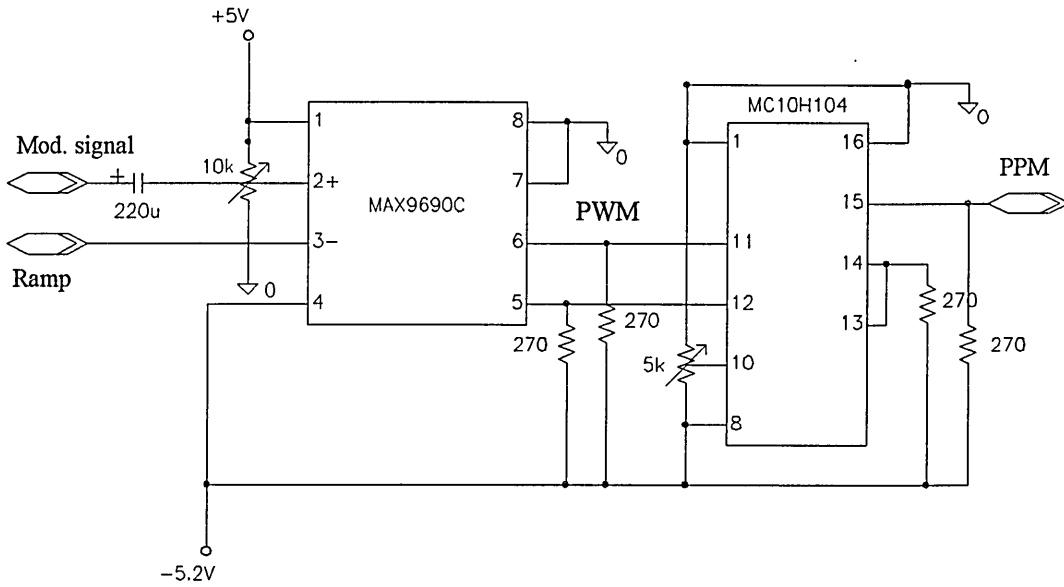


(a) circuit diagram

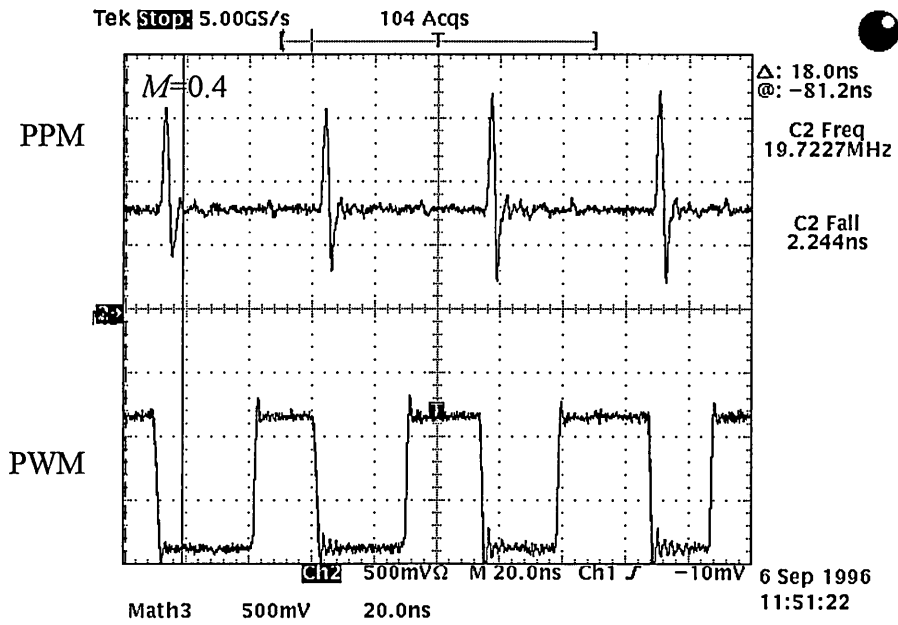


(b) waveforms

Figure 7.13 The ramp generator.



(a) circuit diagram



(b) PPM and PWM signals at a modulation index of 0.4

Figure 7.14 PPM modulator.

It was stated in section 6.2, that key parameters of the PPM modulator, including the amount of non-linear distortion, are primarily determined by the ramp generator. Therefore, in order to minimise the non-linear contribution a highly linear ramp signal is desired. The linearity of the PPM modulator was determined by accounting for the variation of the pulse width at the output of the comparator, for different values of offset voltages. The results are presented and analysed in Chapter 8.

## **7.5 Optical Link**

The PTM signals are transmitted via an optical link, which consists of an optical transmitter, optical fibre and an optical receiver. The choice of optical components is determined by a number of parameters such as system fidelity, cost, reliability, transmission capacity and transmission distance [59]. Details of the optical transmitter and optical receiver are presented in sections 7.5.1 and 7.5.2, respectively.

The performance potential of an optical link is characterised by two system parameters: optical power budget and rise time budget. These two parameters are evaluated in section 7.5.3.

### **7.5.1 Optical transmitter**

Optical transmitter converts the electrical signal into an optical format for transmission via optical fibre. PTM signals are ideal for optical fibre transmission as they can operate lasers at low duty ratios, increasing the device lifetime. Hence a laser source was employed as the optical source for PFM and PPM transmission. However, SWFM

operates with a 50% duty cycle, and due to its reduced bandwidth requirements a LED was adequate for optical transmission.

**LSC 2100** [108], a coolerless laser module operating at 1300 nm, was employed as the optical source for PFM and PPM transmission. The device is well suited for low power applications and can be modulated upto a data rate of 1 Gbit/s. The internal semiconductor laser is based upon InGaAsP buried heterostructure (BH) technology and has a maximum power output of 4 dBm and a typical spectral width (FWHM) of 3 nm. Threshold current of the laser is approximately 20 mA with a temperature co-efficient of 2.5% per °C. The **LSC 2100** package also include a photodiode for monitoring the laser output power and a longhorn type heat sink mounting flange.

The laser source, when operated as an optical transmitter, employs a bias circuit to compensate for temperature fluctuations of the device and a drive circuit to modulate the laser current, as illustrated in Fig. 7.15.

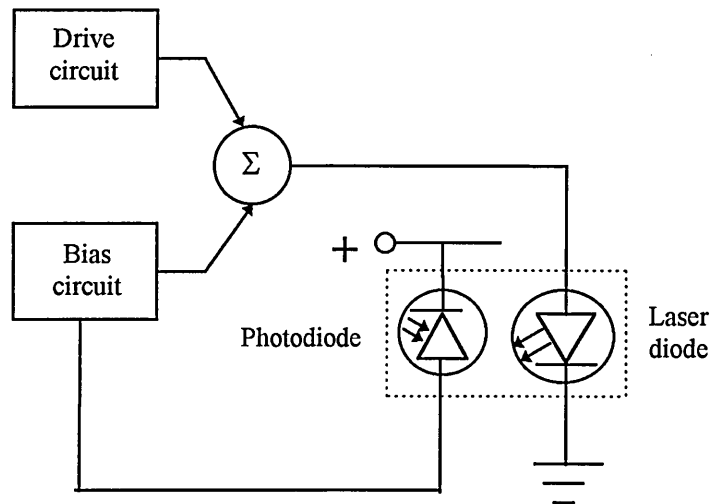


Figure 7.15 Laser source operated as an optical transmitter.

For digital transmission the laser is biased near, but below the threshold current [39]. The laser threshold current is strongly temperature dependent and therefore, a feedback technique is required to compensate for variations of the optical power output against threshold current variations. A simple bias circuit employing monitor photodiode current as the feedback parameter is shown in Fig. 7.16. Here, the monitor photodiode current account for any optical power fluctuations, due to the laser threshold current variations, by changing the bias voltage accordingly. A complete circuit analysis can be found in Appendix 1.

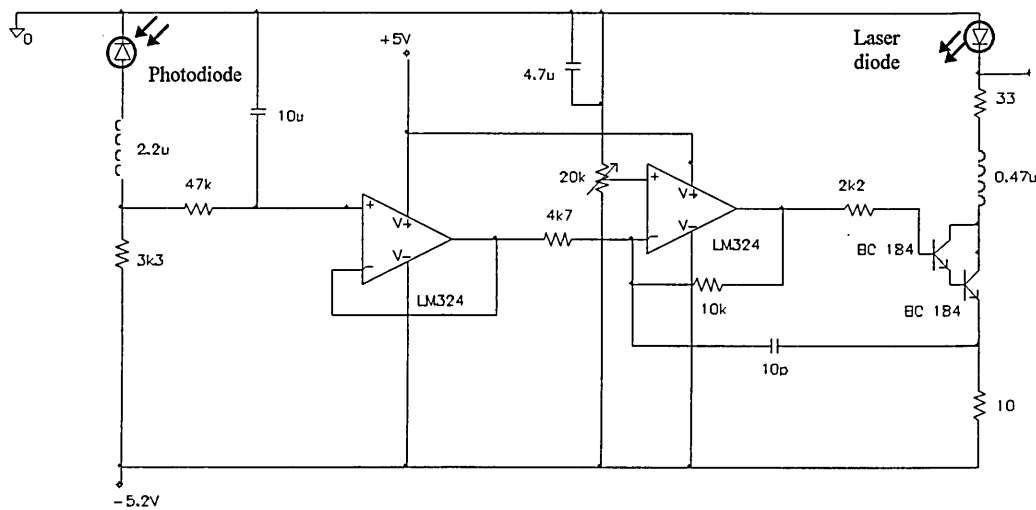


Figure 7.16 Laser bias circuit diagram.

The laser dynamic impedance in the forward current direction is very low and therefore driving the laser source with a low impedance voltage source should be avoided. In order to intensity modulate the ECL pulses, a differential drive circuit [109], which switches the main current from one transistor to the other, was employed. **BFR 93A** high bandwidth, npn RF transistors were used in the drive circuit, illustrated in Fig. 7.17.

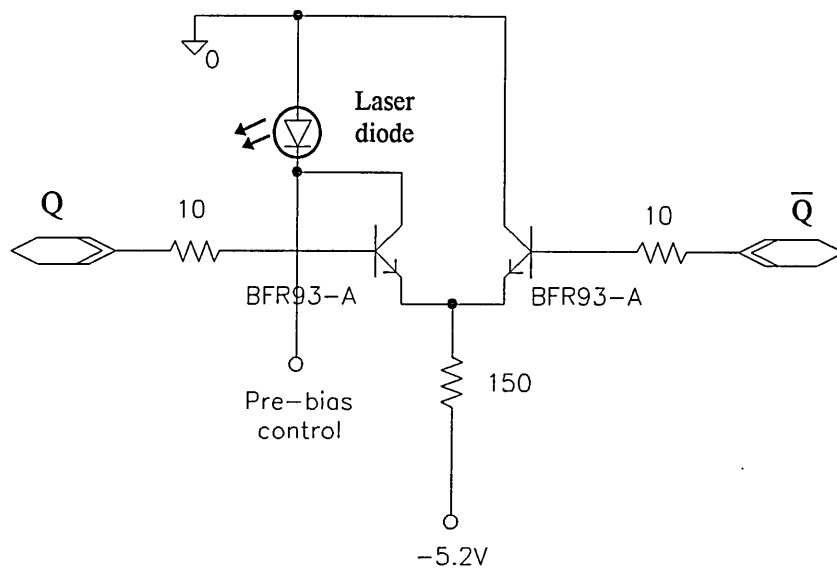


Figure 7.17 Laser drive circuit diagram.

**DL 1040-ST** [110] is a hybrid, optical transmitter-receiver pair. The **DLT 1040-ST** transmitter is a 16 pin dual in line package which employs an advanced edge emitting LED (ELED) as the optical source. The transmitter inputs are pseudo ECL (PECL) compatible i.e. ECL logic operated from a positive supply, and the optical power can be coupled to a 50  $\mu\text{m}$  or 62.5  $\mu\text{m}$  core multi-mode fibre, incorporating ST connectors. The LED operates at 1300 nm and has a maximum power output of -14 dBm and an optical rise time of 3.5 ns. **DLT 1040-ST** was employed to transmit SWFM signal and the circuit diagram is shown in Fig. 7.18.

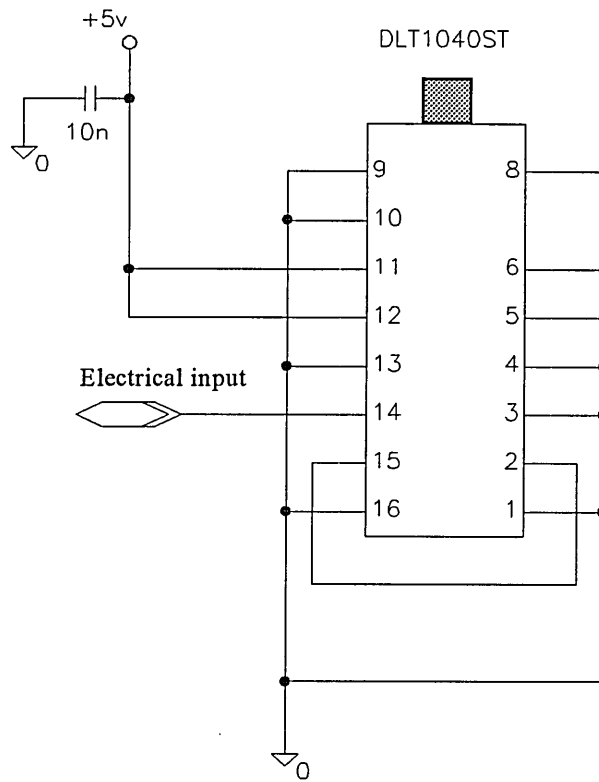


Figure 7.18 Optical transmitter module, employing an ELED.

## 7.5.2 Optical receiver

**DLR 1040-ST** receiver [110], containing an InGaAs/InP photodetector, Si bipolar IC pre-amplifier and a hybrid post-amplifier/decision circuit, was employed as the optical receiver. The photodetector has a maximum input power capability of -14 dBm and a minimum receiver sensitivity of -33 dBm. The optical rise and fall times are typically around 1.5 ns. The data outputs are PECL compatible, when terminated by 510  $\Omega$  resistors to ground. The complementary outputs should be terminated with identical load circuits to avoid unnecessarily large ac currents in the supply lines. A filter network is also present in **DLR 1040-ST**, which bandlimits the preamplifier output noise and thus improve the receiver sensitivity. Circuit diagram of the optical receiver is shown in Fig. 7.19.

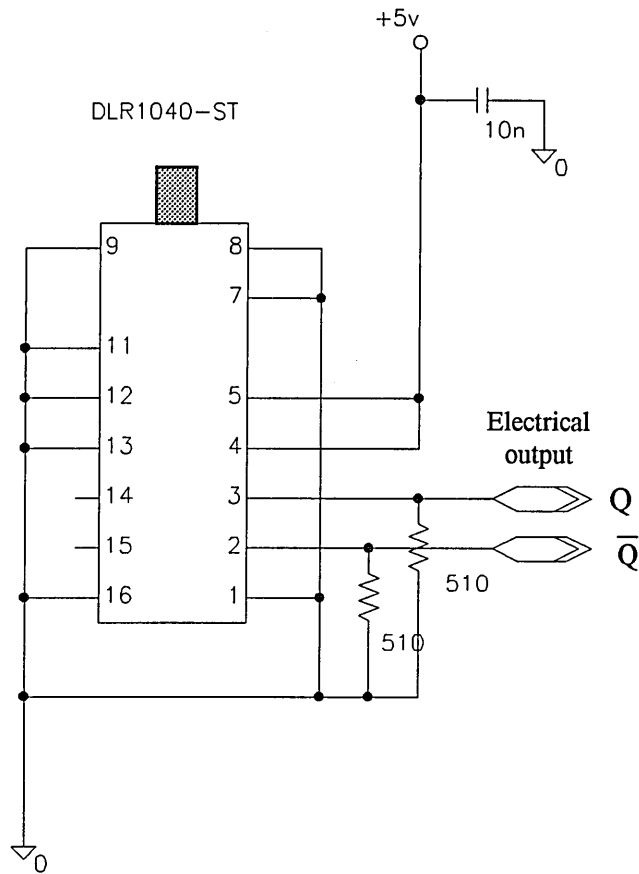


Figure 7.19 Optical receiver circuit diagram.

### 7.5.3 Optical power budget and rise time budget

The concept of an optical power budget was introduced in section 3.5.2. The equation governing the power budget was given by Eqn. (3.21) and is repeated here:

$$P_t = P_r + C_L + M_s$$

where  $P_t$  is the transmitted optical power,  $P_r$  is the received optical power,  $C_L$  is the total channel loss and  $M_s$  is the system margin. Assuming a maximum optical power output for the laser diode operation, a minimum receiver sensitivity for the photodiode and a typical system margin of 7 dB [10], the net optical power available for channel transmission is 32.5 dB ( see Table 7.4).

The channel losses are incurred due to fibre attenuation  $\alpha_f$ , connector losses at the transmitter and receiver  $\alpha_{con}$  and splice losses  $\alpha_{splice}$ . Therefore, the total channel loss  $C_L$  can be expressed as:

$$C_L = \alpha_f + \alpha_{con} + \alpha_{splice} \quad (7.2)$$

Allowing a typical 2 dB value for connector losses [10], 0.1 dB loss for each splice connection placed 1 km apart [5] and a characteristic 0.4 dB/km fibre loss for the 1300 nm wavelength of operation, the optical power restricted, maximum transmission distance  $L$ , of the optical link is 60 km.

In optical communication systems, the purpose of a rise time budget is to ensure that adequate bandwidth is available among optical components for an intended application. The concept of rise time is used to allocate bandwidth since, they are inversely related (refer to section 5.4.2.3 and Eqn. (5.31)). The rise time budget of an optical link is expressed as [10]:

$$T_{sys} = \sqrt{T_t^2 + T_f^2 + T_r^2} \quad (7.3)$$

where  $T_t$  is the transmitter rise time,  $T_r$  is the receiver rise time and  $T_f$  is the fibre rise time. Generally the values of  $T_t$  and  $T_r$  are available from the vendors but  $T_f$  is dependent on fibre dispersion and can be defined as [10]:

$$T_f = \sqrt{T_{mat}^2 + T_{mod}^2} \quad (7.4)$$

where  $T_{mat}$  and  $T_{mod}$  are the dispersion contributions due to fibre material dispersion and modal dispersion, respectively. Agrawal [10] has defined these parameters by the following equations.

$$T_{mat} \approx |D_f| L \Delta\lambda \quad (7.5a)$$

$$T_{modal} \approx \frac{n_1 \Delta}{c} L \quad (7.5b)$$

Here,  $D_f$  represent the fibre dispersion parameter,  $\Delta\lambda$  is the FWHM spectral width of the optical source,  $n_1$  is the refractive index of the fibre core,  $c$  is the speed of light and  $\Delta$  is parameter defined in terms of  $n_1$  and the refractive index of the fibre cladding [111].

In this application a 50/125  $\mu\text{m}$  graded index multi-mode fibre has been used. Since the wavelength of operation is at 1300 nm, the material dispersion is insignificant. Therefore, fibre rise time is solely determined by  $T_{modal}$ , and for the power restricted transmission distance was calculated to be 1.46 ns. This results in an overall rise time budget of 2.32 ns.

When the optical link is operated at the power restricted, maximum transmission distance of 60 km, the rise time budget allows for a system bandwidth of 150 MHz. The parameters used in optical power budget and rise time budget calculations are summarised in Table 7.4.

	Parameter	Value		
<b>Optical Power Budget</b>	$P_t$ (maximum)	4 dBm		
	$P_r$ (minimum)	-35.5 dBm		
	$P_t - P_r$		39.5 dB	
	$M_s$	7 dB		
	$L\alpha_f + (L-1)\alpha_{splice} + \alpha_{con}$		32.5 dB	
	$\alpha_f$	0.4 dB/km		
	$\alpha_{con}$ $\alpha_{splice}$	2 dB 0.1 dB		
$L$		60.8 km		
<b>Rise Time Budget</b>	$T_t$	1.0 ns		
	$T_r$	1.5 ns		
	$T_{mod}$	1.5 ns		
	$n_i$	1.46		
	$\Delta$	0.2		
	$c$	$3 \times 10^8 \text{ ms}^{-1}$		
	$T_{sys}$		2.3 ns	
$B_{sys}$		150.8 MHz		

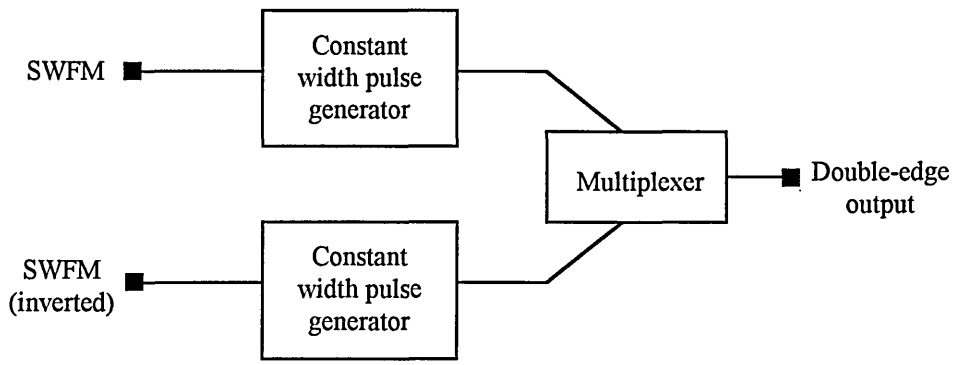
Table 7.4 Summary of system parameters used in optical power budget and rise time budget calculations.

## 7.6 PFM and SWFM Receiver

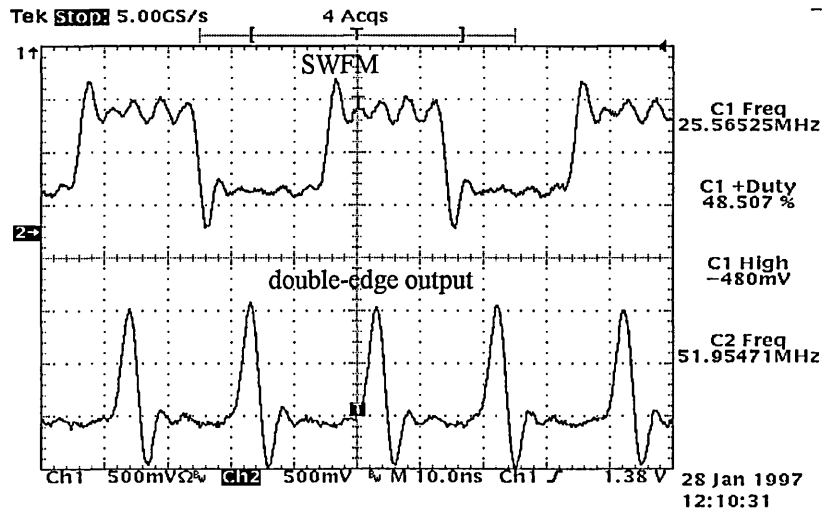
A block diagram of the PFM/SWFM demodulator was shown in Fig. 5.3, where the information is recovered by lowpass filtering the baseband component of a regenerated PFM signal, constructed from the incoming PFM or SWFM signal. The post decision circuit of the **DLR1040-ST** [110] optical receiver generates PECL outputs, which can be converted back into ECL level by applying a dc bias. This signal can then be applied to the constant width pulse generator, discussed in section 7.3.2, in order to produce the regenerated PFM signal. The parabolic relationship identified in section 5.3, for the baseband signal power and the duty ratio of the regenerated PFM signal, will be confirmed by experimental data in Chapter 8.

Double-edge regeneration of SWFM, employing the gate delay technique for pulse generation, was illustrated by Fig. 5.5. The width modulation produced by this technique has already been mentioned in section 7.3.2. In double-edge detection systems, this effect is even more pronounced as the rise and fall times of the SWFM signal are not identical.

Therefore, in order to generate pulses on both edges of a SWFM signal, the approach shown in Fig. 7.20 was used. Here, two constant width pulse generators, described in section 7.3.2, are used to produce pulses at the rising and falling edges of the SWFM signal. The two pulse streams are combined resulting in a double-edge signal.



(a) circuit block diagram



(b) signal waveforms

Figure 7.20 Double-edge SWFM regenerator.

## 7.7 PPM Receiver

The demodulation process of PPM was outlined in section 6.3. The recovery of a clock reference signal from the incoming PPM pulse stream allows for a PWM signal to be regenerated at the receiver. Information is recovered by lowpass filtering the baseband component of the PWM signal. Therefore, the key components of the demodulator are the PLL and the PWM generator. The theory behind PLL operation was presented in section 6.3.3, and its circuit implementation is dealt with in section 7.7.1. The subsection which follows, presents the PWM generator.

### 7.7.1 Phase locked loop (PLL)

The PPM spectral investigation in section 6.3 had shown the strong presence of a clock reference signal at low modulation indices, decaying to its lowest value at a modulation index close to 80%. Figure 7.21 shows the lowest clock component detected for a PPM signal, when modulated at an index of 78%. This illustrates that the clock component is approximately 25 dB above the signal noise floor, allowing adequate margin for a PLL to lock on to it.

NE 564 [112] is a monolithic PLL with TTL compatible inputs and outputs, which can be operated upto a frequency of 50 MHz. The device consists of a limiter, VCO, phase detector and a post detection processor for demodulation applications. The phase detector consists of a double balanced modulator with a limiter amplifier to improve AM rejection.

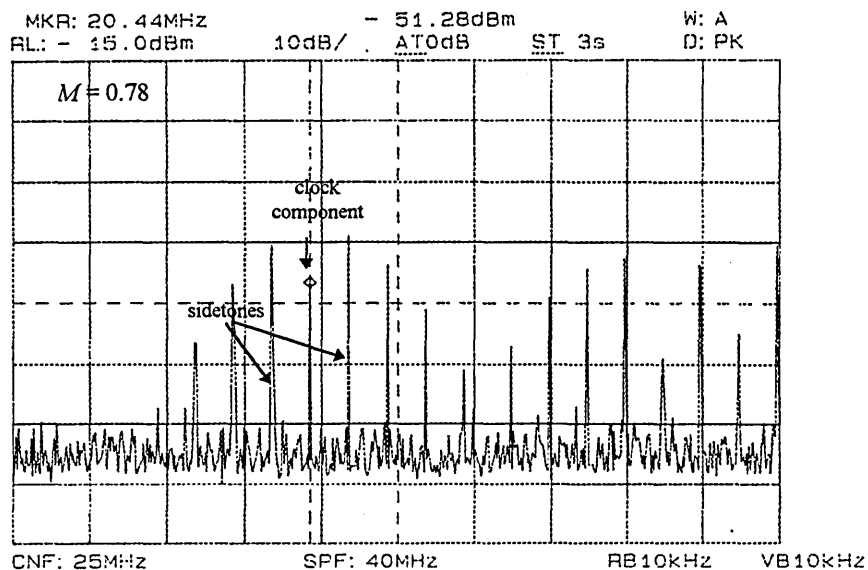


Figure 7.21 PPM spectrum at a modulation index of 78%.

It was stated in section 6.3.3 that the loop filter of a PLL has considerable influence on its operation. In NE 564 the loop filter is a simple first order RC network, and the loop transfer function is given by,

$$f(s) = \frac{1}{1+sRC} \quad (7.1)$$

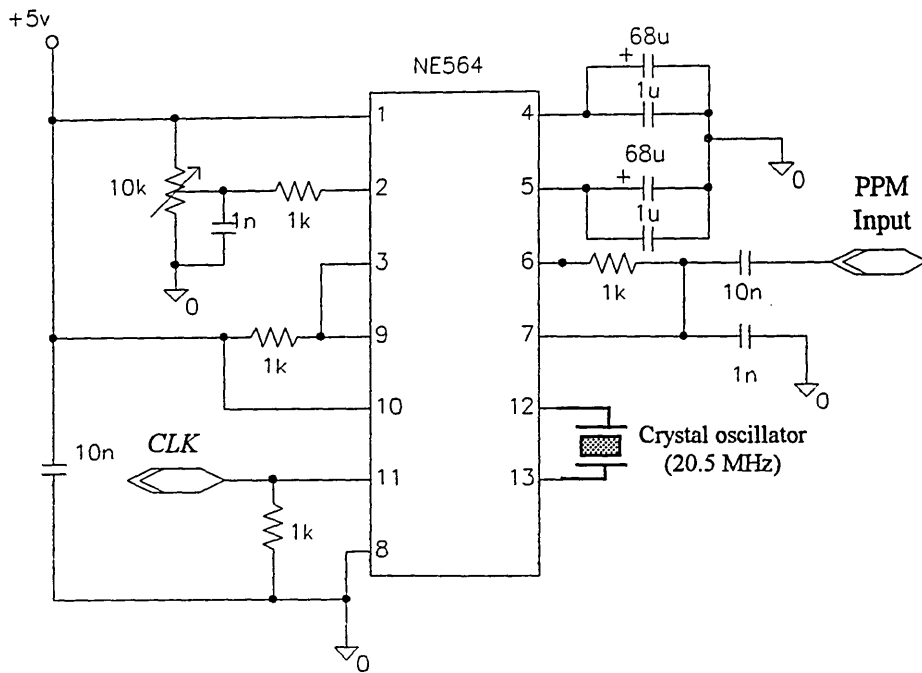
where  $R$  is internal and  $C$  is an external capacitor. The spectral investigation of PPM shows a clock component which has sidebands on either side, at close proximity. Therefore, in order to prevent the PLL from locking onto the sidebands a narrow lock-in-range is desired. This is achieved by making the loop bandwidth as narrow as possible. A narrow loop bandwidth has the added advantages of better noise performance and an extended hold-in-range. A loop filter with a 3 dB cut-off frequency of approximately 6 Hz was used in this application.

To design a small loop bandwidth PLL and to ensure good locking, a crystal controlled VCO is highly desirable. The VCO frequency drift should be controlled to be less than the lock-in range in order to prevent the PLL going out of lock. A crystal controlled VCO, operating at 20.5 MHz was used at the receiver. The frequency offset between the transmitter and the receiver must also be kept to a minimum, so that the VCO frequency drift can be made to be within the lock-in range of the PLL. The carrier frequency of the PPM transmitter was set by the clock signal from a stable function generator (HP 8081A).

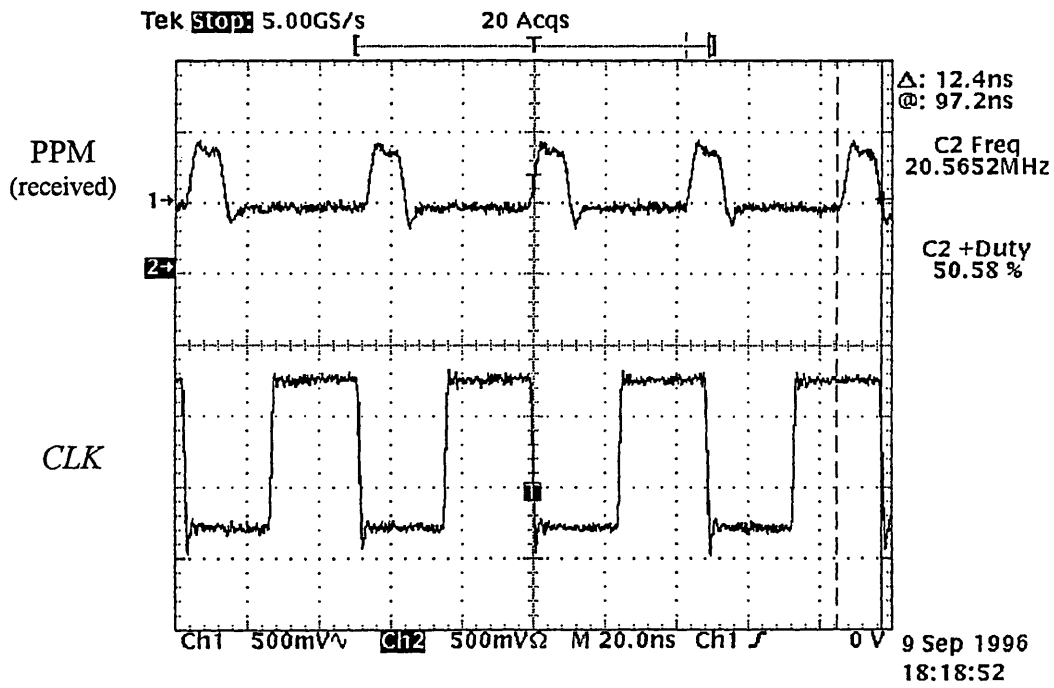
The circuit diagram of the PLL is shown in Fig. 7.22 (a). The received PPM pulse stream and the recovered clock signal is shown in Fig. 7.22 (b).

### **7.7.2 PWM generator**

The signal waveforms associated with the PPM demodulator and its circuit block diagram were shown in Figs. 6.4 and 6.6, respectively. The recovered clock signal and the PPM pulses can be combined to trigger a latch in order to generate the PWM signal. The TTL compatible clock output of the PLL was converted to ECL levels using an ECL comparator and pulses were triggered at the falling edge of the inverted clock signal. These clock pulses were combined with the PPM signal and fed to a dual D-latch, which performs a divide by two operation to generate the PWM signal. The circuit diagram of the PWM generator is shown in Fig. 7.23.



(a) circuit diagram



(b) signal waveforms

Figure 7.22 The phase locked loop.

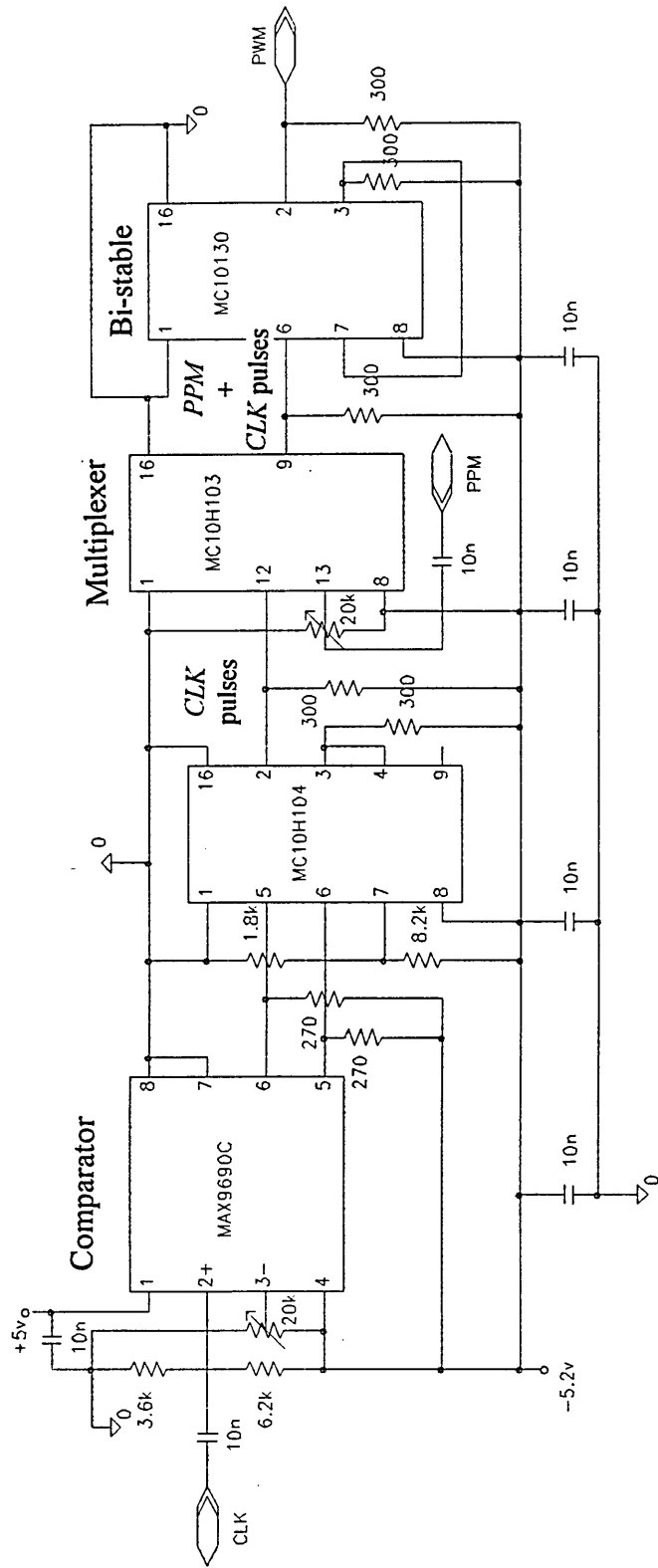


Figure 7.23 PWM generator employed in the PPM receiver.

## 7.8 Demultiplexing and Signal Demodulation

In each PTM technique, baseband regeneration was employed at the receiver. In order to recover the information, subcarrier channels must be isolated and appropriate demodulation techniques should be employed. The implementation of a baseband channel and the commercial availability of filters at the subcarrier frequencies chosen for the prototype, meant filtering was a favourable technique to recover information. In the following sub-sections, the filters used to recover the subcarrier channels from the SCM signal, and demodulation techniques employed to recover signals, are presented.

### 7.8.1 Video signal recovery

Lowpass filters for PAL/SECAM receiver applications are widely available and a 5.5 MHz, lowpass filter from *Toko* [113] was employed to recover the video channel. A differential video amplifier [103], which provides the required gain and bandwidth, was used to amplify the video signal. The circuit diagram for video signal recovery is shown in Fig. 7.24.

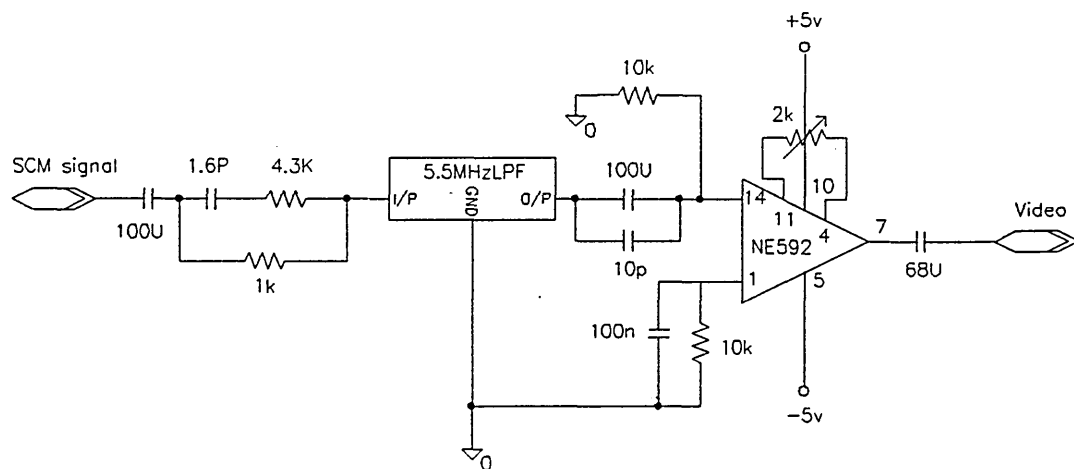


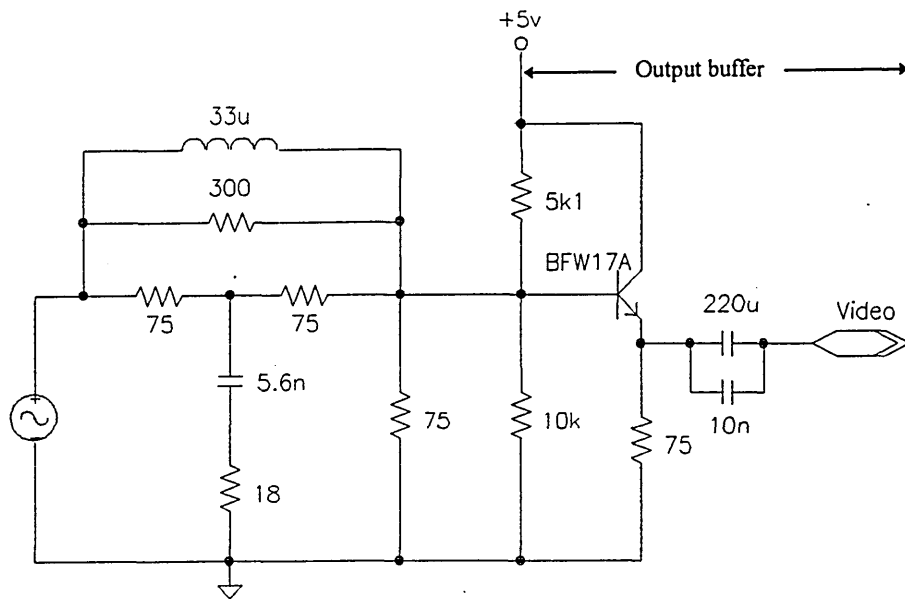
Figure 7.24 Video signal recovery by employing a low pass filter.

Since, pre-emphasis was employed at the transmitter to boost the high frequency signal components, a de-emphasis network is required at the receiver to restore the original signal levels. The video de-emphasis network conforming to CCIR-405 standard and its frequency response are shown in Fig 7.25. An emitter-follower stage was cascaded after the video amplifier to provide the necessary gain adjustment and the required output impedance.

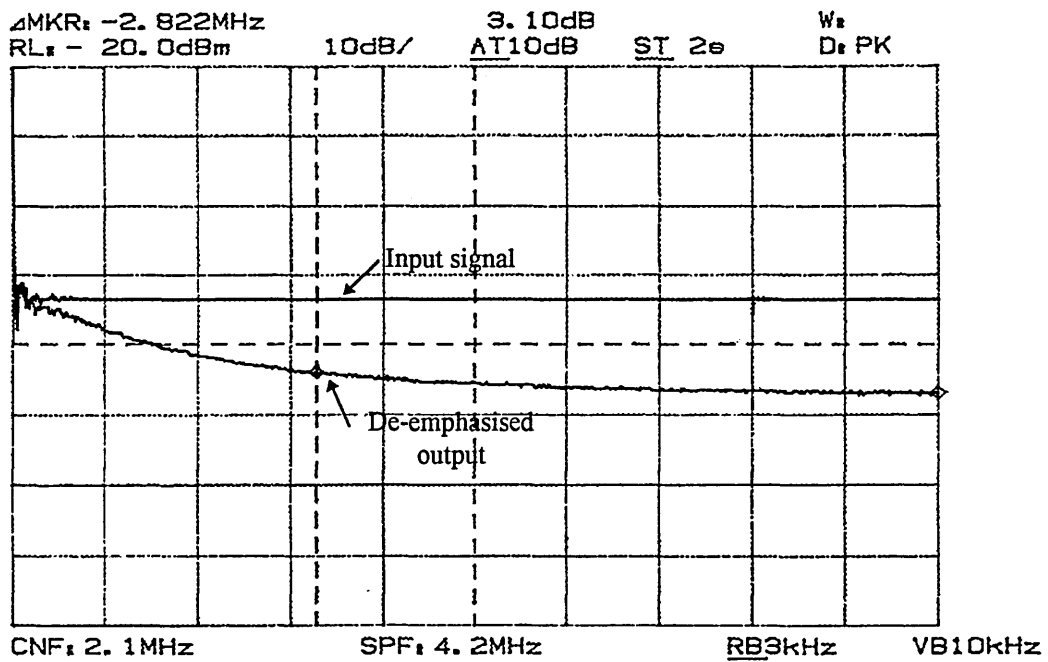
### 7.8.2 Audio signal recovery

Audio signals were recovered by using bandpass filters to filter the FM modulated channels and employing FM demodulators to recover the baseband audio signals. A ceramic filter, custom built for PAL television sound applications [114] was used for the 6.0 MHz channel and a bandpass filter operating at a centre frequency of 7.2 MHz [115] was used for the second audio channel.

The TBA120C [116] monolithic IC, specifically designed for use in the sound section of TV receivers and the FM/IF portion of radio receivers, was used to demodulate the audio channels. The carrier frequency to which the demodulator locks on is determined by an external capacitor and an inductor. The device has a built-in limiter and an IF amplifier, and can operate upto a frequency of 12 MHz. The audio de-emphasis network consists of an external 22 nF capacitor between pin 8 and 11 and a 2.6 k $\Omega$  internal resistor. An audio amplifier[117], designed to deliver 2 W/channel continuous power into a 8  $\Omega$  load, was used for signal amplification. The circuit diagram for the 6.0 MHz audio channel recovery is illustrated in Fig. 7.26.



(a) circuit diagram



(b) frequency response

Figure 7.25 The de-emphasis network for PAL-625 video signal.

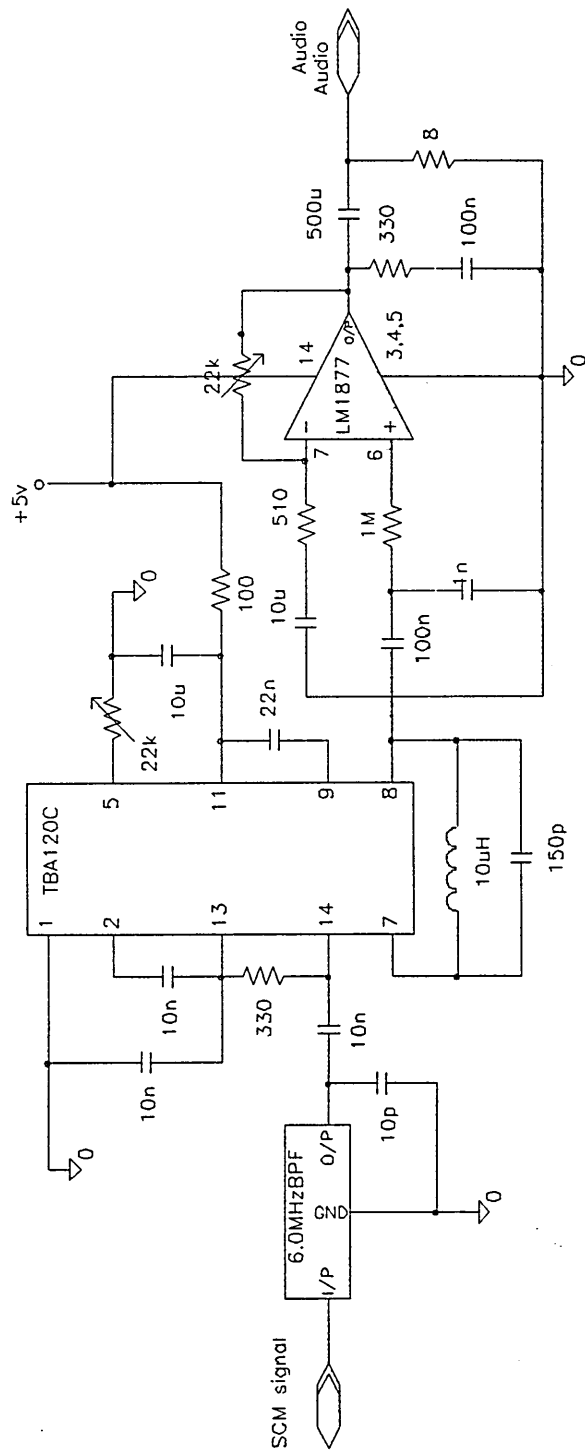


Figure 7.26 Filter and demodulator circuit diagram for the 6.0 MHz audio channel.

### 7.8.3 Data signal recovery

The data channel was allocated the frequency band used for NICAM stereo transmission in a PAL television signal. Therefore, a commercially available NICAM stereo filter [118] was used to filter the FSK signal. The NE564 phase locked loop, described in section 7.7.1, is capable of demodulating FSK signals at data rates in excess of 1 M baud. The centre frequency of the demodulator was selected by a combination of external capacitors. The post detection processor present within the IC convert the mark and space frequencies into DC levels compatible with TTL logic. The circuit diagram for FSK demodulation is shown in Fig. 7.27.

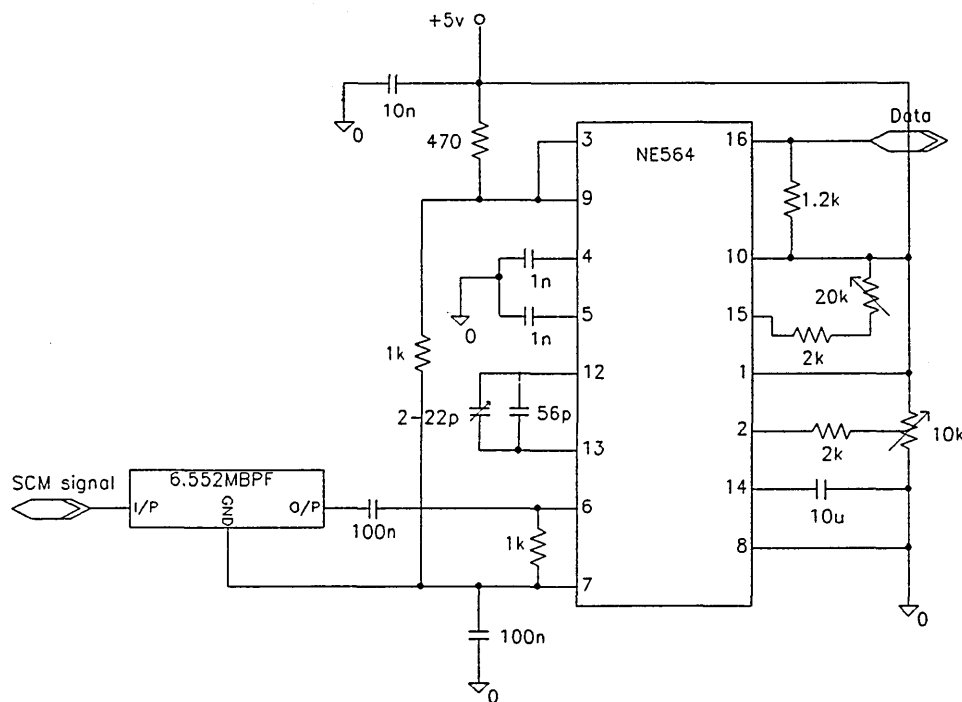


Figure 7.27 Circuit diagram for data channel signal recovery.

## 7.9 Summary

In this chapter the hardware system implementation of the prototype, to demonstrate the technical feasibility of the SCM-PTM concept, was presented. The SCM signal was formed by a video channel, two audio channels and a data channel. The pre-emphasis and de-emphasis networks for the video and audio channels, conforming to the industry standards, were presented. Each PTM technique was implemented using the high speed ECL logic family, and its properties were listed. A *RC* differentiator circuit was nominated as an alternative constant width pulse generator to the gate delay technique. The design of a highly linear ramp generator, critical to PPM operation, was also given.

Details of the bias circuit and the driver circuit for the laser diode operation was given in section 7.5. The optical power budget and the rise time budget calculations have shown a maximum, power restricted transmission distance of 60 km and a system bandwidth of 150 MHz for the optical link. The technique nominated for PPM demodulation in Chapter 6 was implemented by employing a PLL with a narrow loop bandwidth. The commercially available filters at the nominated subcarrier frequencies, and the appropriate demodulation techniques allowed for signal channel recovery.

---

## Results and Analysis

The operational details and theoretical predictions for PFM, SWFM and PPM systems were presented in Chapters 5 and 6. This was followed by details of the prototype system implementation, incorporating each of the above PTM techniques, to transmit a broadband SCM signal. In this chapter, various theoretical predictions made earlier is verified, and the system prototype is used as a test bed to evaluate the performance potential of the SCM-PTM concept.

In the following section the spectral characteristics, baseband signal power variations, the clock component behaviour *etc.* for PFM, SWFM and PPM systems are shown to be in agreement with the theoretical predictions. The implications of baseband distortion for practical SCM-PTM system implementation is discussed in section 8.2. The SNR performance of video and audio channels and the BER performance of the data channel for the implemented PTM techniques are presented in section 8.3. The performance potential of each PTM technique is evaluated and weighed against conventional analogue

techniques. In section 8.4 the linearity of the PTM sub-system, critical to the harmonic performance of the system, is presented. The overall harmonic performance of the system is also presented, by measuring the second and third harmonic performance for each signal channel.

### 8.1 Verification of Spectral Predictions

The general characteristics attributed to PTM spectrums were identified in section 4.3.3. These include the prsence of a carrier frequency and its harmonics and a set of diminishing sidetones centered around each of these frequency componenets. The sidetones are seperated in frequency by an integer multiple of the modulating signal frequency and can be predicted by the Bessel function of the first kind.

In order to verify the theoretically predicted spectrums, frequency domain measurements were carried out on the prototype. The measurement setup is shown in Fig. 8.1, and single tone modulation has been employed in order to simplify the spectral analysis process.

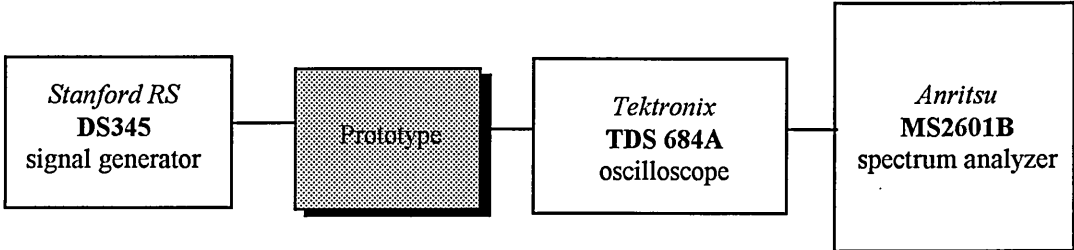


Figure 8.1 Test setup for frequency domain measurements.

### 8.1.1 PFM and SWFM systems

The spectral characteristics of SWFM and PFM systems were identified in section 5.3. A verification of these theoretically predicted spectrums is given in this section. Figure 8.2 shows the spectrum of a SWFM signal, modulated by a 1 MHz sine wave. The presence of a carrier fundamental and odd harmonics, with sidetones around them separated by the modulating signal frequency, can be identified. As predicted, the deviation around the harmonics is greater, compared to the deviation about the fundamental. The even harmonic presence is due to the deviation of the square wave duty cycle from an ideal value of 50%.

The sidetone structure around the carrier fundamental and the harmonics are predicted by Bessel functions of the first kind. The first carrier null detected for the SWFM signal is shown in Fig. 8.3. Theoretically, this corresponds to a  $\beta$  value of 2.408, and this predicts a modulation sensitivity of 20.24 MHz/V for the VCO. This value is in close agreement (within experimental errors) with the experimental data (see Fig. 8.6), conforming the Bessel function behaviour of the sidetones.

The PFM spectrum, when modulated by a 1 MHz sine wave, is shown in Fig. 8.4. Here, the significance is the presence of the modulating signal as a distortionless baseband component, which allow for signal recovery at the receiver. In addition to the carrier fundamental and odd order harmonics side tone structure, as in the case of SWFM, the even order harmonics are also present in PFM systems.

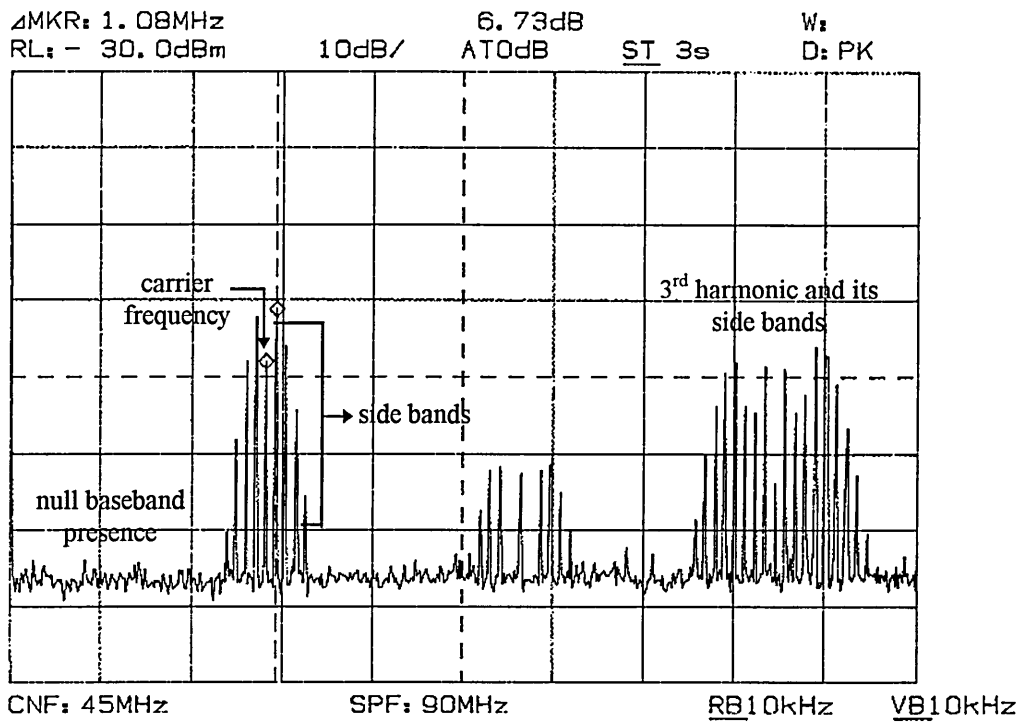


Figure 8.2 SWFM spectrum

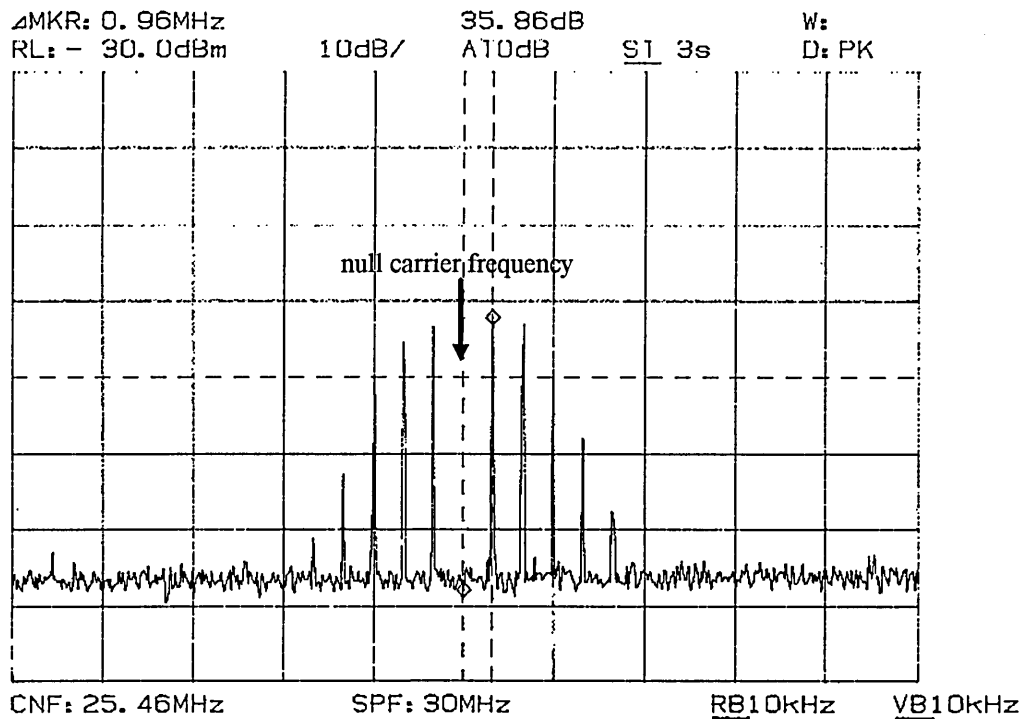


Figure 8.3 SWFM spectrum, indicating a carrier null.

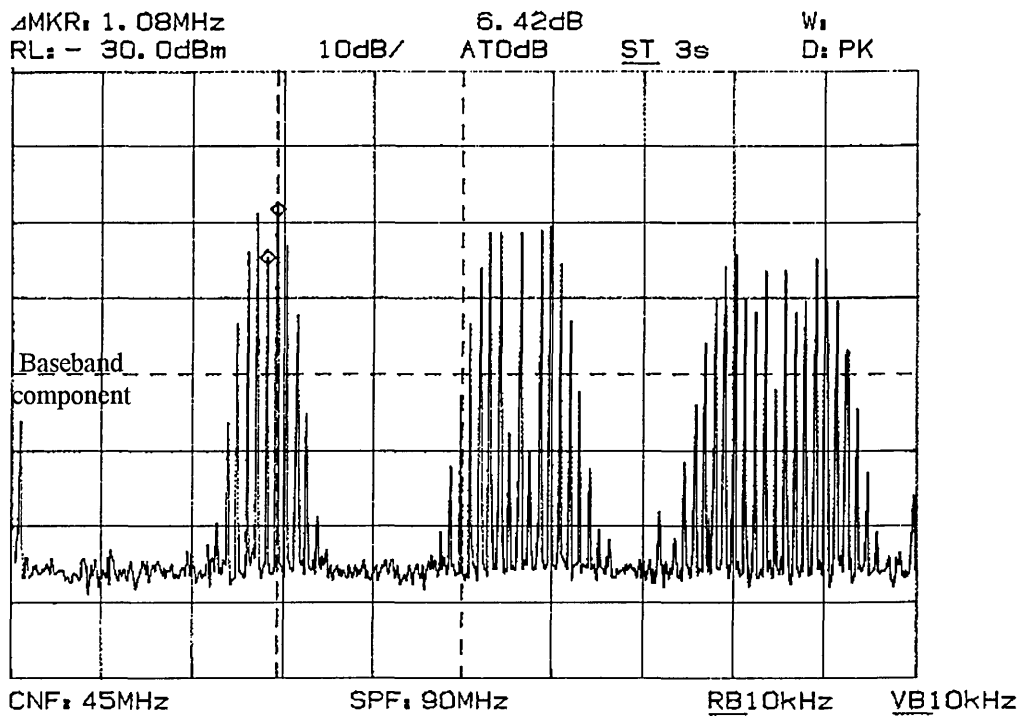


Figure 8.4 PFM spectrum, containing the baseband.

The transmitted PFM pulse width is determined by the required signal-to-noise ratio performance and the available channel bandwidth. A narrow width pulse is desired at the transmitter, as the detected pulse width and the PFM noise power spectral density are inversely related (see section 5.4). However, the achievable SNR performance is constrained by the available channel bandwidth, since shorter pulses require a greater transmission bandwidth (refer to section 5.5.3).

At the PFM receiver, the information is recovered by lowpass filtering the baseband component of the regenerated PFM signal (section 5.3). The relationship between the PFM baseband signal power and the regenerated duty ratio was plotted in Fig. 5.4. Using equivalent system parameters and a sampling ratio,  $R = 28$ , the measured power of the baseband component, for different values of the regenerated PFM duty ratio, is

illustrated in Fig. 8.5. The measured values were fitted to the theoretical curve by applying an appropriate uniform gain factor, confirming the parabolic relationship indicated in Chapter 5. Therefore, as opposed to the transmitter, a wider pulse is advantageous at the output of the PFM regenerator in order to maximise the signal power. Figure 8.5 indicates that when the duty ratio is raised from 20% to 40 %, the baseband signal power increases by a factor of 4, a 6 dB improvement.

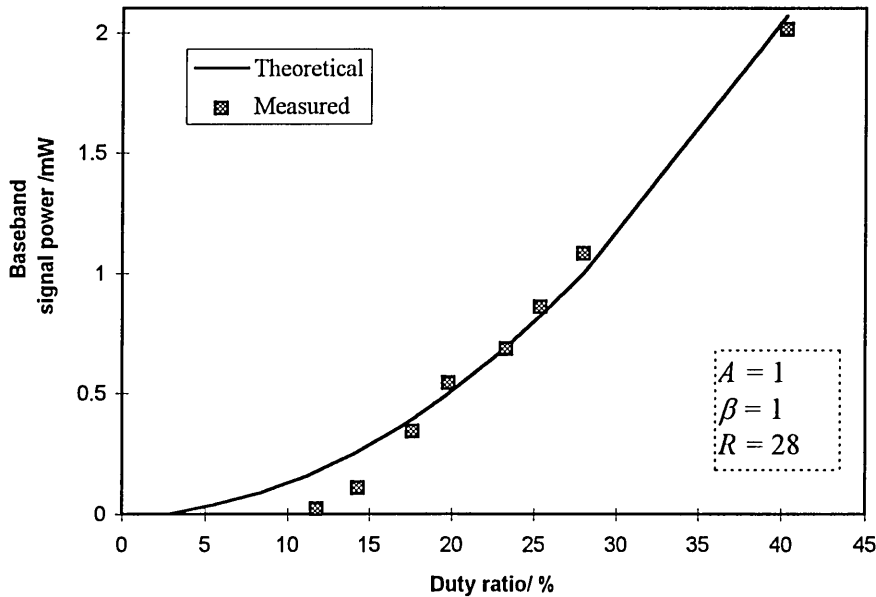


Figure 8.5 PFM baseband signal power variation for different duty ratios.

### 8.1.2 PPM system

The spectral characterisation carried out in section 6.3 revealed the presence of a strong clock frequency component for the PPM spectrum, and a baseband component for the PWM signal. Based on these findings a novel detection technique, based on recovery of the clock component from the incoming PPM pulse train, was introduced. The details of its implementation were presented in section 7.7.

The amplitude of the PPM carrier, normalised to the value of the unmodulated carrier, was plotted for different modulation indices, see Fig. 6.5, using Eqn. (6.9). It showed a strong carrier frequency component at low modulation indices, rapidly decreasing to lower levels at higher modulation. For the same system parameters, the measured amplitude of the PPM carrier (clock) component, normalised to the amplitude of the unmodulated carrier component, for different modulation indices, is indicated in Fig. 8.6, showing excellent agreement with the predicted results.

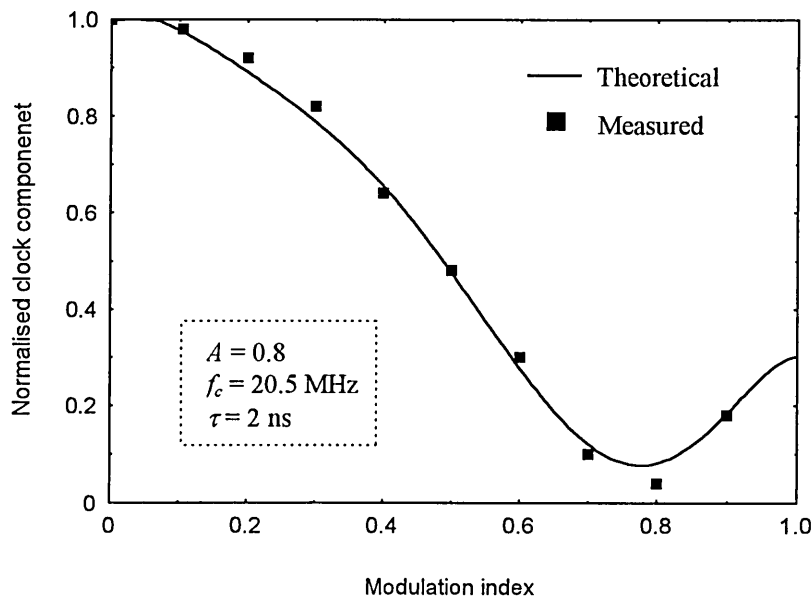


Figure 8.6 Normalised clock component against modulation index for a PPM system.

In order to gain a quantitative understanding, the PPM spectrum containing the lowest clock component, for the modulation range indicated in the graph, was shown in Fig. 7.21. This indicated a frequency component which is approximately 20 dB above the signal noise floor, allowing adequate margin for a PLL to lock and recover the clock component. In fact, the measured lowest clock component corresponded to a modulation index of 78%, in close agreement with the predicted value.

In section 7.7.1 the need for a PLL with a narrow lock-in-range was emphasised because of the presence of sideband components at close proximity, on either side of the PPM carrier. Figure 8.7 shows the measured relative amplitude of the clock (carrier) component to the first sideband pair for different modulation indices. As it can be seen at low modulation indices the sidebands levels are sufficiently below the clock component. However, beyond a modulation index of 60% the sidebands dwarf the clock component, approximately 6 dB higher at 80% modulation. Therefore, at high modulation indices the PLL should be carefully designed in order to prevent it from locking onto the sideband frequencies.

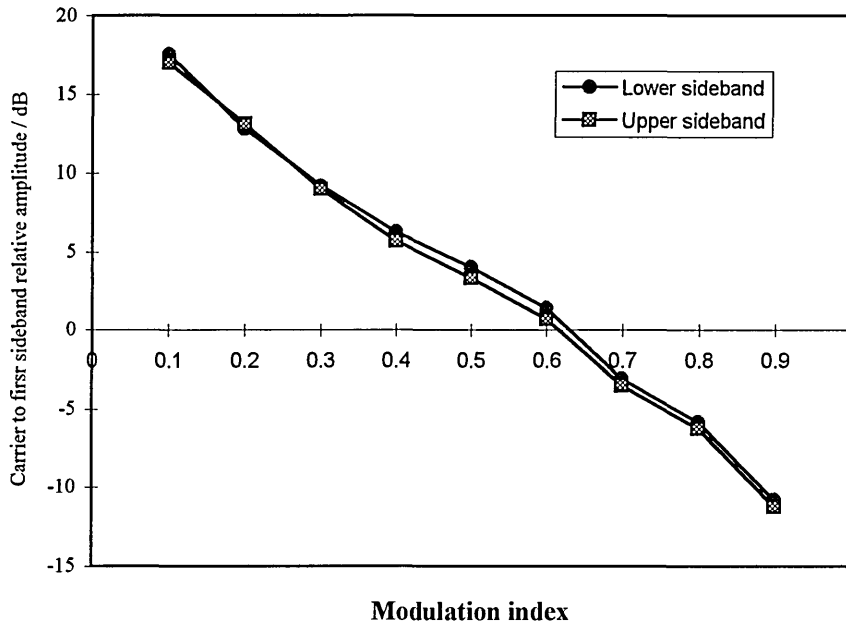


Figure 8.7 Relative amplitude of the PPM clock component to the first sideband pair, under different modulation conditions.

The spectral expression for a naturally sampled, trailing edge modulated PWM signal was given by Eqn. (6.8). The spectral plot of a PWM signal, modulated by a 1 MHz sine wave, is shown in Fig. 8.8. As predicted, a baseband component and sidetones around the carrier frequency and its harmonics can be identified.

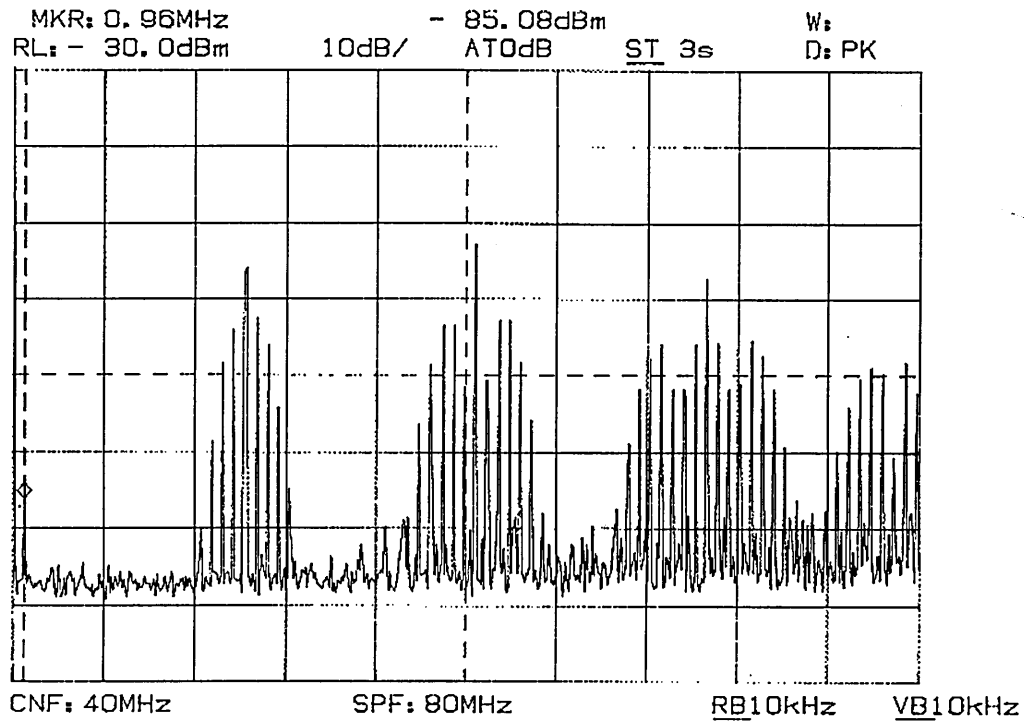


Figure 8.8 PWM signal containing a baseband component.

## 8.2 SNR and BER Performance

The SNR and nonlinear distortion performance are two system parameters which indicate the performance potential of a modulation technique (section 4.3.4). Nonlinear distortion performance of the PTM sub-system and the overall prototype system will be presented in section 8.3. In this section the SNR performance of each PTM technique is presented and analysed. The performance of the video and audio channels are measured in terms of the rms signal power-to-rms noise power ratio. The bit error rate (BER), which defines the ratio of the number of received erroneous bits, to the number of transmitted bits, within a given time period, is used to evaluate the performance of the data channel.

### 8.2.1 SNR measurement

The measurement setup for SNR evaluation is shown in Fig. 8.9. A sine wave at an appropriate signal frequency is used in the SNR measurement of each channel. The recovered signal at the channel output is fed to the spectrum analyser, which measures the system noise floor in a 10 kHz bandwidth for the video channel and a 100 Hz bandwidth for the audio channel. The difference between the signal level and the noise floor is read as the SNR.

An appropriate weighting factor should be applied to the measured values, in order to account for the noise power over the whole frequency range of each signal channel. The weighting factor was calculated using the following equation.

$$\text{Weighting Factor} = 10 \log \left( \frac{\text{resolution bandwidth}}{\text{system bandwidth}} \right) \quad (8.1)$$

Here, the resolution bandwidth refers to the bandwidth in which the system noise floor is measured in. The system bandwidth is the frequency range of each signal channel, 5.5 MHz and 15 kHz for the video and audio channels, respectively.

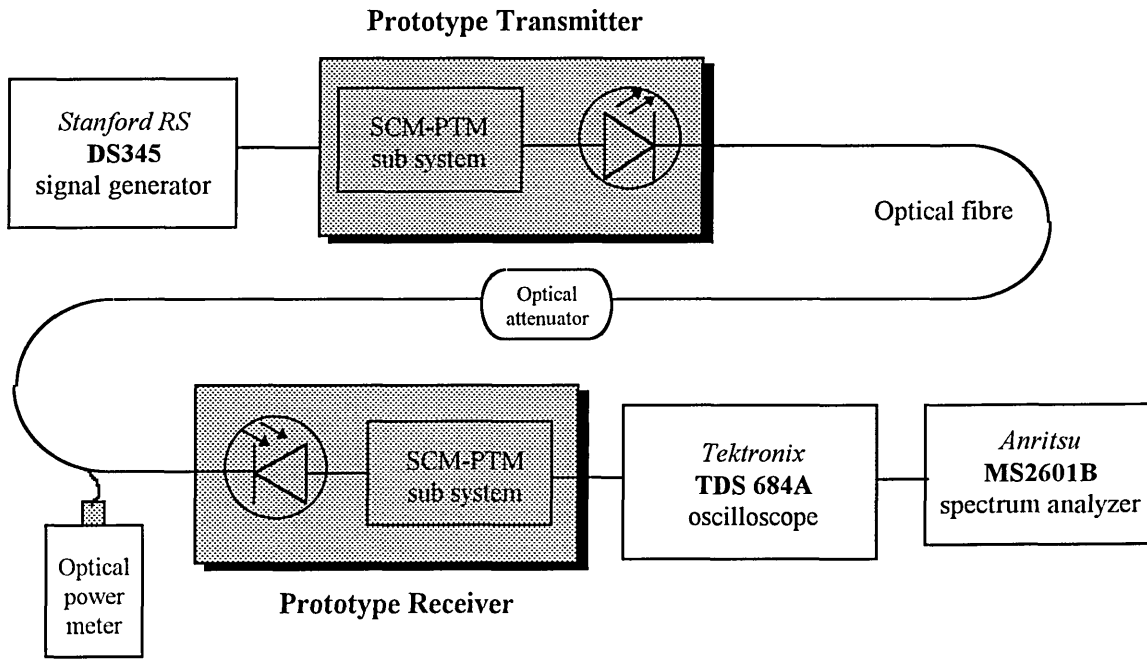


Figure 8.9 Measurement setup for SNR evaluation.

The SNR expressions for PFM, SWFM and PFM systems were derived, employing different pulse models, in Chapters 5 and 6. The conventional approach used to represent SNR performance, in optical communication systems, is to characterise the SNR values against the received optical power. Therefore, the SNR performance of the video and audio channels, for the implemented PTM techniques, are presented using this approach. The parameters used in SNR calculations for the PTM technique, as well as the conventional SCM approach, are also listed. The presented results are analysed in section 8.2.2.

### 8.2.1.1 PFM and SWFM systems

The various parameters of the optical receiver, relevant for rms noise power calculation, are listed in Table 8.1. The mean avalanche gain of the *p-i-n* receiver is unity and a room temperature of 300 K is assumed for the thermal noise calculation.

System parameter	Symbol	Value
Photodiode responsivity	$R_o$	0.75 A/W
Mean avalanche gain	$G$	1
Photodiode dark current	$I_d$	100 pA
Receiver equivalent noise current		2.5 pA/ $\sqrt{\text{Hz}}$
Front-end load resistance	$R_L$	14 k $\Omega$
Absolute temperature	$T_{ab}$	300 K
Boltzman constant	$k$	1.38x10 <sup>-23</sup> JK <sup>-1</sup>
Electron charge	$q$	1.6x10 <sup>-19</sup> C

Table 8.1 Optical receiver parameters for noise power calculation.

The PFM and SWFM parameters of the prototype are listed in Table 8.2. The sampling ratio was allocated according to Eqn. (5.46), allowing adequate frequency guard band in order to limit the baseband distortion. The modulation index for each channel was allocated taking into account the frequency presence and the SNR requirements of the channel. Equivalent modulation indices, used to calculate the performance of conventional SCM approach, are also listed. The ELED limited transmission bandwidth of the SWFM system is approximately 100 MHz. The PFM carrier was operated at a duty cycle of approximately 25%, which results in a similar transmission bandwidth requirement.

PFM/SWFM parameter	Symbol	Value	
Sampling ratio	$R$	3.5	
Modulation index		<i>video</i>	<i>audio</i>
- PFM/SWFM	$\beta_i$	1	0.1
- analogue equivalent	$m_i$	1	0.1
Transmission bandwidth (Duty cycle $d$ ,: PFM=25%, SWFM ~50%)	$B_i$	100 MHz	

Table 8.2 PFM and SWFM system parameters.

The measured rms SNR versus the peak received optical power for the video channel, operated at the PFM/SWFM system parameters listed in Table 8.2, is shown in Fig. 8.10. The measured values of the SWFM double-edge detection technique is also shown. The theoretical curve has been calculated using Eqn. (5.36) representing the Gaussian model. The performance of conventional SCM for equivalent system parameters, calculated using Eqn. (3.15), is also indicated.

Unlike the baseband video channel, the audio signal is FM modulated onto a subcarrier, prior to PTM modulation (section 7.2.2). Therefore, in order to calculate the final output SNR, appropriate gain factors should be employed on the signal recovered at the PTM demodulator. The parameters relevant for the SNR calculation of the FM audio channel are listed in Table 8.3. The FM modulation index  $\beta_{FM}$ , has been calculated for an audio signal bandwidth of 15 kHz and a peak frequency deviation of 50 kHz (Table 7.2). Subjective tests carried out on 50  $\mu$ s pre-emphasis, by the British broadcasting corporation (BBC), has shown a 4.5 dB improvement in the output SNR, compared ordinary FM modulation, and is taken into account in the calculations [119].

Channel parameter	Value
Modulation index ( $\beta_{FM}$ )	3.3
FM gain factor [120]	$\frac{3}{2}(\beta_{FM})^2$
Pre-emphasis gain	4.5 dB
Channel bandwidth	160 kHz

Table 8.3 Audio channel parameters for output SNR calculations.

The performance of the audio channel, for the PFM/SWFM system parameters listed in Table 8.2, is shown in Fig. 8.11. The theoretical curves are produced by the same equations used for the video channel, using the parameters listed in Table 8.3. As before, the measured values for SWFM double-edge detection are also shown.

### 8.2.1.2 PPM system

The system parameters employed in PPM signal transmission are listed in Table 8.4. To obtain a base band distortion of -40 dB or less a sampling ratio of 2.9 was adequate for PPM compared to 3.5 for the PFM system. The video and audio channels were operated at modulation indices of 40% and 10%, respectively.

PPM parameter	Symbol	Value	
Sampling ratio	$R$	2.9	
Modulation index		<i>video</i>	<i>audio</i>
- PPM	$M_i$	40%	10%
- analogue equivalent	$m_i$	40%	10%
Transmission bandwidth	$B_i$	100 MHz	
Duty cycle	$d$	20.5%	

Table 8.4 PPM system parameters.

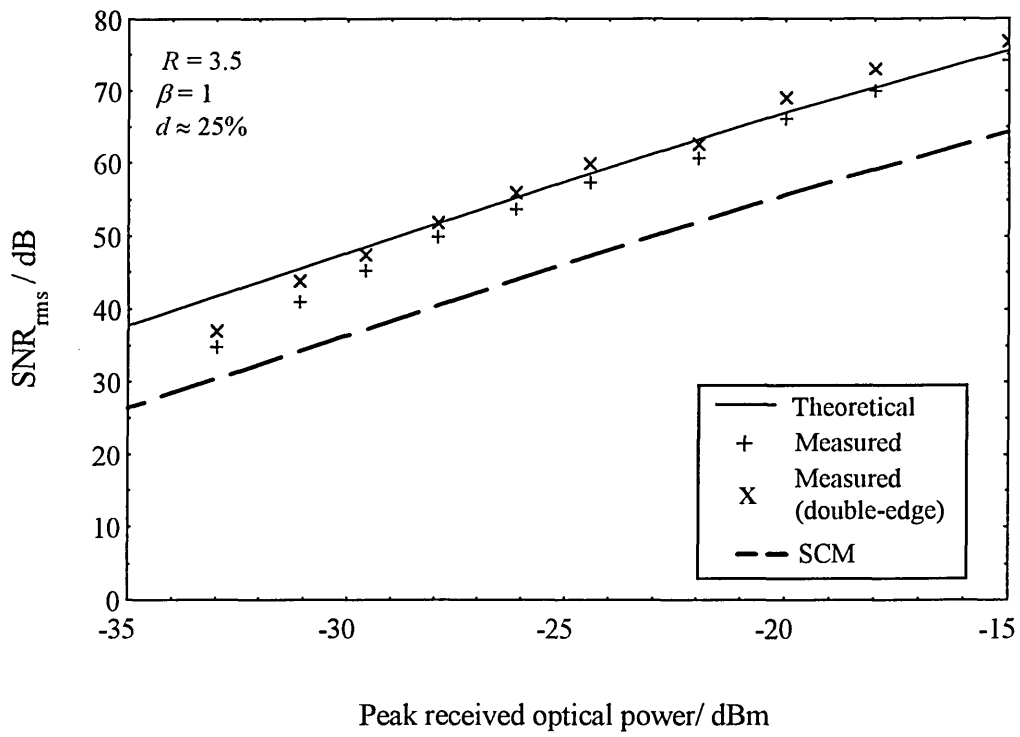


Figure 8.10 SNR performance of the video channel for PFM/SWFM system.

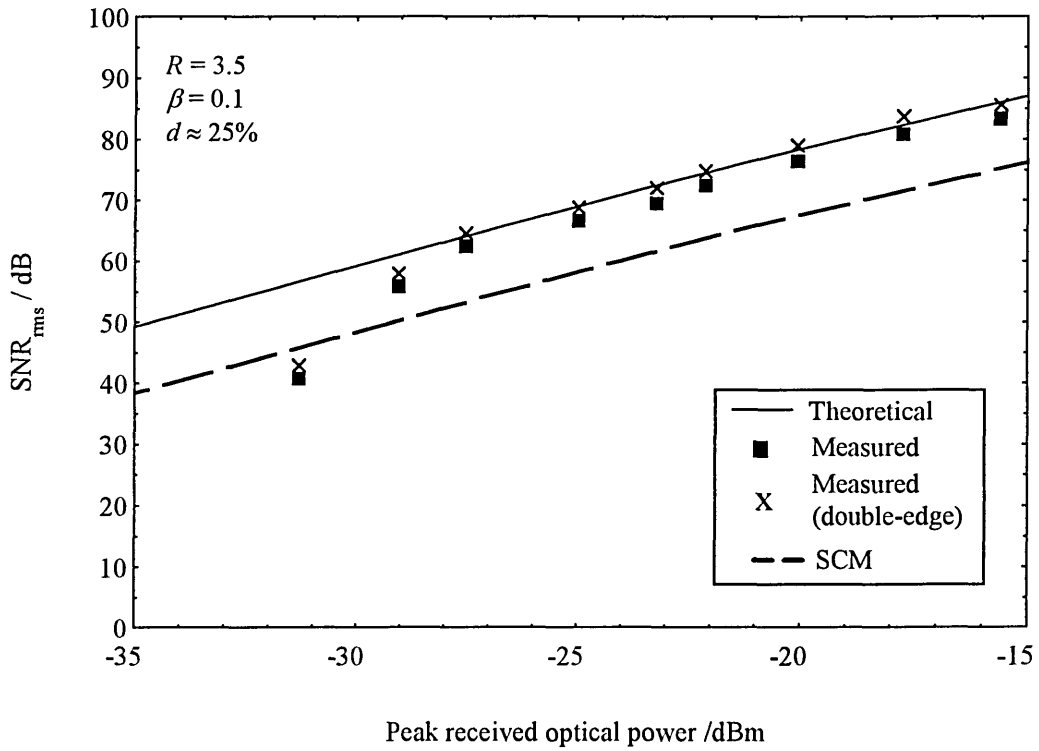


Figure 8.11 SNR performance of the audio channel for PFM/SWFM system.

The SNR performance of the video and audio channels for PPM transmission are illustrated in Figs. 8.12 and 8.13, respectively. The measured values are complemented by theoretical calculations. The PPM theoretical curve has been calculated using the SNR expression given by Eqn. (6.19). For each signal channel the predicted SNR of the conventional SCM approach, employing equivalent system parameters, is also indicated.

### **8.2.2 Performance analysis**

In the previous section the SNR performance of the video and audio channels for SWFM, PFM and PPM systems were illustrated. The system measurements were complemented by theoretical predictions, for both SCM-PTM technique and the conventional method, using the derived SNR expressions and parameters listed in tables 8.1 to 8.4. The SWFM transmission, employing single-edge detection at the receiver, produced SNR values equivalent to the PFM system. By employing double edge detection technique, the SNR performance is improved further by  $\sim 3$  dB as reasoned in Chapter 5, see Figs. 8.10 and 8.11.

The pulses at the optical receiver output are best approximated using a Gaussian pulse, and therefore the SNR expressions representing the Gaussian model has been used in the calculations. The theoretical values are in close agreement with the measured values at higher optical power levels. At lower optical power levels the measured values deviate significantly from the theoretical curve. A possible explanation for this could be the threshold effect, discussed for PFM systems in section 5.4. However, according to the calculations the threshold value correspond to a much lower received optical power level, approximately -40 dBm for the PFM system. On the other hand the limited gain of the optical receiver post- amplifier can limit the sensitivity of the output logic decision

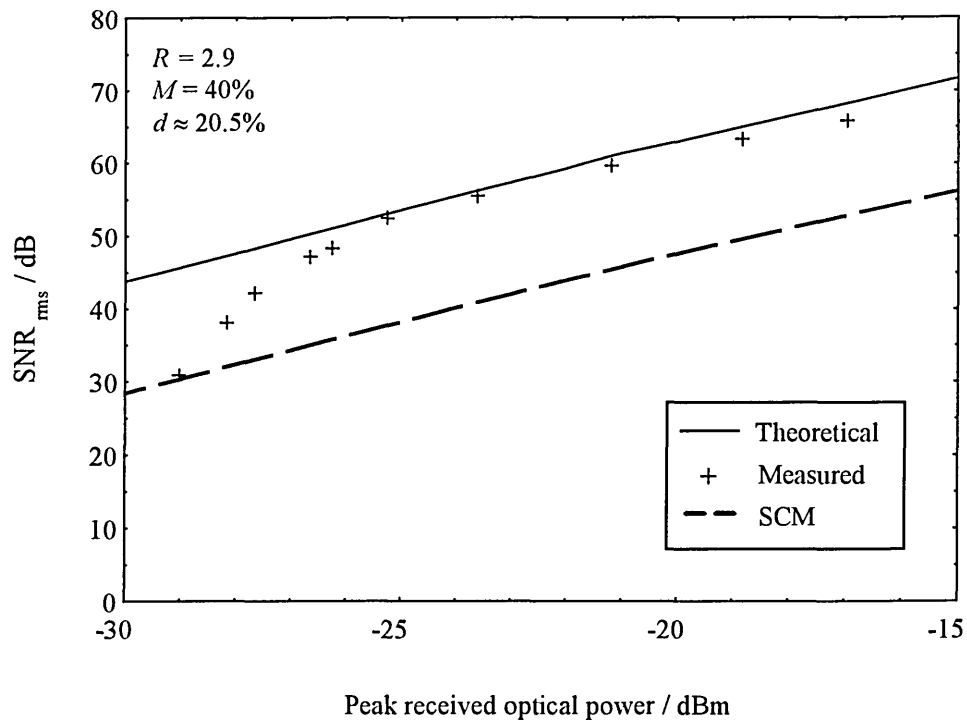


Figure 8.12 SNR performance of the video channel for PPM system.

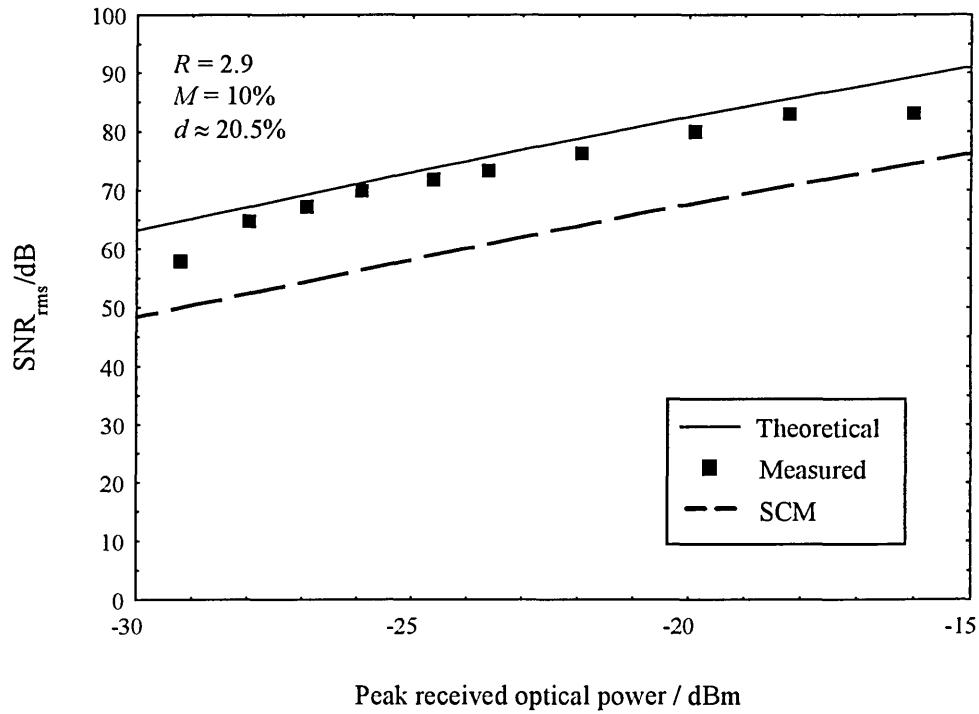


Figure 8.13 SNR performance for the audio channel in PPM system.

circuit at lower optical power levels. Since, the roll-off effect is present in both PFM and PPM systems, this is the most likely cause.

The SNR criterion laid down for each signal channel in Table 7.2 is easily met for both PFM and PPM systems. The PFM system indicates an approximately 6 dB improvement in the optical receiver sensitivity, compared to a conventional SCM system operated using equivalent system parameters. The approximate receiver sensitivity improvement for the PPM system is 8.5 dB. The 2.5 dB increase of the receiver sensitivity in PPM system compared to PFM system, corresponds to the 5 dB SNR advantage predicted for PPM over PFM, in Chapter 6.

The increased receiver sensitivity results in a higher optical power budget which can be utilised to extend the transmission distance and the number of network nodes. For an example, the 8.5 dB improvement in PPM systems results in an increased transmission distance of 17.2 km for the 1300 nm optical window, or 28.6 km for the 1500 nm optical window. An increased transmission bandwidth will further increase the receiver sensitivity. However, this is a trade-off of a number of system parameters such as system capacity, cost and the available channel resources. Similarly a higher modulation index will improve the SNR, but the modulation index that each channel can be operated will depend on the number of channels and the input dynamic range of the PTM modulators.

In order to further validate the above SNR measurements, attempts were made to relate the obtained results with published material. However, due to different system parameters used in other works no meaningful comparisons could be made.

### 8.2.3 BER measurements

The details of the data channel implementation was given in Chapter 7 (sections 7.2.3 and 7.8.3). In order to determine the amount of jitter and the ISI present on a digital bit stream an eye diagram may be displayed on an oscilloscope. The test setup to generate an eye pattern is shown in Fig. 8.14 [121]. Here, the digital bit stream under test is directed into the 'A-input' channel of an oscilloscope. A clock frequency which is either derived from the same source as that which produces the digital signal, or in the absence of this, derived from a clean local source of the same frequency, is used to trigger the oscilloscope. Therefore, the oscilloscope sweep duration corresponds to the clock period and the persistence of vision produces an eye pattern.

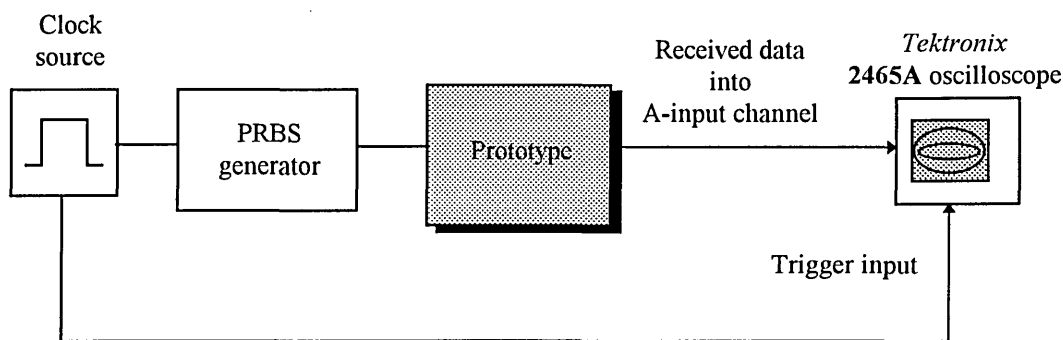


Figure 8.14 Eye diagram test setup

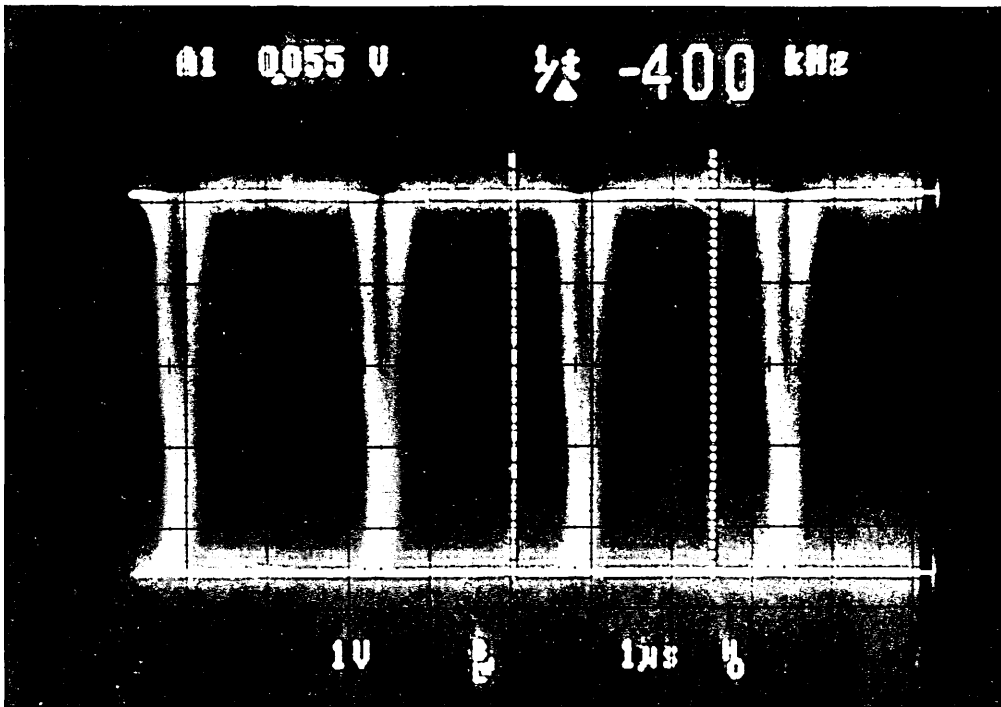
The eye diagram generated for data transmission of the prototype at higher optical power levels is shown in Fig. 8.15. The degree to which the eye is 'open' indicates the ISI degradation, defined in dB units as [121]:

$$\text{ISI degradation} = -20 \log [\text{percentage of eye open}/100] \quad (8.1)$$

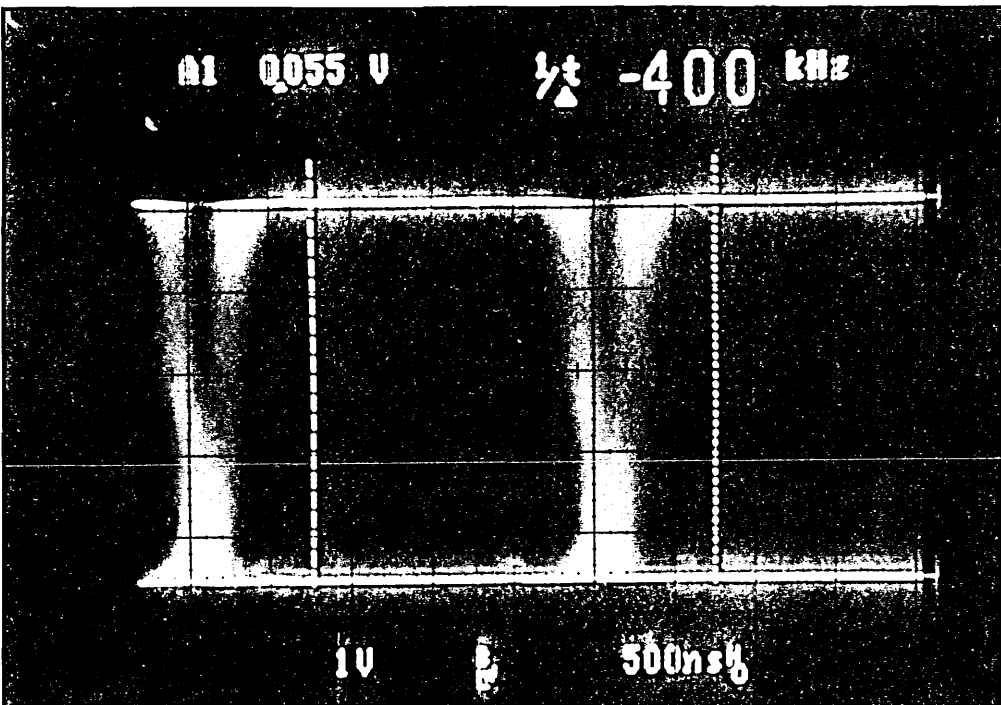
The wide open eye comfortably exceeds the 0.9 dB ISI degradation specified as tolerable for digital data transmission.

The amount of jitter in the system is indicated by the sharpness of the eye corners. In the presence of jitter, the zero crossings of the consecutive bits are variable, resulting in fuzziness at the edges of the eye. The width of the fuzziness is a measure of the peak-to-peak jitter. The measured peak-to-peak jitter of the eye is in the order of ns, providing adequate noise margin for the intended bit rate.

The horizontal crossings of the generated pattern have dropped towards the lower half of the eye. This is due to the slight asymmetry in the mark to space ratio of the data generated by the post detection processor of the FSK demodulator. No significant deterioration in the eye was seen until the power level was dropped below -30 dBm.



(a) 1  $\mu$ s time base



(b) 500 ns time base

Figure 8.15 The generated eye pattern for data transmission.

## 8.3 Nonlinear Distortion Performance

A nonlinear distortion analysis for conventional SCM systems was carried out in Chapter 3. The harmonic and intermodulation distortion resulting from the light-current characteristic of the laser diode was discussed at length. In SCM-PTM technique the overall system linearity is determined by the modulators and demodulators and the associated electronic circuitry, since the constraints on the optical sub-system specification is relaxed. In Chapters 5 and 6, the VCO and the ramp generator were identified as critical system components to deliver acceptable nonlinear distortion levels in PTM systems.

### 8.3.1 PTM sub-system linearity

The amount of non-linear distortion introduced into the SWFM/PFM system is primarily determined by the voltage-to-frequency conversion characteristic of the VCO. In order to evaluate the linearity of the **SP 1658** device, a test was carried out for the intended frequency range of operation for this application. The experimental data, approximated by a second order a polynomial, is shown in Fig. 8.16.

The second order polynomial can be represented by:

$$y = a_0 + a_1x + a_2x^2 \quad (8.2)$$

where  $x$  and  $y$  are input and output respectively and  $a_0$  to  $a_2$  are coefficients. When the input is a single tone of amplitude  $A$  and frequency  $\omega$ , the output signal is:

$$y = \left( a_0 - \frac{a_2 A^2}{2} \right) + a_1 A \sin(\omega t) - \frac{a_2 A^2}{2} \cos(2\omega t) \quad (8.3)$$

Using the above equation, the second order harmonic distortion  $HD_{2dB}$ , relative to the signal fundamental, can be expressed in dB units as:

$$HD_{2dB} = 20 \log \left( \frac{a_2}{2a_1} A \right) \quad (8.4)$$

Applying the above equation to the second order polynomial curve-fit to the voltage-to-frequency conversion characteristic of the VCO, and assuming a modulating signal amplitude of unity, the second order harmonic distortion is predicted to be -33.1 dB.

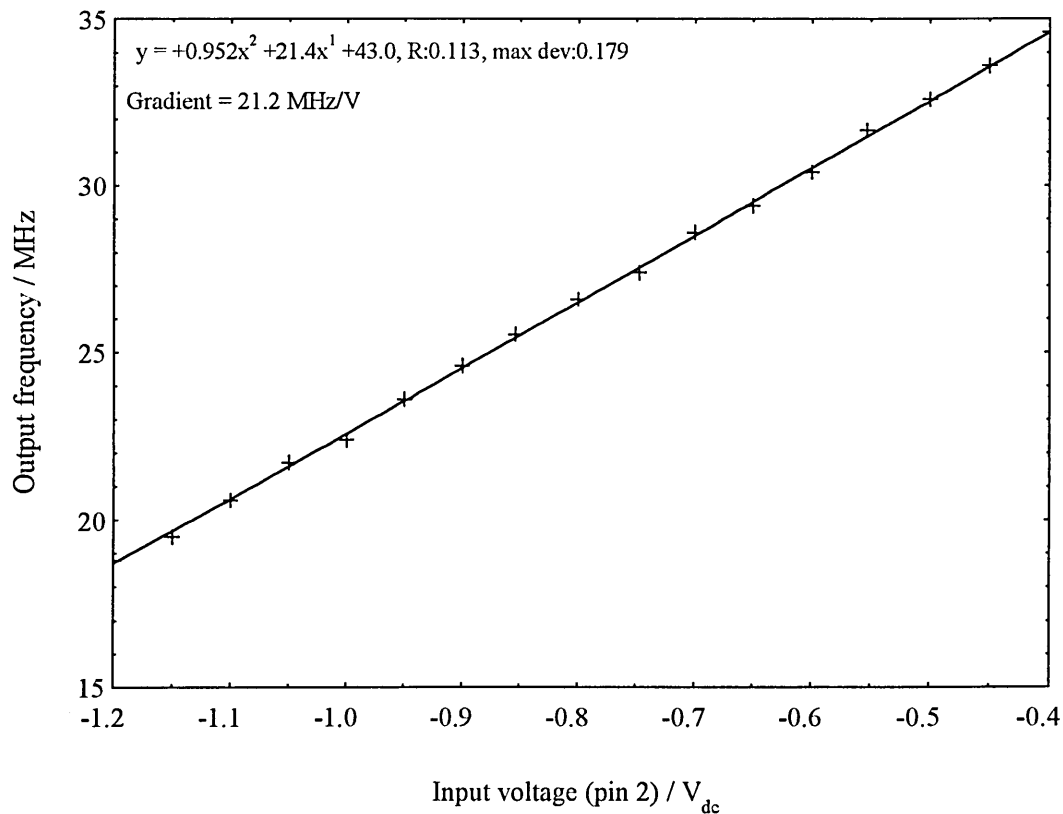


Figure 8.16 Voltage-to-frequency conversion characteristic of the VCO for an external capacitance of 29 pF

It was stated in section 6.2, that key parameters of the PPM modulator, including the amount of nonlinear distortion, is primarily determined by the ramp generator. Therefore, in order to minimise the nonlinear contribution a highly linear ramp signal is desired. The linearity of the PPM modulator was determined by accounting for the variation of the pulse width at the output of the comparator, for different values of offset voltages. Figure 8.17 shows the voltage-to-pulse conversion characteristic, and as before a second order polynomial approximation was obtained for the experimental data. For a modulating input signal of 1 V, the second harmonic distortion predicted by Eqn. (8.3) is:

$$HD_{2dB} = -75.6 \text{ dB}$$

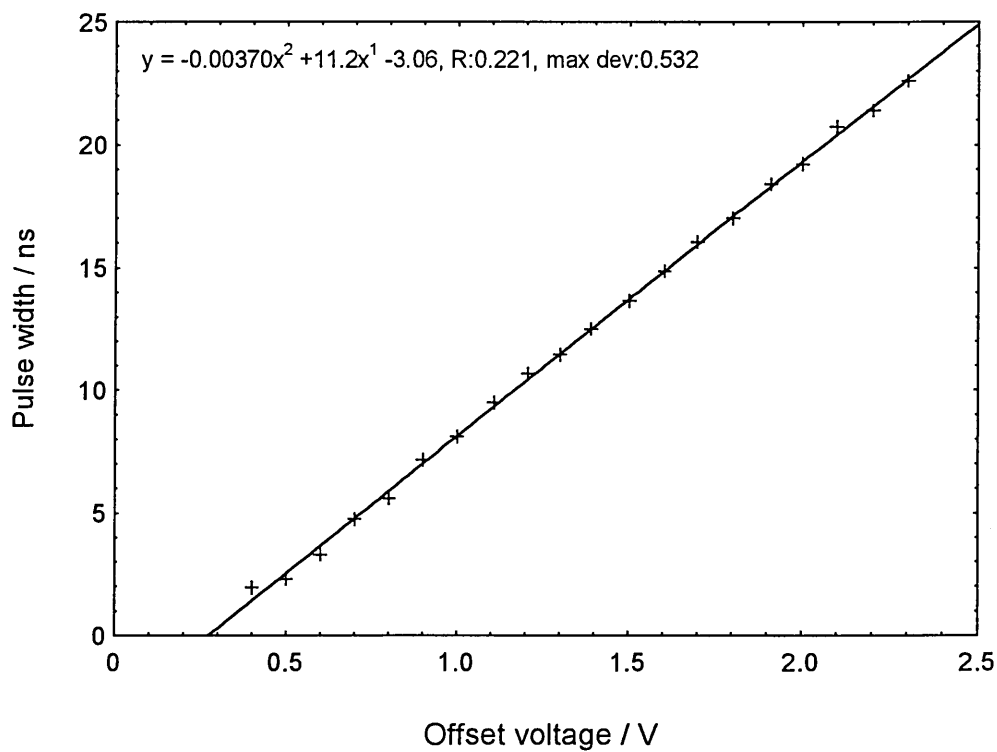


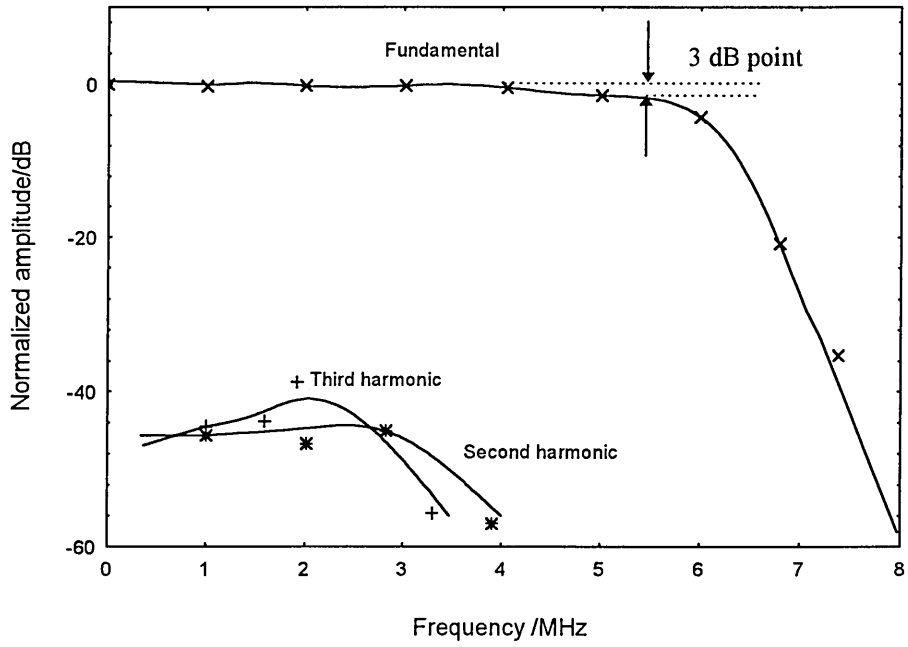
Figure 8.17 Voltage to pulse position conversion characteristic of the PPM modulator.

A third order polynomial curve fit was also considered to characterise the linearity of the VCO and the ramp generator. However, the third order harmonic distortion is significantly lower compared to the second order distortion and therefore, its influence on the overall system linearity is minimal.

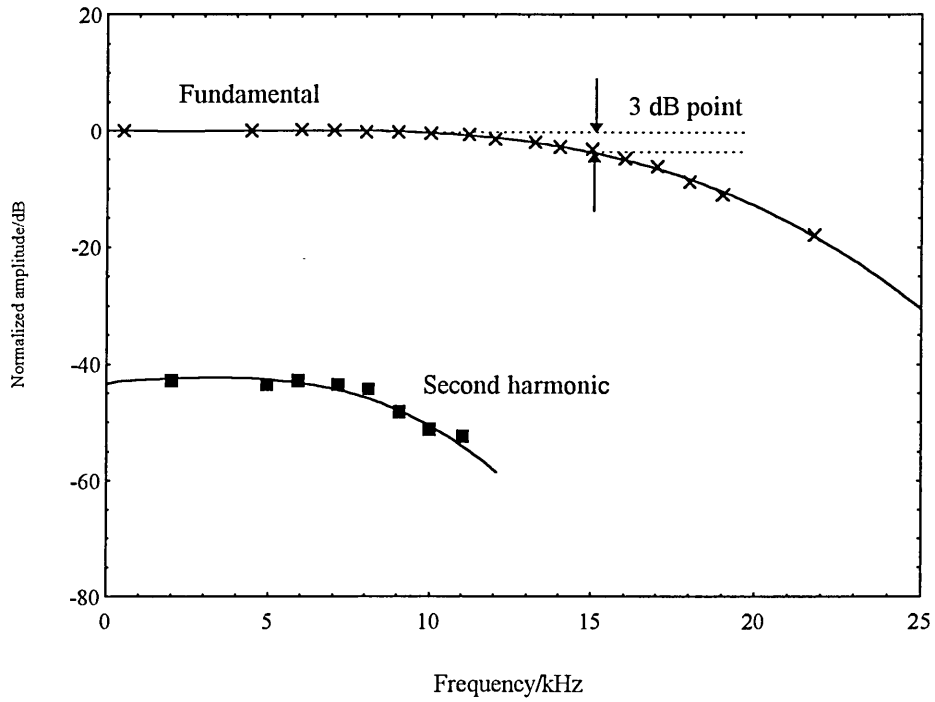
### **8.3.2 Overall system linearity**

In order to evaluate the overall system linearity, the harmonic distortion measurements were carried at the system output. For analogue signals, harmonic distortion is measured in terms of a second and third order nonlinear term with respect to the fundamental. The results obtained for the video and audio channels, when the system was operated using the PFM/SWFM technique, are shown in Fig. 8.18.

Linear distortion results when the frequency response deviates from a consistent level, within the channel passband. The fundamental component for both the video and audio channels are flat throughout their respective channel passbands, and therefore no linear distortion is introduced. The lowpass filter specifically designed for PAL/SECAM television receiver applications has a sharp roll-off of 190 dB/decade, implicating a filter order of 9. The second and third order harmonics of the video channel are below -40 dB, the value specified for adequate signal performance [12, 81]. The roll-off of the audio signal is gradual due to the lower order filter employed. For the audio channel no third order harmonic was detected and the second order harmonic was approximately 44 dB below the fundamental.



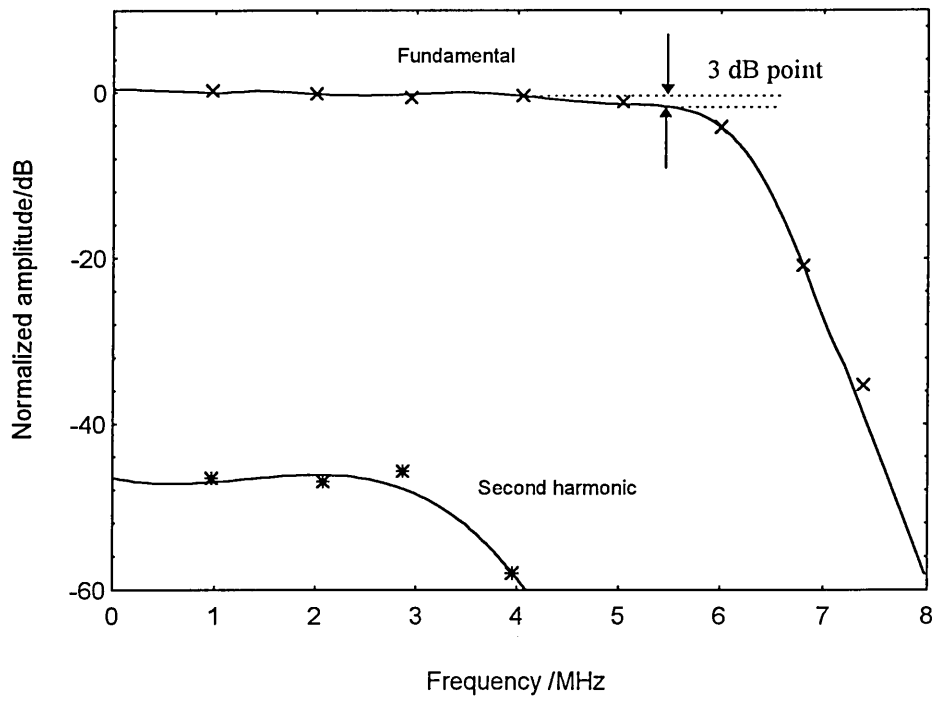
(a) video channel



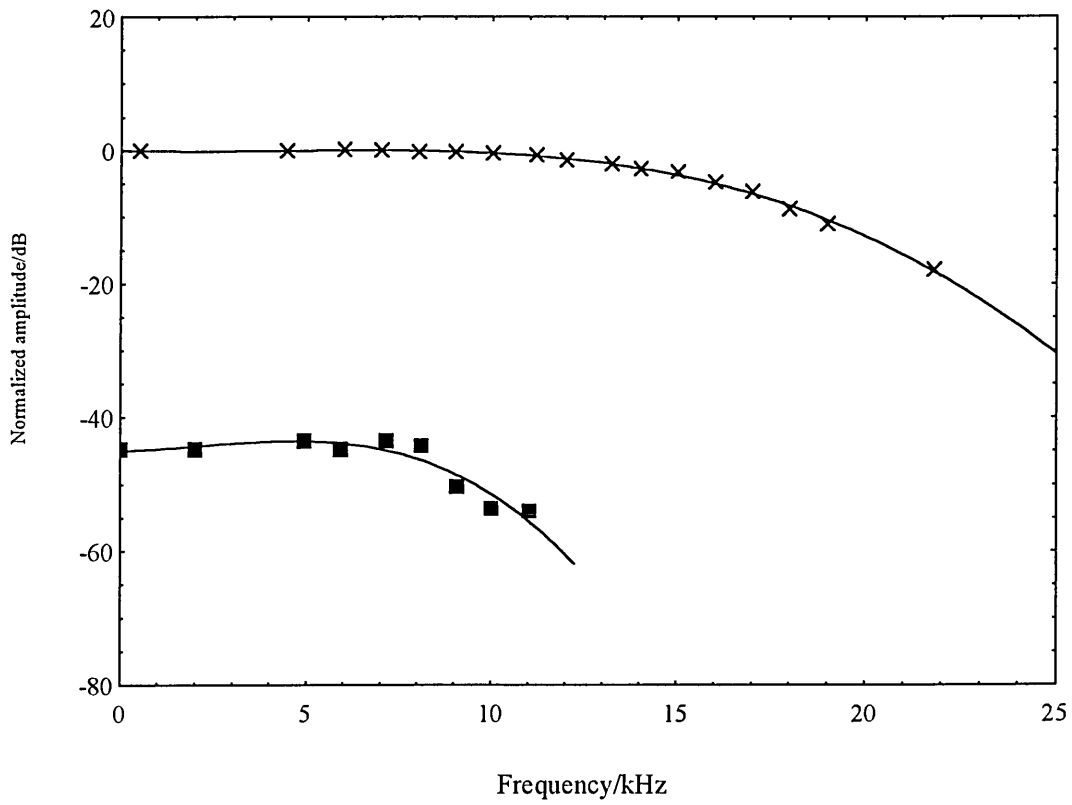
(b) audio channel

Figure 8.18 Harmonic distortion for SWFM/PFM system.

Similar tests were carried out on the PPM system and the results obtained are presented in Fig. 8.19. The second harmonic of the video channel is approximately -48 dB, relative to the fundamental and no significant third order terms could be detected. The performance of the audio channel is also marginally better than the results obtained for the PFM system. The marginally lower harmonic performance of the PPM system compared to the PFM system can be attributed to the excellent linearity of the PPM modulator ( Fig. 8.15).



(a) video channel



(b) audio channel

Figure 8.19 Harmonic distortion in PPM system.

## **Conclusions**

### **9.1 Conclusions**

In conventional SCM systems, the poor receiver sensitivities impose strict noise and nonlinear requirement on the optical link, restricting the power budget. The applications of various second stage modulators, incorporated into SCM systems in order to enhance system performance, have been restricted either due to the limited improvements in receiver sensitivity or in the increased complexity and bandwidth overheads. PTM systems have shown to achieve excellent signal performance to bandwidth trade-off, without compromising system cost and complexity. The work presented in this thesis has demonstrated the viability of PTM as a second stage modulator in SCM systems. The broadband transmission capability of PFM, SWFM and PPM techniques has also been demonstrated. The predicted performance of the PTM techniques has been verified by the implemented prototype system, capable of transmitting a video channel, two audio channels and a data channel.

The simplicity and the similarities of two widely used PTM techniques, PFM and SWFM, were illustrated. The spectral characterisation revealed the presence of a baseband component in the PFM signal, which can be utilised for signal recovery. The voltage-to-frequency conversion characteristic of the VCO determines the input dynamic range of a PFM/SWFM modulator and the commercially available devices were shown to have large transmission capabilities. An alternative pulse generation technique, employing a RC differentiator circuit, was proposed to minimise the width modulation resulting from the gate delay technique. Since, signal demodulation relies on generating a distortion free baseband component, adequate frequency guard band is required to prevent the sidetones around the carrier fundamental making their way into the baseband region. System measurements have indicated adequate system margin can be allowed for by choosing the frequency guard band to be 50% of the modulating signal bandwidth.

Jitter noise was shown to be the dominant noise source in PTM systems operating above a SNR threshold, below which the signal performance deteriorates rapidly due to the presence of impulse noise. The SNR expressions for PFM system were derived using appropriate pulse models for optical communication systems. A raised cosine shaped pulse at the threshold detector results in a 3 dB SNR advantage over a Gaussian or an exponential shaped pulse. The 3 dB SNR improvement, reasoned for double-edge detection SWFM technique, was verified by the prototype system. A transmission bandwidth of  $1/\tau$ ,  $\tau$  being the PFM pulse width, was shown to contain adequate signal energy to recover information at the receiver.

PPM was shown to be an efficient derivative of the PWM technique. Critical to PPM generation is a highly linear ramp generator with a short flyback interval. A ramp signal,

indicating excellent linear characteristics, was generated by charging a capacitor from a constant current source and discharging through an extremely fast transistor in order to achieve short reset times.

An investigation of the PPM spectrum revealed the existence of a clock component, which has a strong presence at low modulation indices, decaying to a minimum at approximately 80% modulation. A quantitative appreciation of the clock component shows adequate system margin for the operation of a PLL to recover the clock reference signal at the receiver. The sidebands on either side of the clock signal are at close proximity and dwarfs the clock component beyond a modulation index of 60%. Therefore, a carefully designed PLL, with a narrow lock-in-range, is required to prevent it from locking onto the sidebands.

Based on reliable clock recovery at the receiver, a novel detection technique was implemented for the PPM technique. The recovered clock pulses are multiplexed with incoming PPM signal to trigger a bi-stable, generating a PWM signal. The spectral investigation of PWM has shown the presence of a baseband component, which is utilised for information recovery. Due to the self-synchronising property of the proposed demodulator no reference pulses are required to be transmitted, and the cost and complexity are also reduced compared to the existing demodulation techniques.

In order to verify the predicted performance of the PTM techniques and their broadband transmission capability, a prototype has been implemented. Video, audio and data signals were employed at the subcarrier stage and the PTM systems have been implemented using the high speed ECL logic. The need for a bias circuit to stabilise laser operation

against optical power fluctuations, due to threshold variations resulting from temperature fluctuations, and a driver circuit to account for the low output impedance of the ECL outputs, were outlined. The optical link was shown to have a maximum, power restricted transmission distance of 60 km, and a transmission bandwidth of 150 MHz for a graded index multi-mode fibre, operating at the power restricted transmission distance. The bandpass filtering technique was preferred to the heterodyne detection due to the implementation of a baseband channel and the commercial availability of filters at the chosen subcarrier frequencies.

The PFM system delivered a 6 dB improvement in receiver sensitivity compared to conventional SCM systems. The PPM system offered an extra 2.5 dB improvement in receiver sensitivity, confirming the 5 dB SNR advantage predicted for PPM over PFM. The increased receiver sensitivity of SCM-PTM technique results in an improved optical power budget allowing for longer transmission distances and a greater number of subscribers in a network. The simplicity and the low cost of PTM techniques mean that this performance enhancement is achieved without compromising other system parameters. The overall harmonic performance of PFM and PPM systems were shown to be within -40 dB, the value specified for video and audio signal transmission.

In summary, the prototype implementation has shown the feasibility of PTM techniques to transmit multi-channel signals, in optical communication systems. The SCM-PTM approach is a hybrid technique for multiplexing signal channels, where hitherto time domain and frequency domain multiplexing of PTM channels have proved inefficient or complex. The commercial availability of VCOs, with extended frequency range of operation, provide for a large transmission capacity in PFM and SWFM systems. In PPM

systems, excellent circuit design techniques are called for in order to produce high frequency, linear ramp generators with short flyback intervals. System measurements have confirmed the predicted SNR performance for the PFM and PPM systems. Novel detection technique, which exploits the self-synchronising property of PPM, has been proposed, reducing the cost and complexity of PPM demodulation. The low cost of PTM implementation and the relaxed specifications on the opto-electronic sub-system means, that the improvement in receiver sensitivity is achieved without compromising other system parameters.

## **9.2 Contributions to Knowledge**

The following is a list of the main contributions to knowledge resulting from the work carried out in this thesis. These original contributions have been supported by the publications listed at the end of the section.

1. The SNR expressions derived for PFM system have been further developed by using appropriate pulse models to represent the detected pulses in optical communication systems. Raised cosine shaped pulses were shown to deliver a 3 dB improvement in SNR over Gaussian and exponential pulses, characteristic for optical fibre transmission. The energy distribution of the PFM signal has shown that approximately 98% of the signal energy is contained within a signal bandwidth corresponding to the inverse of the PFM pulse width.

2. An alternative demodulation technique has been proposed and implemented for PPM demodulation. The characterisation of the PPM carrier frequency and the sideband components on either side, have revealed adequate system margin for PLL operation in order to recover a clock component under variable modulation conditions. The recovered clock pulses are combined with the PPM signal to create a baseband containing PWM signal at the receiver. Due to the self-synchronising property of the proposed demodulator, no reference signal is required to be transmitted and the cost and complexity is also reduced compared to the existing demodulation techniques.
  
3. The prototype implementation has shown the feasibility of the SCM-PTM technique for multi-channel signal transmission over an optical fibre link. Hitherto, time domain and frequency domain multiplexing of PTM channels have proved inefficient and complex. Therefore, the proposed hybrid technique has the ability to transmit multi-channel signals and still exploit the advantages of PTM for optical fibre transmission.

The work carried out in this thesis has produced the following publications:

- [1] Z. Ghassemlooy, A.A. Issa, R. Wickramasinghe and A.J.S. Simmonds  
Compound pulse frequency and width modulation technique  
*Int. Journal of Optoelectronics* 1995, vol. 10, no. 1, pp. 19-23.
- [2] V.R. Wickramasinghe, Z. Ghassemlooy, A.J.S. Simmonds and L. Chao  
Pulse time modulation for subcarrier multiplexed systems

*Proc. of IEEE Singapore Int. Conference on Networks/ Int. Conference on Information Engineering, IEEE SICON/ICIE '95, 3-7<sup>th</sup> July 1995, Singapore, pp. 450-454*

- [3] V.R. Wickramasinghe, Z. Ghassemlooy and L. Chao  
Pulse time modulation for subcarrier multiplexed systems  
*All-Optical Communication Systems: Architecture, control and network issues: SPIE Photonics East '95 Symposium, Oct. 22-26 1995, Philadelphia, USA, vol. 2614, pp. 229-235.*
- [4] V.R. Wickramasinghe, Z. Ghassemlooy and L. Chao  
Optical fibre transmission of a broadband subcarrier multiplexed signal using PTM technique  
*IEEE Trans. on Consumer Electronics May 1996, vol. 42, no. 2, pp. 229-238.*
- [5] V.R. Wickramasinghe, Z. Ghassemlooy and R.G. Harris  
Optical fibre transmission of a broadband SCM signal employing pulse position modulation  
*Third Communication Networks Symposium 8-9<sup>th</sup> July 1996, Manchester, UK, pp. 85-89.*
- [6] V.R. Wickramasinghe and Z. Ghassemlooy  
Pulse position modulation for a subcarrier multiplexed optical fibre transmission system  
*Voice, Video and Data communications, SPIE Photonics East '96 Symposium 18-22<sup>nd</sup> Nov. 1996, Boston, USA.*

## References

- [1] J.R. FORREST: "Telemedia: A survival guide to the fifth dimension", *Electronics & Communication Engineering Journal*, Feb. 1996, vol. 8, no. 1, pp. 13-23.
- [2] B. FURHT: "Multimedia systems: An overview", *IEEE Multi-media*, Spring 1994, pp. 47-59.
- [3] B. FURHT and M. MILENKOVIC: "A guided tour of multimedia systems and applications", *IEEE Computer Society Press*, 1995.
- [4] J.M. ARNOLD: "Solitons in communications", *Electronics & Communication Engineering Journal*, April 1996, vol. 8, no. 2, pp. 88-96.
- [5] J.C. PALAIS: "Fibre optic Communications" 3<sup>rd</sup> edition, *Prentice Hall*, 1996.
- [6] D. FRANKEL: "ISDN reaches the market", *IEEE Spectrum*, June 1995, vol. 32, no. 6, pp. 20-25.
- [7] M. JEFFREY: "Asynchronous transfer mode: the ultimate broadband solution?", *Electronics & Communication Engineering Journal*, June 1994, vol. 6, no. 3, pp. 133-142.
- [8] S.P. FERGUSON: "Implications of SONET and SDH", *Electronics & Communication Engineering Journal*, June 1994, vol. 6, no. 3, pp. 143-151.
- [9] D. LEGALL: "MPEG: A video compression standard for multimedia applications", *Comm. ACM*, April 1991, vol. 34, no. 4, pp. 59-63.
- [10] G.P. AGRAWAL: "Fibre optic communication systems", *MacGraw Hill*, 1993, Chapter 7, pp. 302-310.
- [11] P.A. DAVIES and Z. UREY: "SCM in optical communication networks", *Electronics & Communication Engineering Journal*, April 1992, pp. 65-72.

- [12] M.K. GRACE: "Synchronous quantised SCM for transport of video, voice and data", *IEEE Journal on Selected Areas in Communications*, Sep. 1990, vol. 8, no. 7, pp. 1351-1358.
- [13] R. OHMOTO and H. OHTSUKA: "Performance of FM double modulation for subcarrier optical transmission", *IEICE Trans. on Communications*, Sep. 1993, vol. E76-B, no. 9, pp. 1152-1158.
- [14] K.SATO *et al*: "Fibre optic analogue-digital hybrid signal transmission employing frequency modulation", May 1985, vol. COM-33, no. 5, pp. 433-441.
- [15] D. COOKE, Z. JELONEK, A.J. OXFORD and E. FITCH: "Pulse communication", *Journal of the IEE*, 1947, 94, (IIIA), pp. 83-105.
- [16] B. WILSON and Z. GHASSEMLOOY: "Pulse time modulation techniques for optical communications-a review", *IEE Proc.-J Optoelectronics*, Dec. 1993, vol. 140, no. 6, pp. 346-357.
- [17] Z. GHASSEMLOOY, A.A. ISSA, R. WICKRAMASINGHE and A.J. SIMMONDS: "Compound pulse frequency and width modulation technique", *International Journal of Optoelectronics*, 1995, vol. 10, no. 1, pp. 19-23.
- [18] W.I. WAY: "SCM lightwave systems design considerations for subscriber loop applications", *Journal of Lightwave Technology*, Nov. 1989, vol. 7, no. 11, pp. 1806-1817.
- [19] S. WATANABE *et al*: "Optical coherent broadband transmission for longhaul and distribution systems using SCM", *Journal of Lightwave Technology*, Jan. 1993, vol. 11, no. 1, pp. 116-120.
- [20] M.C. BRIAN *et al*: "Progress towards the field deployment of coherent optical fibre systems", *Journal of Lightwave Technology*, Mar. 1990, vol. 8, no. 3, pp. 210-223.

- [21] R. OLSHANSKY, V.A. LANZISERA and P. HILL: "SCM lightwave systems for broadband distribution", *Journal of Lightwave Technology*, Sep. 1989, vol. 7, no. 9, pp. 1329-1340.
- [22] T.E. DARCIE: "SCM for lightwave networks and video distribution", *IEEE Journal on Selected Areas in Communications*, Sep. 1990, vol. 8, no. 7, pp. 1240-1248.
- [23] S.D. WALKER *et al.*: "Design techniques for SCM broadcast optical networks", *IEEE Journal on Selected Areas in Communications*, Sep. 1990, vol. 8, no. 7, pp. 1276-1284.
- [24] T.E. DARCIE, M.E. DIXON, B.L. KASPER and C.A. BURRUS: "Lightwave system demonstration of SCM", *Electronic Letters*, July 1986, vol. 22, no. 15, pp. 774-775.
- [25] T.E. DARCIE: "SCM for lightwave multiple-access lightwave networks", *Journal of Lightwave Technology*, Aug. 1987, vol. 1, LT-5, pp. 1103-1110.
- [26] R. OLSHANSKY, V.A. LANZISERA and P. HILL: "Simultaneous transmission of 100 Mbit/s at baseband and 60 FM video channels for a wideband optical communication network", *Electronic Letters*, Sep. 1989, vol. 24, no. 19, pp. 1234-1235.
- [27] P.A. ROSHER, S.C. FENNING, M.J. RAMSAY and F.V.C. MENDIS: "Broadband video distribution over a passive optical network using SCM techniques", *Electronic Letters*, 1989, vol. 25, no. 2, pp. 115-117.
- [28] F.V.C. MENDIS, T.T. TJHUNG and B. SELVAN: "20 km single mode optical fibre system for multi-channel video", *Electronic Letters*, 1988 vol. 24, no. 7, pp. 442-443.

- [29] H.M. GUNDER, R. STANNARD and U. SCHOLZ: "Optical fibre CATV distribution system for 12 TV and 12 FM stereo radio channels", *ECOC conference digest, 9<sup>th</sup> European Conference on Optical Communication*, Holland 1983, pp. 559-563.
- [30] T.E. DARCIE and G.E. BODEEP: "Lightwave SCM-CATV transmission systems", *IEEE Trans. on Microwave Theory Technology*, joint special issue, May 1990, vol. 38, pp. 524-533.
- [31] E. YONEDA *etal* : "Fully engineered multi-channel FM-SCM video distribution systems", *Journal of Lightwave Technology*, Feb. 1994, vol. 12, no. 2, pp. 362-367.
- [32] N. KANNO and K. ITO: "Fibre-optic subcarrier multiplexing video transport employing multilevel QAM", *IEEE Journal on Selected Areas in Communications*, Sep. 1990, vol. 8, no. 7, pp. 1313-1319.
- [33] D.G. TANG: "Design and performance of a fibre optic video distribution system using BPSK microwave subcarriers", *IEEE Journal on Selected Areas in Communications*, Sep. 1990, vol. 8, no. 7, pp. 1304-1311.
- [34] R. OLSHANSKY *etal*: "SCM broadband service network: A flexible platform for broadband subscriber services", *Journal of Lightwave Technology*, Jan. 1993, vol. 11, no. 1 pp. 60-69.
- [35] J.R. FOX and S.T. JEWELL: "A broadband distributed star network using subcarrier fibre transmission", *IEEE Journal on Selected Areas in Communications*, Sep. 1990, vol. 8, no. 7, pp. 1223-1228.
- [36] P.D. SARGIS, R.E. HAIGH, K.G. McCAMMON: "Dispersion reduction technique using subcarrier multiplexing", *All optical communication systems*:

- Architecture, control and network issues, *SPIE Photonics East '95*, Oct. 1995, pp. 104-17
- [37] W.D. REEVE: "Subcarrier loop, signalling and transmission handbook-Analog", *IEEE Press*, NY, 1992.
- [38] B. WILSON, Z. GHASSEMLOOY and I. DARWAZEH: "Analogue optical fibre communications", *The Institution of Electrical Engineers*, 1995, Chapter 1.
- [39] J.M. SENIOR: "Optical fibre communications: principles and practice", *Prentice Hall*, 1992.
- [40] R. OLSHANSKY, R. GROSS and M. SCHMIDT: "Subcarrier multiplexed coherent lightwave systems for video distribution", *IEEE Journal on Selected Areas in Communications*, Sep. 1990, vol. 8, no. 7, pp. 1268-1275.
- [41] K. ALAMEH and R. MINASIAN: "Ultimate limits of SCM lightwave transmission", *Electronic Letters*, July 1991, vol. 27, no. 14, pp. 1260-1262.
- [42] F.V.C. MENDIS and B.J. TAN: "Overmodulation in SCM video FM broadband optical networks", *IEEE Journal on Selected Areas in Communications*, Sep. 1990, vol. 8, no. 7, pp. 1285-1289.
- [43] R. OLSHANSKY, V. LANZISERA and P. HILL: "Design and performance of wideband SCM lightwave systems", *Proceedings of 14<sup>th</sup> European conference on optical communication*, 1988, pp. 143-146.
- [44] K. SATO: "Intensity noise of semiconductor laser diodes in fibre optic analogue video transmission", *IEEE Journal on Quantum Electronics*, 1983, vol. QE-19, pp. 1380-1391.
- [45] A.T. PHAM: "Nonlinear distortion due to laser intrinsic nonlinearity and clipping in lightwave CATV SCM systems", *18<sup>th</sup> Australian conference on optical fibre technology*, New South Wales, Australia, Nov.-Dec. 1993, pp. 27-29.

- [46] GEC PLESSEY SEMICONDUCTORS: "Intermodulation, phase noise and dynamic range", *Professional products: IC handbook*, GEC Plessey semiconductors, May 1991, pp. 4.25-4.33.
- [47] C.A.A. WASS: "A table of intermodulation products", *Journal of Institute of Electrical Engineers*, Jan. 1948, part III, pp. 31-39.
- [48] J. DALY: "Fiber optic intermodulation distortion", *IEEE Trans. on Communications*, Aug. 1982, vol. COM-30, no. 8, pp. 1954-1958.
- [49] J. ANGENENT: "Simple model for calculation of distortion in an optical analogue subcarrier multiplexed CATV system", *Electronic Letters*, Nov. 1990, vol. 26, no. 24, pp. 2049-2050.
- [50] A. SALEH: "Fundamental limit on number of channels in subcarrier multiplexed lightwave CATV system", *Electronic Letters*, June 1989, vol. 25, no. 12, pp. 776-777.
- [51] K. ALAMEH and R. MINASIAN: "Optimum optical modulation index of laser transmitters in SCM systems", *Electronic Letters*, Aug. 1990, vol. 26, no. 16, pp. 1273-1275.
- [52] A. RAINAL: "Laser intensity modulation as a clipped Guassian process", *IEEE trans. on communications*, Feb./Mar./Apr. 1995, vol. 43, no. 2/3/4, pp. 490-494.
- [53] N. FRIGO, M. PHILLIPS and G. BODEEP: "Clipping distortion in lightwave CATV systems: models, simulations and measurements", *Journal of Lightwave Technology*, Jan. 1993, vol. 11, no. 1, pp. 138-145.
- [54] E. DESURVIRE: "Erbium doped fibre amplifiers", *John Wiley & sons*, 1994.
- [55] D.A. CHAPMAN: "Erbium-doped fibre amplifiers: the latest revolution in optical communications", *Electronics Communication Engineering Journal*, April 1994, vol. 6, no. 2, pp. 59-67.

- [56] H. YONETANI *et al.*: "Analysis of dispersion induced distortion in multi-channel analogue transmission", *IOOC-ECOC '91 17<sup>th</sup> European conference on integrated optics and optical fibre communications*, 1991, vol. 3, pp. 571-580
- [57] C. IH and W. GU: "Fibre induced distortions in a subcarrier multiplexed lightwave system", *IEEE Journal on Selected Areas in Communications*, Sep. 1990, vol. 8, no. 7, pp. 1296-1303.
- [58] G. STREMLER: "Introduction to Communications Systems", *Addison-Wesley publishing*, 3<sup>rd</sup> edition, 1990.
- [59] R.J. HOSS: "Fibre optic communications design handbook", *Prentice Hall International*, 1990.
- [60] "Specification of television standards for 625-line System I transmission in the UK", *Dept. of Trade and Industry*, London 1984.
- [61] S.D. WALKER and A.C. BOUCOUVALAS: "Optimum design of subcarrier optical networks for local loop applications", *IEE colloquium on fibre optic LANs and techniques for the local loop*, London Mar. 1989, paper 12.
- [62] D.G. CUNNINGHAM, A. COLES, A.C. BOUCOUVALAS: "Intensity noise in lightwave fibre systems using LED transmitters", *Electronic Letters*, Oct. 1989, vol. 25, no. 22, pp. 1481-82.
- [63] L.M. JOHNSON and H.V. ROUSSELL: "Linearization of an interferometric modulator at microwave frequencies by polarization mixing", *IEEE Photonics Technology Letter*, Nov. 1990, vol. 1, no. 11, pp. 810-811.
- [64] M.L. FARWELL: "An electro-optic intensity modulator with improved linearity", *IEEE Photonics Technology Letter*, Sep. 1991, vol. 3, no. 9, pp. 792-795.

- [65] M. SHIKADA and N. HENMI, "Evaluation of power penalty due to beat noise induced by connector reflection", *Electronic Letter*, Sep. 1988, vol. 24, pp. 1126-1128.
- [66] A.S ANDRAWIS and I. JACOBS: "A new compound modulation technique for multi-channel analogue video transmission on fibre", *Journal of Lightwave Technology*, Jan. 1993, vol. 11, no. 1 pp. 49-54.
- [67] W.B. PENENNBAKER and J.L. MITCHELL: "JPEG still image data compression standard", *Van Nostrand Reinhold*, 1993.
- [68] B. FOX: "Dawn of digital TV in Europe", *IEEE Spectrum*, April 1995, vol. 32, no. 4, pp. 50-53.
- [69] B. WILSON, Z. GHASSEMLOOY and L. CHAO: "High speed pulse time modulation techniques", *SPIE: Multigigabit Fiber Communications*, 1992, vol. 1787, pp. 292-302.
- [70] M.M. LEVY: "Some theoretical and practical considerations of pulse modulation", *Journal of the IEE*, 1947, vol. 94, no. IIIA, pp. 565-572.
- [71] N.A. AL-ANANI, Z. GHASSEMLOOY, A.K. RAY and B. WILSON: "An experimental optical fibre communication link using pulse slope modulation", *Proc. IEE 2<sup>nd</sup> Int. Symp. on Communication Theory and Applications*, UK 11-16<sup>th</sup> July 1993, pp. 106-110.
- [72] Z. GHASSEMLOOY, R. REYHER, E.D. KALUARACHCHI and A.J. SIMMONDS: "Digital pulse interval and width modulation", *Microwave and Optical Technology Letters*, March 1996, vol. 11, no. 4, pp. 231-236.
- [73] M.N. CALVERT *etal*: "Experimental optical fibre digital pulse position modulation system", *Electronic Letters*, 1988, vol. 24, pp. 129-131.

- [74] B. WILSON, Z. GHASSEMLOOY and I. DARWAZEH: "Analogue optical fibre communications", *The Institution of Electrical Engineers*, 1995, Chapter 4.
- [75] B. WILSON, Z. GHASSEMLOOY and D.J.T. HEATLEY: "Properties and applications of pulse time modulation techniques for fibre broadband communication networks", *Proc. of the ICIE '91*, Singapore 2-5<sup>th</sup> Dec. 1991, pp. 693-702.
- [76] A. OKAZAKI: "Still picture transmission by pulse interval modulation", *IEEE Trans. on Cable Television*, Jan. 1979, vol. CATV-4, no. 1, pp. 17-22.
- [77] Y. UENO and T. YASUGI: "Optical fibre communication systems using pulse interval modulation", *NEC Research & Development*, Jan. 1978, no. 48, pp. 45-51.
- [78] S.D. MAROUGI and K.H. SAYHOOD: "Signal-to-noise performance of the pulse-interval and width modulation system", *Electronic Letters*, July 1983, vol. 19, no. 14, pp. 528-530.
- [79] B. WILSON, Z. GHASSEMLOOY and J.C.S. CHEUNG: "Optical pulse interval and width modulation for analogue fibre communications", *IEE Proc.-J*, Dec. 1992, vol. 139, no. 6, pp. 376-381.
- [80] A.I. DURAKEV: "Noise performance and SNR threshold in PFM", *IEEE Trans. on Communications*, July 1985, vol. COM-33, no. 7, pp. 708-711.
- [81] B. WILSON, Z. GHASSEMLOOY and L. CHAO: "Squarewave frequency modulation techniques", *IEEE Trans. on Communications*, Feb./March/April 1995, vol. 43, pp. 1505-1512.
- [82] L. CHAO: "Optical transmission of wideband video signal using SWFM", *PhD Thesis*, University of Manchester Institute of Science and Technology, UK, Oct. 1990.

- [83] E. FITCH, "The spectrum modulated pulses", *Journal of the IEE*, vol. 94, part 3A, pp. 556-564, 1947.
- [84] B. WILSON, Z. GHASSEMLOOY, I. DARWAZEH, L. CHAO and D. CHAN: "Optical SWFM for wideband instrumentation and video signals", IEE colloquium on analogue optical communications, London, 1989, digest 1989/165, paper 9.
- [85] J.G. PROAKIS and M. SALEHI: "Communications systems engineering", *Prentice Hall International*, 1994, chap. 5, pp. 340.
- [86] R.P. WEBB: "Output noise spectrum from demodulator in an optical PFM system", *Electronic Letters*, July 1982, vol. 18, no. 14, pp. 634-636.
- [87] TAUB and SCHILLING: "Principles of communication systems", McGraw-Hill, 1986.
- [88] V. DI-BIASE, P. PASSERI and R.PIETROIUSTI: "Pulse analog transmission of TV signal on optical fibre", *Alta Frequenza*, June 1987, vol. LVI, no. 4, pp.195-203.
- [89] V.R. WICKRAMASINGHE, Z. GHASSEMLOOY and L. CHAO: "Optical fiber transmission of a broadband subcarrier multiplexed signal using PTM technique, *IEEE Trans. on Consumer Electronics*, May 1996, vol. 42, no. 2, pp. 229-238.
- [90] "1-800-OSCILLATOR", *MODCO*, Nevada, 1995.
- [91] S.F. HEKER, G.J. HERKOWITZ, H. GREBEL and H. WICHANSKY: "Video transmission in optical fibre communication systems using PFM", *IEEE Trans. on communications*, Feb. 1988, vol. 36, no. 2, pp. 191-193.
- [92] Z. GHASSEMLOOY: "Pulse position modulation spectral investigation", *International Journal of Electronics*, Jan. 1993, vol. 74, no. 1, pp. 153-158.

- [93] M. SCHWARTZ: "Information transmission, modulation and noise: a unified approach to communication systems, *McGraw-Hill*, 3<sup>rd</sup> edition, 1980.
- [94] R.D. STUART: "An introduction to Fourier analysis", *Chapman & Hall*, 1982.
- [95] H.S BLACK: "Modulation theory", *Van Nostrand*, 1953, Chapter 17.
- [96] W.R. BENNET: "New results in the calculation of modulation componenets", *Bell System Technology Journal*, 1933, issue 12, pp. 228-243.
- [97] S.Y. SUH: "Pulse width modulation for analog fiber-optic communications", *Journal of Lightwave Technology*, Jan. 1987, vol. LT-35, no. 1, pp. 102-112.
- [98] V.R. WICKRAMASINGHE, Z. GHASSEMLOOY and R.G. HARRIS: "Optical fibre transmission of a broadband SCM signal employing pulse position modulation", *Third Communication Networks Symposium* 8-9<sup>th</sup> July 1996, Manchester, UK, pp.85-89.
- [99] H.H. HAUSIEN: "Pulse position modulation for optical fiber local area networks", *PhD Thesis*, University of Bath, 1991.
- [100] W.S. HOLDEN: "An optical frequency pulse position modulation experiment", *Bell System Technical Journal*, Feb. 1975, vol.54, no.2, pp. 285-296.
- [101] *Motorola*: "MC1376 FM modulator circuit", Linear/Interface Devices.
- [102] Texas Instruments: "SN74S124 dual voltage controlled oscillator", The TTL data book, 1987, vol. 1, pp. 3-375 to 3-380.
- [103] *Philips Semi-conductors*: "NE 592 Video amplifier", General purpose / Linear ICs data handbook, April 1992, pp. 159-166.
- [104] "MECL Data", *Motorola Inc., Logic integrated circuits division*, 1993.
- [105] *GEC Plessey Semi-conductors*: "SP 1658 Voltage-controlled multi-vibrator", Data converters & Data comms, July 1991, pp. 3-32 to 3-35.
- [106] *Siemens*: "BFR 183 npn Silicon RF transistor", RS Technical data,, 1996.

- [107] *Maxim*: "MAX 9690C Ultra fast ECL output comparator".
- [108] *BT&D Technologies*: "LSC 2100 14 pin coolerless BH laser module", publication no. DS005/L, March 1992, revision 2.
- [109] *Laser Diode Laboratories Inc.*: "CW lasers and LEDs", Application note A/N101.
- [110] *BT&D Technologies*: "DLT 1040-ST transmitter, DLR 1040-ST receiver fibre optic data links", publication no. DS092/095, Jan. 1993, revision 2.
- [111] *Seastar Optics*, "Optical devices and laser diode instrumentation", 1990, pp. 8-10.
- [112] *Philips Semi-conductors*: "NE 564 Phase-locked loop", General purpose / Linear ICs data handbook, April 1992, pp. 259-267.
- [113] *Toko Inc.*: "5.5 MHz LPF", part no. TH317LTPS-2726PGD.
- [114] *Murata Manufacturing Co. Ltd.*: "SFE6.0MBF", part no. T335BBTS-0352.
- [115] *Toko Inc.*: "7.20BPF", part no. TH335BBTS-0304.
- [116] *Motorola*: "TBA120C FM IF amplifier, limiter and detector", Linear/Interface Devices, pp. 9-137 to 9-141.
- [117] *National Semiconductor*: "LM1877 dual power audio amplifier" RS technical data 1996.
- [118] *Toko Inc.*: "6.552 MHz BPF NICAM stereo filter", part no. TH316BQM-2110QDAF.
- [119] G. KENNEDY: "Electronic communication systems", 3<sup>rd</sup> edition, *McGraw Hill*, 1985.
- [120] S. HAYKIN: "Communication systems", *John Wiley & sons*, 3<sup>rd</sup> edition, 1994.
- [121] A.R. TOWNSEND: "Digital line-of-sight radio links: a handbook", *Prentice Hall International*, 1988.



But  $V_E$  can be expressed in terms of the base-emitter voltage of Q2,

$$V_E = V_2 - 2V_{BE} \quad (A6)$$

Hence,

$$I_b = \frac{V_2 - 2V_{BE} - V_{EE}}{R_E} \quad (A7)$$

The laser power fluctuations are detected by the monitor photodiode current, which determines the  $V_1$  voltage. The  $V_2$  voltage is sensitive to the  $V_1$  voltage. The dependence of  $I_b$  on  $V_2$  compensate for power fluctuations by changing the laser bias current accordingly.

The following closed form expression is used to calculate the laser bias current,  $I_b$

$$I_b = \frac{3V_s - 3V_{EE} - 2V_{BE}}{(2R_o \eta R_1 + R_E)} \quad (A8)$$

# Prototype Transmitter

